

# **Development and Testing of an Acoustic Combustion Sensor for Domestic Gas Boilers**

*by*

**Thomas David Neeld**  
UCL Energy Institute  
University College London  
2018

## **Declaration**

I, Thomas David Neeld, confirm that the work presented in this thesis is my own. Where information has been derived from other sources, I confirm that this has been indicated in the thesis.

Signed:

Tom Neeld

(September 2018)

## Abstract

For reasons of energy security, affordability and decarbonisation, future gas supply in the UK and Europe will likely be characterised by a wider variety of gas specifications. Due to variations of burn conditions associated with different gases, this shift necessitates the integration of technologies capable of detecting and adapting accordingly. Presented here are the results of a novel flame detection technology based on combustion acoustics, i.e. an acoustic combustion sensor. For the boilers investigated, this study has shown that pitch related acoustic features can be used to predict the equivalence ratio ( $\varphi$ ) of the burn with a root-relative-squared-error (RRSE) of less than 3%. This was achieved for an  $\varphi$  range of 0.75-0.88, independent of gas type and for the full range of transducers tested. Transducers tested included a piezoelectric contact microphone costing 1-2 USD. Additionally, independent of variations in  $\varphi$ , it was possible to predict gas type using combustion acoustics to 100% accuracy; this was achieved across four gas types investigated (G20, G21, G25 and G222). The minimum number of dimensions required to predict  $\varphi$ , to less than 3% RRSE, varied from 12 to 26 depending on boiler and transducer combination. For all data gathered, it was found that ML algorithms based on pitch related acoustic features significantly outperformed those based on ionisation current and CO concentration data for tracking  $\varphi$  and detecting gas type. Thus, it appears that a system based on a practical combustion acoustics sensor could outperform current, industry standard, commercially available systems.

## Impact Statement

This thesis presents a new approach to diagnosing the operational state of gas combustion systems within domestic boilers. The approach developed outperforms current industry standards and can seemingly be retrofitted to any boiler. Additionally, the proposed approach is not vulnerable to a common failure mode, namely that which occurs in the case of hydrogen-hydrocarbon gas mixes. The approach utilises the information hidden within the acoustic signals of flames to determine the operational air-to-gas ratio of the burn and the composition of the gas. The proposed diagnostic approach is named an 'acoustic combustion sensor'.

Sensors that diagnose the operational state of flames, otherwise known as combustion sensors, are essential to any combustion control system. Combustion control systems aim to maintain preferred burn conditions so that efficiencies and emissions are sustained. Preferred burn conditions are largely controlled by the operational air-to-gas ratio of a system, which can remain stable if gas compositions remain constant. However, for reasons of energy security, affordability and decarbonisation, there would ideally be flexibility in the permissible gas compositions throughout a gas network. For example, there is considerable interest in injecting hydrogen into the gas mix to help in decarbonising the wider power grid (Markillie, 2016). Similarly, injecting shale gas directly into the gas mix could improve energy security and affordability of host nations without the need for expensive refinery procedures. Thus, to improve the environmental and economic sustainability of energy systems, flexibility of gas composition is desirable, and to have flexibility, effective combustion sensors are required.

For industry, this thesis demonstrates that cheap, reliable, and highly accurate thermoacoustic combustion control systems can be developed. These systems out-perform existing combustion control systems, and if applied would allow combustion control of a wider range of gases. For governments, this has direct benefits on the economic and environmental sustainability of combustion of gases, particularly the combustion of green gases such as hydrogen currently being tested as a pathway to decarbonise gas as an energy vector for heating. For academia, this work demonstrates the application of interdisciplinary fields from combustion dynamics to machine learning. The thesis brings together methods not previously combined or applied in this context and demonstrates the potential of using thermoacoustic features with machine learning methods to diagnose and interpret flames. The methods presented offer a new approach to researchers to investigate origins of combustion acoustics and use the information contained within combustion acoustics for diagnostic purposes.

# Table of Contents

Declaration .....	2
Abstract .....	3
Impact Statement.....	4
Table of Contents .....	5
List of Figures.....	9
List of Tables .....	14
Acknowledgements .....	16
Published Work .....	17
List of Acronyms .....	18
1. Introduction.....	19
1.1 The 'Preferred' Equivalence Ratio .....	20
1.2 Variable Gas Compositions.....	21
1.3 Combustion Sensors .....	23
1.4 Scope of the Thesis.....	24
1.5 Structure of the Thesis .....	25
2. Background.....	27
2.1 Gas Specifications throughout Europe .....	27
2.1.1 Current Gas Specifications in Europe .....	28
2.1.2 Future Gas Specifications in the UK.....	30
2.2 The Domestic Gas-Fired Boiler .....	33
2.2.1 Working Principles.....	33
2.2.2 Impact of Varying Gas Specifications .....	34
2.3 Combustion Sensors .....	39
2.3.1 Combustion Overview .....	39
2.3.2 Commercially Available Combustion Sensors in Boilers.....	43
2.3.3 Potential Combustion Sensors for Practical Application .....	45

2.4	Aims and Objectives.....	52
3.	Literature Review .....	53
3.1	Combustion Acoustics.....	53
3.1.1	Overview .....	53
3.1.2	Direct Combustion Noise .....	56
3.1.3	Indirect Combustion Noise .....	59
3.1.4	Confinement .....	60
3.1.5	Relationship between Equivalence Ratio and Acoustics .....	61
3.2	Machine Learning.....	64
3.2.1	Unsupervised Machine Learning.....	64
3.2.2	Supervised Machine Learning .....	65
3.2.3	Feature Reduction.....	72
3.2.4	Training and Testing.....	73
3.3	Application Areas of Machine Learning.....	74
3.3.1	General.....	75
3.3.2	Combustion .....	76
3.3.3	Acoustics .....	79
3.3.4	Combustion Acoustics.....	82
4.	Pilot Study.....	86
4.1	Introduction .....	86
4.1.1	Hypothesis and Assumptions .....	87
4.2	Method .....	88
4.2.1	Setup .....	88
4.2.2	Experiments .....	91
4.2.3	Analysis .....	92
4.3	Results.....	93
4.3.1	Visual Analysis .....	93
4.3.2	Machine Learning.....	97

4.4	Conclusions.....	101
4.5	Uncertainties and Unanswered Questions.....	102
5.	Method of Primary Study .....	106
5.1	Predicting $\phi$ from Combustion Acoustics.....	106
5.1.1	Setup.....	106
5.1.2	Experiments.....	110
5.1.3	Data Analysis.....	112
6.	Results of Primary Study.....	119
6.1	Acoustic Combustion Sensor .....	119
6.1.1	Predicting $\phi$ .....	119
6.1.2	Predicting Gas Type .....	139
6.2	Ionisation and CO Combustion Sensor .....	140
6.2.1	Predicting the Equivalence Ratio.....	140
6.2.2	Predicting Gas Type .....	143
6.3	Summary.....	144
7.	Discussion .....	146
7.1	Significance of the results.....	146
7.1.1	Summary.....	146
7.1.2	Significance .....	147
7.2	Assumptions and Limitations .....	152
7.2.1	Repeatability and Scalability.....	152
7.2.2	Intermediate Gas Specifications.....	153
7.3	Analysis of the Results .....	154
7.3.1	Algorithms .....	154
7.3.2	Boilers.....	155
7.3.3	Microphones.....	156
7.4	Directions for Commercial Development.....	157
8.	Conclusions.....	160

References .....	162
9. Appendix .....	175
9.1 Heat Exchangers.....	175

## List of Figures

Figure 1 CO and NO <sub>x</sub> emissions for methane-air reaction at atmospheric conditions in a domestic gas-fired boiler, based on measurements made by the author. The boiler was a Worcester Bosch Greenstar 28i Junior. The CO and NO <sub>x</sub> traces have been smoothed for illustration purposes – the unsmoothed version is presented as Figure 6.....	21
Figure 2 Graph showing Wobbe Index regulations for European countries based on data gathered from a report by project Gasqual (Kimpton and Brown, 2010), as approved by the European Committee for Standardisation (CEN). If not specified the gas is of Group H as defined in standard EN 437:2003 (CEN, 2009, p.8). Note, specifications quoted are standardised to the reference conditions of 15 °C for combustion and 15 °C and 101.325 kPa for volume.....	30
Figure 3 Illustration of the specification of different gas types as adapted from (SGN, 2016) ...	32
Figure 4 Cross section showing the working principle of a condensing gas-fired heating appliance, as adapted from (Kiefer et al., 2012).....	34
Figure 5 Illustration of the relationship between adiabatic flame temperature ( $T_{ad}$ ) and equivalence ratio ( $\phi$ ) for methane-air combustion under standard conditions (Wang, 2015) ..	35
Figure 6 CO and NO <sub>x</sub> emissions for methane-air reaction at atmospheric conditions in a domestic gas-fired boiler. The boiler was a Worcester Bosch Greenstar 28i Junior. Note, the gas sensor for CO had a maximum range of 525 ppm.....	37
Figure 7 CO emissions and equivalence ratio for different test gases for two domestic gas-fired boilers. Note, the gas sensor for CO had a maximum range of 525 ppm .....	38
Figure 8 Composition, temperature and heat release rate ( $q$ ) profiles for stoichiometric CH <sub>4</sub> -air reaction at atmospheric temperature and pressure. As adapted from Glassman and Yetter (2014, p. 171). Note, 'Flame coordinate' refers to the distance along the flame from base to tip. ....	40
Figure 9 Flow diagram showing the main reaction mechanisms involved in methane oxidation in air. The circled radicals' CH*, OH* and CO <sub>2</sub> * are responsible for chemiluminescence phenomena. Note that C <sub>2</sub> * has not been included which gives a blue-green colour. This figure was adapted from Najm et al. (1998, p.325). The green arrows underlying the image indicated the dominant reaction path for the high-temperature mechanism of methane oxidation as summarised by Glassman and Yetter (2014, p. 113) .....	41

Figure 10 Image of the flame in a Worcester Bosch Greenstar 25Si Compact ErP condensing combi boiler (Worcester Bosch Group, 2015) burning G20 gas at an equivalence ratio of 0.75. .... 42

Figure 11 Image of the flame in a Worcester Bosch Greenstar 25Si Compact ErP condensing combi boiler (Worcester Bosch Group, 2015) burning G231 (85% CH<sub>4</sub> and 15% N<sub>2</sub>) gas at an unknown equivalence ratio. .... 43

Figure 12 Illustration of combustion noise sources from a closed system as adapted from Dowling and Mahmoudi (2015) ..... 56

Figure 13 Sound pressure level (SPL) vs frequency for direct combustion noise from an open premixed lean methane-air flame, as adapted from Rajaram (2007) ..... 58

Figure 14 Sound Pressure Level (SPL) vs frequency for combustion acoustics from an auxiliary power unit. Indicated are the contributions from direct combustion noise and indirect combustion noise. Adapted from Tam et al. (2013) ..... 60

Figure 15 Illustration of various contributions of combustion noise from heat release rates ( $Q$ ) and turbulence ( $z$ ). Adapted from Petela and Petela (1983) ..... 62

Figure 16 Direct noise from flame with same parameters but with  $\phi=0.73, 0.85$  and  $0.96$ . Adapted from Rajaram and Lieuwen (2003)..... 63

Figure 17 Illustration of an ANN with one hidden layer and three hidden neurons. Where  $x_1..n$  are the inputs,  $w_{1,1}(1)$  is the weight from neuron 1 in the first layer to neuron 3 in the second layer, and  $a(1)$  is the activation function for the first hidden layer ..... 70

Figure 18 Illustration of the soft margin loss setting as applied to SVM for regression. Figure adapted from Schölkopf and Smola (2002) ..... 71

Figure 19 Picture of the WB6 heat exchanger with labels indicating components of interest.. 88

Figure 20 Picture of the burner used in the WB6 heat exchanger ..... 89

Figure 21 Pictures highlighting the various positions of Microphones 1 and 2..... 91

Figure 22 Spectrograms of acoustics from Microphone 1 and Microphone 2 while sweeping through a range of equivalence ratios from 1 to 0.55..... 94

Figure 23 Averaged spectrogram for each interval of  $\phi$  investigated - Microphone 1 in Position 2. The spectrogram has been normalised with respect to the mean amplitude for that interval ..... 96

Figure 24 Averaged spectrogram for each interval of  $\phi$  investigated - Microphone 2 in Position 4. The spectrogram has been normalised with respect to the mean amplitude for that interval ..... 96

Figure 25 Pictures of the WB6 and WB7 heat exchangers with labels indicating components of interest ..... 107

Figure 26 Pictures of Burner 1, 2 and 4 used in Boilers 1 and 2..... 107

Figure 27 Picture of Microphone 3, a ceramic piezoelectric transducer, and a circuit diagram of the preamplifier used ..... 109

Figure 28 Pictures of the positions of all microphones for Boilers 1 and 2..... 110

Figure 29 Spectrograms of recordings from Dataset 5 for G20 gas. The 'Cold-Flow' represents all boiler noises without the presence of combustion, the 'Signal' represents the original recording with combustion present and the 'Cleaned Signal' is a spectral subtraction of the two previous signals. A smoothing filter of nine seconds was applied to all images. Figure (a) displays the frequency range from 0-2 kHz. Figure (b) displays the frequency range from 0-11 kHz ..... 121

Figure 30 Spectrograms of three separate recordings for Microphone 2, Boiler 2 and G20 gas. The value of  $\phi$  was varied between each recording as indicated at the top of each image. The PSD has been normalised to a range of -1 to 1. The frequency range is limited to 200-1000 Hz to highlight changes occurring in the spectrogram. A smoothing filter of nine seconds was applied to all images..... 122

Figure 31 Information-gain merit score for each frequency bin of Dataset 1\_NFC. The frequency range is limited from 2-8 kHz for illustration purposes only ..... 124

Figure 32 Information-gain merit score for each frequency bin of Dataset 1\_NFC as split by gas type for the frequency range of 2-4 kHz ..... 125

Figure 33 Information-gain merit score for each frequency bin of Dataset 1\_NFC. Labelled are the top seven peak frequency regions from 150-10000 Hz ..... 126

Figure 34 Normalized average values of 20 MFCCs for Dataset 3_MFCC .....	127
Figure 35 Plots of the resultant average RRSE after running ten iterations of 10-fold CV using kNN algorithms split by dataset, plotted against the number of dimensions in the data. The data used in the algorithms was varied by changing the granularity of frequency bins and by removing the number of frequency regions from '7' to '1' .....	130
Figure 36 Plots of the resultant average RRSE after running ten iterations of 10-fold CV using kNN algorithms split by dataset, plotted against the number of dimensions in the data. The data used in the algorithms varied by the number of MFCCs calculated over the same range of frequencies .....	132
Figure 37 RRSE results of kNN using 10-fold CV to all datasets (before application of wrapper methods). 'Original' refers to the original datasets (Datasets 1-6) without the removal of any instances. 'Reduced' refers to datasets with non-fully time-smoothed data points removed (2-4% fewer instances) .....	135
Figure 38 A bubble chart of the resultant average RRSE after running 10-fold CV using kNN, SVM and ANN algorithms on both NFC and MFCC features for all datasets. The size of bubbles represents the number of dimensions .....	136
Figure 39 Plots of the resultant average RRSE after running ten iterations of 10-fold CV using kNN algorithms split by dataset, plotted against the number of dimensions in the data. The data used in the algorithms was varied by changing the granularity of frequency bins and by removing the number of frequency regions included from 7 to 1 .....	138
Figure 40 Plots of the resultant average RRSE after running ten iterations of 10-fold CV using kNN algorithms split by dataset, plotted against the number of dimensions in the data. The data used in the algorithms was varied by changing the number of MFCCs included from 70 to 10 .....	138
Figure 41 Plot of ionisation current against $\phi$ as split by gas type for data collected from Boiler 2 .....	142
Figure 42 Plot of CO concentration against $\phi$ as split by gas type for data collected from Boiler 2 .....	143

Figure 43 Actual vs predicted per estimates from SVM algorithms based on MFCC (Dataset 6\_MFCC), ionisation current (Ion) and CO concentration (CO) feature data for Boiler 2. The black dotted line represents the correct prediction..... 147

Figure 44 CO and NO<sub>x</sub> emissions for methane-air reaction at atmospheric conditions in a domestic gas-fired boiler. The boiler was a Worcester Bosch Greenstar 28i Junior. The CO and NO<sub>x</sub> trace has been averaged significantly for illustration purposes ..... 148

Figure 45 Illustration of the potential variations in gas type ..... 153

Figure 46 Plot of CO<sub>2</sub> percentages and associated standard deviations for each recording block for Boilers 1 and 2 G20 data points ..... 156

Figure 47 Blue prints of the WB6 Heat Exchanger ..... 175

Figure 48 Blue prints of the WB7 Heat Exchanger ..... 176

## List of Tables

Table 1 Range of gases within the second group of gas families, group H, L and E, as defined in standard EN 437:2003 (CEN, 2009, p.8).....	28
Table 2 Prediction results of a range of different machine learning algorithms to the datasets analysed. Results reported are the consequence of applying 10-fold cross-validation .....	99
Table 3 Coefficients for Equation 5.1 for the various gas types investigated .....	108
Table 4 Table summarising compositions of all gas types tested.....	112
Table 5 Summary of datasets available for analysis .....	120
Table 6 Frequency region ranking for each dataset as based on the information-gain evaluator .....	126
Table 7 The lowest RRSE values achieved for each of the machine learning algorithms tested for each dataset. Also included is the standard deviation of the average RRSE.....	129
Table 8 The average RRSE after running ten iterations of 10-fold CV using kNN algorithms split by dataset. The selection of dimensions is based on selecting data-point with the lowest dimensions at the point that algorithms asymptote. Included in the table are the frequency regions, the number of dimensions and the frequency granularity.....	131
Table 9 Resultant average RRSE before and after running wrapper methods for Datasets 1-6_NFC. Also listed are the changes in dimensions.....	133
Table 10 Resultant average RRSE before and after running wrapper methods for Datasets 1-6_MFCC. Also listed are the changes in dimensions.....	134
Table 11 Summary of datasets available for analysis for Section 6.1.2.....	137
Table 12 Confusion matrix showing the predicted gas type as based on acoustic data. ....	140
Table 13 Summary of the average RRSE results of the best performing ML algorithms for Ionisation current and CO concentration data as split by gas type and for all gas types combined .....	141

Table 14 Confusion matrix for predicting gas type using J48 ML algorithm for ionisation current data. Also included are the Kappa statistic and the percentage correct ..... 144

Table 15 Confusion matrix for predicting gas type using J48 ML algorithm for CO concentration data. Also included are the Kappa statistic and the percentage correct ..... 144

Table 16 Summary table of prediction results for data gathered form the acoustic sensor, ionisation sensor and CO gas sensor for all gas types (G20, G21 and G222). Boiler 2 only..... 145

## Acknowledgements

I am grateful for the funding I have received from the Engineering and Physical Sciences Research Council through the London-Loughborough Centre for Doctoral Training in Energy Demand (LoLo), under grant numbers EP/L01517X/1 and EP/H009612/1.

I acknowledge all the help and support the Worcester Bosch R&D team have provided to me. Many of the experiments performed in this thesis were only possible due to the support of the technical staff within Worcester Bosch. I must thank Andrew Butler and Tom Collins for their support during experiments. I also thank the Director of R&D Richard Evans for supporting me during my research and some inspired ideas as I progressed through the PhD.

I am very grateful for the help and support received from my supervisors Professor David Shipworth and Professor Bob Lowe, without which none of this would have been possible. I would also like to acknowledge the help received by James Eaton from the department of Electrical and Electrical Engineering at Imperial College London who advised me throughout my PhD with regard to signal processing approaches.

## **Published Work**

### Peer-Reviewed Journal Publications

Neeld, T., Eaton, J., Naylor, P.A. and Shipworth, D., 2016. A novel method of determining events in combination gas boilers: Assessing the feasibility of a passive acoustic sensor. *Building and Environment*, 100, pp.1-9.

## List of Acronyms

ANNs – Artificial Neural Networks

CCS – Combustion Control System

CH<sub>4</sub> – Methane

CO – Carbon monoxide

CO<sub>2</sub> – Carbon Dioxide

G20 – Natural gas with a composition of 100% methane

G21 – Natural gas with a composition of 87% methane and 13% propane

G222 – Natural gas with a composition of 77% methane and 23% hydrogen

G23 – Natural gas with a composition of 92.5% methane and 7.5% nitrogen

G25 – Natural gas with a composition of 86% methane and 14% nitrogen

GS(M)R – Gas Safety Management Regulations

kNN – K-Nearest Neighbour algorithm

LFCC - Linear-Frequency Cepstral Coefficients

LGR – Logistic Regression

LR – Linear Regression

MFCC – Mel-Frequency Cepstral Coefficients

NO<sub>x</sub> – Nitrous Oxides

RRSE – Root Relative Squared Error

SVMs – Support Vector Machines

$\varphi$  - Equivalence ratio of combustion ( $\varphi > 1$  is fuel rich)

# 1. Introduction

For reasons of energy security, affordability and decarbonisation, future gas supply in the UK and Europe will likely be characterised by a wider variety of gas quality and composition. Due to the impact such variations have on the burn conditions of gas combustion technologies, such a shift requires:

- a. that gas networks are split regionally and each region has a region-specific gas specification range and consequently region-specific combustion technologies (this has been done in Germany); or
- b. control systems are introduced into gas combustion technologies which can deal with the impact of varying gas specifications; such technologies are referred to as Combustion Control Systems (CCSs).

CCSs automatically adjust the air-to-gas ratio of a combustion system in response to changes in burn conditions. Such a device aims to avoid adverse impacts that varying gas compositions may have on emissions, efficiencies and the safety of the combustion device. A CCS typically achieves this by adjusting an electronic gas valve in response to readings from a combustion sensor. The combustion sensor infers directly or indirectly the operational state of the flame, such as the operational air-to-gas ratio. For example, if the combustion sensor has detected that the air-to-gas ratio is lower than required, then the partition on the gas valve can be reduced until the reading is normalised. A gas valve partition is typically referred to as the Ratio Adjuster on gas valves but quite simply restricts the flow of gas for a given negative pressure.

The domestic gas boiler is a critical technology globally and in many countries, is the technology via which most domestic energy is consumed. Unsurprisingly significant effort has been by many manufacturers to develop CCSs for integration into domestic gas boilers. From the perspective of manufacturers, the primary incentives of developing gas-independent boiler technologies are to future-proof their product and widen their market. However, most if not all the CCSs developed employ combustion sensors which fail during potentially critical scenarios, namely when hydrogen is included into the gas mix. There is thus a need for more research. This work investigates the feasibility of a new type of combustion sensing technology, namely an acoustic combustion sensor.

An investigation into new combustion sensing solutions is pertinent for several reasons:

1. The current portfolio of practical combustion sensors have been shown to fail when significant proportions of hydrogen are added into the gas mix.
2. The current portfolio of practical combustion sensors cannot determine the composition of the gas being burnt and thus cannot achieve a 'preferred' air-to-gas ratio during operation - a 'preferred' air-to-gas ratio refers to the air-to-gas ratio value considered preferred for the unique gas composition being burnt. This applies for hydrogen containing gases in addition to 100% hydrocarbon gases.
3. The portfolio of potential combustion sensors either require direct access to the flame, or a line-of-sight measurement of the flame, or access to exhaust gases; all of which can suffer from degradation and/or fogging issues.

The present investigation indicates that an acoustic combustion sensor can: operate accurately regardless of changes in gas composition (including significant admixtures of hydrogen); estimate gas composition and thus achieve a close-to 'preferred' air-to-gas ratio; be developed cheaply; be retrofitted to a domestic gas boiler; and does not require line-of-sight access to the flame. Thus, an acoustic combustion sensor potentially does-away with many of the issues apparent in current approaches. To relate combustion acoustics to operational combustion parameters of interest, machine learning methods are integral. Note that additional work is required to investigate the impact of background noise for an operational CCS using the proposed combustion acoustic sensor.

### *1.1 The 'Preferred' Equivalence Ratio*

The 'preferred' air-to-gas ratio, or 'preferred' equivalence ratio ( $\varphi$ ), in a gas combustion system will vary depending on: the combustion system under consideration; the gas composition; the operational power output of the system; and environmental conditions. Due to emission constraints, all gas combustion systems operate fuel-lean ( $\varphi$  less than one). Efficiencies are maximized at stoichiometric conditions ( $\varphi$  approaching unity), but efficiency is not the only relevant criterion – boilers must also not exceed  $\text{NO}_x$  and CO emission constraints. Consequently, most gas combustion systems aim to maximise  $\varphi$  so long as emission criteria are maintained. For methane-air reactions a value of  $\varphi$  in the range of 0.7 to 0.9 is normally selected. Note,  $\varphi$  is defined as the actual fuel to oxygen ratio divided by the stoichiometric fuel to oxygen ratio.

Figure 1 illustrates the change in emission concentration ( $\text{NO}_x$  and CO) with  $\varphi$  for a unique gas boiler and gas type combination. As observed, a value of  $\varphi$  in the range of 0.72 appears optimum

for this combination of gas composition, power output and combustion system. Such a value is preferred as it maintains emission criteria, with minimal degradation of efficiency. If such a value was set for a particular gas type, then the preferred  $\phi$  would be achieved if the calorific content of the gas remained constant. However, as the calorific content of the gas shifts,  $\phi$  would be moved from its set point as the proportion of air-to-gas has altered relative to its stoichiometric value. In addition, a different gas composition would result in a unique  $\text{NO}_x$  and CO curve and therefore change the preferred value of  $\phi$  from 0.72 to a new value. For example, high proportion Hydrogen-Hydrocarbon gases contain less carbon and therefore can typically be run at a higher value of  $\phi$ . To manage both impacts, a combustion sensor must estimate the operational  $\phi$  and gas composition. Such an estimate can be used to determine the revised 'preferred'  $\phi$  and estimate  $\phi$  while adjustments are made to attain said value. Note, the instantaneous operational power output of the boiler is assumed to be known independently of the estimation of  $\phi$ ; this is because the power output of every boiler can be estimated accurately from the speed of the pre-mix fan, the speed of which is controlled by the CPU of the boiler.

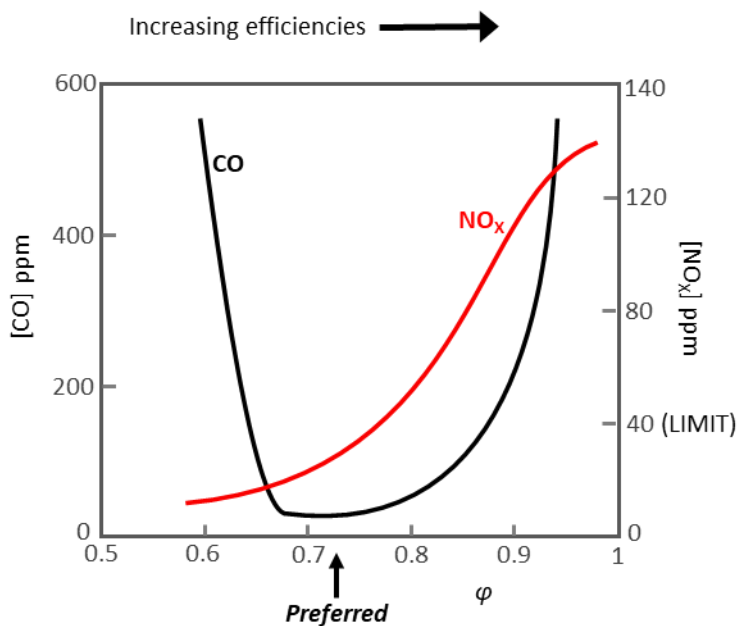


Figure 1 CO and  $\text{NO}_x$  emissions for methane-air reaction at atmospheric conditions in a domestic gas-fired boiler, based on measurements made by the author. The boiler was a Worcester Bosch Greenstar 28i Junior. The CO and  $\text{NO}_x$  traces have been smoothed for illustration purposes – the unsmoothed version is presented as Figure 6.

## 1.2 Variable Gas Compositions

If gas compositions within a gas combustion system could be tightly controlled, and the system performed consistently over its lifetime, there would be no need for a CCS or indeed a

combustion sensor. If, however the gas composition is subject to considerable variation over time a CCS would be required to maintain preferred burn conditions. Within the UK, gas compositions are tightly controlled and thus CCSs are to-date not essential. In the rest of Europe however the ranges of acceptable gas type and gas quality vary substantially. For example, networks in Poland are segregated into high-quality and low-quality gas regions. This has traditionally led to region-specific gas combustion technologies. If a gas network sought to deliver a larger variation of gas composition throughout the entire network, CCS would be required in all gas combustion systems. There are three main reasons why varying gas compositions are desirable: energy security, affordability and decarbonisation. These aspects will be discussed below from the perspective of the UK.

Security and affordability of gas supply in the UK is subject to competitively priced reliable sources of natural gas. Traditionally the UK has been reliant on UK Continental Shelf (UKCS) gas. UKCS gas has been affordable, reliable and consistent in composition. However according to the national grid (National Grid plc, 2016a), by 2040 the UK may either have about 20-45% of its total gas supply coming from UK shale or be highly reliant on gas imports. Shale gas composition would be expected to "...vary widely with the local geology" (National Grid plc, 2013, p.99), in addition the composition of imports cannot be guaranteed: "Over the next decade, gas arriving in Europe (to the UK) may come from more diverse sources and may therefore be characterised by a wider range of gas quality" (Ofgem, 2016). Thus, due to market factors it may be necessary for the UK to transmit a larger variation in gas composition throughout the network.

Regarding decarbonisation, steps need to be taken globally to reduce the carbon footprint of consumed energy. Within the UK, the government is committed to a 80% reduction in carbon emissions by 2050 relative to 1990 levels (Parliament, 2008). To meet these targets the decarbonisation of space heating within the domestic environment is key. This requires either the electrification of heating (heat pumps) combined with the decarbonisation of the electricity network, or decarbonisation of gas transmitted through the gas network and continued use of gas heating technologies. According to energy system models, both hydrogen and biogas are potential avenues for a carbon-free gas network (Dodds and McDowall, 2013). Hydrogen inclusion into the gas network has gained notable traction in recent years. Processes such as Power-to-Gas present attractive means to storing energy during periods of electricity surplus. The HyDepoly project for example has gained seven million pounds of Ofgem funding to "...inform a further public trial of the use of hydrogen-blended natural gas in the UK grid, with

the intention of then rolling out the use of hydrogen blends nationwide (in 2020)” (Markillie, 2016).

Shale gas, hydrogen containing gas, and biogas will all likely fail to meet the current restrictions imposed in the UK by the Gas Safety (Management) Regulations (GS(M)R), although the benefits of such would potentially improve energy security, affordability and carbon emissions. For shale and biogas GS(M)R restrictions could be met via costly refining processes, however for hydrogen blends no such option exists. Thus, without refining, a significant barrier to the adoption of shale, hydrogen and biogas is the ability of gas combustion technologies to manage variations in composition. To manage such variations, effective CCSs are required. Essential to the performance of CCSs are combustion sensors. Ideally such combustion sensors would accurately predict the gas composition and the operational value of  $\varphi$  so that the ‘preferred’  $\varphi$  can be achieved (as discussed in Section 1.1). For practical consideration, these sensors should also be affordable, reliable and safe.

### *1.3 Combustion Sensors*

To-date, commercially available domestic gas boilers featuring combustion sensors use either a CO gas sensor or an ionisation probe to diagnose the state of the flame. Both systems have advantages and disadvantages associated with them. Ionisation sensors are low cost but accuracies are poor, particularly for hydrogen containing gas types - CO flue gas sensors are accurate, expensive and fail when high proportion hydrogen mixes are considered. Within the literature, a variety of potential combustion sensors have been researched covering a wide range of subject areas including spectroscopy, solid-state physics, chemical kinetics, machine vision and fluid dynamics. From this literature, other combustion sensing options include: emission/absorption spectroscopy, flame imaging and combustion acoustics.

Emission/absorption spectroscopy is an approach largely applied for research purposes. Spectroscopy combustion sensing based approaches have been applied in commercial systems (Ebert et al., 1998, Ebert et al., 2005) but are not practical for integration into domestic appliances due to cost and fogging/design issues associated with a line-of-sight sensor. Flame imaging as a combustion sensing approach has been developed within experimental combustion rigs (Lu et al., 1999) however the approach similarly suffers from fogging/design issues associated with a line-of-sight sensor. Studies into the usage of combustion acoustics as a combustion sensor have shown some promise (Petela and Petela, 1983, Sanz et al., 2008), however significant research is still required, particularly for the case of varying gas

specifications in a practical combustion system. Considering the weaknesses of current combustion sensor technologies and the demand for CCSs within domestic gas combustion systems, alternatives should be considered.

Petela and Petela (1983) and Ramachandra (1983) were the first to explicitly identify combustion acoustics as a potential diagnostic mechanism for flames. Petela and Petela (1983) found the acoustic intensity, within certain frequency bands, varied as a function of the  $\varphi$ . More recently (Norris et al., 2005, Kleppe et al., 2004) found a strong relationship between peak frequency of their system and the  $\varphi$  of the burn for a limited dataset. They also proposed that passive acoustic methods could be used to determine the operational  $\varphi$ . In general however research in this area has been limited, as indicated by a recent review: "...these studies clearly demonstrate that the information contained in acoustic flame signals is intimately related with the very nature of the combustion process and, therefore, may offer interesting possibilities for flame monitoring" (Ballester and García-Armingol, 2010, p.397). One possibility for the stagnation of the development of practical acoustic combustion sensors may be the failure to apply recent technological advances in data mining techniques and computational resources. By applying modern methods of machine learning to this subject area, such as those applied in automatic speech recognition, the application of an acoustic combustion sensor could be realised.

Consequently, the focus of the present study is on the application of combustion acoustics as the basis for low cost and accurate combustion sensor for domestic gas boilers. To deal with the complexity of acoustic data emanating from combustion, particularly for the case of a confined system, modern methods in machine learning are utilised.

### *1.4 Scope of the Thesis*

The scope of this thesis is to determine if combustion acoustics can be used as an indirect measure of the operational  $\varphi$  for gas combustion within domestic gas-fired boilers. A pilot study will be used to answer this question for a single boiler and gas type. Additional experiments will be used to determine if detection of  $\varphi$  can be made independently of gas type in addition to determining if an accurate estimate of gas composition can be made. This will be performed across several domestic gas boilers with differing heat exchangers and burners using an array of acoustic sensors. Equivalence ratios will be varied from 0.6 to 1.0 for the pilot study and across a tighter range of 0.75 to 0.88 for the remainder of the experiments. The equivalence ratio will be varied via two methods, firstly by manually altering the partition of the gas valve and secondly by manually altering the speed of the pre-mix fan.

The hypothesis for this study is as follows:

Noise from a flame (aka combustion roar) is closely related to unsteady heat release rates, which will vary as air to gas ratios change, under the influence of changing gas composition. By applying machine learning algorithms one can use data from these complex pressure signals to accurately and reliably predict the operational equivalence ratio. Additionally, noise from a flame is closely related to the composition of the gas being burnt and therefore machine learning algorithms can be used to accurately and reliably predict gas composition. This can be achieved in a domestic gas boiler using a combination of low-cost transducer with machine learning algorithms.

### *1.5 Structure of the Thesis*

First a background of gas specifications in the UK and Europe is provided with consideration to the future of gas specifications in the UK. Next an overview of the domestic gas-fired boiler is given and the impacts that varying gas specifications have on the emissions and/or efficiencies of these systems. Following that the solution to such variations is introduced, namely a combustion control system. Such systems require combustion sensors to determine the state of combustion. Thus, an overview of commercially available combustion sensors and the array of potential combustion sensors are given. The end of this section highlights the potential of pressure fluctuations as a diagnostic tool.

Following the background, a literature review will be given regarding combustion acoustics. Such a review highlights the complexities associated with combustion acoustics, especially for scenarios where the flame is confined. From this and reviewing previous studies, it is clear machine learning techniques will be required to relate combustion acoustics to variables of interest; consequently, a literature review regarding machine learning is given next. In this review, focus will be in the context of machine learning applied to combustion related and acoustic related phenomena. The methods and techniques discovered within this review informed the pilot study.

The pilot study is reported next. In this study boiler acoustics are analysed for large variations in air-to-gas ratios for a single system and gas type combination. The pilot study is performed to determine if the potential of such methods can be realised. The output of the pilot study was very positive and provided impetus for further investigation. Highlighted from the pilot study

were however many uncertainties and unanswered questions. This instigated another phase of experiments carried out in the primary study.

The experimental and analytical methods required to complete the primary study are then given. These include the setup of experimental apparatus, the running of the experiments and the data analysis required.

The results from the primary study are then presented. This includes the results of multiple microphones, across two boilers with two different heat exchangers and four different burners; burning a wide range of gas types and changing the method by which air-to-gas ratios are varied. Due to the large data volumes and range of analysis covered in this section, it is split into a number of logical steps: first a visual analysis is performed of the acoustic impact of varying air-to-gas ratios; following this the observed features are used within the machine learning paradigm and tested; next more sophisticated but less intuitive features and machine learning algorithms are explored.

The results of the investigation are followed by a detailed discussion and conclusions.

## 2. Background

### *2.1 Gas Specifications throughout Europe*

Gas networks throughout Europe contain gases defined within the second grouping of gas families. This family contains gas Groups E, H and L, as defined in standard EN 437:2003 (CEN, 2009). The second grouping of gas families are primarily made of methane, varying amounts of other alkanes, nitrogen, carbon dioxide, and can include up to 23% hydrogen. This gas family is often referred to as natural gas and will be referred to simply as “gas” for the rest of this report. The full range of test gases for this family has been summarised in Table 1. Although many gas appliance testing procedures throughout Europe include all gases in Table 1, constraints on transmitted gases, and therefore long term operation, vary significantly by country. This will be discussed in the following section.

Note, gas specifications are defined in terms of the Wobbe Index (WI): The WI is equal to the higher heating value of gas divided by the square root of the specific gravity as compared to air; it is a particularly useful metric because, “for a particular orifice at a constant supply pressure, heat input is directly proportional to Wobbe number [WI]” (Jones, 1989, p. 10).

Group	Gas code	Composition, vol-%	Gross calorific value <sup>1</sup> , MJ/m <sup>3</sup>	Gross Wobbe index <sup>1</sup> , MJ/m <sup>3</sup>	Stoichiometric air-to-gas ratio
H/E	G20	CH <sub>4</sub> = 100	37.78	50.72	9.52
H/E	G21	CH <sub>4</sub> = 87 C <sub>3</sub> H <sub>8</sub> = 13	45.28	54.76	11.38
H/E	G222	CH <sub>4</sub> = 77 H <sub>2</sub> = 23	31.86	47.87	7.88
H	G23	CH <sub>4</sub> = 92.5 N <sub>2</sub> = 7.5	34.95	45.66	8.81
E	G231	CH <sub>4</sub> = 85 H <sub>2</sub> = 15	32.11	40.9	8.45
L	G25	CH <sub>4</sub> = 86 N <sub>2</sub> = 14	32.49	41.52	8.19
L	G26	CH <sub>4</sub> = 80 C <sub>3</sub> H <sub>8</sub> = 7 N <sub>2</sub> = 13	36.91	44.83	9.29
L	G27	CH <sub>4</sub> = 82 N <sub>2</sub> = 18	30.98	39.06	7.81

<sup>1</sup> Reference conditions of 15 °C for combustion and 15 °C and 101.325 kPa for volume.

*Table 1 Range of gases within the second group of gas families, group H, L and E, as defined in standard EN 437:2003 (CEN, 2009, p.8)*

### 2.1.1 Current Gas Specifications in Europe

Throughout Europe acceptable gas specifications vary significantly. Figure 2 provides a summary of the acceptable ranges by country (Kimpton and Brown, 2010); unless otherwise stipulated, all gas types reported in are within Group H. As observed in Figure 2, Ireland, Portugal and Spain's regulations allow for the transmission of all gases within Group H (CEN, 2009); Germany allows for transmission of all gases defined within the second family (Group H, E and L). Note, the restrictions labelled EASEE represent standards defined by The European Association for the Streamlining of Energy Exchange. The EASEE "...develop and promote standard European business practices to simplify and streamline gas transfer and trading across Europe" (EASEE-gas, 2016). Gas specifications as defined by the EASEE have WI ranges of 46.45 - 53.99 MJ/m<sup>3</sup> containing "insignificant levels of hydrogen" but with no restriction on ballast gas (N<sub>2</sub>, CO<sub>2</sub>, etc.) (EASEE-gas, 2008). There are gas groups outside of the internationally marketed groups outlined

in EN 437:2003 (CEN, 2009), Group 2S is an example of a special category for Hungary (similar to Group L but with a higher CO<sub>2</sub> content). These special categories can only be marketed nationally. Note that the Author could not find WI regulations for Bulgaria, Finland, Lithuania, Romania, Slovakia and Slovenia. All Finish, Bulgarian, Lithuanian and almost all Slovakian (98% in 2014) (URSO, 2014) gas is imported from Russia (Gazprom Export, 2016). All Russian gas is exported by Gazprom PJSC which has exclusive rights to export Russia's natural gas (Gazprom, 2016).

Of note, in recent news (as of early 2017), the low quality (L-gas) supplies from the Netherlands to other EU countries are expected to fall significantly. In Germany alone this will impact approximately five million households by 2030 (Morris, 2017). To ensure appliances continue to operate safely, this transition will either require adjustments to current appliances or that current appliances be replaced by new ones. Of particular concern is how the changeover impacts domestic gas boilers (Frahm, 2015). It also appears that Belgium, France and the Netherlands will be transitioning from L-gas to H-gas, although no specific sources have yet been identified (Broenink, 2015). The decision in the Netherlands to reduce production of natural gas has come about due to mounting public pressure with regard to extraction-induced subsidence in the Province of Groningen; a phenomenon which has gained significant public attention since a particularly bad tremor in 2012 (van der Voort and Vanclay, 2015). To avoid additional subsidence, extraction has been reduced from 48 bcm/yr in 2011 to a maximum of 24 bcm/yr from 2017-2022 (Reuters Staff, 2016).

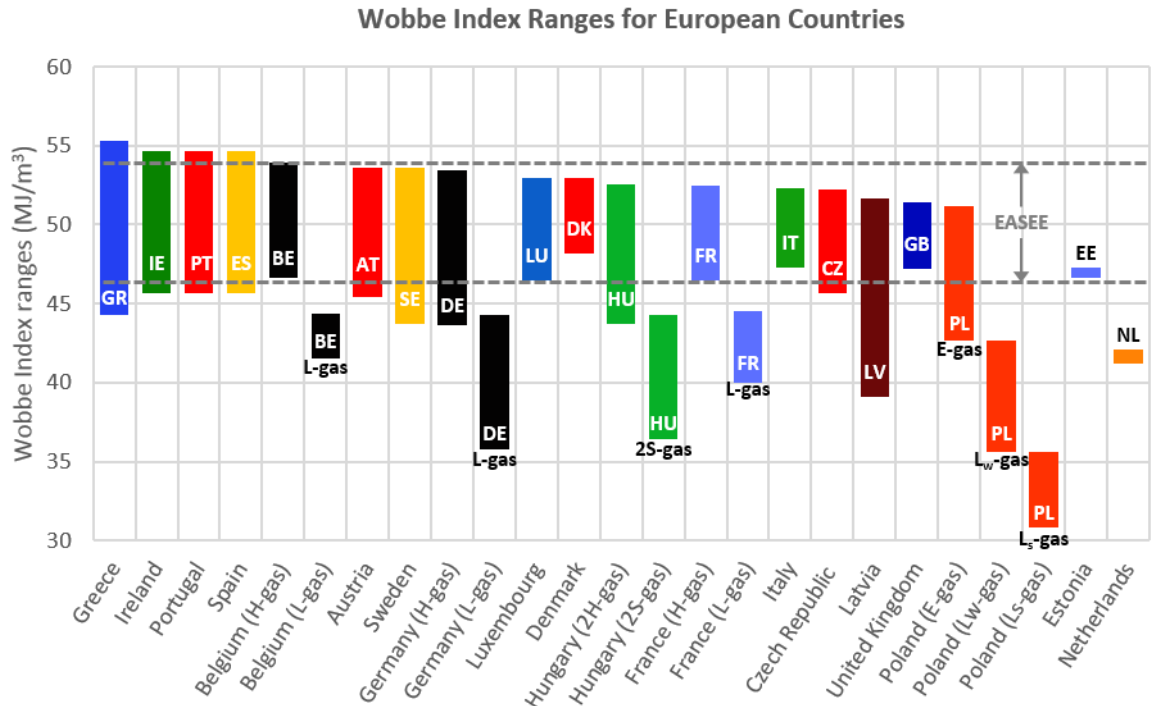


Figure 2 Graph showing Wobbe Index regulations for European countries based on data gathered from a report by project Gasqual (Kimpton and Brown, 2010), as approved by the European Committee for Standardisation (CEN). If not specified the gas is of Group H as defined in standard EN 437:2003 (CEN, 2009, p.8). Note, specifications quoted are standardised to the reference conditions of 15 °C for combustion and 15 °C and 101.325 kPa for volume

### 2.1.2 Future Gas Specifications in the UK

Since 2000 the UK's reliance on UK Continental Shelf (UKCS) gas has dropped from supplying over 98% of consumed gas in 2000 to 39% in 2014. To meet the consumption gap the UK has relied exclusively on gas imports largely from Norway, Qatar and the Netherlands (DECC, 2015). In general, since 2000, the UK market has undergone a transition from "one of supply self-sufficiency to one of import dependency: not only for annual supply but also for seasonal flexibility" (Rogers, 2011, p.17). The LNG and gas pipeline import infrastructure in the UK, as of 2013, had a total capacity of 150 bcm/yr (Kopp, 2015), close to double the annual consumption of 2014 (78 bcm/yr). There are currently four planned LNG import infrastructure projects in the UK. In total these projects could increase import capacity by another 35 bcm/yr (National Grid plc, 2016b, p.209).

The future of the gas network in the UK, according to the National Grid (National Grid plc, 2016b), is one of continued import dependence with the potential of inclusion of UK shale. Of the four scenarios considered, the National Grid (National Grid plc, 2016b) concluded that by

2040 gas imports could make up over 90% of supply; alternatively supply dependence could be reduced by the inclusion of UK shale reserves, which could make up to 25% of supply. The predicted forecast of UKCS gas is at most 10% of supply by 2040, this is less than half of what it was in 2014.

With reliance on import channels and potentially inclusion of UK shale, the future of gas specifications is uncertain. The Office of Gas and Electricity Markets state that “Over the next decade, gas arriving in Europe may come from more diverse sources and may therefore be characterised by a wider range of gas quality” (Ofgem, 2016); The National Grid have noted the issues shale gas will cause regarding alignment to the Gas Safety (Management) Regulations (GS(M)R) (HM Government, 1996) in addition to potential of local variation: “(Shale) Gas quality will need to be considered due to GS(M)R (...) and may vary widely with the local geology.” (National Grid plc, 2013, p. 99). There is no indication to-date of the WI of UK or EU shale reserves, however based on MacKay and Stone’s (2013, p. 17) data on US shale quality, which found that WI values varied from 31.4 - 53.4 MJ/m<sup>3</sup> due to varying ratios of nitrogen to methane, UK and EU shale gas may cover a large range of qualities.

Within the UK, the government is committed to a 80% reduction in carbon emissions by 2050 relative to 1990 levels (Parliament, 2008). To meet these targets the decarbonisation of space heating within the domestic environment is key. This requires either a shift to electric heating (heat pumps) combined with the decarbonisation of the electricity network, or decarbonisation of the gas transmitted through the gas network. Thus, in addition to energy security and affordability of gas, one must also consider decarbonisation.

According to energy system models, both H<sub>2</sub> and biogas are potential avenues for a carbon-free gas network (Dodds and McDowall, 2013). Although H<sub>2</sub> and biogas scenarios are not currently projected by the National Grid (National Grid plc, 2016b), the HyDepoly project, due to start in 2017, will “...be used to inform a further public trial of the use of hydrogen-blended natural gas in the UK grid, with the intention of then rolling out the use of hydrogen blends nationwide (in 2020)” (Markillie, 2016). The HyDeploy project will provide a framework to develop the Power-to-Gas market in the UK. Power-to-Gas is a process whereby surplus electricity (generated via renewables or otherwise) is used to extract H<sub>2</sub> via electrolysis. Thus, storing surplus energy and stabilising the electricity grid. H<sub>2</sub> can then be injected into the gas network for use in domestic combustion systems, or converted to electricity by any of several gas-to-power technologies. Germany has a number of operational Power-to-Gas facilities of this type (ITM-Power 2015).

As a summary, an illustration of the relevant gas supply channels discussed, and their estimated WI values, has been provided in Figure 3.

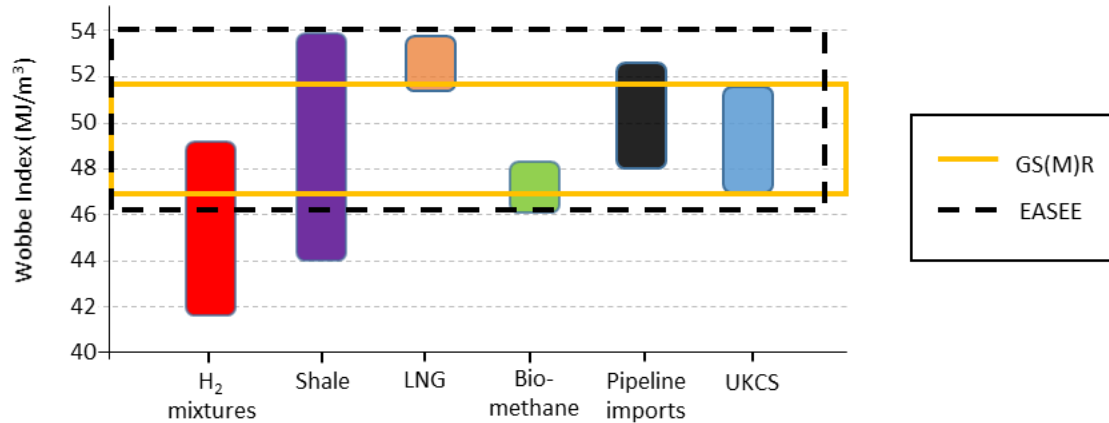


Figure 3 Illustration of the specification of different gas types as adapted from (SGN, 2016)

Because of what has been discussed above, UK gas standards defined by the GS(M)R have been strongly challenged. For example, the Oban Project run by Scottish Gas Networks (SGN) aimed “To demonstrate that gas which meets EASEE Gas specification but sits outside GS(M)R can be conveyed safely and efficiently in the GB (UK) gas network.” (SGN, 2015). The culmination of the project was a 13-month field trial injecting gas of EASEE range into the Oban network - 1,104 properties in total. However, during the field trials a much smaller range from 48.75 - 53 MJ/m<sup>3</sup> was tested. Indeed for over 95% of the period WI ranges were between 49.5 MJ/m<sup>3</sup> and 52.5 MJ/m<sup>3</sup> (SGN, 2016) which is only 1 MJ/m<sup>3</sup> above GS(M)R restrictions. Thus the Oban project field trial failed to prove or disprove decisively if EASEE gas specifications can be “...conveyed safely and efficiently in the GB (UK) gas network” (SGN, 2015). Field tests were also performed within the scope of the Oban project. It was found that “Having been correctly adjusted with a ‘standard gas’ (G20) all of these [about 700] room sealed boilers will operate safely on WI up to 53.25 MJ/m<sup>3</sup> and down to about 48.00 MJ/m<sup>3</sup>” (SGN, 2016, p. 80). For the full EASEE WI range about 1.5-3% of boilers failed per the CO/CO<sub>2</sub> ratio safety action level of 0.008; this is once the boilers had been adjusted to G20, thus exempting potential post adjustment air-to-gas ratio shifts. The results of the field tests potentially explained why gas ranges were limited to a smaller than planned range during the field trial.

## *2.2 The Domestic Gas-Fired Boiler*

Within European gas networks one vital gas consuming technology is that of the domestic gas-fired boiler - in the UK approximately 72% of energy delivered to dwellings is consumed in gas-boilers for the purposes of central heating and hot water production (DECC, 2014); western European domestic heating markets are dominated by condensing gas-fired boilers (BSRIA, 2015). Typically, domestic gas-fired boilers are connected to mains gas networks, thus varying gas compositions in the network directly impact operation of gas boilers and so must be considered. As mentioned, the biggest impact associated with parts of Germany, France, Belgium and the Netherlands shifting from L-gas to H-gas, is the impact on the operation of domestic gas boilers. The shift is requiring intervention to adjust settings and perform safety checks in over five million homes in Germany (Frahm, 2015).

### *2.2.1 Working Principles*

The typical working principle of domestic condensing gas-fired boilers has been illustrated in Figure 4 (Kiefer et al., 2012). As seen in the figure: gas, via the gas valve (2), and air, via the air inlet (1), are mixed by the pre-mix fan (3), forced into the combustion chamber (4) and burnt; the heat exchanger (5) then transfers heat from the products of combustion (4) to the water circuit (6); near the bottom region of the heat exchanger, cold returning water (6) is heated when hot-wet exhaust gases condense - this additional level of heat transfer via the process of condensing highlights the difference between non-condensing and condensing boilers; to gather the condensate, a water sump (7) is required. The exhaust gases are extracted via the flue pipe (8).

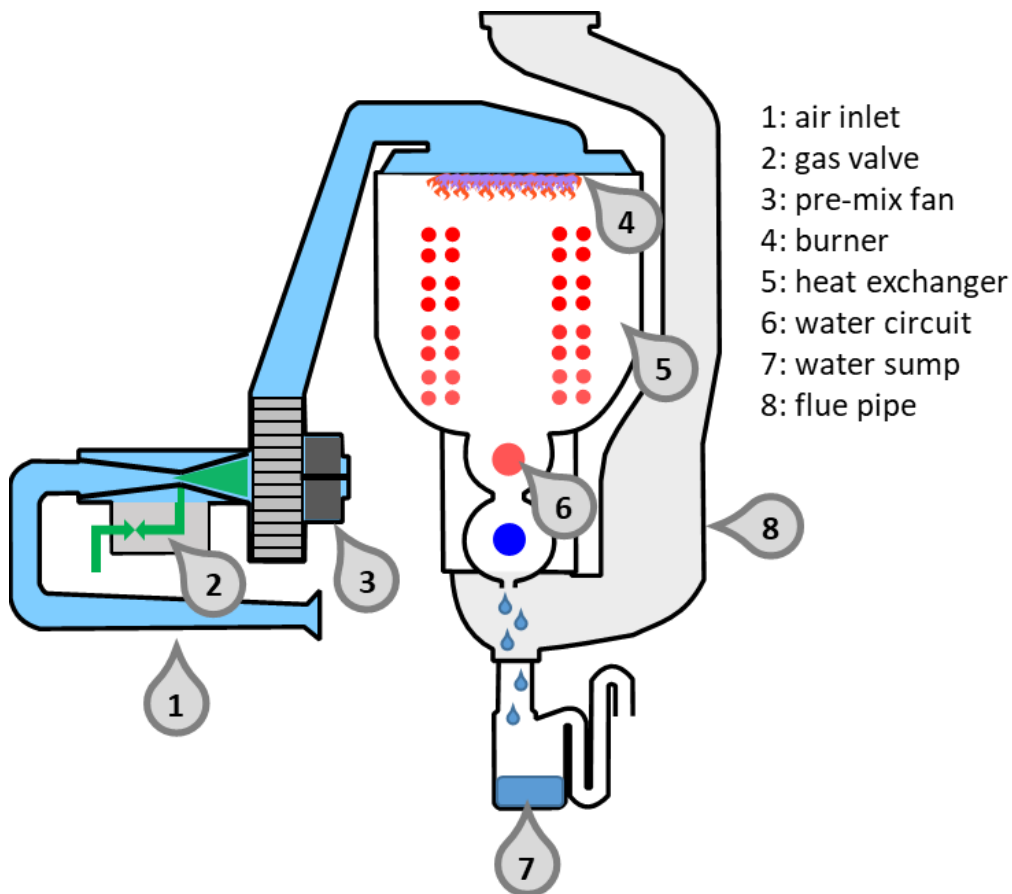


Figure 4 Cross section showing the working principle of a condensing gas-fired heating appliance, as adapted from (Kiefer et al., 2012)

### 2.2.2 Impact of Varying Gas Specifications

Most modern gas boilers use a pneumatic gas valve such as the 848 Sigma (SITGroup, 2018) to deliver gas to the combustion chamber - there are relevant exceptions to this design which will soon be discussed. A pneumatic system enforces that the amount of gas delivered to the gas chamber is a single-valued, close-to-linear, function of the negative pressure; therefore the air-to-gas ratio is roughly constant and any adjustments to the ratio must be done manually by an engineer. Such a setup is fine assuming no significant variation occurs in gas composition during the lifecycle of the boiler and the boiler works in accordance with design. If variations do occur to gas composition the 'preferred' air-to-gas ratio will change but the boiler's air-to-gas ratio setting will not. This could result in combustion becoming inefficient, unsafe and emissions increasing. To circumvent this boiler engineers manually adjust gas valve partitions during service if necessary. These adjustments are made based on CO to CO<sub>2</sub> ratio readings from the exhaust gases.

Note, to avoid confusion moving between different gas types, the equivalence ratio ( $\varphi$ ) is used as an analogous measure of the air-to-gas ratio. It is defined in Equation 2.1 as the actual fuel to oxygen ratio divided by the stoichiometric fuel to oxygen ratio. Accordingly, if  $\varphi > 1$  then the reaction is fuel rich, if  $\varphi < 1$  then the reaction is fuel lean and if  $\varphi = 1$  then the reaction is stoichiometric.

$$\varphi = \frac{m_{fuel}/m_{ox}}{(m_{fuel}/m_{ox})_{st}} \quad (2.1)$$

From an efficiency perspective, it has been shown empirically that near stoichiometric conditions, reactions produce the highest adiabatic flame temperatures (Glassman and Yetter, 2014, Edwards, 1974). As observed in Figure 5, the peak adiabatic flame temperature aligns with an equivalence ratio just above unity. For methane, under standard conditions, the peak aligns with an equivalence ratio in the range of 1.05-1.10 (Glassman and Yetter, 2014, Wang, 2015).

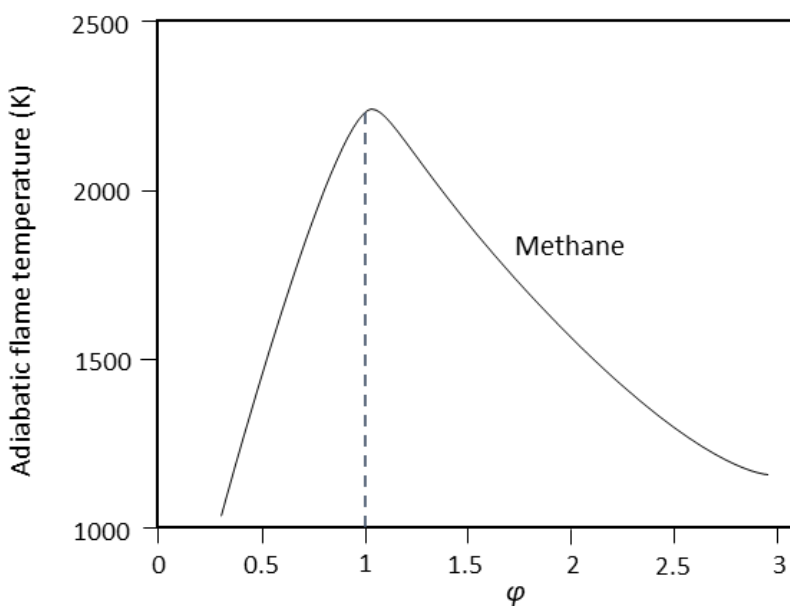


Figure 5 Illustration of the relationship between adiabatic flame temperature ( $T_{ad}$ ) and equivalence ratio ( $\varphi$ ) for methane-air combustion under standard conditions (Wang, 2015)

From an emissions perspective one must consider the production of Carbon Monoxide (CO) and Nitric Oxide/Nitrogen Dioxide ( $\text{NO}_x$ ). According to standard EN 15502-1 (NBS, 2012), from September 2018 a  $\text{NO}_x$  limit of 56 mg/kWh is required on newly manufactured boilers, this corresponds to 31.8 ppm assuming 3% excess  $\text{O}_2$ . Regarding CO emissions, in general if they exceed 200 ppm, an engineer will service the boiler and likely adjust the air to gas ratio.

CO and NO<sub>x</sub> emissions vary with  $\varphi$ . For  $\varphi > 1$  CO emissions increase due to incomplete combustion. For  $\varphi$  approximately less than 0.6 (although this value is burner and fuel dependant) CO emissions also increase; this is because CO oxidation occurs via an OH mechanism, and OH concentrations decrease with temperature, and temperature decreases when  $\varphi$  decreases from unity (Bowman, 1975). NO<sub>x</sub> emissions in gas combustion systems primarily occur via the extended Zeldovich mechanism (Zeldovich et al., 1947), known as thermal-NO<sub>x</sub>. Thermal-NO<sub>x</sub> increases with temperature and can be reduced by setting  $\varphi < 1$ . Additionally, thermal-NO<sub>x</sub> can be reduced via application of specialised burners designed to limit the maximum temperatures seen in the post-flame zone. Thus, CO emissions can increase if  $\varphi$  is too low (due to low temperatures), and NO<sub>x</sub> emissions can increase if  $\varphi$  is too high (due to high temperatures). Consequently, for a unique boiler and gas type, there exists a 'preferred' value of  $\varphi$  whereby NO<sub>x</sub> and CO production are minimised, and efficiencies are maximised. The exact value of the 'preferred'  $\varphi$  depends on the burner design, power output, gas type, and environmental conditions such as humidity. Refer to Glassman and Yetter (2014) and Flagan and Seinfeld (2013) respectively for a thorough overview of the mechanisms of NO<sub>x</sub> and CO production during combustion of natural gas.

An example of how emissions vary with  $\varphi$  can be seen in Figure 6 (based on data gathered during this project). As observed, when designing this boiler one must select a value of  $\varphi$  which is a compromise between efficiencies and emissions. In theory, the closer  $\varphi$  gets to unity the higher the efficiencies of the burn; however, this comes at the compromise of releasing more emissions. If for example CO emissions were limited to 100 ppm and NO<sub>x</sub> emissions to 40 ppm, then a value of  $\varphi$  in the range of 0.8 would be a compromise to maximise efficiencies while ensuring emission standards are maintained. The 'preferred'  $\varphi$  value for a unique boiler and gas type can only be confirmed upon completion of emission and efficiency tests as specified by EN 15502-1 (NBS, 2012).

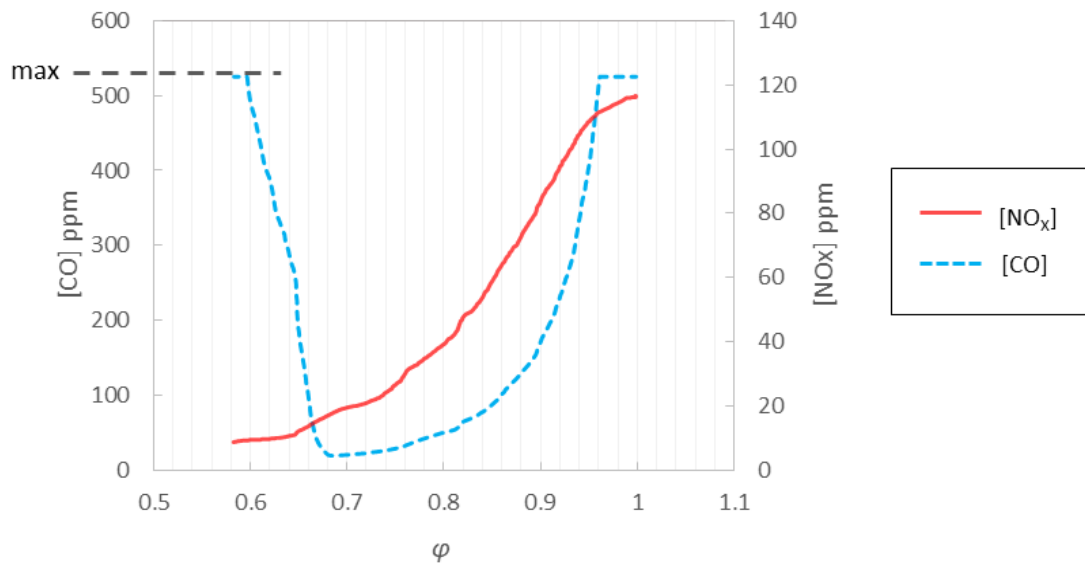


Figure 6 CO and NO<sub>x</sub> emissions for methane-air reaction at atmospheric conditions in a domestic gas-fired boiler. The boiler was a Worcester Bosch Greenstar 28i Junior. Note, the gas sensor for CO had a maximum range of 525 ppm

As gas compositions vary within boilers containing pneumatic gas valves, the operational  $\phi$  value also varies. Plotted in Figure 7 are the impacts on  $\phi$  and CO emissions due to changing gas types for two gas fired condensing combination boilers (this figure was based on data gathered during this project). As observed, when the gas type was changed from G20 to G25 (refer to Table 1),  $\phi$  varied from 0.80 to 0.60. This increased CO emissions from 38 ppm to >525 ppm (525 ppm was the maximum reading of the equipment used). Variations in  $\phi$  and CO emissions going from G20 to G21, G23, or G222 aren't as severe. Regardless, the value of  $\phi$  for any change in gas specification varies from its 'preferred' position and therefore negatively impacts emissions and/or efficiencies. It should also be noted that flames leaner than optimum also risk becoming unstable or blown out (Ballester and García-Armingol, 2010).

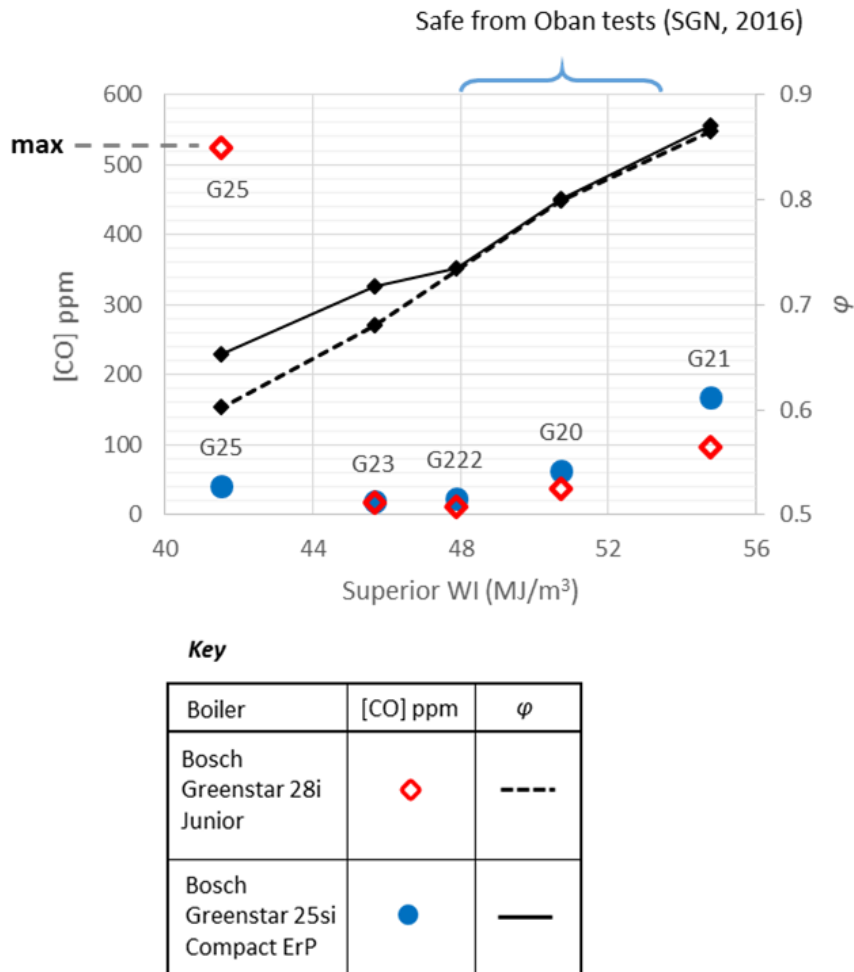


Figure 7 CO emissions and equivalence ratio for different test gases for two domestic gas-fired boilers. Note, the gas sensor for CO had a maximum range of 525 ppm

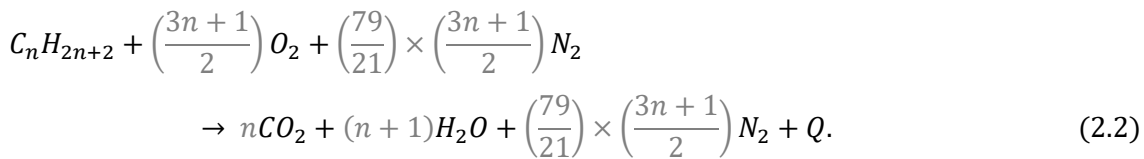
The mechanism required to negate the impact on  $\phi$ , due to changing gas compositions, is referred to as a Combustion Control System (CCS). The principle of a CCS is to automatically adjust the  $\phi$  value depending on the state of combustion with the aim of maintaining the 'preferred'  $\phi$  value independent of variations in gas composition. Critical in the operation of a CCS, is a combustion sensor. A combustion sensor is a device designed to determine the operational  $\phi$  and operational gas composition. In practice, commercially available combustion sensors will only detect the operational  $\phi$  and not the gas composition. This allows the CCS to attain a fixed  $\phi$  and not the 'preferred'  $\phi$  for that gas composition. Adjustments to  $\phi$  are typically achieved by adjusting an electronically controlled gas valve in response to the signal from the combustion sensor. The following section will provide an overview of combustion and combustion sensors.

## 2.3 Combustion Sensors

As mentioned the principle of a CCS in domestic gas-fired boilers is to automatically adjust the  $\varphi$  value depending on the state of combustion as determined by a combustion sensor. The aim of a combustion sensor in this instance is to give a measure of the current  $\varphi$  value and the gas composition (ideally). In this section an overview of combustion in general will be given before reviewing the literature on combustion sensors. This will be in the context of practical combustion systems burning lean premixed natural gas, where the range of gas includes all those within the second group of gas families (Table 1).

### 2.3.1 Combustion Overview

Combustion of natural gas involves the oxidation of alkanes to form oxidation products and the release of heat ( $Q$ ). Assuming air consists of 79% nitrogen and 21% oxygen the stoichiometric oxidation of alkanes is given by:



Thus, for a fuel containing 100% methane, 2 molecules of oxygen or 9.52 molecules of air are required. For a fuel containing 10% nitrogen and 90% methane the stoichiometric air-to-fuel ratio changes to 8.57.

Figure 8 shows how the concentration of reactants and products varies in a one-dimensional representation of the flame front during  $CH_4$ -air combustion. Also, included in the figure is the temperature and heat release rate  $\dot{q}$  – the heat release rate will be discussed in more detail in Section 3.1. The width of the reaction zone for methane combustion is in the region of 0.9mm (Glassman and Yetter, 2014). Note, Figure 8 is applicable for a laminar flame with  $\varphi=1$  at atmospheric temperature and pressure.

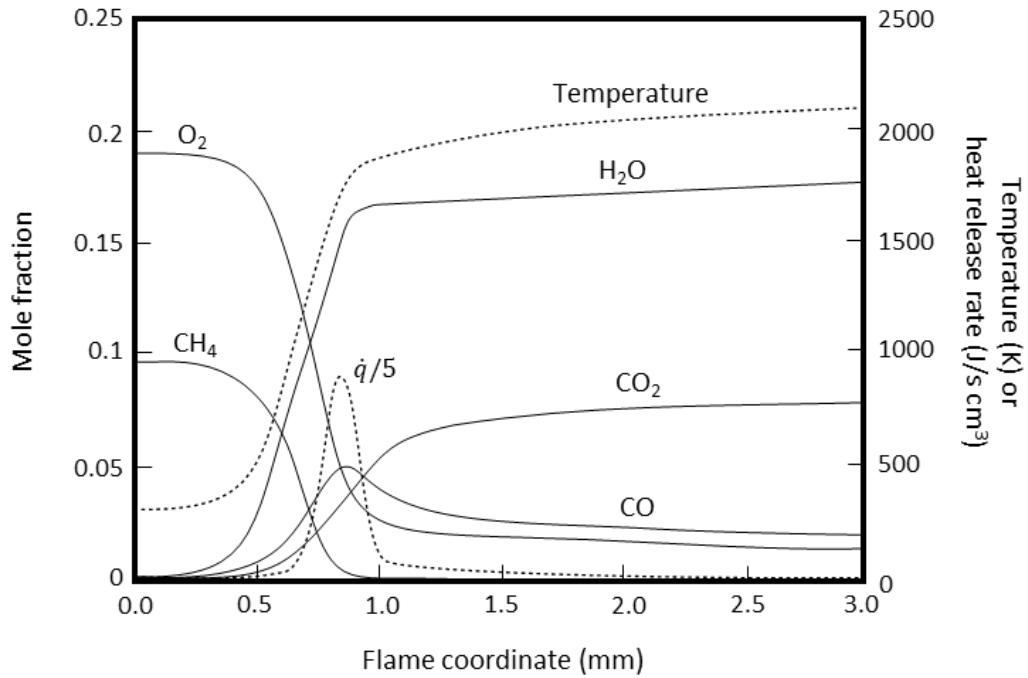


Figure 8 Composition, temperature and heat release rate ( $\dot{q}$ ) profiles for stoichiometric  $\text{CH}_4$ -air reaction at atmospheric temperature and pressure. As adapted from Glassman and Yetter (2014, p. 171). Note, 'Flame coordinate' refers to the distance along the flame from base to tip.

Equation 2.2 stipulates that, for methane, one alkane molecule reacts with two oxygen molecules simultaneously with enough energy to break the binding energy of the reactants; this representation however is purely theoretical. In reality the probability of such an occurrence, in what is a random process, is nearly zero (Wang, 2015). A thorough examination of the oxidation mechanism for methane reveals much more complex processes are at play. Figure 9 gives a summary of the overall reaction mechanisms for methane oxidation in air. The green arrows in the figure highlight the dominant reaction pathways for the high-temperature mechanism of methane oxidation as summarised by Glassman and Yetter (2014, p. 113). As observed, the reaction mechanism for methane oxidation is complex. Indeed ongoing research efforts are currently underway to determine rate constants; thus the mechanisms of methane oxidation are "...not necessarily definitive" (Glassman and Yetter, 2014, p. 117). Note that within the mechanism for methane ethane is produced via recombination of methyl radicals. Warnatz (Warnatz, 1981a, Warnatz, 1981b) have estimated that for lean methane-air mixtures, 30% of methyl radicals recombine to form ethane, for fuel-rich mixtures this can rise to 80%.

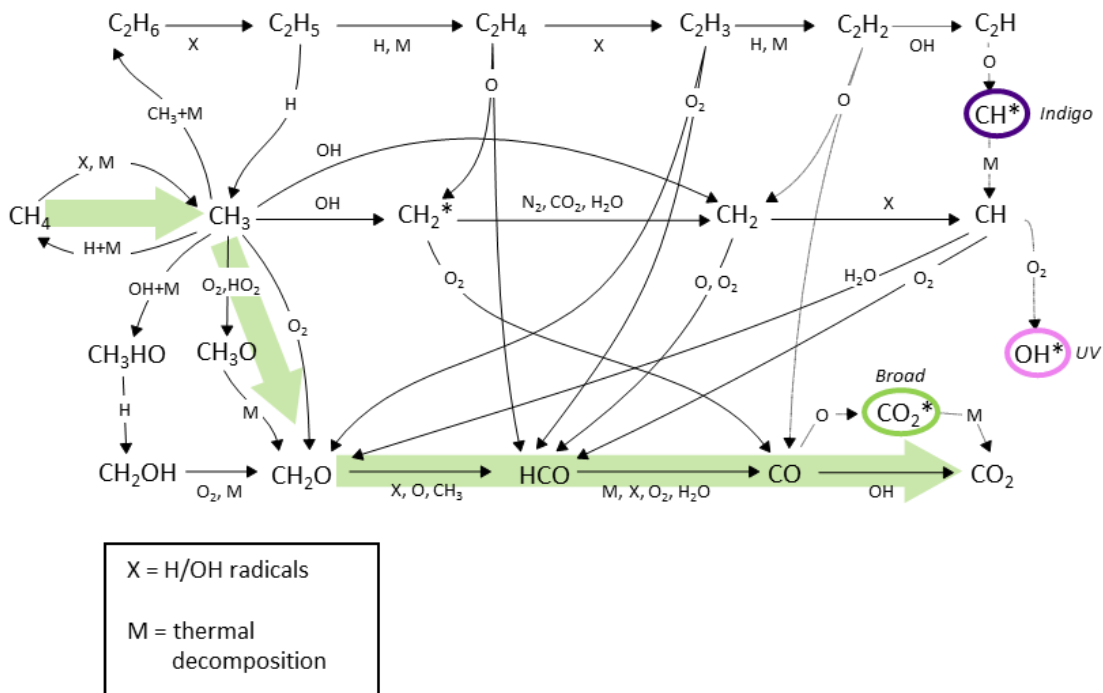


Figure 9 Flow diagram showing the main reaction mechanisms involved in methane oxidation in air. The circled radicals  $\text{CH}^*$ ,  $\text{OH}^*$  and  $\text{CO}_2^*$  are responsible for chemiluminescence phenomena. Note that  $\text{C}_2^*$  has not been included which gives a blue-green colour. This figure was adapted from Najm et al. (1998, p.325). The green arrows underlying the image indicated the dominant reaction path for the high-temperature mechanism of methane oxidation as summarised by Glassman and Yetter (2014, p. 113)

Beside for chemical kinetics, a major factor impacting the properties of combustion is the unsteadiness of the combustion process i.e. turbulence. The standard measure for turbulence is given by the Reynolds number. Typically Reynolds numbers less than 2300 indicate a laminar (steady) flow, for Reynolds numbers over 4000 the flow is considered turbulent. The classic example of a laminar flame is that formed by a Bunsen burner when burning a premixed mixture of air and gas. A laminar flame on the Bunsen burner is characterised by a stable blue cone. The position of the cone is at the point where the laminar flame speed is equal to the premixed gas flow velocity normal to the flame front. The cone is blue / bluish-green due to the chemiluminescence of  $\text{C}_2$  and  $\text{CH}$  radicals; colours in the post flame front zone are due to oxidation of species such as  $\text{CO}$  (refer to Figure 9). If combustion is laminar, the shape of the Bunsen cone will remain steady, if the incoming premixed gas flow is turbulent then the surface of the cone will randomly move around a mean position. Such movement induces vorticity into the flow and can impact chemical kinetics and fluid dynamics downstream. In general, turbulence allows for faster mixing and faster flame propagation (Peters, 2000). Note, a Bunsen flame operating without any premixing behaves as a diffusion flame and is often turbulent in nature

The Reynolds number for the flow in a circular pipe can be approximated by the following equation (Fay, 1994):

$$Re = \frac{\textit{inertial forces}}{\textit{viscous forces}} = \frac{uD_H}{\nu} = \frac{QD_H}{\nu A}$$

Where  $u$  is the mean velocity of the fluid,  $Q$  is the volumetric flow rate of the fluid,  $D_H$  the hydraulic diameter of the pipe,  $\nu$  is the kinematic viscosity of the fluid and  $A$  is the cross sectional area of the pipe. For premixed domestic gas boilers, burners typically contain thousands of 1mm diameter holes (refer to Figure 24). On the surface of each hole a flame is formed similar to that of a Bunsen cone, using the equation above one can estimate the Reynolds number of a typical domestic gas boiler. During the experiments performed in this study, the premix gas-air flow rates were typically around 35 m<sup>3</sup>/hour. Assuming that the flow is evenly split across all holes the Reynolds number at the surface of each burner hole can be approximated at 500-1000 i.e. less than 2300 and therefore laminar. However, as observed in Figure 10 (Boiler 2 used in this study), the premix flow is not evenly split across all holes, potentially leading to a mix of turbulent and laminar flames. Additionally the position of each flame front is extremely close to another flame front, which could induce unsteadiness into the flow. Watching a video clip of the flame in Figure 10 indicates that most flame fronts are steady beside for the ones at the peripheral of the burner. However, when running at undesired equivalence ratios the flame fronts can become very unsteady due to factors such as flame lift - refer to Figure 11.

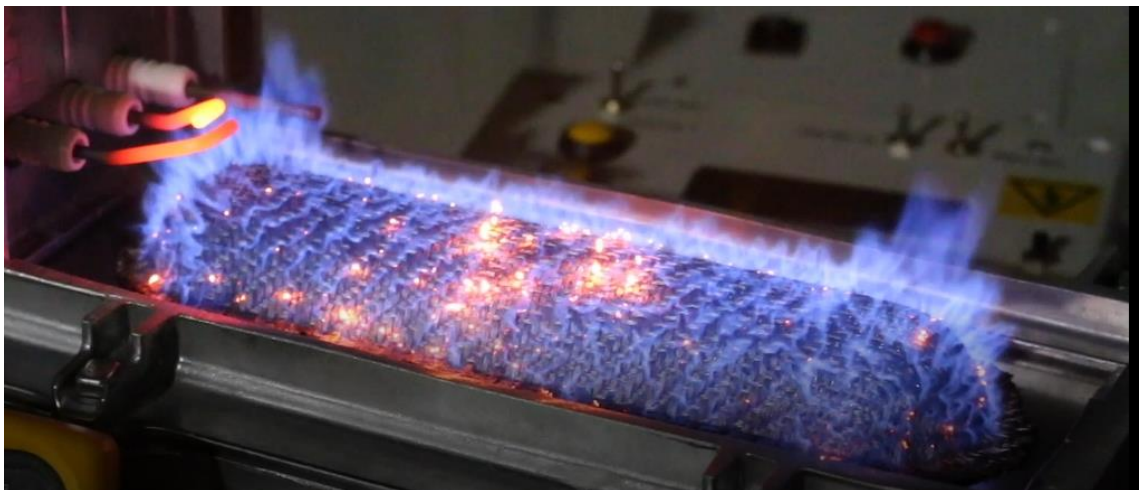


Figure 10 Image of the flame in a Worcester Bosch Greenstar 25Si Compact ErP condensing combi boiler (Worcester Bosch Group, 2015) burning G20 gas at an equivalence ratio of 0.75.

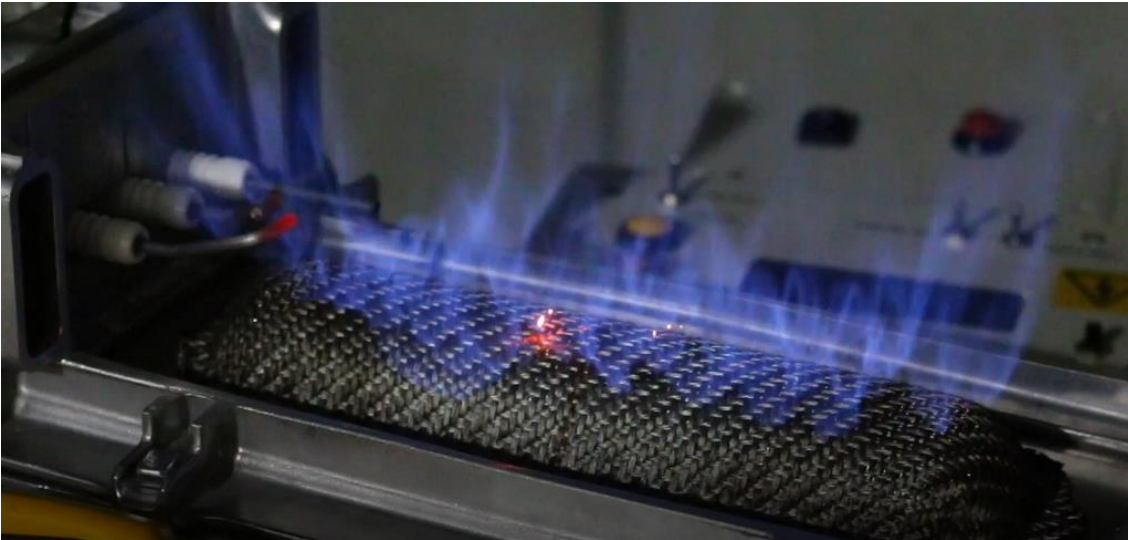


Figure 11 Image of the flame in a Worcester Bosch Greenstar 25Si Compact ErP condensing combi boiler (Worcester Bosch Group, 2015) burning G231 (85% CH<sub>4</sub> and 15% N<sub>2</sub>) gas at an unknown equivalence ratio.

### 2.3.2 Commercially Available Combustion Sensors in Boilers

Commercially available boilers containing CCSs, and thus combustion sensors, have been developed independently by Weishaupt, Viessmann, SIT and Vaillant. Examples include: Viessmann's Vitodens 200-W Wall Mounted Boiler (Viessmann, 2017); Weishaupt's WTC 15A to 60A range (Weishaupt, 2017); Vaillant's ecoTEC plus range (Vaillant, 2017); and SIT's VestaSIT combustion system (SITGroup, 2017). These devices are categorised as I<sub>2N</sub> gas-fired condensing appliances according to standard EN 437:2003 (CEN, 2009); this means that they meet emission and efficiency standards for the range of gas specifications in second family of gases (Group H, L and E) with a WI range of 39.1-54.8 MJ/m<sup>3</sup>. Such devices are gaining popularity in countries like Germany and Poland where gas specifications can vary significantly. Weishaupt, Viessmann and SIT have developed ionisation sensors as combustion sensors: Weishaupt the 'SCOT' (Safety Combustion Technology) sensor, Viessmann the 'Lambda Pro' sensor and SIT the 'VestSIT' sensor. Vaillant have developed a CO gas sensor as a combustion sensor (Näslund, 2014) – the commercial name is unknown. As noted previously, these combustion sensors aim to detect the operational  $\varphi$  only and not the gas composition, thus these devices work to maintain a set  $\varphi$  and are not used to dynamically infer the 'preferred'  $\varphi$  which is also dependent on gas composition.

Nitschke-Kowsky and Radtke (2011) have tested the performance of four commercially available I<sub>2N</sub> appliances with CCSs using a mix of ionisation and CO gas sensors as combustion sensors. The results are very positive showing that the CCS are "...extremely effective and reliable for all

gases”: the  $\varphi$  value was found to remain within an apparently acceptable range of 0.74-0.83 irrespective of gas type for all boilers tested; in addition, field trials showed the CCS operating as expected “some time” after an initial calibration, indicating positive long-term behaviour. This report however is not peer reviewed and it was noted that although gases containing hydrogen are listed as required test gases for  $I_{2N}$  devices, results for gases containing hydrogen (such as G222 in Table 1) were not reported (Nitschke-Kowsky and Radtke, 2011). Data collected by E.ON Ruhrgas (Nitschke-Kowsky and Wessing, 2012) using the ‘SCOT’ ionisation sensor have shown that CCSs do not correctly adjust  $\varphi$  during changes in hydrogen-hydrocarbon blends. It is suggested this is a fundamental weakness of ionisation sensors because of the unique nature of ion production and flame height variation in hydrogen-hydrocarbon gases (Näslund, 2014, p.15). No tests were available to verify if the same weaknesses is present when using CO sensors, however it is stated that “The technology [CO gas sensor] seems to be fuel independent” (Näslund, 2014, p.15). However, in theory a CO gas sensor would start to fail once the high proportions of hydrogen containing gases are considered. This is because of hydrogen-air reactions do not produce any CO. Viessmann claim their ‘Lambda Pro’ sensor can handle gases with WI values ranging from 36.0 - 58.0 MJ/m<sup>3</sup> (Viessmann, 2013), which is beyond the range of the second gas families - no data can be found in the literature that validates this claim.

Important aspects of combustion sensors to consider for practical application include accuracy, reliability, integration and cost. The accuracy and reliability of commercially available combustion sensors in domestic boilers have been reviewed briefly above, although the amount of publicly available data is very limited. From an integration perspective, ionisation sensors can be easily integrated in a gas boiler in place of a standard flame sensor; a CO gas sensor is a little more of a challenge for integration but has been done so by Valliant by modifying the exhaust duct. From a cost perspective, ionisation sensors are considered to be a very low cost solution as the hardware is already present in most systems, the cost of a replacement Weishaupt ionisation probe is in the range of 25 USD (IBHS Ltd., 2017); the cost of CO gas sensors appear significantly more expensive with today’s technology, a replacement sensor for the Valliant system discussed is in the range of 90-95 USD (HRB, 2017, MHS, 2017, Ersatzteilmfachmann, 2017).

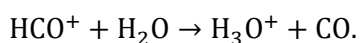
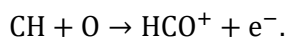
Additional details regarding said commercially available combustion sensors in addition to all other potential combustion sensors has been given below.

### 2.3.3 Potential Combustion Sensors for Practical Application

Potential combustion sensors for practical systems include ionisation sensors, flue gas sensors, flame emission spectroscopy, laser absorption spectroscopy, flame imaging and pressure fluctuations. See Ballester and García-Armingol (2010) and Docquier and Candel (2002) for detailed reviews.

#### 2.3.3.1 Ionisation Sensors

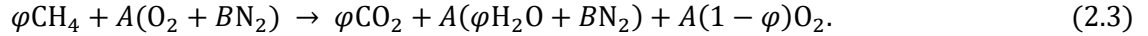
Ions are yielded during most chemical reactions (chemi-ionization). For flames, the rate of chemi-ionization is closely related, among other factors, with the instantaneous properties of combustion: chemi-ionization concentrations are typically found to vary as a function of  $\varphi$ , peaking near stoichiometry and reducing either side (Clements and Smy, 1976). Thus, in theory, by placing an ionisation probe in contact with a flame the rate of chemi-ionization can be determined from the probes' current and an indirect measure of the  $\varphi$  value made. However, chemi-ionization occurs in a very narrow region in the chemiluminescence zone of the flame (approximately 0.1mm in width for  $\varphi=1$ ) and concentrations decay rapidly in the post-flame zone (Fialkov, 1997, Calcote and King, 1955); in addition the ion current from chemi-ionization species in hydrocarbon fuel-lean flames are very low. This is due to the high activation energy required to produce the principle source of ions ( $H_3O^+$ ) shown in the reaction equations below (Ballester and García-Armingol, 2010, Calcote, 1962, Fialkov, 1997):



Consequently, in practical applications of ionisation probes in domestic gas-fired boilers, it has been found that currents from ionisation probes were dominated by thermionic emission of electrons from the rod rather than chemi-ionization (Huppelshausen et al., 2001, Ballester and García-Armingol, 2010). Because thermionic emission rates are correlated with temperature, and temperature is related to the instantaneous  $\varphi$  value, ionisation probes detecting thermionic emissions in flames can be, and are, used to indirectly measure of the operational  $\varphi$  value. Thermionic principles underpin the operation of the 'SCOT' combustion sensor (Ballester and García-Armingol, 2010). In general, the absolute signal from ionisation sensors "...is influenced by the design of the burner, the combustion chamber geometry and the ionisation probe as well as the burner load and the aging of the probe. For this reason, the ionisation signal must be calibrated in the field." (Nitschke-Kowsky and Radtke, 2011, p.4).

### 2.3.3.2 Flue Gas Analysis

Measuring the concentration of various species in the exhaust gases of combustion gives a direct measure of the operational  $\varphi$  value (Spindt, 1965), such methods are very common in industry test facilities and research labs alike. Assuming complete oxidation for fuel-lean mixtures ( $\varphi < 1$ ), and that air contains oxygen and nitrogen only, the global reaction of methane in air can be expressed as:



where  $A = 2.0$  and  $B \approx 3.76$  (depending on the assumed ratio of  $\text{N}_2$  to  $\text{O}_2$  in the atmosphere). Thus by measuring the mole fraction of  $\text{O}_2$  ( $X_{\text{O}_2}$ ) in dry exhaust gases, the equivalence ratio can be estimated from the following relation (Docquier and Candel, 2002):

$$\varphi = A \frac{1 - (1 + B)X_{\text{O}_2}}{A + X_{\text{O}_2}}. \quad (2.4)$$

Equivalently by measuring the mole fraction of  $\text{CO}_2$  ( $X_{\text{CO}_2}$ ) in dry exhaust gases:

$$\varphi = \frac{X_{\text{CO}_2}}{\alpha + \beta X_{\text{CO}_2}}, \quad \text{where } \alpha = \frac{1}{A(B + 1)} \text{ and } \beta = \frac{A - 1}{A(B + 1)}. \quad (2.5)$$

Similarly, for other fuels  $\alpha$  and  $\beta$  can be derived by constructing equivalent excess air combustion equations: for G222  $\alpha=0.0975$  and  $(\beta \cdot 100) = 0.112$ , for G30  $\alpha=0.129$  and  $(\beta \cdot 100) = 0.081$  etc. Equation 2.3, and thus 2.4 and 2.5, are applicable for the complete combustion of methane when  $\varphi < 1$  and atmospheric air comprises of oxygen and nitrogen only. Chan (1996) showed that  $\varphi$  can be calculated accurately, for oxidation of any hydrocarbon in general atmospheric conditions, by measuring four exhaust gas emission concentrations:  $\text{CO}$ ,  $\text{CO}_2$ ,  $\text{O}_2$  and  $\text{HC}$ .

The most common lab-based technique for determining the concentration of various gas species relies on Infrared Chromatography (IC). Such systems however occupy a significant amount of physical space and not practical for integration into domestic gas boilers. Solid-state gas sensors are however small and can potentially be made cheap enough for practical consideration. Solid-state gas sensors can be split into three broad categories: electrolyte, catalytic and semiconducting. Zirconia sensors are a common type of electrolyte sensor used for the measurement of oxygen concentration and have been used within the automotive industry in order to control the air-to-gas ratios of combustion (Moseley, 1997). Metal-oxide semiconductors represent the most recent developments in this field - refer to Korotcenkov

(2007) for an review. Other sensing techniques include the use of novel materials such as graphene for CO<sub>2</sub> detection (Yoon et al., 2011).

### 2.3.3.3 Flame Emission Spectroscopy

Analysis of electromagnetic radiation emitted by flames is a valuable tool for combustion research (Kohse-Höinghaus and Jeffries, 2002). An overview of flame emission spectroscopy and methods suitable for practical application for lean methane-air combustion is given below.

Flames emit electromagnetic radiation due to three main phenomena:

1. Solid bodies emit black-body radiation when heated. The spectrum of this radiation is directly related to the temperature of the solid-body. Solid bodies in combustion include soot, ash and char particles.
2. Gas molecules at high temperatures emit rotation-emission bands.
3. Excited species produced during chemical reactions emit radiation when reverting to their ground state, this process is known as chemiluminescence. Excited species of note during methane oxidation are CH\*, C<sub>2</sub>\*, CO<sub>2</sub>\* and OH\*.

Detection of black-body radiation, typically in the IR part of the spectrum, has led to the development of radiation thermometers - see DeWitt and Nutter (1988) for an overview. Techniques reliant on black-body emissions are applicable to particle-laden flows, thus the literature regarding analysis of black-body radiation is dominated by diffusion flames (Siddall and McGrath, 1963, Köylü and Faeth, 1996, Correia et al., 2000), coal combustion (Obertacke et al., 1996, Leipertz et al., 1996) or in the case of premixed hydrocarbon combustion when  $\varphi > 2$  (Choi et al., 1994, Xuan and Blanquart, 2016). For fuel-lean combustion of premixed gas, combustion flows are effectively particle free and thus black-body radiation emissions are essentially negligible.

Detection of rotation-emission bands from major combustion products (H<sub>2</sub>O, CO<sub>2</sub> or CO) can be used to determine the temperature and relative concentrations of combustion products. These bands can be identified using a Fourier transform IR (FTIR) spectrometer. Brenez et al. (2000) and Solomon et al. (1988) have applied these techniques to premixed natural gas boilers to measure temperature and species concentration. However it is considered that FTIR spectrometers are too bulky, expensive and time-response too slow for practical application as combustion sensors (Docquier and Candel, 2002).

Chemiluminescence phenomena have been related heat release rates (Price et al., 1969, Docquier et al., 2000, Balachandran et al., 2005, Ayoola et al., 2006), local flame structure (Kim et al., 2002, Ducruix et al., 2003, Hardalupas et al., 2004) and the operational  $\varphi$  (Cheng et al., 2006, Von Drasek et al., 1999, Docquier et al., 2000). The main chemiluminescence emitters for lean combustion of gas are  $\text{CH}^*$ ,  $\text{C}_2^*$ ,  $\text{CO}_2^*$  and  $\text{OH}^*$ . Figure 9 shows the mechanisms for the creation of three of these excited species - other mechanisms are known to exist for creation of these excited species however research is ongoing to determine the details. Note  $\text{C}_2^*$  species are formed when  $\text{CH}_2$  reacts with carbon or when  $\text{C}_3$  reacts with a single oxygen atom (Kathrotia, 2011).  $\text{CO}_2^*$  gives off a continuous spectrum (350-600nm),  $\text{CH}^*$  indigo (387.1 and 431.4 nm),  $\text{OH}^*$  ultraviolet (282.9 and 308.9 nm) and  $\text{C}_2^*$  a blue-green colour (513 and 516.5 nm) (Ballester and García-Armingol, 2010).

For a methane-air flame the relative intensities of certain chemiluminescence bands vary with temperature, turbulence, fuel composition, pressure and  $\varphi$  (Ballester and García-Armingol, 2010). For lean methane-air flame  $\text{OH}^*$  and  $\text{CH}^*$  intensities have been reported to peak near stoichiometric conditions (Docquier et al., 2000, Hardalupas et al., 2004) and vary with  $\varphi^{5.23}$  (Higgins et al., 2001b) and  $\varphi^{2.72}$  (Higgins et al., 2001a) respectively. Most studies have been performed on laminar flames, thus an important objective in the field was the development of diagnostic methods applicable to turbulent flames. Nori and Seitzman (2009) found that for  $\text{CH}^*$  emission the effect of turbulence diminishes with spatial and temporal averaging of the signal. In addition monitoring of  $\text{OH}^*/\text{CH}^*$  ratios has been shown to have a number of advantages, including being relatively immune to changes in strain rate and turbulence intensities (Ballester and García-Armingol, 2010). Good results (95% confidence) relating  $\text{OH}^*/\text{CH}^*$  ratios to operational  $\varphi$  have been obtained by Muruganandam et al. (2005) for Reynolds numbers (measure of turbulence) from 11,700 to 23,300 for lean methane-air flames. However the shape of chemiluminescence vs  $\varphi$  signals vary significantly with fuel composition, for example the inclusion of  $\text{H}_2$  into the fuel mix has a similar effect to a decreasing  $\varphi$  value for  $\text{OH}^*$  and  $\text{CH}^*$  intensities (Ballester et al., 2009). Chemiluminescence monitoring of  $\text{OH}^*/\text{CH}^*$  ratios have been incorporated into a control system designed to regulate the  $\varphi$  value of combustion, however this has only been done for methane-air combustion systems (Docquier et al., 2002, Scott et al., 2002).

Thus, managing fuel variations remains an outstanding challenge in the application of chemiluminescence as a combustion sensor in practical turbulent systems. One potential solution has been the application of supervised machine learning (ML) techniques. Supervised

ML techniques were selected for such application as they are well suited to estimating unknown variables of interest, within sets of complex features, when functional dependences are unknown - see Section 3.2 for an overview. Methods using chemiluminescence signals in combination with broadband emissions, and applying ML techniques to classify the flame, have been applied by Ballester et al. (2009). Ballester et al. (2009) found that such an approach “might be adequate for a wide range of pressures and fuel types”; however only methane-hydrogen mixes were tested. Thus, analysing chemiluminescence and broadband signals using ML techniques may result in methods for monitoring the operational  $\varphi$  value for practical systems with varying gas compositions.

#### *2.3.3.4 Laser Absorption Spectroscopy*

Laser absorption spectroscopy is based on the principle that the attenuation of a light beam across a gas is characteristic of the different chemical species within the gas. This principle is summarised by the Beer-Lambert’s law - refer to Kohse-Höinghaus et al. (2005) for a detailed review on the topic of laser absorption spectroscopy in combustion systems. The methods can be adapted for the measurement of temperature, species concentration (e.g., CO and O<sub>2</sub>), velocity and pressure. Note, that by being able to detect species concentrations one can also determine the operational  $\varphi$  value (see Section 2.3.2.2). So, called Tuneable Diode Laser Absorption Spectroscopy (TDLAS) constitutes the best option for practical measurements in high temperature flows due to the robustness, high spatial and temporal resolution, and low maintenance of diodes. In one study TDLAS combustion temperature measurements could be made with a temporal resolution of 100ms (Furlong et al., 1998); such a fast response time is advantageous over conventional methods of temperature and gas sensing (e.g., thermocouples and extractive sampling) (Ballester and García-Armingol, 2010).

TDLAS sensors as a diagnostic tool have been used in waste incinerators by Ebert et al. (Ebert et al., 2005, Ebert et al., 1998) to detect fluctuations in stoichiometry (by tracking O<sub>2</sub> and CO concentrations) and harmful emissions. For this application, the fast response of TDLAS is an important advantage due to regular variations in the properties and feeding rate of waste (fuel). TDLAS sensors have also been applied in coal-fired plants by Teichert et al. (2003), an environment which contains high concentrations of solid-bodies, making line-of-sight sensing (such as TDLAS) challenging; however the results show that accuracies in CO concentration estimates of  $\pm 200$  ppm can still be achieved. Feasibility for TDLAS as a diagnostic tool for gas turbines and pulse detonation engines has been demonstrated by Hanson et al. (2005) and by

Sanders et al. (2002) respectively. The authors have found no examples where TDLAS sensors have been applied to lean premixed continuous gas combustion systems.

### *2.3.3.5 Flame Imaging*

Passive imaging techniques have long served as useful visualisation tools for researchers to describe or understand important features of the flame. To detect flame images, charge-coupled devices (CCD) are typically selected, this is because of their relative low-cost. Integrating a CCD sensor into combustion systems typically requires modifications to the chamber to avoid fouling and damage to the sensor.

Analysis of blackbody radiation from CCD sensors has been used to determine the temperature of the flame for coal and sooty gas flames (Huang et al., 2000). Again, analysis of blackbody radiation is applicable to particle-laden combustion systems only and thus not of interest for lean gas combustion systems. Radiation from chemiluminescence phenomena, as discussed in section 1.4.1.3, is however of interest for lean gas combustion systems. Chemiluminescence emissions can be related to flame parameters (e.g., heat release rates,  $\varphi$ ) and can be detected using a CCD. By combining a CCD with a bandpass filter, emission bands of interest can be extracted. Tao and Burkhardt (1995) used a CCD in combination with filters and artificial neural networks (a ML algorithm) to analyse emissions from CH\* (filtered at 430nm).

Processing of flame images to derive interesting quantitative information about the flame has been performed in several ways. Some studies have derived relationships based on a physical interpretation of flame dynamics. Other studies have used data analysis techniques to categorise the flame images, some via unsupervised ML and others via supervised ML. A flame-imaging combustion sensor was integrated into a spray frame rig by Allen et al. (1993). Allen et al. (1993) used an artificial neural network, with spatial features of the flame, to determine the atomising air flow rate of the flame so that adjustments could be made to the combustion regime. Such a method was similarly used by Hernandez and Ballester (2008). Hernandez and Ballester (2008) used a number of ML approaches to predict combustion states from flame images for an experimental natural gas burner rig.

### *2.3.3.6 Pressure Fluctuations*

Combustion acoustics are intimately related to flame properties. Efforts have thus been made to correlate acoustics to flame properties. Petela and Petela (1983) and Ramachandra and Strahle (1983) were the first to, seemingly independently, suggest using the acoustic signature

from flames as a combustion diagnostic tool. Since then however the primary motivation for research in this area has been to prevent combustion instabilities. For example Hermann and Hoffmann (2004) used a piezoelectric transducer to detect and prevent the onset of instabilities in a commercial gas turbine.

For practical systems where flames are enclosed, the relationship between acoustics and flame properties becomes extremely complex, thus lends itself to the application of ML methods. Seemingly the only attempt at using combustion acoustics as a diagnostic tool for confined flames has been performed by Sanz et al. (2008), and required the application of ML. Sanz et al. (2008) used frequency band data from pressure fluctuations in combination with neural networks to predict  $\text{NO}_x$  emissions for a gas diffusion industrial burner. The burner rig investigated by Sanz et al. (2008) was a water-cooled experimental furnace. The  $\varphi$  of combustion in addition to the fuel type (methane) was held constant for all tests performed. Variations in the combustion properties were made by adjusting the air distribution between primary and secondary registers, and by adjusting the swirl numbers. It was found that  $\text{NO}_x$  emissions could be estimated to a good accuracy, with an absolute error of 0.96% using acoustic features.

There are no examples in the literature whereby combustion acoustics has been used as an indirect measure of  $\varphi$  for combustion within a closed environment. In general research in this area has been limited, as indicated by a recent review: "...these studies clearly demonstrate that the information contained in acoustic flame signals is intimately related with the very nature of the combustion process and, therefore, may offer interesting possibilities for flame monitoring" (Ballester and García-Armingol, 2010, p.397). More specifically, within the literature there are no examples whereby combustion acoustics has been used as a feature to determine any combustion related properties independent of fuel type. If combustion acoustics can be used to track  $\varphi$  in a practical system independent of gas composition, then such a system could be used as a viable combustion sensor for application in domestic appliances. Additionally, if combustion acoustics can give insight into the gas composition of the gas, then combustion acoustics could be used to achieve the 'preferred'  $\varphi$ , a feat which has not been attained by any existing combustion sensor. It is consequently the focus of the study to determine the feasibility of such a sensor. Accordingly, the following section will give an overview of the aims and the objectives of the study, following this a literature review regarding combustion acoustics and machine learning will be provided.

## *2.4 Aims and Objectives*

The aim of this study is to determine if combustion acoustics can be used as an indirect measure of the operational  $\varphi$  of combustion for domestic gas-fired boilers. The primary aim of this study is to develop techniques of estimating the operational  $\varphi$  of combustion, for domestic gas-fired boilers, from combustion acoustics. This method should be independent of fuel composition and apply to a range of boilers. The technique will also likely require the application of supervised machine learning methods. The technique should be scalable to practical application as a combustion system and thus cost, accuracy, robustness and integration should be considered. The secondary aim of this study is to use combustion acoustics to predict the composition of the gas being burnt. Such an estimate of gas composition should be made independently of  $\varphi$ .

In order to achieve these aims the following objectives will be met: selection and testing of acoustic sensors; gathering acoustic data from a single boiler and gas type combination for a range of equivalence ratios; development and evaluation of different machine learning methods for analysis of acoustic data. After completing these objectives, the next steps of the study will be determined. As this is a relatively new area of research, the investigation lends itself to a Pilot Study followed by a Primary Study format.

For the next chapter a literature review will be completed regarding combustion acoustics within confined environments and the application of machine learning techniques in the domain of combustion and acoustics.

### 3. Literature Review

In accordance with the objectives in Section 2.4 it is imperative to review literature on combustion acoustics and machine learning. Specifically, combustion acoustics for confined turbulent premixed gas-air flames; and applications of machine learning as applied to combustion and acoustic related phenomena. Reviewing these aspects will inform the methods applied and the interpretation of the results obtained in this study.

#### 3.1 Combustion Acoustics

Combustion is inherently unsteady and thus a source of noise. Experimentally it has been shown that "...in the absence of feedback instabilities, a combusting system will typically radiate about  $10^{-6}$  -  $10^{-5}$  of the thermal power as sound; for unstable burning in a combustion chamber, the efficiency can be as high as  $10^{-4}$ ." (Howe, 1998, p.502). Formative works on the matter were aimed towards combustion noises in an open environment i.e. a consideration of 'direct' combustion noises only. However, in practical combustion systems confinement is required – to convert chemical energy into useful heat or work. Confinement complicates matters of combustion noise significantly by introducing 'indirect' noise sources, system resonances and combustion feedback effects. Research into combustion noise emanating from practical systems is ongoing. See the review by Dowling and Mahmoudi (2015) and the lecture series by Candel (2016) for recent overviews of the field.

In this section a short overview of combustion noise will be given, this will be followed by specific literature regarding direct combustion noise, indirect combustion noise and combustion noise within a confined environment. Following this review, literature reporting on the relationship between combustion noise and the operational equivalence ratio ( $\phi$ ) will be given. As the focus of this study is regarding turbulent lean premixed gas-air combustion, the review of combustion acoustics will be specific to these types of flame. Note, virtually all practical combustion systems involve a turbulent process (Griffiths and Barnard, 1995), indeed turbulence is necessary in order to maximise efficiencies (Glassman and Yetter, 2014).

##### 3.1.1 Overview

For a complete overview of combustion noise, one should examine the full set of equations governing sound radiation from a region of chemically reacting species; the complete derivation of which has been covered by Howe (1998), Dowling and Mahmoudi (2015) and Candel et al.

(2009, 2016). In summary, one should start by considering the conservation equations for mass, momentum, energy and species. From this a general acoustic wave equation, can be derived. For the case of combustion of a premixed gas one can generally assume the following: generated pressure waves are in the low Mach limit ( $M \ll 1$  pressure perturbations are small compared with the surrounding mean pressure, that the system is nearly isobaric (mean pressure is constant) and that the gas behaves as an ideal gas (Candel et al., 2009). Note, 100 dB represents a pressure perturbation of less than 0.02% relative to atmospheric pressure, thus the assumption of pressure perturbations being small compared with the surrounding pressure is generally valid.

In addition to the above, it is generally accepted that all the terms associated with transfer of momentum, species and heat at the molecular level do not constitute important source terms in combustion noise and can be neglected (Candel et al., 2009). These assumptions lead to the expression of the wave equation for combustion noise phenomena for a turbulent premixed gas flame:

$$\left( \frac{1}{c_0^2} \frac{\partial^2}{\partial t^2} - \nabla^2 \right) p' = S_1 + S_2 + S_3 + S_4 + S_5. \quad (3.1)$$

Where:

$$S_1 = \frac{\gamma - 1}{c_0^2} \frac{\partial \dot{q}}{\partial t}; \quad S_2 = \rho_0 \frac{\partial}{\partial t} \left[ W \frac{\partial}{\partial t} \left( \frac{1}{W} \right) \right];$$

$$S_3 = \rho_0 \nabla \mathbf{v} : \nabla \mathbf{v}; \quad S_4 = \rho_0 \nabla \cdot \left[ \left( \frac{1}{\rho} - \frac{1}{\rho_0} \right) \nabla p' \right];$$

$$S_5 = -\rho_0 \frac{\partial}{\partial t} \left[ \left( \frac{1}{\rho c^2} - \frac{1}{\rho_0 c_0^2} \right) \frac{\partial p'}{\partial t} \right].$$

The left-hand side of Equation 3.1 has the form of a wave operator acting on the fluctuating pressure, the right-hand side can be seen as containing the acoustic source terms of different nature from  $S_1$  to  $S_5$ . Although some source terms also contain variables characterising the wave field, this separation has been accepted and is reasonable when the sound field only weakly interacts with the sources (Candel et al., 2009, Doak, 1973). Note that the suffix  $0$  denotes the mean value in the distant acoustic field.  $c$ ,  $W$ ,  $\gamma$ ,  $\rho$ ,  $\mathbf{v}$ ,  $p'$  and  $\dot{q}$  respectively represent the speed of sound within the flame, the molar mass, the heat capacity ratio, local density, velocity vector, fluctuating pressure and the rate of heat release per unit volume in the combustion region. We will now discuss each of the source terms in Equation 3.1.

Terms  $S_1$  and  $S_2$  represent so called 'direct' noise sources, these are sources that emanate from the reaction zone of the flame. These sources are monopole in character.  $S_1$  is dominated by changes in the heat release rate within the reaction zone.  $S_2$  is noise due to rapid changes in molar content. It has been found that the  $S_2$  term can be neglected for air-burning systems (Candel et al., 2009) and thus can be disregarded. Note, term  $S_2$  isn't considered in the derivation of Equation 3.1 by Howe (1998, p.500).

Terms  $S_3$  and  $S_4$  represent the so called 'indirect' noise sources. Indirect combustion noise sources occur downfield from the flame front at the point of constriction (if existent). Source  $S_3$  is the classic Lighthill quadrupole aerodynamic sound associated with velocity fluctuations (Howe, 1998, Ch.2). Source  $S_4$  is what is known as the entropy wave source and is caused by the change of momentum due to density inhomogeneities (Marble and Candel, 1977). Source  $S_5$  is another indirect noise source term, the strength of which "...is determined by differences between the adiabatic compressibility inside the source region and the ambient medium" (Candel et al., 2009, p. 13). However contributions from  $S_5$  are very small, especially in the low Mach regime of interest – see Sinai (1980); it will thus be disregarded.

Accordingly, the dominate source terms for turbulent premixed gas-air combustion are: one direct source term due to changes in heat release rates emanating from the reaction zone ( $S_1$ ); and two indirect source terms ( $S_3$  and  $S_4$ ), one due to vorticity waves, the other due to entropy waves. Not included in this analysis is the modifications and interactions the surrounding environment can cause.

Within a confined environment one must also consider how the system responds to acoustic stimuli i.e. the resonant modes of the system. For the resonant modes of rectangular and cylindrical cavities this can be performed analytically by modelling the systems as a Helmholtz resonator. For an arbitrarily shaped cavity the acoustic modes can be resolved by either performing finite element simulations or performing experiments. In addition to resonant modes, reflections within a combustion chamber, or indirect noises travelling upstream, can give rise to interactions between combustion acoustics and the flame front. This will result in modifications to the overall dynamics of the flame and can lead to combustion driven oscillations (Klein, 2000). Thus far such an interaction has not been considered: as mentioned previously, the concept that the right-hand side of Equation 3.1 represents the source terms of combustion noise is only valid when the acoustic field interacts weakly with the source terms.

In summary the acoustics of a confined combustion chamber has been illustrated in Figure 12 - adapted from Dowling and Mahmoudi (2015). Included in this figure are acoustics produced from direct ( $S_1$ ) and indirect combustion sources ( $S_3$  and  $S_4$ ), in addition to modifications by the system resonant modes and upstream components within the chamber which can then potentially modify the flame. Not included in this analysis is additional acoustics caused by combustion instabilities, these include effects such as vortex shedding (Syred, 2006).

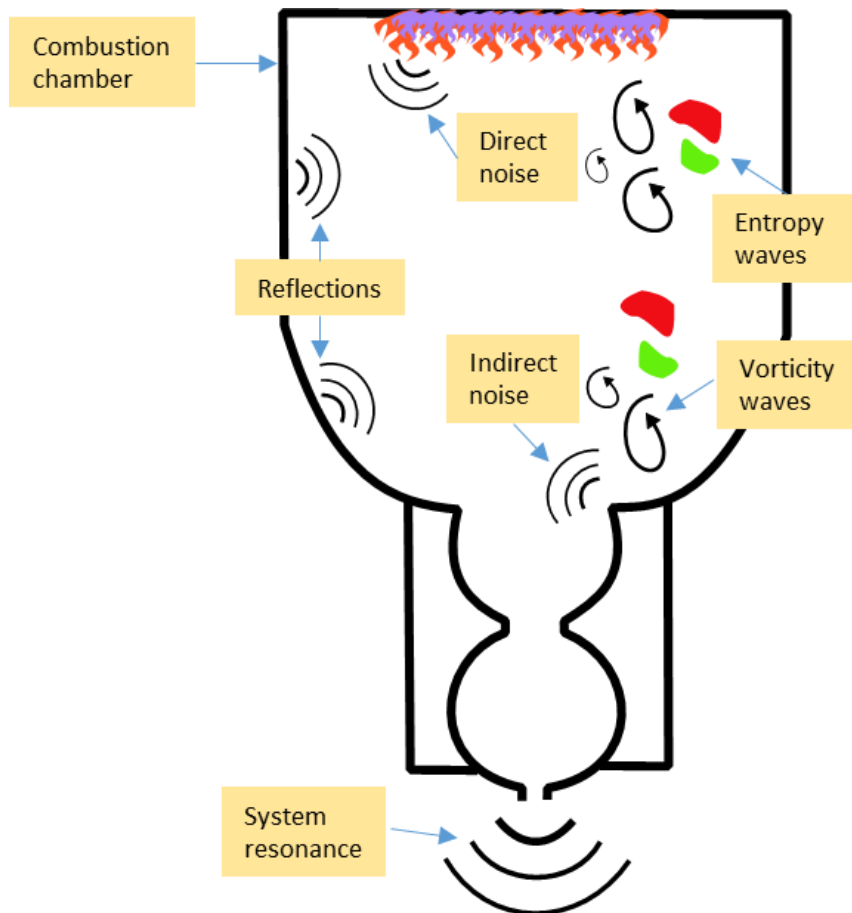


Figure 12 Illustration of combustion noise sources from a closed system as adapted from Dowling and Mahmoudi (2015)

### 3.1.2 Direct Combustion Noise

The seminal experimental work investigating direct combustion noise source was in accordance with work formed by Thomas and Williams (1966). In view of the complexity of a fully developed turbulent flame model, Thomas and Williams (1966) aimed to simulate combustion noise in its simplest form. As established by Smith and Kilham (1963) and Bragg (1963), direct combustion noise was thought to be equivalent to a statistical distribution of simple monopole sources throughout the combustion zone. Consequently, to mimic a monopole source of combustion

noise, Thomas and Williams (1966) analysed the pressure waves produced from the ignition of a premixed gas confined within soap bubbles. Since the size of the soap bubbles was small compared to the wavelength of the pressure waves being investigated, the soap bubbles were considered as monopole sources of sound. The experiments showed that the pressure perturbation created from a monopole source of sound, due to combustion at a distance  $r$  from the point of ignition, was given by the following equation:

$$p'(r, t) = \frac{\rho}{4\pi r} \ddot{V}(t - r/c_0).$$

Where  $\ddot{V}$  represents the second rate of change of the volume of the bubble.

Although a simple experiment, Thomas and Williams (1966) highlighted the key aspect underlying the source of direct combustion noise: that the sound is generated by unsteadiness in the rate of expansion by combustion of gas. Studies by Hurle et al. (1968) and others have shown the results obtained by Thomas and Williams (1966) are equally applicable to open turbulent flames.

One can also determine aspects of direct combustion noise by solving the acoustic wave equation. In the far field, for a compact turbulent premixed flame, considering direct combustion noises only, a general solution to Equation 3.1 is given by (Crighton et al., 1992, Strahle, 1971):

$$p'(x, t) = \frac{(\gamma - 1)}{4\pi c_0^2 |x|} \iiint \ddot{q}(\mathbf{y}, t - |\mathbf{r}|/c_0) d^3 \mathbf{y}. \quad (3.2)$$

Where the integral is over the entire combustion zone within  $\mathbf{y}$ . The point of measurement is at position  $\mathbf{r}$ , due to the far-field and compact flame assumptions,  $\mathbf{r}$  has been approximated to  $\mathbf{x}$ . Equation 3.2 indicates that the instantaneous pressure fluctuations from open turbulent premixed flames are generated from the rate of change in the total heat release rates. For acoustic measurements, the instantaneous value of pressure perturbations is not of interest. However, from Equation 3.2 one can determine an expression for the stochastic mean square pressure perturbations of the flame, which is of interest for acoustic measurements:

$$\overline{p'^2(\mathbf{x})} = \left( \frac{(\gamma - 1)}{4\pi c_0^2 |x|} \right)^2 \iiint \overline{\ddot{q}^2(\mathbf{y}, t)} V_{corr}(\mathbf{y}) d^3 \mathbf{y}. \quad (3.3)$$

Where  $V_{corr}(\mathbf{y})$  is the correlation volume – refer to Dowling and Mahmoudi (2015). Equation 3.3 can be used as a basis to derive scaling laws. For example, Strahle and Shivashankara (1974)

derived scaling laws relating the total radiated acoustic power,  $P$ , from an open flame to: the burner diameter ( $D$ ), laminar flame speed ( $S_L$ ), fuel to air ratio ( $F$ ), and mean flow velocity ( $U_{ave}$ ). The derived law aligned closely with experimental results. The law was as follows:

$$P \propto F^{-0.42} S_L^{2.16} U_{ave}^{1.82} D^{3.44}.$$

Other examples of similar scaling laws have been derived by include Roberts and Leventhall (1973) and Kilham and Kirmani (1979).

Regarding the spectral characteristics of direct combustion noise, it is well established that direct combustion noise is largely broadband in nature with emissions ranging from 100 Hz to over 10 kHz exceeding background noise, with frequency peaks in the range of 200-1000 Hz (Mahan, 1984). Rajaram (2009) characterised the spectral characteristics of direct combustion noise for turbulent premixed flames. This was done so by determining, for a particular flame, the value of the peak frequency ( $F_{peak}$ ), slope of the low frequency components ( $\beta$ ) and slope of the high frequency components ( $\alpha$ ) - refer to Figure 13. Rajaram (2009) analysed a scaling law derived from Equation 3.3 that equates peak frequency to the mean flow velocity divided by the flame length i.e.  $F_{peak} = U_{ave}/L_f$ . Results indicated a strong correlation between  $F_{peak}$  and the  $U_{ave}/L_f$  for the three fuel types investigated.

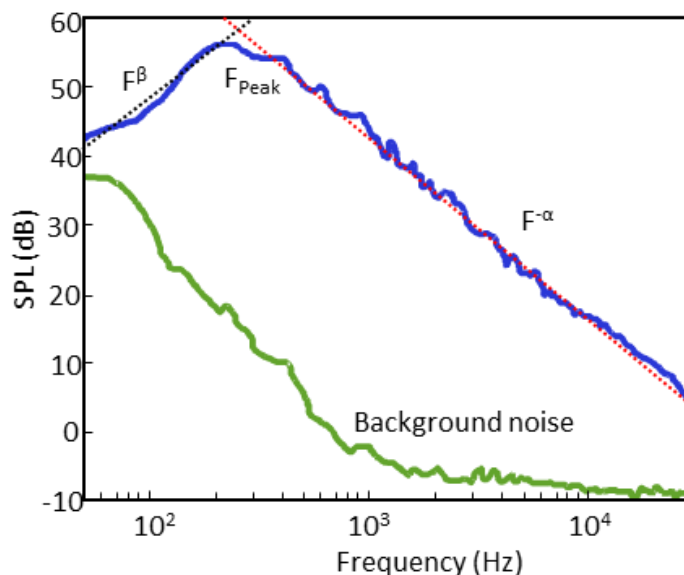


Figure 13 Sound pressure level (SPL) vs frequency for direct combustion noise from an open premixed lean methane-air flame, as adapted from Rajaram (2007)

### 3.1.3 Indirect Combustion Noise

Indirect combustion noise was first identified in the seventies by Marble and Candel (1977) and Morfey (1973).

As discussed there are two source terms of indirect noise for naturally aspirated combustion, they are present when entropy and vorticity waves are accelerated, typically via a downstream constriction. Entropy waves are created when there is some temporal and spatial variation in the rate of combustion at the flame front, this is common in any turbulent system. The variation produces hot spots, aka entropy waves, which are swept downstream with the flow (advect with the local flow). When these entropy waves are accelerated by a constriction downstream, they produce pressure perturbations (Bake et al., 2007). Vorticity waves are created because combustion generates unsteady shear at the flame front (Dowling and Mahmoudi, 2015, Chu and Kovásznay, 1958), this is also common in any turbulent system. As these waves advect downstream and are accelerated by a constriction, they produce pressure perturbations. Thus, energy contained within entropy and vorticity waves can be converted to an acoustic mode downstream. Indirect combustion noises propagate upstream towards the flame front and downstream through the exhaust duct. Upstream components can interact with the flame front and modify the downstream propagation of waves, in some instances causing thermoacoustic instabilities (Polifke et al., 2001). Generally entropy noise is considered to be more significant than vorticity noise (Morgans and Duran, 2016). A constriction may in the form of a nozzle or turbine blade. The shape of the constriction dictates the rate of acceleration in the flow and thus the relative energy of indirect noises.

A recent review by Morgans and Duran (2016) summarises progress in analysing entropy noise. Tam et al. (2013) separated the relative contribution of direct and indirect combustion noise for an auxiliary power unit. The study concluded that there is a high chance the system produced indirect noise in the region of 1.7-3.5 kHz range. Figure 14 was adapted from Tam et al. (2013) and illustrates the estimated contribution of indirect noise. Bake et al. (2007) analysed entropy noise for aero-engine combustors. Entropy noise was shown to be the dominant source of pressure fluctuations in the exhaust duct. The noise was broadband ranging from 1-3.5 kHz. In general “The relative contribution to the overall radiated noise from indirect and direct noise components is an ongoing issue...” (Dowling and Mahmoudi, 2015). Mahmoudi et al. (2017) found, similarly to other studies (Morgans and Duran, 2016), that vorticity noise is negligible

compared to entropy and direct noise. Additionally Mahmoudi et al. (2017, p. 21) found that “...entropy noise is the main mechanism of noise generation at the downstream duct.”

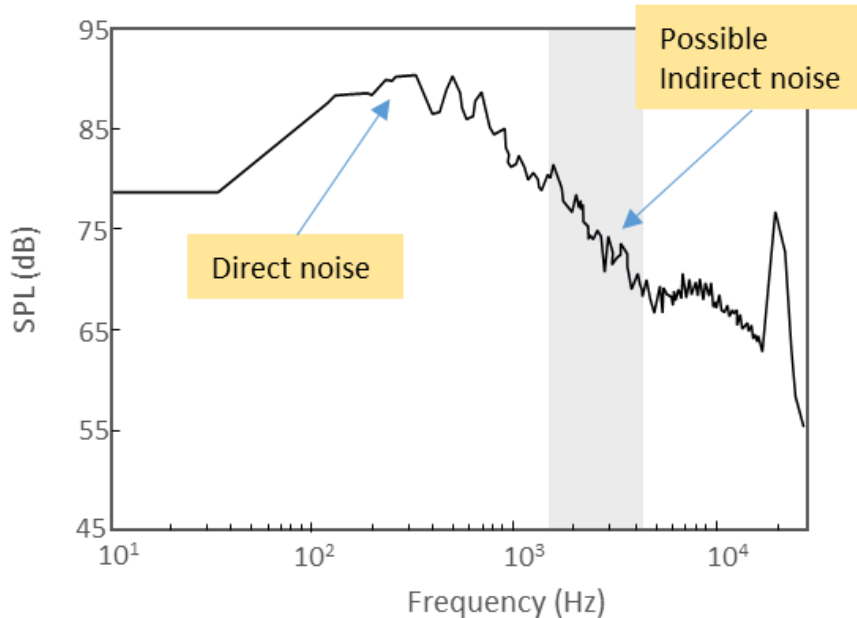


Figure 14 Sound Pressure Level (SPL) vs frequency for combustion acoustics from an auxiliary power unit. Indicated are the contributions from direct combustion noise and indirect combustion noise. Adapted from Tam et al. (2013)

### 3.1.4 Confinement

By confining a flame in unbounded space, although required for any practical combustion system, complicates mechanisms of combustion acoustics and interpretation of acoustics in the far field. As discussed, entropy and vorticity waves are advected by the mean flow and will transfer energy to an acoustic mode via a non-linear interaction such as a nozzle (Dowling and Mahmoudi, 2015). Thus, confinement typically results in the presence of indirect combustion noise.

Reflection of direct combustion noise, in addition to indirect noise travelling upstream, can interact with the flame front causing feedback effects. If this interaction is weakly coupled, then the flame front is not modified significantly. If, however the interaction between acoustics and the flame front is strongly coupled, then self-sustained oscillations can occur leading to increased noise production and a modified spectrum. “In these regimes, unsteady flow, combustion and acoustics are intimately coupled.” (Candel et al., 2009, p. 34).

Confinement of the flame also influences the flame dynamics, the impacts of such has been investigated in detail by Birbaud et al. (2007). Birbaud et al. (2007) found that even small confinement factors can modify flame dynamics to an appreciable extent. To illicit a significant change in combustion acoustics confinement is required to be tight within the bounds of the flame. However, this affect will depend on the type of flame under investigation.

The sound produced by direct and indirect combustion noise will also likely be modified by the natural frequencies of the system; these typically manifest as discrete peaks in the frequency spectrum. For example, when analysing combustion noise from a premixed methane industrial burner, Sanz et al. (2008) concluded that spectral peaks at 35 Hz were due to resonant modes of the combustion chamber and exhaust duct; this was confirmed by analysing the system as a Helmholtz resonator. Additionally Sanz et al. (2008) observed peaks at 220 and 370 Hz, these were either considered to be due to vortex-shedding (a combustion instability associated with swirl burners), or resonant modes of the burner. For combustion noise from a gas turbine, Tao et al. (2016) observed multiple frequency spikes around 2324 Hz; these were thought to be due to the longitudinal resonant mode of the combustion chamber. System resonances can be determined by modelling the system, analytically or numerically, or by performing experiments to find the transfer function of the system. The transfer function of the system “...includes both time-domain effects (echoes, discrete reflections, statistical reverberant tail) and frequency-domain effects (frequency response, frequency dependent reverberation)” (Farina, 2000). These effects can be summarised by calculating the system’s impulse-response. The impulse-response can be calculated via the swept-sine technique pioneered by Farina (2007, 2000).

### *3.1.5 Relationship between Equivalence Ratio and Acoustics*

Petela and Petela (1983) analysed the impact equivalence ratio had on acoustic intensities for premixed lean hydrogen-air flames in an open environment. Using the solution to the inhomogeneous wave equation proposed by Strahle (1971), Petela and Petela (1983) performed an order of magnitude analysis to conclude that the main source of pressure fluctuations from an open flame is the fluctuation of energy release rate due to combustion i.e. source  $S_1$  in Equation 3.1. Petela and Petela (1983) determined that in the far-field the acoustic intensity  $I$  due to combustion at position  $x$  from the flame was a function of the average heat release rate per unit volume,  $\langle \dot{q} \rangle$ , divided by  $c_p T$ , and some measure of turbulence which they labelled  $z$ . This can be expressed as:

$$I(x) = I \left\{ \frac{\langle \dot{Q} \rangle}{c_p T}, z \right\}. \quad (3.4)$$

For an ideal laminar flame, there is no turbulence and thus the flame intensity is a function of the average heat release rate only. For a turbulent jet without a flame  $z$  is nonzero and  $\dot{q}$  is zero, this noise source is referred to as 'cold flow' in the literature. For any practical flame both  $z$  and  $\dot{q}$  are nonzero. This interpretation was then used to analyse the impact of a varying  $\varphi$  on the acoustic intensity of the flame. It is expected that both  $\dot{q}$  and  $z$  will vary as a function of  $\varphi$ . From a theoretical point of view the combustion intensity in the primary kinetic flame front, synonymous with  $\dot{q}$ , is expected to be at a maximum when  $\varphi = 1$ , for fuel lean mixtures ( $\varphi < 1$ ) and fuel rich mixtures ( $\varphi > 1$ ) this will drop off as the mixture becomes more dilute. With regards to turbulence ( $z$ ) it is expected that this will decrease monotonically with  $\varphi$  i.e. the reaction zone turbulence will increase as the mixture becomes more lean (Petela and Petela, 1983). Thus, for lean flames ( $\varphi < 1$ ) the effects of  $\dot{q}$  and  $z$  are opposed. This has been summarised in Figure 15.

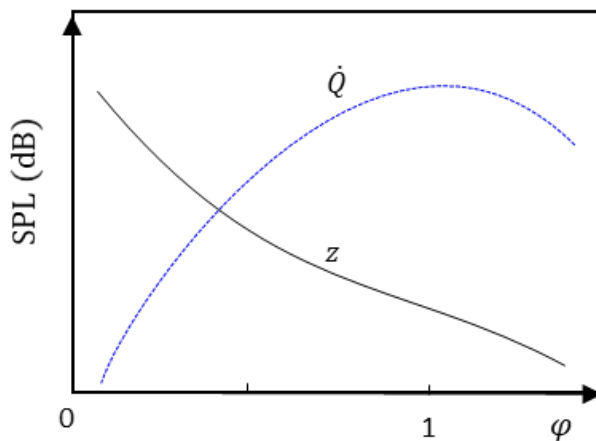


Figure 15 Illustration of various contributions of combustion noise from heat release rates ( $\dot{Q}$ ) and turbulence ( $z$ ). Adapted from Petela and Petela (1983)

Petela and Petela (1983) thus analysed the acoustic intensity, within frequency bands from 2-20 kHz, for a range of  $\varphi$  for a hydrogen-air flames. For lean flames, they found that for Reynolds numbers  $Re < \sim 17,000$  that the effect of  $\dot{q}$  is dominant, and thus the acoustic intensity decreases as  $\varphi$  decreases from unity. However, for  $Re > \sim 17,000$  turbulence starts to govern the acoustic intensity, and thus the acoustic intensity starts to increase as  $\varphi$  decreases from unity. Thus, the variation of acoustic intensity appears to be complex if turbulence is sufficient. Petela and Petela (1983) consequently proposed that flame acoustic intensity could be used as an indirect measure of flame parameters, such as  $\varphi$ , and hence used as a diagnostic tool.

Norris et al. (2005) and Kleppe et al. (2004) found a strong relationship between peak frequency and fuel/air ratios for jet engine turbines. They proposed that passive acoustic methods could be used to determine the operational equivalence ratio. They reported two separate sets of measurements taken 30 minutes apart for four fuel/air ratios, because the fuel is not reported one cannot determine the effective equivalence ratios. The peak frequencies appear to be in the range of 580-670 Hz. No prediction accuracies were reported.

Shivashankara et al. (1975) and Hassan (1974) developed empirical correlations between combustion acoustics and flame properties. They found that the position at which combustion acoustics peak was a function of  $\phi$ . Rajaram and Lieuwen (2003) showed that the acoustic spectra of turbulent methane-air flames, for a fixed burner diameter, for  $Re = 10,000 - 30,000$  has a “nearly universal shape” with the same peak whose total power increases with  $\phi$  for lean flames i.e. the total area under the spectra increases as a lean flame approaches stoichiometry. Results from Rajaram and Lieuwen (2003) have been summarised by Figure 16.

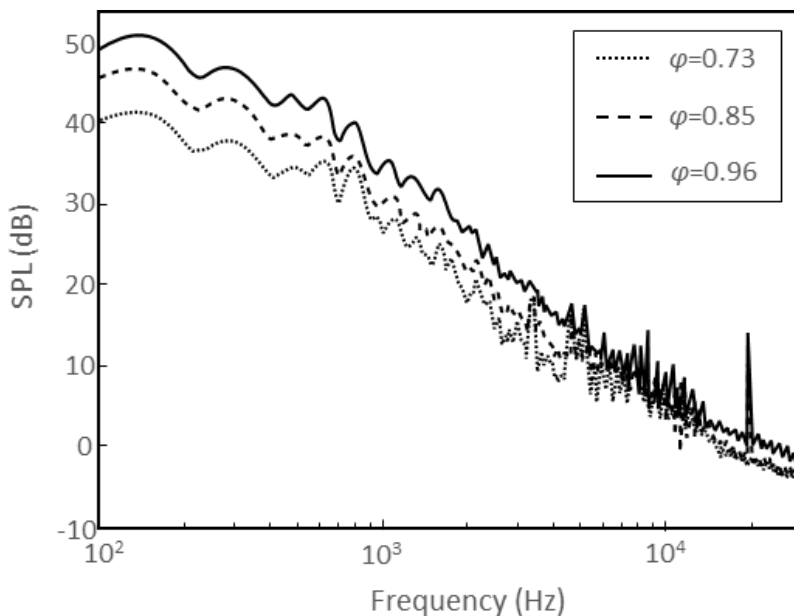


Figure 16 Direct noise from flame with same parameters but with  $\phi=0.73, 0.85$  and  $0.96$ . Adapted from Rajaram and Lieuwen (2003)

Hirsch et al. (2007) developed a model to theoretically determine the spectral content of direct combustion noises. In doing so the authors performed experiments of direct combustion noise for a range of parameters. They presented several spectrograms of combustion noise from premixed methane-air turbulent flames in an open environment. Similarly to the work

presented by Rajaram and Lieuwen (2003), they showed that increasing  $\varphi$  towards a value of unity increases the total acoustic power of the combustion noise without impacting the general shape of the spectra. Although one should note, as with Rajaram and Lieuwen (2003), the increase in total power does not occur equally across the entire spectra: most of the variation in acoustic power resides in the low frequency regions (<1000 Hz). Additionally, in the work Hirsch et al. (2007), the relative acoustic spectra of methane and hydrogen-methane (50% hydrogen) combustion for a fixed  $\varphi$  are reported. Interestingly, the change in acoustic spectra moving from methane to hydrogen-methane gas, has a similar effect increasing  $\varphi$  towards unity. Thus, the acoustic impact of changing  $\varphi$  may be similar to the acoustic impact of changing gas type.

### *3.2 Machine Learning*

Machine learning (ML) includes a broad set of algorithms which infer unknowns from knowns without being explicitly programmed. It can be seen as learning if the algorithm performs better at the inference task after being given example data. ML is useful to help in tasks whereby: the task cannot be defined well except for by example input and output pairs; relationships and correlations are hidden within large piles of data; the amount of knowledge required is too large for explicit programming; and/or the environmental conditions are adapting over time (Nilsson, 1996). ML algorithms can be split into two broad categories, those ML algorithms which learn when the outcome is known, and those which learn when the outcome is unknown; these are called supervised and unsupervised ML respectively. The most commonly applied ML algorithms are supervised ML. After giving a brief overview of unsupervised ML, the focus will be on supervised ML techniques and the primary nuances and pitfalls of training and testing ML algorithms.

#### *3.2.1 Unsupervised Machine Learning*

Unsupervised ML algorithms learn from unlabelled features, thus there is no defined target output(s) for the features to be mapped to. Typically, the problem in this instance is cluster the data. Clustering quite simply groups together similar data items into clusters: “These [obtained] clusters should reflect some mechanism at work in the domain from which instances or data points are drawn, a mechanism that causes some instances to bear a stronger resemblance to one another than they do to the remaining instances.” (Witten et al., 2016).

Often unsupervised methods are applied before the application of supervised methods so that assumptions about the distribution of the data can be made. Most clustering schemes are parametric and can be split into generative or reconstructive methods. Reconstructive methods try and minimise a cost function whereas generative models are based on assuming some probability distribution. An overview of some of the most popular unsupervised ML algorithms will be given below - refer to Fung (2001) for a more detailed overview.

A popular reconstructive clustering algorithm is *K*-means: Given an initial distribution of clusters where the number of clusters (*K*) has been defined. This algorithm assigns points to each cluster, calculates the mean of that cluster and repositions the centre of the cluster to that mean value. Repeating this until the cluster centre is stable splits the data into *K* clusters. Correctly initialising the position of the clusters is imperative to the performance of *K*-means: one option is running *K*-means multiple times, using a random initialisation each time, and a cost function to decide the best clustering; another option is to similarly run *K*-means multiple times but initialise clusters based on distance metrics. Popular applications include image segmentation (Dehariya et al., 2010) and analysing gene data (Gasch and Eisen, 2002).

A popular generative clustering algorithm is a Gaussian mixture model (GMM): This algorithm models clusters as Gaussian probability density functions. Clusters can be overlapping in this space. The position, covariance and height of each Gaussian are updated using the expectation maximisation (EM) algorithm. The number of clusters is defined by the user and position is often initiated using *K*-means. The EM algorithm iteratively updates the position and covariance of the clusters by: (1) measuring the probability that each data point belongs to each cluster; and (2) updating the position and covariance of each cluster by an amount weighted by the probability values determined in step (1). Consequently, if a set of data points are strongly assigned to one cluster over another, then the cluster parameters (mean and covariance) will be adjusted by an amount to be more representative of those points. For a point in the feature space, the GMM returns a probability that it belongs in each cluster, thus the model is generative. Application areas include automatic speech recognition (Reynolds et al., 2000) and object tracking in moving images (Santosh et al., 2013)

### *3.2.2 Supervised Machine Learning*

Supervised ML algorithms learn how best to map the features (inputs) to the desired class (outputs) given examples of both features and the corresponding class i.e. inductive learning. For example, to build a face recognition algorithm, the algorithm would require input features

representative of facial and non-facial images (e.g. the intensities of pixels) and the corresponding class value (1 for an image of a face, 0 otherwise). The algorithm then trains itself using this data so that it performs well classifying a new image it has not seen – curve fitting is an example.

Often ML is suited to an ill-posed problem. This is because, in most examples, there does not exist a single ‘best’ hypothesis which fits the training data, thus ML algorithms must select the most general hypothesis from a selection of options. Each algorithm does this in its own unique way, giving the algorithm its own inductive bias when building a hypothesis. Some of the main groups of algorithms will be discussed later in this section.

From a learning perspective, if the algorithm is not given enough instances (examples) for all classes then the algorithm will struggle to develop applicable rules for unseen data. If the feature space is too large then this can lead to what is known as ‘the curse of dimensionality’ (Bellman, 2015). In ML ‘the curse of dimensionality’ refers to a set of problems caused by trying to work with data in high dimensional space when the number of instances (examples) is insufficient. The problems are caused because the density of data points in such spaces is very low. For example, for 100 dimensions, a training set of a trillion examples only covers  $10^{-18}$  of the feature space (Domingos, 2012). However, if the space occupied by the training and testing sets is small in comparison with the total feature space, it can be the case that even for high dimensionality spaces learning algorithms work well. For example  $k$ -nearest neighbour for handwritten digit recognition is known to work very well for 400 dimensions (20x20 images) given 60,000 instances (LeCun et al., 1995). Dimensionality reduction is a widely researched topic in itself refer to Tenenbaum et al. (2000).

Critical to ML is to assess the predictive capacity of the algorithm. A major error is to test the algorithm on the data used to train it; doing so would return misleadingly high predictive accuracies. The algorithm must be tested on data it has not seen. The primary goal of a ML algorithm is for it to be able to generalise. When an algorithm performs poorly for data it has not seen relative to data it has, it has likely over-fitted itself to the training data. In other words, it may have become overly complex so that the broader, more generally applicable rules governing say the recognition of faces are overlooked for other aspects which may be unrelated. Thorough strategies of training and testing algorithms include leave-one-out cross-validation (CV),  $k$ -fold CV and bootstrap aggregation (or bagging) (Breiman, 1996). These strategies should show poor accuracy and/or consistency if the algorithm is over-fitting the training data. Over-fitting can be due to the model itself being too complex or many the input features being

unnecessary i.e. not related to the desired output. It can be possible to under-fit the data if the model is not complex enough and/or there is not enough information within the features. However, over-fitting is much more common, thus substantial effort in the field of ML is dedicated to feature selection, feature reduction, and complexity limiting techniques such as regularization. Again, the primary goal of a ML algorithm is for it to be able to generalise.

The general purpose of feature reduction schemes is to remove irrelevant features without impacting algorithm performance. These are features which do not give any additional information with respect to determining the class, such features could also be deemed noise. In this study, we will split feature reduction schemes into ML-dependent and ML-independent feature reduction schemes. An example of a ML-dependent feature reduction scheme is the wrapper method (Kohavi and John, 1997). The wrapper method evaluates subsets of the feature space by using a ML algorithm, the subset that returns the highest testing accuracy for that ML algorithm is selected. There are several methods for searching through the feature space, for example best-first, exhaustive, genetic etc. An example of a ML-independent feature reduction scheme is correlation-based feature selection. Correlation-based feature selection is based on the hypothesis that “A good feature subset is one that contains features highly correlated with (predictive of) the class, yet uncorrelated with (not predictive of) each other” (Hall, 1999, p. 4). Thus, it evaluates the worth of a subset of features by calculating the individual predictive ability of each feature along with the degree of redundancy between them using a search method similar to wrapper methods.

Regularization on the other hand penalises ML algorithms for complexity – often compared to ‘Occam’s razor’. During training a ML algorithm will often optimise itself to minimise a loss function. The loss function is a measure of the algorithms current performance during training and is normally set equal to the squared error i.e. the square of the difference between the current estimates and the actual class. To avoid creating algorithms which are too complex, or in other words contain additional complexity for little benefit, a complexity penalising heuristic is added to the loss function. This is known as regularisation. For example, when deriving a polynomial fit, the regularisation term could be set as some regularisation factor multiplied by the square sum of the polynomial parameters, thus favouring a simpler hypothesis. ML algorithms such as instance based learners do not contain any loss function, and indeed do not go through a training process, thus such methods are not applicable. In the case of instance based learners, model complexity is entirely controlled by the selection of features.

In general, there are two main groupings of supervised ML algorithms; they are lazy-learners (aka instance-based learners) and eager-learners. A lazy-learner compares an unknown data point with instances seen in the training dataset. Eager-learners create a single hypothesis based on the training set and generalise that hypothesis to all unknown data points. Thus eager-learners must commit to a single hypothesis to cover the entire instance space, whereas lazy-learners can effectively use a richer hypothesis space, since many local linear functions can exist to form an implicit global approximation to the target function (Mitchell, 1997). The main disadvantage of lazy-learners is that the database of known instances must be kept in memory for the algorithm to perform. Within the groupings of lazy and eager-learners there are a range of ML algorithms which all pertain to an inductive bias.

Some of the main types of supervised ML algorithms applied in research are  $k$ -nearest neighbour (kNN), decision trees, artificial neural networks (ANNs) and support vector machines (SVM). An overview of these algorithms will be given below.

#### *3.2.2.1K-Nearest Neighbour*

First proposed in 1968 by Cover and Hart (1967). This algorithm is a lazy-learner and determines the class of an unknown data point by matching it to its nearest neighbours in the training feature space. It does this by calculating the Euclidean distances (although several distance functions can be applied) in the feature space between an unknown data point and the training dataset, and assigns a class by averaging the  $k^{th}$  nearest data points in the training dataset. If the class is labelled, then a majority vote of the  $k^{th}$  nearest data points determines the class. Although the kNN algorithm requires no training time, it requires all training data to be stored in memory. The 'curse of dimensionality' is prevalent when applying kNN. This is because, as the feature space becomes large, the distance to the nearest neighbour approaches the distance to the farthest neighbour. Thus, nearest neighbour matching becomes unstable and meaningless. Beyer et al. (1999) analyse this problem in detail, discussing exceptions and analysis procedures. Regardless the simplicity of the algorithm means that it is widely used so long as precautions are taken. kNN can be summarised by the following saying: "If it looks like a duck, swims like a duck, and quacks like a duck, then it is probably a duck" (Gorunescu, 2011, p. 256)

#### *3.2.2.2Decision Trees*

This includes a range of algorithms which in general pertain to a tree structure whose internal nodes represent tests or decisions and leaf nodes represent outputs. Inputs filter through the

tree structure moving down different branches via the nodes until an output is attained. The tree is constructed during training and the method of construction depends on the algorithm applied. Popular decision tree algorithms include C4.5 (Quinlan, 1993) and CART (Breiman et al., 1984). When constructing the tree, the most popular method of selecting a suitable test and feature combination at each node, is to do so based on that which maximises the information gain per the test data; iteratively inducing this scheme on each sub-list of data forms the tree. The tree stops splitting once a split is found not to improve the information gain by some threshold amount. A process of pruning is then sometimes applied to reduce tree complexity. Such a method implicitly performs feature selection, using an information gain heuristic, and regularisation, via pruning. The output of a tree algorithm can be observed by a user. Simplicity of application, in addition to the potential level of model complexity, and the interpretability of the output, explain the popularity of decision trees. The Random Forest algorithm (a very popular ML algorithm) is developed by constructing an ensemble of decision trees built on data selected via a bootstrapping approach.

### *3.2.2.3 Artificial Neural Networks*

Although the concept of artificial neural networks (ANNs) was first coined in 1943 (McCulloch and Pitts, 1943), it wasn't until the early 80's that the field was invigorated due to the invention of the back-propagation algorithm and increasing processing power. Today ANNs or Deep Neural Networks are integral to some of the biggest advances in ML. ANNs are inspired by the way in which the brain processes information - via neurons interconnected with synapses to form networks. For example, the primary visual cortex, allowing us to recognise images, contains 140 million neurons with tens of billions of connections. Such image recognition problems, although simple for our brains, are very difficult to program because one cannot explain them explicitly, especially when considering all possible caveats. ANNs are very useful techniques for developing ML algorithms which solve complex problems such as image recognition (Nielsen, 2015).

An ANN links inputs to some number of hidden neurons via synapses to an output neuron (if a multi-class problem there are numerous output neurons). The number of hidden layers, the structure of the neurons, and the number of neurons can be varied by the designer – an example has been given in Figure 17 of one hidden layer with three hidden neurons. Each synapse contains an adjustable weight which is multiplied by the data at the start of the synapse. At the end of each synapse is a neuron which sums all the incoming values and applies an activation function (typically a sigmoid function). The final neuron(s) in the structure are the output(s). All data moves from inputs to outputs via synapses and neurons. During training the algorithm

adjusts the weights in the training process to minimise the loss function. This is typically performed via back-propagation i.e. the algorithm aims to improve the cost function on each iteration by varying the weights while moving back through the layers. By calculating the derivative of the loss function with respect to each weight, the direction to adjust the weights can be determined, aka gradient decent. The amount of adjustment is determined by the slope of the gradient and the learning rate. A momentum term can be used to increase the rate of learning. The number of epochs defines how many times the weights are adjusted by the learning procedure.

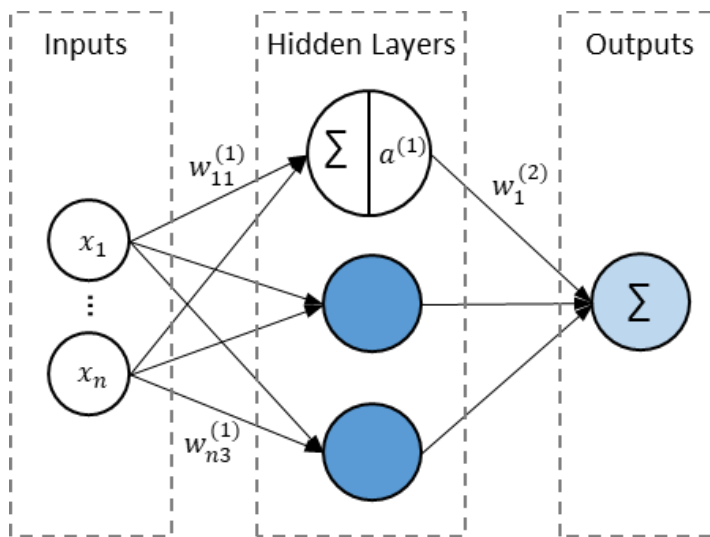


Figure 17 Illustration of an ANN with one hidden layer and three hidden neurons. Where  $x_{1..n}$  are the inputs,  $w_{1,1}^{(1)}$  is the weight from neuron 1 in the first layer to neuron 3 in the second layer, and  $a^{(1)}$  is the activation function for the first hidden layer

Typically, the number of weights in ANNs are large, thus they take a long time to train. For example, 40 inputs and 20 neurons in one hidden layer result in 821 weights. There are many parameters which can be tuned in an ANN, these include the network structure, the learning rate, the loss function, number of training epochs and momentum. Thus, significant testing and know-how is required to build optimum networks. Significant efforts are ongoing to develop techniques to interpret ANNs (Montavon et al., 2017) in addition to help automate parameter selection and network structure (Leung et al., 2003, Tsai et al., 2006).

### 3.2.2.4 Support Vector Machines

Support vector machines (SVMs) were developed throughout a 20-30 year period by Vapnik and Chervonenkis (1974), Vapnik and Kotz (1982) and Vapnik (1995). A detailed overview of SVM methods as applied to classification and regression problems have are provided by Dibike et al.

(2001) and Schölkopf and Smola (2002) respectively. A basic overview of the regression problem will be given below.

Given training data  $(x_1, y_1), \dots, (x_n, y_n)$  in the input space. The aim of SVMs for regression (aka  $\epsilon$ -SV regression) is to determine a linear function  $f(x)$ , which is at most a certain distance  $\epsilon$  from attaining  $y_i$  for all training instances  $x_i$ , and is at the same time as flat as possible (Smola and Schölkopf, 2004). It may not be possible to encompass all training instances within a range  $\epsilon$ , additionally one may not want to attempt this to avoid overfitting. Thus 'slack variables',  $\zeta$ , are introduced (analogous to the 'soft-margin' used in the SVM classification problem) to allow some number of instances to exist outside of the imposed restriction – refer to Figure 18.

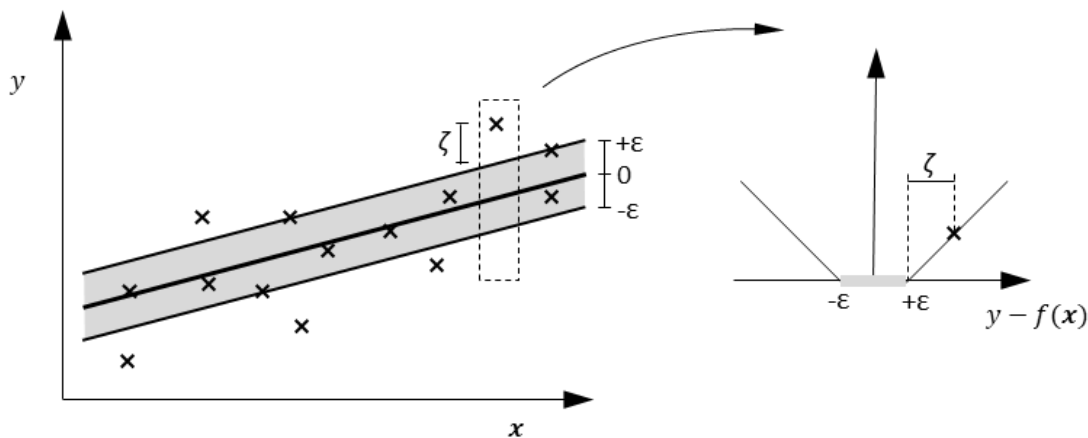


Figure 18 Illustration of the soft margin loss setting as applied to SVM for regression. Figure adapted from Schölkopf and Smola (2002)

In most practical learning scenarios relationships are non-linear. However, the mathematics underpinning SVMs only require consideration of the dot products of the input space, thus a kernel trick can be applied. The kernel applied transforms the input space to a high-dimensional feature space where, in principal, non-linear relationships can be represented in a linear form (Üstün et al., 2006). Thus, for the training data the target function is given by the following linear function in the space determined by the kernel  $K$ :

$$f(x) = \sum_{i=1}^n (\alpha_i - \alpha_i^*) K(x_i, x) + b, \quad 0 < \alpha_i < C.$$

Where  $x$  a test/unknown data point,  $\alpha_i$  are the Lagrange multipliers and  $b$  the offset of the function. The values of  $\alpha_i$  and  $b$  are determined during training. The larger the value of  $C$  the more leniency is given to points outside the region in  $\epsilon$  i.e. the softer the margin of the hyperplane. The selection of kernel, the value assigned to  $C$  and the value assigned to  $\epsilon$  are

critical in the performance of SVMs. There are no strict rules for selection of these parameters, thus SVMs are often combined with some optimisation procedure, such as a grid search (Thissen et al., 2004). Popular choices for kernel functions include: the linear and polynomial inner-product kernel and the radial basis function (RBF). However, one can avoid experimentation with permutations of various kernel functions by applying the Pearson VII universal kernel (PUK). “In general, PUK can be used as a universal kernel that is capable to serve as a generic alternative to the common linear, polynomial and RBF kernel functions” (Stanimirova et al., 2010, p. 55). Note, the selection of kernel is constrained by Mercer’s condition (Mercer, 1909). SVMs are appealing as they are considered to generalise well without making prior assumptions on the distribution of instances (Mountrakis et al., 2011).

### *3.2.3 Feature Reduction*

Feature reduction techniques are split into three broad model types: filter, wrapper and embedded models. Filter models analyse the data without the input of ML algorithms. Filter models score each feature for its relevance with respect to the class. A cut-off is typically selected whereby features below a certain score are removed. By analysing only intrinsic properties of the data, filter methods can provide levels of insight otherwise missed using wrapper or embedded models. In addition, filter methods are computationally fast and simple. The main disadvantages of filter models are that, because they are ML algorithm independent, they may not optimise the performance of a classifier. Additionally, most filter models treat features independently, thus potentially miss feature dependencies. Examples of filter methods which treat features independently include: Chi-squared, Information-gain, gain-ratio and one-rule (Ben-Bassat, 1982). Examples of filter methods which consider interactions between features include: Correlation-based feature selection (Hall, 1999) and Markov blanket filter (Koller and Sahami, 1996).

Wrapper and embedded models consider a particular ML algorithm when determining the optimum selection of features. Wrapper models select the feature set, out of all possible combinations, which maximises the accuracy of a ML algorithm. As exhaustive searches are computationally intractable, key in applying wrapper models is the search method. There are many search methods including methodical searches such as best-first (Kohavi, 1994), stochastic such as random hill-climbing (Skalak, 1994), and heuristic, such as sequential forward/backward selection/elimination (Kittler, 1978). Wrapper models are largely considered to result in the optimum selection of features for a particular ML algorithm (Guyon and Elisseeff, 2003). The

method is brute force and therefore computationally expensive. Additionally, the risk of overfitting is higher relative with other models.

The final feature reduction model is embedded. This is where the feature selection is built into the construction of the ML algorithm. An example of this includes the construction of decision trees: as previously discussed decision trees typically use an information gain heuristic to determine which feature to split on and where to split. Thus, feature reduction is embedded into the scheme. Like wrapper models, embedded models consider a particular ML algorithm only, however they are comparatively less computationally expensive. Other embedded methods include weighted naïve Bayes (Duda et al., 2012) and using the weight vectors of SVM (Weston et al., 2003). The main disadvantage of embedded methods is the small number of methods available and therefore their lack of range across various inductive biases available in the array of ML algorithms.

### *3.2.4 Training and Testing*

As mentioned the primary goal of a ML algorithm is for it to be able to generalise. To test if, within a dataset with  $n$  instances, the ML algorithms developed can generalise, strategies of training and testing need to be considered.

The simplest approach to this problem is to train and test ML algorithms on the same data. This approach does not test how well a ML algorithm would deal with a point it has not seen before. Such a strategy is rare as it returns overly optimistic results in most instances. A more thorough approach, more common throughout the literature, is referred to as the holdout method. This method randomly partitions the data into training and testing sets. Typically, the split is two thirds training and one third testing. This method, unless repeated multiple times and an average taken, can still lead to an unbiased view of the general performance of the ML algorithm.

An extension of the holdout method is to rotate the data so that every portion of the data is used for both training and testing. This method is called  $k$ -fold cross validation (CV). For  $k$ -fold CV the data is split into  $k$  segments,  $k-1$  of which are used for training and the remaining used for testing. This is repeated  $k$  times so that every instance has been used once for testing. The average result of all  $k$  tests is then calculated and used as an estimate of predictive accuracy and variance. This method is very popular within the literature. Another popular method, referred to as the leave-one-out method, trains algorithms on all but one instance and tests on the

remaining instance. This is repeated for all points and an average taken. For the methods mentioned above, a random number seed is used to make the initial split in the data, for completeness this random number seed can be changed and the process repeated. This is to ensure that the selected split in the dataset does not impact the results.

Another thorough testing approach is called bootstrap aggregating (aka bagging) (Breiman, 1996). In this scheme the data is first split into a training and testing set; next, for the training set, a sampling technique called bootstrapping is applied. This involves randomly sampling, with replacement, the training instances into  $m$  ‘bags’. The number of instance in each bag is typically less than or equal to the total number of training instances. The number of bags,  $m$ , is typically incrementally increased from a starting value of 10 until variations in the predictive accuracies attained remain constant. ML algorithms are then trained on each ‘bag’ of data. The testing set is applied to the  $m$  ML algorithms and an average predictive accuracy result taken. This can be repeated multiple times with different training and testing partitions. The resultant average accuracy of applying this method, per by central limit theorem, should get close to the correct answer. This is because each bag should provide a different weighting of the data, highlighting all variance involved in the dataset.

Note, a good error metric to compare ML algorithms is the root-relative-squared-error (RRSE). The RRSE metric returns an absolute value and takes into account what the error would have been if a ‘simple predictor’ had been applied. ‘Simple predictor’ refers to a predictor which will always predicts the average of the training classes. The equation for the RRSE is:

$$RRSE = \sqrt{\frac{\sum_{i=1}^N (\hat{\varphi}_i - \varphi_i)^2}{\sum_{i=1}^N (\bar{\varphi} - \varphi_i)^2}}, \quad (3.5)$$

Where  $\hat{\varphi}_i$  is the predicted value of the  $i^{\text{th}}$  data point using some algorithm,  $\varphi_i$  is the corresponding correct value and  $\bar{\varphi}$  the mean of all  $N$  data points investigated.

### ***3.3 Application Areas of Machine Learning***

Below an overview of ML application areas are given. This has been split into general, combustion, acoustic and combustion acoustic related applications.

### 3.3.1 General

In the past 20-30 years, ML has been applied to a vast array of tasks. These can be divided into formal, expert and mundane tasks. Formal tasks include logical tasks such as Chess, mathematical proofs etc.; expert tasks are designed to aid or improve on a user, they include medical diagnostics, scheduling etc.; mundane tasks are those which a human typically performs with ease, they include speech analysis, visual perception, object manipulation, driving etc. (Fridman, 2017). Some generally applicable and notable applications of ML will be given below.

A well-developed and ongoing application area in ML is bioinformatics. Bioinformatics is a field characteristic of many of the challenges associated with the application of ML; these include class imbalance, high dimensional feature spaces, missing data and class noise (Larranaga et al., 2006). For example, within genomics ML is used to understand the relationship between gene expression data and inherent physiological characteristics of interest. As characteristic with these problems, the relative proportion of cases to controls is very low and number of features (gene expression data) is in the order of thousands, containing large amounts of noise – both class-noise (variation within a class) and feature-noise (missing gene data). As such, blind application of ML algorithms can be computationally costly and often lead to over-fitting (Toivonen et al., 2005). Consequently feature selection schemes are essential, along with appropriate evaluation metrics (Libbrecht and Noble, 2015). Ramaswamy et al. (2001) for example used ML techniques to determine the relationship between gene expression data and the prevalence of cancers. To deal with issues of over-fitting associated with the high dimensional gene expression data, the authors applied an embedded feature reduction scheme: similarly to Guyon et al. (2002) they used SVM methods based on recursive feature elimination to select genes correlated with various forms of cancer. In doing so, Ramaswamy et al. (2001) developed a more accurate classification algorithm relative to previous attempts. In a review of feature selection as applied in bioinformatics, it was found: “...an advisable practice is to pre-reduce the search space using a univariate filter method, and only then apply wrapper or embedded methods, hence fitting the computation time to the available resources.” (Saeys et al., 2007, p. 2512).

A noteworthy and recent application of ML has been AlphaGo Zero (Silver et al., 2017b). AlphaGo Zero is Google’s self-learning program developed to master the game of Go. Considering the timing of this achievement, in addition to being “...a feat previously thought to be at least a decade away” (Silver et al., 2016, p. 484), it is worth briefly reviewing here. Unlike Chess, the

game of Go cannot not be solved by brute force and domain knowledge alone. This is because in the game of Go the number of potential moves is much larger than Chess and mid-game heuristics are not useful i.e. it is hard to know who is winning at a given point. As such, a different approach was required. Silver et al. (2017b) developed a program called AlphaGo Zero which learnt to play Go via self-play only i.e. the learning algorithm had no prior knowledge of the game. It took AlphaGo Zero 72 hours to learn how to play Go beyond human expert level and 40 days to advance far beyond human-level play. Some Go strategies which are common in professional games were discovered by AlphaGo Zero, and interestingly over time some of these were disregarded for better options. The playing style of the algorithm is still being analysed by Go players world-wide as it is adding to the knowledge of a game which has been studied by humans for thousands of years. A similar self-learning algorithm called AlphaZero has also been applied to Chess (Silver et al., 2017a) and has convincingly outperformed expert Chess algorithms. The architecture employed by AlphaZero (like that of AlphaGo Zero) is a deep convolutional neural network trained via reinforcement learning. For more details refer to Silver et al. (2016, 2017a, 2017b).

### *3.3.2 Combustion*

Relevant to the current study is the application of ML in the field of combustion. Specifically, in the pursuit of developing control systems aiming to optimise combustion conditions. The focus here will be with regards to ML procedures applied to the analysis and optimisation of combustion systems.

As mentioned in Section 2.3.3.5, Allen et al. (1993) used a CCD camera in combination with ML to develop a combustion diagnostic method for a liquid-fuelled spray flame burner. The ML algorithm used in this instance was an ANN. The ANN was trained on spatial representations of the flame consisting of 1024 features. The ML algorithm could determine, based on 5000 training and testing images the atomising air flow rate of the flame in ten discrete bands. This was used as a part of a control loop for executing desired fluctuations in atomising air flow rates. Lu et al. (1999) similarly coupled an ANN-based image analysis technique, using data from CCD camera, within a combustion control loop for butane gas flames. Both these studies were performed in laboratory rigs. Hernandez and Ballester (2008) report on the use of flame images to predict combustion states for a natural gas burner rig. A CCD camera, housed in a water-cooled jacket, was used to get images. Three approaches were applied to predict desired combustion states ( $\text{NO}_x$ , CO and air-to-gas ratios) from 49 acquired images across a range of

flame types; they included self-organising feature maps, ANN-based prediction using PCA as feature reduction and a 'probabilistic approach'. Good results were achieved for a fixed fuel composition. Note, images in all the aforementioned studies were averaged in time to smooth out fluctuations due to turbulence or flame oscillations.

Ballester et al. (2009) used broadband chemiluminescent signals from a photomultiplier and photodiode in combination with ANNs to predict equivalence ratios and emission concentrations in premixed methane-hydrogen flames with varying levels of hydrogen. Good results were obtained, for the laboratory scale setup, for the prediction of CO, NO<sub>x</sub> and equivalence ratios using an ANN with one hidden layer. This was in accordance with formed for datasets containing varying amounts of hydrogen from 0-40% and thus the techniques were applicable independent of hydrogen concentration. Additionally, the ML algorithms developed could predict the hydrogen content of the fuel. Features applied were the average and standard deviation of broadband signals from a photomultiplier and photodiode.

Many studies have utilised ML approaches to optimise burn conditions in industrial combustion systems. In these systems, the power output or feed in rates can vary depending on the demand requirements. Additionally, the fuel composition can vary by a known amount. ML algorithms are used in these studies to determine the required operational parameters to optimise emissions for a unique set of inputs. Typically, the input parameters are fuel/air flow rates, exist temperatures and input air temperatures, air swirl angles, burner positioning (tilt angle etc.), and fuel composition (C, H and O content of fuel). ML algorithms are trained as based on computational fluid dynamic (CFD) models, historical data and operational data. Examples of such studies include Hao et al. (2001), Chu et al. (2003), Tan et al. (2006), Zhou et al. (2012), Ilamathi et al. (2013), Iliyas et al. (2013), Krzywanski et al. (2015) and Song et al. (2017).

Tan et al. (2006) and Iliyas et al. (2013) for example trained ANNs (Iliyas et al. (2013) used an RBF neural network) to replace the need to run computational fluid dynamic (CFD) models in a pulverised coal / biomass co-combustion and gas fired boilers respectively. CFD models are useful for predicting the ideal operational constraints of a combustion system, however they are computationally intensive, hence ANNs were developed to replace them. Tan et al. (2006) trained ANNs by running CFD models over a large range of constraints. ANNs were designed to predict exhaust gas emissions and carbon burnout from: flow rates of fuel, air swirl angles, air flow rates, and fuel composition. The results indicated ANNs were very good at replicating CFD models for the range of outputs tested. Thus, during operation of the rig, flow rates and swirl

angles were varied, depending on the incoming fuel properties, to optimise emissions as based on the output of the ANNs. During experiments this method worked well.

Similarly Mayes (1999) utilised ANN to represent the complexity of a large coal fired boiler in order to optimise carbon burnout given some input constraints on fuel type, fuel rate and oxygen rate. For Mayes (1999) retraining of the ANN was required as the system varied over time. In this vein Gu et al. (2011) developed an adaptive ML approach so that system variability can be controlled for to optimise efficiencies in coal boilers.

For diesel engines, NO<sub>x</sub> emissions are of concern. Controlling emissions is possible by managing temperatures in the combustion chamber by use of techniques such as exhaust gas recirculation. Consequently, operational monitoring of NO<sub>x</sub> is of use for a control procedure or to indicate when a service is required. However, NO<sub>x</sub> sensors are typically expensive and require periodic recalibration, thus so called soft surrogate sensor techniques have been investigated. Some of which utilise ML algorithms in combination with the data available from on-board management systems. Examples of such approaches include Ismail et al. (2012), Liu et al. (2016) and Taghavifar et al. (2016)

Liu et al. (2016) developed a ML algorithm to determine NO<sub>x</sub> from on-board parameters. They used principal component analysis (PCA) for dimension reduction and a SVM in combination with a genetic algorithm (GA) to optimise parameters. As inputs about 40 parameters were considered, from an empirical evaluation these were reduced to 15; these included engine torque, engine speed, oil temperature, coolant temperature, air intake temperature, atmospheric pressure etc. NO<sub>x</sub> emissions were recorded using a gas analyser in order to train algorithms. Data was collected running at 180 different combinations of engine load and engine speed. PCA was used to reduce this feature space from 15 to 5 dimensions. Note, that PCA methods were not mentioned in Section 3.2.3, this is because they do not limit the features considered; PCAs reduce dimensionality by summarising the variance across all features into eigenvectors (a linear combination of all features). SVM was used with a Gaussian RBF as a kernel. A GA was applied to optimise selection of parameters for the SVM, such parameters included the penalty factor, often referred to as C, and the kernel shape. The resultant algorithm could predict NO<sub>x</sub> emissions with a mean absolute percentage error of 4.65% on testing data, outperforming ANN and SVM without the implementation of a GA. This study did not consider the long-term application of such techniques. Taghavifar et al. (2016) used ANNs to predict NO<sub>x</sub>, CO<sub>2</sub> and soot. For this study the algorithms were trained based on a CFD model of the engine. Testing was completed using said CFD model for two engine speeds. Ismail et al. (2012) used an

ANN to predict nine engine output parameters including CO<sub>2</sub>, CO and NO. This was based on only four engine parameters including engine speed, torque, fuel mass flow rate, and biodiesel fuel composition. ANN were trained and tested on about 322 using a network with one hidden layers and ten neurons. Good results were obtained tracking emissions for the test engine used. A holdout testing strategy was applied.

### 3.3.3 Acoustics

As it is the focus of this study to investigate the application of ML techniques in the domain of combustion acoustics, it is relevant here to consider applications in acoustics. Applications in acoustics cover a broad range of fields including fault detection in machinery (Tandon and Choudhury, 1999, Ocak and Loparo, 2001), music emotion recognition (Kim et al., 2010), diagnosing Parkinson's disease from speech (Tsanas et al., 2010), bird species identification (Briggs et al., 2012) etc. Of all the fields, the one which has been most widely researched is the field of automatic speech recognition (ASR). Thus, it is of interest to briefly review ASR techniques with focus on the acoustic features applied.

Automatic speech recognition (ASR) is one of the most widely researched application areas in computing. The first notable success of which dates back to 1952 when Bell laboratories developed a system for isolated digit recognition for a single speaker (Davis et al., 1952). In the past, few decades, as sophisticated ASR has become more attainable, research has been particularly intensive. The aims of ASR systems vary depending on the required sophistication. Ideally ASR systems can handle: spontaneous speech in the presence of noise, in the far field, for a huge vocabulary, which is accent-independent and speaker-adaptive (Senior, 2017).

Variations in utterances can be observed by transforming a sampled acoustic signal onto the time vs frequency domain. Such a representation is achieved by calculating the speech spectrogram. A spectrogram is calculated by windowing, and commonly overlapping, the time domain signal into chunks, and calculating the discrete Fourier transform of each chunk. For speech audio, to capture stationary segments of speech, the windows are typically 25 ms in length with 15 ms of overlap. This leads to a frequency representation of the signal every 10 ms of the audio - each 10 ms chunk is commonly referred to as a periodogram. From speech spectrograms it is possible for people to 'read' the speech by visually studying the images (Lamel, 1988); thus the information contained within spectrograms is sufficient for some kind of speech recognition analysis.

When applying ML techniques to speech spectrograms it is common to summarise the data in each periodogram in the form of a feature vector. Ideally this summarised form of the periodogram contains useful information for identifying linguistic content while disregarding unnecessary information. Examples of unnecessary information include background noise and needless frequency granularity - it is known that the human auditory perception cannot typically identify between frequencies separated by less than 3Hz (Smith, 1997). Popular feature vectors include: Mel-Frequency Cepstral Coefficients (MFCC) (Davis and Mermelstein, 1980), perceptual linear prediction (PLP) (Hermansky, 1990), perceptual minimum variance distortionless response (PMVDR) (Yapanel and Hansen, 2008), power-normalized cepstral coefficients (PNCC) (Kim and Stern, 2012), etc. Regardless, “The overwhelming majority of speech recognition systems today make use of features that are based on either MFCCs [...] or features based on PLP” Stern and Morgan (2012, p. 218).

By calculating the MFCCs the spectral shape of the frequency distribution is maintained while the spectral details are discounted. Furthermore, the mel-scale, in addition to the logarithm, replicates the human auditory response – refer to Stern and Morgan (2012) for more information. Details of how the MFCCs are calculated are provided in Section 5.1.3.3 The PLP algorithm is in principle like MFCC but differs in implementation (for example, a Bark-scale is applied instead of a mel-scale). In fact, most ASR acoustic feature vectors are based on some sort of representation of the smoothed spectral envelope (Benzeghiba et al., 2007). By quantifying the spectral envelope, features are generally more robust with respect with acoustical variability, such as noise, relative to features based on the original periodogram alone. Additionally, this representation is much lower in dimensionality - typically the first 12 MFCCs are used for ASR. Kim and Stern (2012) have shown that PNCCs perform better than MFCCs and PLPs for signals with high reverberation or low signal to noise ratios. Before acoustic features are calculated, a pre-emphasis filter is often applied to boost higher frequencies. Additionally, often an additional layer of background noise removal is applied to the original speech signal; examples include spectral subtraction by Boll (1979), feature vector Taylor series (Moreno, 1996). As speech is not constant from frame-to-frame, some dynamic representation of the features is normally included. A common method is to include a first and second order derivative of each coefficient. In addition, some measure of the overall acoustic energy contained in each time frame is normally included. This results in 39 ‘standard ASR’ dimensions for each time frame (Stevens, 2000): 12 MFCC/PLPs and one energy measure for the current time frame; 13 for the first order derivative and 13 for the second order derivative.

The aim of ASR systems is to determine a word sequence from speech audio. The universal paradigm of determining a word sequence is as follows: The estimated word sequence  $\hat{\mathbf{W}}$  is equal to the maximum posterior probability (the maximum *a posteriori*) of a hypothesised word sequence given acoustic data. The posterior probability, in accordance with Bayes' rule, is equal to the probability of the word sequence irrespective of the acoustic data (called the 'language model') multiplied by the likelihood of the acoustic data given the hypothesised word sequence (called the 'acoustic model'). This can be expressed as follows (sometimes referred to as the fundamental equation of ASR):

$$\hat{\mathbf{W}} = \underset{\mathbf{W}}{\operatorname{argmax}} p_{\Gamma}(\mathbf{W}) p_{\Lambda}(\mathbf{X}|\mathbf{W}).$$

Where  $p_{\Lambda}(\mathbf{X}|\mathbf{W})$  is the acoustic model for acoustic features  $\mathbf{X}$ , conditioned on the word sequence  $\mathbf{W}$ .  $p_{\Gamma}(\mathbf{W})$  is the language model. The language model is biased towards word sequences which are more likely, for example, following the word '*the*', the probability of the next word being noun is high, whereas the probability of the next word being '*the*' is low.

Although the language model applied in ASR systems is imperative to performance, over the past few decades the main hindrance to improved ASR has been the acoustic model. The acoustic model estimates the probability of the acoustic data given the word sequence. Word sequences are typically split into individual phonemes or sub-phoneme units (start, middle or end of individual phonemes). In the English language there are about 42 phonemes and thus about 74,000 classes - this can be reduced down to about 10,000 using clustering techniques (Senior, 2017). The acoustic model is thus required estimate sub-phoneme units from speaker data. Considering the complexity of speech data given a variety of different speakers in noisy environments, this problem is highly complex. Thus has been best solved using ML with large datasets – Google's ASR systems contain about 3 million utterances from anonymised live traffic (Senior, 2017). Up until 2010, the most successful acoustic models applied hidden Markov models (HMMs) combined with Gaussian mixture models (GMMs). As of 2010 however the application of deep neural networks (DNNs) were shown to significantly outperform the probabilistic approach of GMM-HMM, culminating in a resurgence in ASR. Progress has been helped by a combination of increasing processing speeds, access to larger datasets and interest in developing ASR in mobile devices (Yu and Deng, 2014, Li et al., 2015).

The optimum selection of acoustic features is dependent on the acoustic model and vice versa. The 'standard ASR' dimensions summarised above are a typical selection for GMMs. This is because GMMs do not perform well with large feature spaces. DNNs however have been shown

to eliminate the need for such hand-crafted feature engineering and perform well using 'raw' features like the original waveform. The speech waveform has been used as features by Tüske et al. (2014) and Hoshen et al. (2015) for DNN acoustic models and shown to produce excellent recognition results: "Experiments on a simulated multichannel dataset show that the proposed acoustic model [DNN using 'raw' waveforms] outperforms a DNN that uses log-mel filterbank magnitude features under noisy and reverberant conditions" (Hoshen et al., 2015, p. 1)

### *3.3.4 Combustion Acoustics*

As mentioned in Section 2.3.2.6, the most applicable application of ML techniques in combustion acoustics was performed by Sanz et al. (2008). Sanz et al. (2008) presented a "proof-of-concept study" utilising ML to estimate combustion related parameters of a combustion system from acoustics. The combustion system of interest was an industrial furnace burning methane with a fixed equivalence ratio of 0.88. The class of interest in this study were NO<sub>x</sub> emissions and the air distribution between primary and secondary registers. Note, the air distribution between primary and secondary registers was expressed as a fraction of secondary air over the total air flow (referred to as AR). The features used to estimate NO<sub>x</sub> emissions and AR were six frequency bands calculated using Welch's method: 14-25; 25-45; 45-81; 81-146; 146-263; 263-473 Hz. There were 400 instances investigated with 20 variations in NO<sub>x</sub> from about 14 - 42 ppm. NO<sub>x</sub> emissions were impacted primarily by adjusting the AR, and in part by adjusting the swirl numbers (S1 and S2). The training / testing strategy applied was the holdout method, with 75% of data used for training and 25% used for testing. The only ML technique reported was ANNs, the architecture of which had one hidden layer. Regularisation and early stopping techniques were applied to avoid over-fitting. The resultant ANN could predict NO<sub>x</sub> with 0.96% 'root-mean-absolute-error' (one would assume this is a typo and it was the mean of the 'relative-absolute-error').

The ML methods and testing procedures employed by Sanz et al. (2008) appear to be following the expected standards: the training and testing accuracies aligned well, suggesting over-fitting was avoided; regularization methods were implemented and training of the ANN only took 40 epochs; the feature space applied had a low dimensionality, signifying no issues regarding the 'curse of dimensionality'. All suggesting correlations were present between acoustics and the predicted parameters. However, it would have been better if more than one ML method was reported to cement the analysis. In addition, the training and testing strategy employed was not very thorough, considering the small number of instances used, bootstrap aggregation would

have been very suited to this problem. Although it has not been performed it seems that NO<sub>x</sub> could be easily predicted from S1, S2 and AR as input vectors without the need for pressure fluctuations, although it may be the case that these variables cannot be determined during operation. As mentioned in Section 2.3.2.6, the primary weakness of this study lies in the presumed relationship between combustion acoustics and NO<sub>x</sub>: it could be argued that the acoustic variations observed were caused by varying AR alone and not due to varying combustion noise; cold flow recordings or results from the downstream microphone could have shed light on this. Additionally, potentially insightful combustion parameters were not varied, these included equivalence ratio and fuel type, doing so may have been of interest in relating combustion acoustics to various combustion parameters.

Tan et al. (2003) developed a hybrid neural network to detect and monitor slag deposits in a pulverised-coal fired combustion rig from combustion acoustics and infra-red (IR) emissions. Slag deposits can severely impact the stability of the burner and thus should be monitored and if possible size predicted. This study created two artificial slag deposits of differing sizes and aimed to determine the deposit class from a combination of combustion acoustics and IR emissions – resulting in three class values. The hybrid neural network (HNN) applied consisted of two layers: a self-organising map (SOM), to reduce the number of dimensions and visualise the data; and a radial-basis-function neural network (RBFNN), to map inputs to a class value. The SOM reduces dimensions of the original space to the number of neurons defined in the application of the SOM, normally this a 2D grid – in essence data points that are nearby in the higher-dimensional space will also be nearby in the SOM. The RBFNN is a supervised ML algorithm to map outputs of the SOM to class value probabilities, similarly to the description of an ANN given in Section 3.2.2.3 but with RBFs as activation functions. The study applied the SOM as a visualisation tool and discovered the three class values were highly clustered using either acoustic features or IR features. However, application of features from both sensors allowed classes to be segregated. Acoustic and IR features consisted of: normalised frequency components from 0-1000 Hz; the entropy of the power spectral density; the frequency centroid; and the shape factor (standard deviation/mean). In total 13 features were used for IR data and 15 for acoustic data. About 20-30 instances were available for each class, the instances were split 50:50 for training and testing (holdout method). Using both IR and acoustic features, the HNN returned classification accuracies in the range of 99-100 %. This was independent of coal type for the two coal types investigated. Note, coal feed and primary air supply rates were held constant for all data collected; secondary air rates were varied, changing the excess air percentage from 1.3-21.6%.

The application by Tan et al. (2003) highlighted that information contained in combustion acoustics and IR radiation can be correlated with variations in burner exit shapes (slag deposits). Again, the study is not without its criticisms and should be considered proof of concept for practical application of slag detection devices. As stated by the authors: "Further work is required to address additional questions, such as the ability of the system to be able to classify 'real' unsymmetrical eyebrows as well as the need to investigate the effect of a wider range of coals". Similarly to Sanz et al. (2008), the training and testing strategy employed could have been improved, with such a low number of instances (estimated to be below 100), k-fold CV or bootstrap aggregation should be considered. Again, the dimensionality of feature data was not a concern for application of ML techniques. Of particular interest in the application by Tan et al. (2003) was the fuel independence for slag detection. Although only two fuel types were investigated, the potential of algorithms in determining combustion parameters of interest independently of fuel is relevant to the aims and objectives of the current study.

Studies which have aimed to detect, predict or actively dampen faults within combustion systems by utilising combustion acoustics and ML techniques include: Ortmann and Glesner (1998), Liu and Daley (1999), Blonbou et al. (2000), Sharkey et al. (2000), Kokanovic et al. (2006) and Bahri et al. (2016). This could be in the form of mechanical faults, combustion faults and combustion instabilities. As applied to internal combustion engines or gas combustion turbines.

Ortmann and Glesner (1998) developed ANN to help in the detection of knock in diesel engines using data from a pressure sensors. Note, knocking should be avoided as it is known to damage the engine. Tests were performed of this system for databases under almost 'on road' conditions by Ortmann et al. (1998). In-cylinder pressure data or accelerometer data can be used as a method of estimating one of three classes: no-knock, borderline knock and hard knock. Rychetsky et al. (1999) used 24 features from accelerometer data, including the amplitude, mean and variance of the first eight frequency bands. Rychetsky et al. (1999) found that the application of SVM, with polynomial and RBF kernels, performed knock detection better than ANNs. SVMs returned misclassification rates in the range of 1.5% whereas ANNs were in the range of 8.5%.

Sharkey et al. (2000) developed an early warning fault diagnostics system in diesel engines using pressure signals from cylinders. The faults under consideration were cylinder exhaust valve or cylinder fuel injector faults. The feature data used was the in-cylinder pressures every other revolution of the engine for 100 consecutive revolutions – 50 dimensions in total. Across all three classes, 3600 instances were available at various engine conditions. An ANN was

developed using a holdout method for training and testing. The ANN developed could correctly classify the fault 86% of the time. This considerably outperformed a decision tree algorithm and a human expert.

Bahri et al. (2016) used an ANN to estimate the combustion noise level within a homogeneous charge compression ignition (HCCI) engine from in-cylinder pressure signals. Of specific concern for HCCI engines is the onset of excessive noise due to the so-called ringing region. The ANN developed could predict the combustion noise level for the HCCI engine with less than 0.5% average error and thus could be applied within in a control loop to avoid the onset of exponentially increasing noise levels. To train the algorithm, pressure data at four crank angles was used, a 50:50 holdout method was applied with 200 instances.

## 4. Pilot Study

The purpose of the pilot study was to determine if within the system of interest (a domestic gas boiler) the operational equivalence ratio ( $\varphi$ ) can be predicted from combustion acoustics.

### 4.1 Introduction

As observed in Section 3.1.5, combustion acoustics appear to be correlated with  $\varphi$ . As such one might expect a similar correlation to exist for combustion acoustics produced within the combustion chamber of a domestic gas boiler. However, results reported in Section 3.1.5 were based on open systems; for open systems combustion acoustics originate predominantly from direct combustion noise sources and are not modified significantly by environmental factors. For closed systems (such as a domestic gas boiler) combustion acoustics will likely originate from a combination of direct and indirect combustion noise sources, in addition these sources are modified by the environment via resonant modes and acoustic feedback interactions (refer to Section 3.1.1). Thus, any correlation between combustion acoustics and  $\varphi$  within a practical system, such as a domestic gas boiler, are likely to be complex and difficult to determine. In addition, due to a multitude of background noises in boilers (fan noise, pump noise etc.), correlations between recorded acoustics and variations in  $\varphi$  are likely to be difficult to discern. However, as observed in Section 3.3, machine learning (ML) techniques are particularly useful in determining correlations in complex acoustic datasets. As such ML techniques were utilised to determine the correlations between combustion acoustics and  $\varphi$  for domestic gas boilers.

Supervised ML algorithms use example data (training data) to develop models relating input(s) to output(s). In this case the inputs are combustion acoustics (combined with other boiler noises) and the output is  $\varphi$ . The training data required comprises of recordings of the combustion chamber in addition to the  $\varphi$  value of the burn at the time of recording. Ideally the training data volumes would be as large as possible and cover all practical scenarios. For a unique boiler and operating mode, this includes all feasible gas types and all feasible values of  $\varphi$ . In addition to this, to ensure techniques could be applied irrespective of environment, additional training datasets would ideally also cover all feasible boiler component variabilities; boiler power outputs; boiler operating modes; and boiler failure modes. For the purposes of the pilot study various practical restrictions were imposed on the ideal training dataset.

In practical domestic gas boilers  $\varphi$  does not vary considerably, this is largely due to tight restrictions on gas type. As observed in Figure 7, if a wide range of gas types are delivered to a

boiler without a combustion control system,  $\varphi$  can vary from about 0.6 to 0.9. For the purposes of this pilot study a large range of  $\varphi$  was selected from 0.55 to 1.0. Such a large range was selected to increase the chance of observing variations in combustion acoustics due to varying  $\varphi$ . Additionally, to simplify the analysis the pilot study was limited to a single gas type and a single boiler operating in one mode. Such restrictions are not reflective of all practical scenarios but were considered sufficient for the purposes of the pilot study.

The focus of this pilot study was to determine if  $\varphi$  can be predicted from combustion acoustics and not to analyse the nature of such a relationship. As such the interpretability of ML algorithms tested were not prioritised. Regardless thorough testing methodologies were applied so that ML results were indicative of true predictive performance.

#### *4.1.1 Hypothesis and Assumptions*

The basic working hypothesis at the start of the pilot study was: For a single gas type a relationship exists between combustion acoustics emanating from the combustion chamber of a domestic gas boiler and the operational  $\varphi$  of the burn.

Several assumptions have been made in developing a method to test such a hypothesis; these include:

- Combustion acoustics originate within the combustion chamber (direct combustion noise) and directly downstream of the combustion chamber (indirect combustion noise).
- Variations in combustion acoustics are detectable using a contact or contactless transducer on the surface or within the vicinity of the domestic boiler.
- Varying the  $\varphi$  of combustion induces no additional acoustic variations within the system beside for variations in combustion noise.
- The relationship between combustion acoustics and  $\varphi$  can be determined by applying machine learning algorithms on acoustic features.

A method to test this hypothesis will be given followed by the results. Conclusions drawn from the pilot study will then be summarised along with any uncertainties and outstanding questions. How these results fit within the larger context of this study will then be discussed followed by an updated hypothesis.

## 4.2 Method

### 4.2.1 Setup

For this pilot study a Worcester Bosch Greenstar 28i Junior condensing combi boiler (Worcester Bosch Group, 2013) was used. The boiler is set-up during manufacture so that, for G20 gas,  $\varphi$  equals 0.88 for the minimum power output (7.38 kW) and 0.93 for the maximum power output (28 kW). The variation of  $\varphi$  with power output is by-design and achieved via a differential pressure in the pneumatic gas valve. Such variation with  $\varphi$  is desirable due to how emission and efficiency test are defined in EN 15502-1 (NBS, 2012).

The combustion chamber of the boiler exists within the WB6 primary heat exchanger - nicknamed the 'kebab' heat exchanger. The heat exchanger is a truncated cone with water spiralling around the outside of the combustion chamber. Returning water is pumped in from the bottom of the heat exchanger and leaves at the top. Heat is absorbed from the condensing of exhaust gases at the bottom of the heat exchanger and from the flame as the water circulates vertically. Figure 19 shows the aforementioned heat exchanger, highlighting the positions of the burner, air/gas inlet, exhaust flue and sump. A blue print for the heat exchanger has been provided in Appendix 9.1 for the interest of the reader.

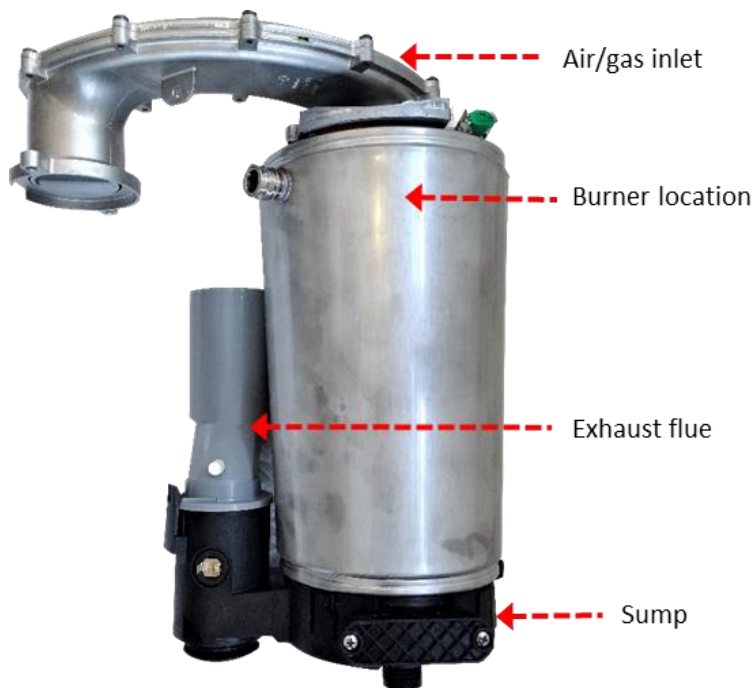


Figure 19 Picture of the WB6 heat exchanger with labels indicating components of interest

The burner in the WB6 heat exchanger is a cylindrical burner with thousands of 1mm diameter holes surrounding the 21cm circumference. This burner has been pictured below in Figure 20.



*Figure 20 Picture of the burner used in the WB6 heat exchanger*

The boiler was operated in central heating mode at a constant load. The load was the maximum output of the boiler (28 kW) which was equivalent to a pre-mix fan motor speed of  $108 \pm 1$  Hz. The gas used for the duration of the pilot study analysis was G20 i.e. 100% CH<sub>4</sub>. The boiler was placed in an environment whereby the surrounding noise was largely constant and minimised where possible.

A test-rig controlled the flow of water entering and exiting the heat exchanger (average of 19.3 L/min with 0.11 standard deviation) and the gas meter pressure (average of 20.0 mbar with less than 0.2 standard deviation). Depending on the power output of the flame, the return flow temperature to the primary heat exchanger varied from 30-35 °C with an average of 32.5 °C and standard deviation of less than 1 °C.

To vary the  $\phi$  of the burn several options were available, they included: adjusting the rate of incoming gas while keeping the rate of incoming air constant; adjusting the rate of incoming air while keeping the rate of incoming gas constant; or varying the quality of gas entering the combustion chamber. For the purposes of the pilot study the gas type was held constant while adjusting the rate of incoming gas. This option was selected for a number of reasons: firstly, because it was a simple operation to adjust the gas valve partition on the pneumatic gas valve; secondly because said adjustment in theory had no acoustic impact on any other boiler component; thirdly because varying gas composition by incremental values was not an option with the equipment available; and finally, because adjusting the proportion of gas to air in said manner is almost directly comparable to adjusting the quality of G20 gas.

To determine the operational  $\varphi$  of hydrocarbon oxidation one can perform a calculation based on concentrations of exhaust gases. As explained in Section 2.3.1.2, for a lean hydrocarbon mixture, an accurate calculation of  $\varphi$  can be made from the mole fraction of CO<sub>2</sub> ( $X_{CO_2}$ ) in dry exhaust gases. For example, for G20 gas  $\alpha=0.10482$  and  $\beta=0.104$  in Equation 4.1:

$$\varphi = \frac{X_{CO_2}}{\alpha + \beta X_{CO_2}} \quad (4.1)$$

Thus, the concentration of CO<sub>2</sub> species in dry exhaust gases was used as a method of determining the operational  $\varphi$  of the combustion chamber. To determine the concentration of CO<sub>2</sub> species in dry exhaust gases a gas analyser was used. The gas analyser was a Siemens Ultramat 23 and used Infrared Chromatography to determine the concentration of CO<sub>2</sub> species. The analyser also reported the concentration of CO and NO<sub>x</sub> species. Data from the gas analyser was logged every second.

For the purposes of the pilot study the largest range of  $\varphi$  values possible for testing was selected. A large range was selected to magnify any correlations between combustion acoustics and  $\varphi$ . Without causing operational failure in the boiler the largest range was determined to be approximately 0.55 to 1.00. Per Equation 4.1, for G20 gas, this corresponds to CO<sub>2</sub> percentages from about 6 to 12%. Note, that within most domestic hot water boilers, if the operational  $\varphi$  was less than 0.6 or greater than 0.9, emissions would likely exceed regulations (see Section 2.2.2). Thus, values far above 0.9 and below 0.6 are not expected to occur in practice.

To measure combustion acoustics two microphones were attached to the boiler in various locations and audio recorded at a sampling frequency of 44.1 kHz. Audacity software was used to make digital recordings of both microphones. Microphone 1 was a piezoelectric transducer contact microphone developed by Barcus-Berry for professional recording of musical instruments. Microphone 2 was a contactless omnidirectional condensing microphone developed by DPA Microphones for application in voice recording. Both microphones required preamplifiers of various types for optimal operation. The Barcus-Berry manufacturer supplied a proprietary preamplifier specific to the contact microphone which required one 9V battery to run. Microphone 2 required a 48 Volt phantom power supply to run.

Various positions for said microphones were tested. As seen in Figure 21 Position 1 was Microphone 1 on the surface of the primary heat exchanger, so as to be in closest physical proximity to the burner. Position 2 was Microphone 1 on the surface of the flue outlet, so as to be strongly coupled with the combustion chamber. Position 3 was Microphone 2 about 5cm in-

front of the top centre of the boiler with the cover of the boiler off. Position 4 was Microphone 2 protruding about 5cm below the flue opening.

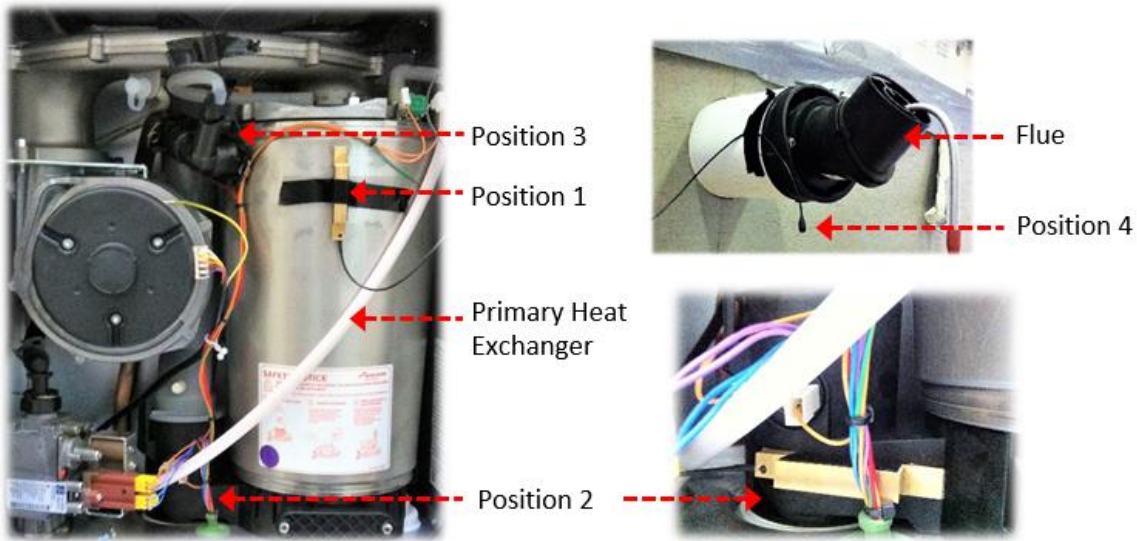


Figure 21 Pictures highlighting the various positions of Microphones 1 and 2

#### 4.2.2 Experiments

Three datasets were collected during the pilot study to test different positions of Microphones 1 and 2 and to test continuous and static changes in  $\varphi$ . For Datasets 1 and 2 incremental changes were made in  $\varphi$ , for Dataset 3  $\varphi$  was varied continually.

Dataset 1:

- Microphone 1 was placed in Position 1 and Microphone 2 in Position 3. The boiler was turned on and set to meet a constant central heating demand at maximum power output. A manual adjustment was made to the ratio adjuster on the gas valve so that the CO<sub>2</sub> concentration, as read from the exhaust-gas spectrometer, was approximately 12%. Once the CO<sub>2</sub> reading settled the microphones were set to record simultaneously for a duration of two minutes. The data from the test rig and exhaust-gas spectrometer was also logged during this period. One minute after the recording finished, another two-minute recording was made; this process was repeated until four separate two minute recordings had been made. The ratio adjuster was then manually adjusted until a drop of 0.5% was observed in the CO<sub>2</sub> concentration. Once the CO<sub>2</sub> levels settled another four sets of two minute recordings were made. This process was repeated until the CO<sub>2</sub> concentrations reached

approximately 6%. This concluded the range of air to gas ratios of interest. Note that during experiments the boiler was restarted on multiple occasions to replace gas bottles.

Dataset 2:

- This dataset was the same as Dataset 1 however Microphone 1 was placed in Position 2 and Microphone 2 in Position 4.

Dataset 3:

- For this dataset, manual manipulations to the air to gas ratio were made constantly during audio recordings. The microphones were positioned so that Microphone 1 was placed in Position 2 and Microphone 2 in Position 4 (the same as Dataset 2). The air to gas ratio was set by manipulating the ratio adjuster on the gas valve so that the CO<sub>2</sub> concentration was at 12%. The boiler was set to run at a fixed power output. The microphones were then set to record simultaneously. The data from the test rig and exhaust-gas spectrometer was logged. The ratio adjuster on the gas valve was then manually manipulated slowly over approximately a five-minute duration until the CO<sub>2</sub> concentration was at 6%. This was repeated three times going from 6% CO<sub>2</sub> concentration to 12% or vice versa.

### 4.2.3 Analysis

The first step in the analysis was to convert acoustic data gathered into features which summarise the acoustic characteristics of interest. After this the feature space considered could be reduced via analysis (visual or otherwise) of how the acoustic data varied with the quantity of interest, i.e.  $\varphi$ . ML algorithms could be trained and tested on the reduced feature space.

It was the aim of the investigation to use tonal variations of the acoustic data as a basis to correlate combustion acoustics with  $\varphi$ . This was because tonal features are relatively robust compared with features based on variations in loudness. Consequently, the time-varying acoustic signal was converted into normalised frequency components using Welch's method (Welch, 1967). Welch's method overlaps segments of a signal, applies a window function, calculates the discrete Fourier transform (DFT) of the windowed functions and averages out the resultant DFTs over a fixed interval. Once the average periodogram for the one second interval was calculated, it was normalised by dividing it by the mean energy per frequency bin. As such, if one second interval was on average louder than the next, this would not be discernible from the feature vector, i.e. loudness was not used as a feature.

To reduce the feature space used when applying ML algorithms, visual analysis of the tonal qualities of the signal was performed. This was done by plotting spectrograms for the data collected in Dataset 3. Those frequency ranges that appeared to vary with  $\varphi$  were used as feature vectors for further analysis.

Once the feature vectors had been calculated and filtered, ML algorithms could be tested. For the pilot study a range of ML algorithms were tested, the range represents some of the fundamental methods of machine learning for regression and classification problems. The ML algorithms tested included: linear regression (LR); logistic regression (LGR); k-Nearest-Neighbour (kNN); C4.5 decision trees; and M5P decision trees. For application of these methods,  $\varphi$  was treated as both a discrete value and a continuous value. For the discrete representation,  $\varphi$  was binned into twelve distinct classes, for the continuous representation  $\varphi$  was kept as the original value as calculated by Equation 4.1.

A thorough method for testing the predictive accuracy of a machine learning algorithm on a given dataset is to apply 'stratified  $k$ -fold cross-validation (CV)'. For completeness multiple iterations of stratified  $k$ -fold CV were applied. Refer to Section 3.2.4 for a description of  $k$ -fold CV.

## **4.3 Results**

Over a period of two days' acoustic, flue-gas and test-rig data was collected from a gas-fired domestic hot-water boiler. In total, approximately 100 minutes of acoustic data was collected for each microphone in each position for a range of  $\varphi$  values ranging from 0.55 to 1.00 (CO<sub>2</sub> percentages ranging from 6% to 12%). This data was used to establish if, in the setup outlined in Section 4.2.1, a correlation existed between combustion acoustics and the operational  $\varphi$ .

### *4.3.1 Visual Analysis*

Spectrograms were used to visually analyse the acoustic data gathered. Note, a spectrogram shows the energy contained within the frequency components of an acoustic signal over time by applying successive discrete Fourier transforms (DFTs) to the signal. The signal was split into discrete time windows of one second, overlapped with neighbouring windows by 70% and windowed using a Hamming window. A time window of one second was applied because the signal was slowly varying in time and frequency clarity could be prioritised. The number of DFTs

calculated for each window was selected to maximise the visual clarity of the resultant spectrograms.

For Dataset 3 changes in  $\varphi$  were made continuously during recordings and thus serve as a useful dataset to analyse visually in the form of spectrograms. To help highlight acoustic variations within spectrogram images, Gaussian smoothing was also applied. As seen in Figure 22 the Gaussian smoothed spectrogram of the acoustic signal appears to vary with  $\varphi$  for both microphones in the frequency range of 1.5-3.5 kHz. All data from Dataset 3 appears to show the same variations with  $\varphi$ . Note, that observations of other frequency components did not appear upon visual inspection to show correlations with  $\varphi$ .

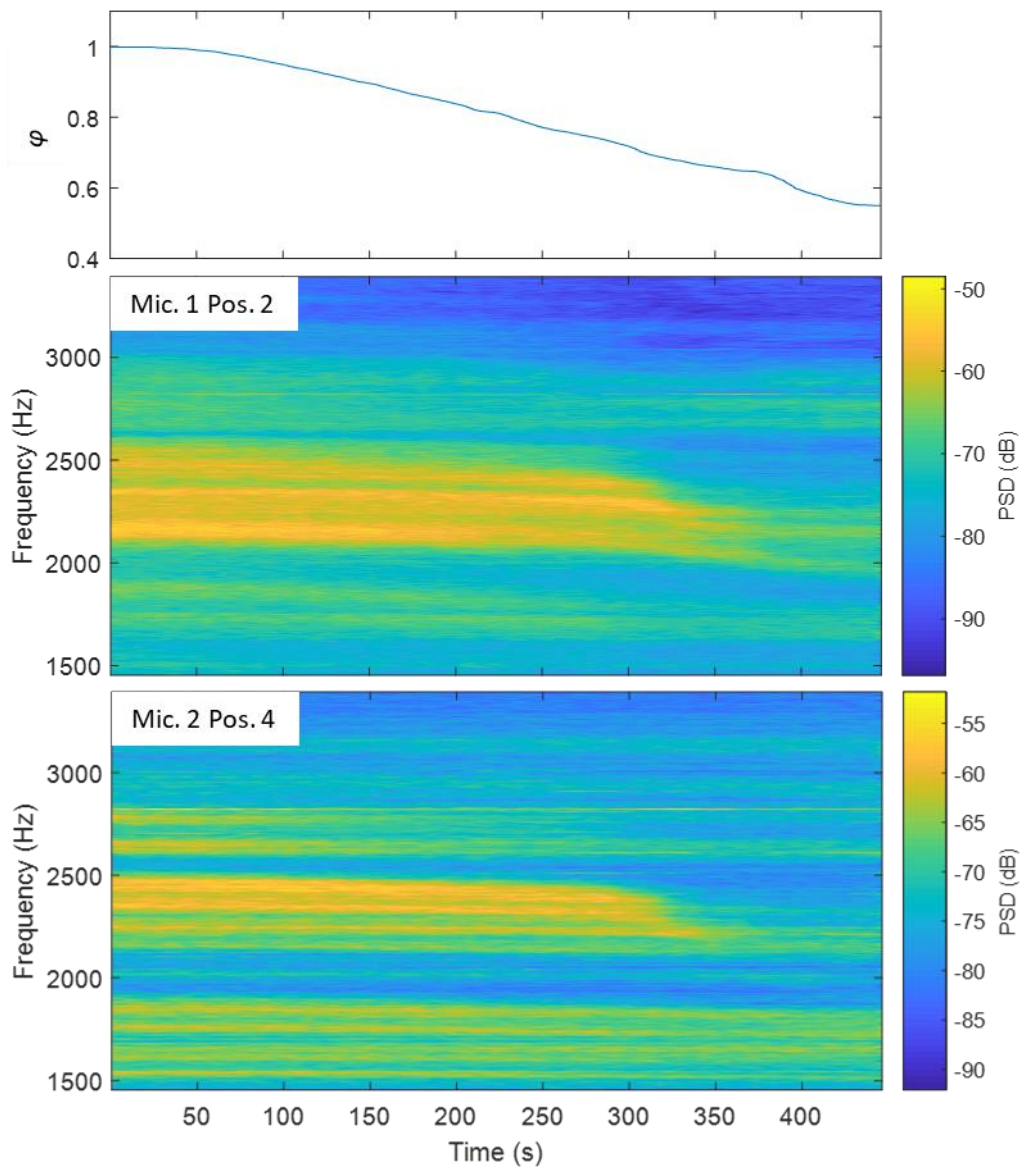


Figure 22 Spectrograms of acoustics from Microphone 1 and Microphone 2 while sweeping through a range of equivalence ratios from 1 to 0.55

From this analysis, it was conjectured that frequency components in the range of 1.5-3.5 kHz was correlated with  $\varphi$ . To analyse this potential correlation, the 1.5-3.5 kHz normalised frequency components (NFCs) for Datasets 1 and 2 was extracted using Welch's method and compared with the value of  $\varphi$ .

To calculate the NFCs, the signal was first down-sampled from 44.1 kHz to 8.82 kHz (to save on processing without breaching sampling theorem) and Welch's method was applied with a Hamming window length of 0.1 seconds, overlap of 60%, 900 DFTs and an averaging period of one second. Note, Welch's method is comparable to calculating a spectrogram but with an averaging window. Once the average periodogram for each one second period had been calculated, it was normalised by dividing it by the mean energy per frequency bin - accordingly a value of one represented the mean. This analysis resulted in 205 normalised frequency bins from 1.5-3.5 kHz for each second of data collected. There were 5760 seconds of data collected for each dataset and for every second, the data was linked with the CO<sub>2</sub> concentration at that time interval (per the log from the gas-analyser). From the CO<sub>2</sub> concentration  $\varphi$  was calculated from Equation 4.1. Consequently, for Datasets 1 and 2 there were 5760 instances of acoustic data (NFCs) matched with the variable of interest for prediction ( $\varphi$ ).

Figures 23 and 24 below show the result of applying Welch's method for both microphones in Dataset 2. The frequency distributions shown in the figures have been averaged across periods where  $\varphi$  varied by less than 1% i.e. the figures show the average acoustic distribution of the 12 values of  $\varphi$  tested. As observed in the figures, the frequency distribution varies depending on the value of  $\varphi$  and appears unique for each range of  $\varphi$  investigated. For both microphones the frequency variations with  $\varphi$  show similar patterns. To determine the relationship between the frequency distribution of the signal and  $\varphi$  machine learning algorithms were applied.

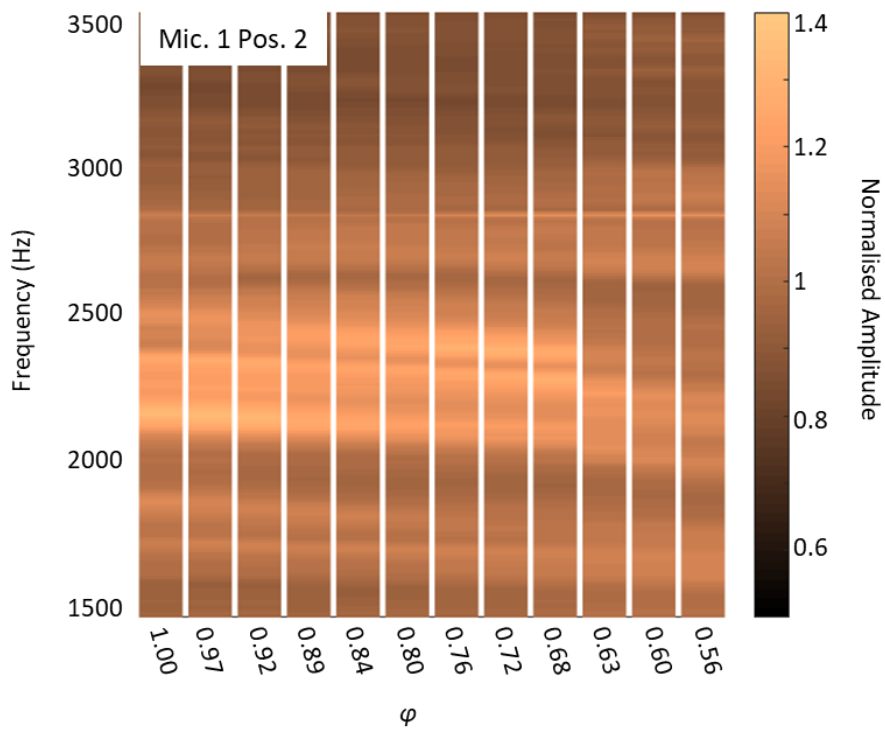


Figure 23 Averaged spectrogram for each interval of  $\phi$  investigated - Microphone 1 in Position 2. The spectrogram has been normalised with respect to the mean amplitude for that interval

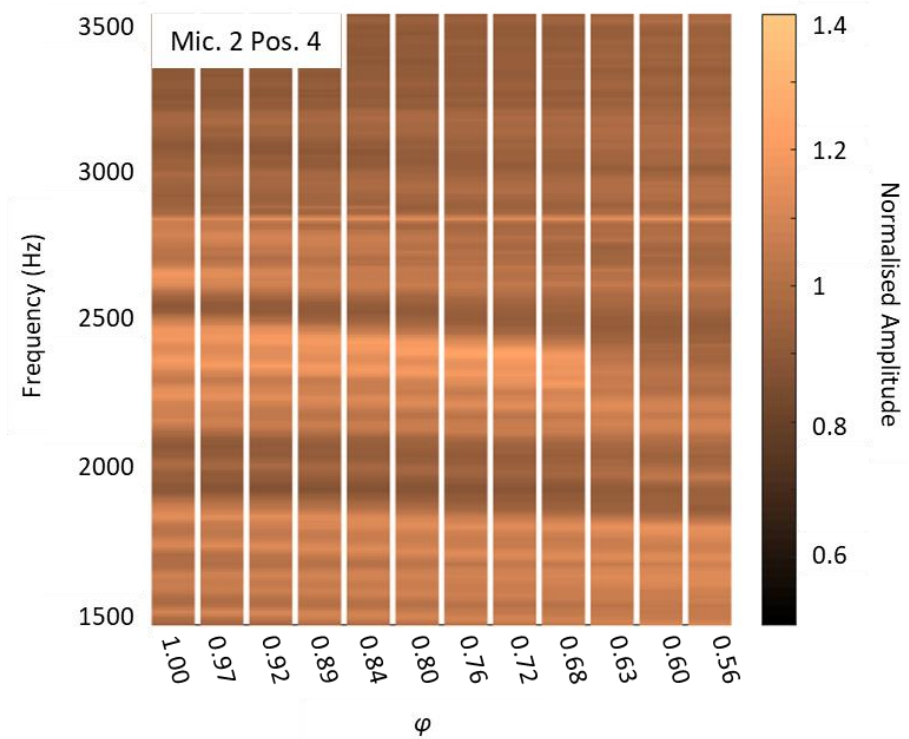


Figure 24 Averaged spectrogram for each interval of  $\phi$  investigated - Microphone 2 in Position 4. The spectrogram has been normalised with respect to the mean amplitude for that interval

### 4.3.2 Machine Learning

Defining  $n$  as the number of example data points (aka instances),  $d$  is the number of frequency intervals (aka dimensions) and  $\mathbf{A}$  as the normalised amplitude vector as calculated from Welch's method: for Datasets 1 and 2  $n = 5760$ ,  $d = 205$  (number of frequency bins) and  $\varphi$  ranges from 0.56-1.00. The aim of the investigation was to use the data collected to find a function  $\mathcal{F}$  that relates combustion acoustics to  $\varphi$  i.e.

$$\mathcal{F}(\mathbf{A}) \cong \varphi : (\mathbf{A}^{(1)}, \varphi^{(1)}), \dots (\mathbf{A}^{(n)}, \varphi^{(n)}). \quad (4.2)$$

From Section 3.1 the acoustic distribution is dependent on changes occurring to the state of combustion, one such state indicator being  $\varphi$ . Thus  $\mathbf{A}$  is the dependent variable and  $\varphi$  the independent variable. There may be no exact function that describes the relationship between combustion acoustics and  $\varphi$ , however, if correlations exist, supervised machine learning is very suited to developing approximate functions to such a problem (see Section 3.3). By splitting the dataset  $(\mathbf{A}^{(1)}, \varphi^{(1)}), \dots (\mathbf{A}^{(n)}, \varphi^{(n)})$  into training  $(\mathbf{A}^{(T)}, \varphi^{(T)})$  and testing data  $(\mathbf{A}^{(t)}, \varphi^{(t)})$ , machine learning algorithms can be developed and tested for their ability to predict  $\varphi$  for an unknown acoustic signal.

In this study stratified 10-fold CV was performed ten times as described in Section 3.2.4. The output was the average predictive accuracy of an algorithm and the variance associated with that average. Thus, for each iteration,  $(\mathbf{A}^{(T)}, \varphi^{(T)})$  was the randomly selected training set containing 90% of the data and  $(\mathbf{A}^{(t)}, \varphi^{(t)})$  the remaining test data.

The application of machine learning algorithms depends on the data-type of the variable being predicted ( $\varphi$  in this case); if the data-type is numeric the problem is a so-called regression problem, if the data-type is categorical the problem is a so-called classification problem. For Datasets 1 and 2  $\varphi$  values could be treated as categorical or numeric. For categorical treatment, the 12 distinct values of  $\varphi$  tested were converted to labels. Some loss of accuracy occurred during this process as  $\varphi$  was not constant during each of the 12 intervals tested. However, variations in  $\varphi$  were less than 1% during recordings (for three standard deviations) and thus the loss of accuracy in predicting  $\varphi$  was of the order of 1% when comparing regression results with classification results. As a classification problem, there were 480 instances of each of the 12 classes of  $\varphi$ . As a regression problem, the value of  $\varphi$  was in accordance with Equation 4.1 and no rounding was made.

As described, the features extracted for this analysis were the normalised amplitude components of 205 frequency bins from 1.5-3.5 kHz. These features were extracted every second of the acoustic recordings (5760 seconds for Datasets 1 and 2). Also, analysed here are the same features but smoothed over a nine second window. The smoothing function takes the current one second interval frequency bin and averages across those of the previous four seconds and the next four seconds (nine second window); this is performed for every frequency bin.

In Table 2 the results of the machine learning algorithms described for all microphones in all positions. The table also presents the results of one second feature data with and without nine-second time smoothing applied. For each algorithm, the average and standard deviation of ten iterations of 10-fold CV are given. For the regression problem, the root-relative-squared-error (RRSE) was reported, for the classification problem the percentage correct was reported. The percentage correct represents the expected percentage of classes correctly predicted by the algorithm. The RRSE is the root of the total squared error of the prediction normalised by the total squared error of a simple predictor (predicting the average) – refer to Equation 3.5.

One second acoustic data		Regression			Classification		
		kNN (k=5)	LR	M5P	kNN (k=5)	LGR	C4.5
		RRSE (%) (standard deviation)			Percentage correct (standard deviation)		
Mic. 1	Pos. 1	0.89 (0.11)	7.71 (0.26)	7.00 (2.29)	99.2 (0.3)	92.3 (0.5)	90.1 (1.4)
	Pos. 2	2.84 (0.28)	9.25 (0.27)	7.37 (0.65)	98.1 (0.5)	90.2 (1.7)	89.2 (1.3)
Mic. 2	Pos. 3	16.42 (0.81)	27.66 (1.18)	25.11 (2.22)	84.5 (1.8)	76.3 (3.4)	77.2 (3.2)
	Pos. 4	3.61 (0.28)	9.3 (0.34)	7.46 (0.55)	96.4 (0.8)	89.1 (1.7)	90.0 (1.2)
One second acoustic data with nine second smoothing		Regression			Classification		
		kNN (k=1)	LR	M5P	kNN (k=1)	LGR	C4.5
		RRSE (%) (standard deviation)			Percentage correct (standard deviation)		
Mic. 1	Pos. 1	0.26 (0.03)	3.45 (0.21)	4.95 (2.3)	100.0 (0)	99.8 (0.1)	99.3 (0.1)
	Pos. 2	0.19 (0.01)	4.19 (0.19)	5.07 (3.2)	100.0 (0)	99.6(0.3)	99.1 (0.4)
Mic. 2	Pos. 3	0.52 (0.15)	14.82 (0.91)	11.15 (2.62)	100.0 (0)	92.1 (1.2)	93.1 (1.1)
	Pos. 4	0.19 (0.01)	4.70 (0.22)	2.81 (0.59)	100.0 (0)	99.9 (0.1)	99.0 (0.4)

Table 2 Prediction results of a range of different machine learning algorithms to the datasets analysed. Results reported are the consequence of applying 10-fold cross-validation

For Microphone 1, for one second time intervals, Position 1 was shown to be more accurate relative to Position 2. Once a moving average was applied to the acoustic data the differences in accuracy between the two positions became arbitrary. Accordingly, it could be presumed that the data gathered from Position 1 contains less noise with respect to Position 2. Note, that because Position 1 was in contact with the hot-surface of the heat exchanger, it may not be advisable to continue to rely on the position because:

- a) the surface temperature could impact the data recorded as the response of any piezoelectric microphone will vary with temperature and;
- b) the contact microphone may become damaged over time due to the surface temperature.

For Microphone 2, Position 4 produced significantly better results compared to Position 3. Position 3 was at the flue extraction point and separated from all boiler components by an artificial wall; Position 4 was directly in-front of the boiler. Position 4 therefore detected more noise from the boiler components relative to Position 3 (this can be heard by listening to recordings). Such boiler component noises include the pre-mix fan motor, electrical transistors and the circulation pump (Neeld et al., 2016). At Position 3 the noises detected were dominated by the air-flow from the combustion chamber and out of the flue. Such a result suggests that to improve predictions in  $\varphi$  from boiler acoustics, acoustics which are coupled closer to the air flow in the combustion chamber are more beneficial or that acoustics which are less coupled with other boiler component noises are more beneficial. In other words, the correlation between the acoustic data recorded and  $\varphi$  are more apparent when the acoustics are more related to the noises from the combustion chamber relative to other boiler component noises. This is a positive result with respect to the initial hypothesis and can be used to help quell doubt on concern that the correlations determined by machine learning algorithms are associated with changes in non-combustion related acoustic variations.

Comparing Microphone 1 with Microphone 2 in Position 4, the predictive accuracy of the resultant algorithms were very similar. This suggests that for the experiments performed, a contact microphone serves no observable benefit over a contactless microphone. This may not be true if external background noises were increased as such noises would likely be more readily detected by a non-contact microphone.

Applying a nine second moving average to the frequency bin data increased the predictive accuracy of all algorithms. The increase in predictive accuracy was less notable for kNN when

the value of  $k$  was increased. Increasing the value of  $k$  in the kNN algorithm has the effect of averaging the results of multiple data points in the feature space, thus it is not surprising that increasing  $k$  and increasing the time-smoothing had a similar outcome. Regardless, time-smoothing appeared to help with the results of all machine learning algorithms regardless of changes in parameters. It appears therefore that acoustic data one second in length contains some additional acoustic variation which is not directly associated with  $\varphi$ . Any practical scenario of  $\varphi$  variance due to gas composition changes would occur over a period of minutes and not seconds. Thus, responses over the period of one second would likely never be required and time-smoothing should be used where beneficial.

Out of all the algorithms tested, kNN produced the best results. Why this is the case is not clear. Due to the sparsity associated with high-dimensional spaces, kNN approaches can suffer from the curse of dimensionality and thus such an approach should be treated with caution. However, as other predictive approaches such as decision trees and linear regression show very positive results, it is unlikely that the positive predictive results observed are not due to a misapplication of kNN. Many algorithms used throughout acoustic related machine learning tasks were not tested during this pilot study. They include artificial neural networks, Gaussian mixture models and support vector machines. Testing these algorithms would indicate the potential of using machine learning on this problem.

#### *4.4 Conclusions*

Acoustic data gathered from a domestic gas boiler was used as an accurate predictor of the equivalence ratio ( $\varphi$ ) of the combustion system. This was for the limited scenario when  $\varphi$  varies in 12 steps from 0.56-1.00 and the boiler burns a single gas type (G20) at a set power output. The acoustic data was attained using a contact microphone on the surface and sump of the primary heat exchanger; and by using a contactless microphone placed near the extraction flue outlet.  $\varphi$  was predicted from boiler acoustics by applying machine learning. Machine learning algorithms were trained on the 1.5-3.5 kHz normalised frequency components of the system. These features were calculated in one second intervals however time smoothing was shown to improve the results. Machine learning algorithms tested included decision trees, linear regression, logistic regression and kNN. The most accurate result was obtained using the kNN algorithm (with  $k=1$ ), this gave a predicted RRSE of 0.19% after applying  $k$ -fold cross-validation over multiple iterations.

The  $\varphi$  values investigated in this pilot study cover a large range from 0.5 to 1.0 with only 12 steps between. The large range was selected to exaggerate any acoustic variation, if present. The acoustics from the boiler for these 12 values of  $\varphi$  appear distinct from the accuracies of the algorithms developed. However, for practical cases the  $\varphi$  range could vary continuously from about 0.7 to 0.9 at most, in addition variation may be caused by variations in gas composition. Thus, the results of the investigation presented here are only representative of the data gathered and should not be extrapolated to realistic scenarios. Several uncertainties and unanswered questions have been highlighted below to guide future work.

#### *4.5 Uncertainties and Unanswered Questions*

There are many uncertainties and unanswered question associated with this pilot study. Below these are listed out, explained and solutions proposed. These solutions will feed into the main study:

- Are variations observed in acoustic signals emanating from changes in combustion acoustics?

From the pilot study correlations between the acoustic data gathered and  $\varphi$  have been observed visually, and indirectly discerned from the accurate predictive results of machine learning algorithms. However, it is still uncertain that the acoustic variations observed are due to variations in combustion acoustics. In other words, the argument could be made that the origin of acoustic variation is due to some arbitrary system component not associated with variations in combustion acoustics, thereby invalidating the premise of the investigation. The system in question contains many potential sources of noise from component noise (fan, pump, diverter valve etc.) to flow noise (water or gas). As shown in a previous study for this boiler (Neeld et al., 2016), the premix fan appeared to be the largest contributor to noise, however this component cannot easily be isolated from combustion noises as they occur in unison. One solution is to measure and subtract the so-called cold-flow noise. The cold-flow noise would be the noise produced when the boiler is in normal operation but without combustion being present i.e. all noise sources except combustion noise. The cold-flow measurements could then be subtracted from the boiler acoustics (via spectral subtraction) during normal operation, thus isolating combustion noise (albeit combustion noise enhanced by the environmental conditions induced by boiler operation) and testing thoroughly if the acoustic variations observed are indeed due to variations in combustion acoustics. During these cold-flow recordings all boiler components should be

operating as before but without a flame present. To test this further, experiments should be performed on a different boiler. If after these experiments, analogous correlations are found between the acoustic data and  $\varphi$ , then it is likely acoustic variations are indeed due to variations in combustion acoustics.

- Are acoustic correlations due to the impact of a varying  $\varphi$  or the impact of varying the proportion of gas?

As discussed in Section 3.1.5, it is expected that changes in  $\varphi$  would impact combustion acoustics due to changes in the chemical kinetics of the flame. In this pilot study  $\varphi$  has been varied by increasing or decreasing the proportion of gas entering the combustion chamber while holding the total volume of gas and air mix constant (constant pre-mix fan speed). Such variation is potentially acoustically different compared to altering  $\varphi$  by varying the proportion of air entering the system or by altering the calorific content of the gas entering the system. To test if correlations between acoustics and  $\varphi$  are due to variations in chemical kinematics as hypothesised, it would be thorough to perform experiments for all other ways of varying  $\varphi$ . Analysis of this data would reveal the relationship between combustion acoustics and  $\varphi$  for various scenarios and a common relationship may be established.

- Are the algorithms developed generalising well?

By applying machine learning algorithms to datasets with high dimensional feature spaces issues of over-fitting and the curse of dimensionality become a concern. During this pilot study 205 dimensions were used to develop machine learning algorithms, consequently such algorithms may be unstable. In particular, kNN is susceptible to the curse of dimensionality due to the sparsity of data points - in high dimensional spaces, it is possible that a small change in the value of a data point causes the kNN algorithm to assign a data point to the wrong cluster. Such impacts need to be considered and efforts made to reduce the feature space so that algorithms developed are both accurate and robust for practical application. In addition, other algorithms should be considered such as neural networks and support vector machines.

- Can the same results be obtained for a smaller range of  $\varphi$ ?

For the purposes of the pilot study a very wide range of  $\varphi$  values were tested. Such a range would likely not occur in practice, instead a smaller range should be investigated from about

0.7-0.9. In addition, the steps within this range should be made small so that granular prediction of  $\varphi$  can be tested.

- Can the same results be obtained independent of gas type?

In the wider context of this study, a combustion sensor would only be practically useful if it could detect  $\varphi$  across the range of gases expected in future networks. This can be broken down into two questions: Can the same results be obtained for a different gas type? Can the same results be obtained when the gas type is unknown? For the former, data should be gathered in the same way for other gas types in the second grouping of gases i.e. G21, G222, G23 and G25. Regarding the latter, acoustic datasets of various gas types can be combined and machine learning algorithms developed. The algorithms would not know the gas type and potentially identify correlations associated with  $\varphi$  only while ignoring those associated with gas type. If such a gas-type-independent prediction algorithm can be developed, it would be very useful in practical scenarios whereby gas composition can change by an arbitrary amount.

- Can the same results be obtained for any domestic gas boiler?

Results have thus far been based on the data gathered for a single boiler. Combustion noise would be expected to vary significantly if changes were made to the burner and combustion chamber. Thus, it would be of interest to test the impact of changing the burner in addition to testing the impact of changing the combustion chamber. To change the combustion chamber, a different primary heat exchanger should be tested, which may necessitate testing a different boiler model. If possible burner designs should also be varied within the same boiler.

- Can the same results be obtained in the presence of noise?

In the wider context of this study, a combustion sensor must be able to manage any expected environmental changes. For an acoustic sensor, a vital environmental change to consider is the impact of noise. Environmental noises can be simulated to a certain extent; however, a thorough analysis would necessitate extensive field trials. This topic is re-visited in Section 7.2.1 where hardware / software solutions to background noises are discussed.

- What is the nature of the combustion noise within the combustion chamber of a boiler?

As discussed in Section 3.1 combustion noises within a confined environment are four-fold: direct combustion noise, indirect combustion noise, reverberation of the confinement and feedback interactions. As already mentioned, it may be possible to use cold-flow noises to isolate combustion noises within the primary heat exchanger. It may then be of interest to analyse combustion acoustics further by removing the reverberating effect of the environment. This can be done by determining the impulse response of the acoustic chamber, in this case the primary heat exchanger. Using the inverse impulse response one can determine the combustion noise occurring within the primary heat exchanger, thus removing one of the four effects associated with combustion noise within a confined environment.

- Is it possible to develop an affordable acoustic combustion sensor?

Any practical combustion sensor for inclusion into domestic appliances must be affordable. Within the pilot study affordability was not considered and the two transducers tested cost in the range of 200-300 pounds' sterling. In bulk these costs would reduce, however one should consider cheaper transducers and see if the quality of the audio gathered from cheap sensors is sufficient.

- Is an acoustic combustion sensor more accurate than other sensor options?

As discussed in Section 2.3.3 ionisation and gas sensors have been used as combustion sensors in commercially available domestic hot water boilers. It would be useful in the context of this study to compare the results of the sensors with the results of an acoustic combustion sensor.

It is the aim of the rest of this thesis to build upon the pilot study, addressing the unanswered questions and uncertainties highlighted in the best way possible.

## 5. Method of Primary Study

### 5.1 Predicting $\varphi$ from Combustion Acoustics

It was aim of this study to determine if combustion acoustics can be used as an indirect measure of the operational  $\varphi$  of combustion for domestic gas-fired boilers. For the setup in the Pilot Study, it was shown that a strong relationship exists between boiler acoustics and  $\varphi$ , and that machine learning (ML) algorithms can be used to accurately predict  $\varphi$  from said acoustics. However, several limitations, uncertainties and unanswered questions have been raised by the Pilot Study. In this section a method is proposed to answer these questions and quell the uncertainties highlighted.

#### 5.1.1 Setup

For the main study two boilers were tested. Boiler 1 was a Worcester Bosch Greenstar 28i Junior condensing combi boiler (Worcester Bosch Group, 2013) with a WB6 primary heat exchanger. Boiler 2 was a Worcester Bosch Greenstar 25Si Compact ErP condensing combi boiler (Worcester Bosch Group, 2015) with a WB7 heat exchanger. Figure 25 shows the heat exchangers, highlighting the positions of the burners, air/gas inlet, exhaust flue and the sump. A blue print for each heat exchanger has been provided in Appendix 9.1 for the interest of the reader. For both these heat exchangers returning water is pumped in from the bottom and leaves at the top. Heat is absorbed from the condensing of exhaust gases at the bottom of the heat exchanger, then from the flame as the water circulates vertically.

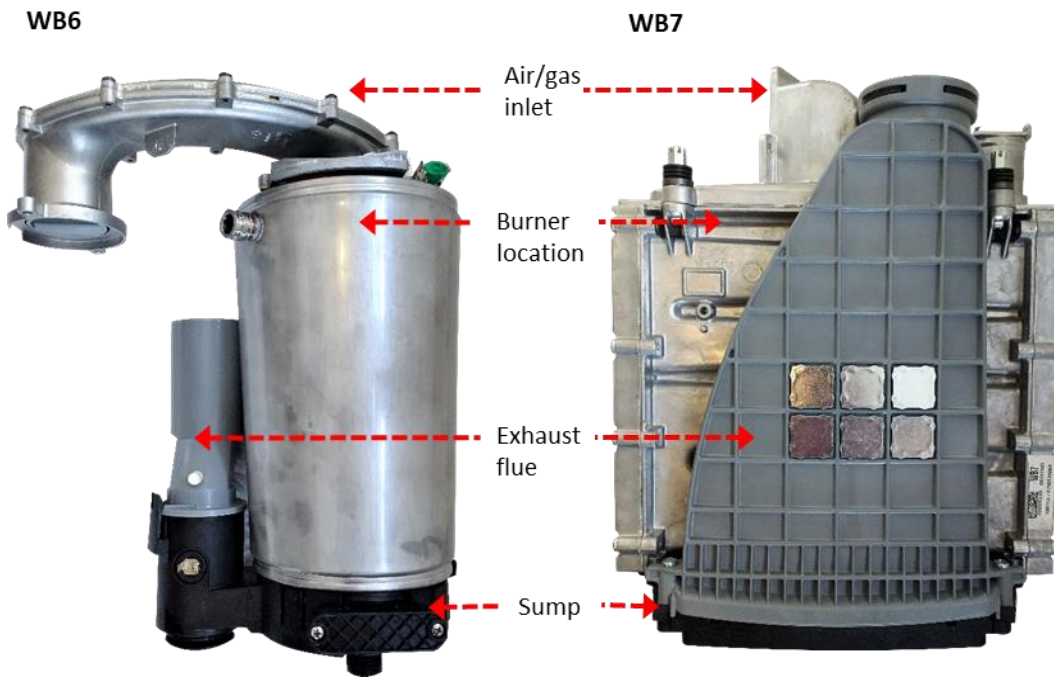


Figure 25 Pictures of the WB6 and WB7 heat exchangers with labels indicating components of interest

For Boiler 1 three different burners were used during experiments. These burners were all cylindrical burners, with thousands of holes surrounding the circumference, but with slight variations. Burners 1 and 3 had the same circumference design but with a slightly different internal design controlling the flow of air and gas. Burner 2 had a different design of holes surrounding the circumference - see Figure 26 (blueprints not available). Boiler 2 contained a mesh burner, labelled Burner 4. Note, in the figure Burner 4 is facing out-of-the-page, in WB7 it would be facing downwards. There were no variations of burner available for WB7.



Figure 26 Pictures of Burner 1, 2 and 4 used in Boilers 1 and 2

A test-rig controlled the flow of water entering and exiting the heat exchanger (average of 19.3 L/min with less than 1.2 standard deviation) and the gas meter pressure (average of 20.0 mbar with less than 0.2 standard deviation). Depending on the power output of the flame, the return flow temperature to the primary heat exchanger varied from 30-35 °C with an average of 32.5 °C and standard deviation of less than 1 °C.

Measurement of CO<sub>2</sub> species in dry exhaust gases was used, in combination with Equation 5.1, as a method of determining the operational  $\varphi$  of combustion. CO<sub>2</sub> concentrations (as well as CO and NO<sub>x</sub> concentrations) were logged by the Siemens Ultramat 23 gas analyser. For Boiler 2 data was also gathered from the on-board Energy Management System (EMS) of the boiler. This data included the signal from the ionisation probe in micro amperes.

The range of  $\varphi$  values tested in this study was 0.75-0.88, this tight range was selected to accurately simulate real world variations. After discussions with members of the Worcester Bosch team it was apparent that  $\varphi$  values in this approximate range were the most relevant in a practical scenario. Within this range 12 intermediate values of  $\varphi$  were tested. The gases used during this study included G20 (100% CH<sub>4</sub>), G23 (92.5% CH<sub>4</sub>, 7.5% N<sub>2</sub>), G25 (86% CH<sub>4</sub>, 14% N<sub>2</sub>), G21 (87% CH<sub>4</sub>, 13% C<sub>3</sub>H<sub>8</sub>) and G222 (77% CH<sub>4</sub>, 23% H<sub>2</sub>). As seen in Table 3 coefficients  $\alpha$  and  $\beta$  in Equation 5.1 change depending on gas type being burnt.

$$\varphi = \frac{X_{CO_2}}{\alpha + \beta X_{CO_2}} \quad (5.1)$$

Gas Type	$\alpha*100$	$\beta*100$
G20	10.482	0.104
G23	10.482	0.096
G25	10.482	0.88
G21	11.052	0.099
G222	9.754	0.112

*Table 3 Coefficients for Equation 5.1 for the various gas types investigated*

The  $\varphi$  was varied within the boilers via several methods:

- a. In accordance with the Pilot Study, by manually altering the gas valve partition while keeping the incoming air flow constant
- b. By altering the incoming air flow while keeping the gas flow constant. This was done by electronically controlling the speed of the premix fan while keeping the gas valve partition constant.

To record combustion acoustics three microphones were used. Microphones 1 and 2 were in accordance with the Pilot Study: Microphone 1 was a piezo electric transducer contact microphone developed by Barcus-Berry; Microphone 2 was a contactless omnidirectional condensing microphone developed by DPA microphones. Microphone 3 was a ceramic piezoelectric transducer contact microphone with a custom built 9V preamplifier; these components were very cheap, costing a total of 1-2 USD at the time. Figure 27 shows the modified ceramic piezoelectric transducer used and the design of the preamplifier.

The high impedance of piezoelectric sensors requires an amplifier with high-input impedance, hence an amplifier containing a junction gate field-effect transistor was selected (Karki, 2000); the exact design of the preamplifier was based on suggestions from amateur enthusiasts (Tillman, 2005). The ceramic piezoelectric transducer was modified by applying an epoxy resin to the non-contact surface; this was done to improve the stability of the microphone and thus the reliability of results obtained. Note, several preamplifiers were tested and this one was found to exhibit good signal-to-noise ratios considering the simplicity of design.

### Ceramic piezoelectric

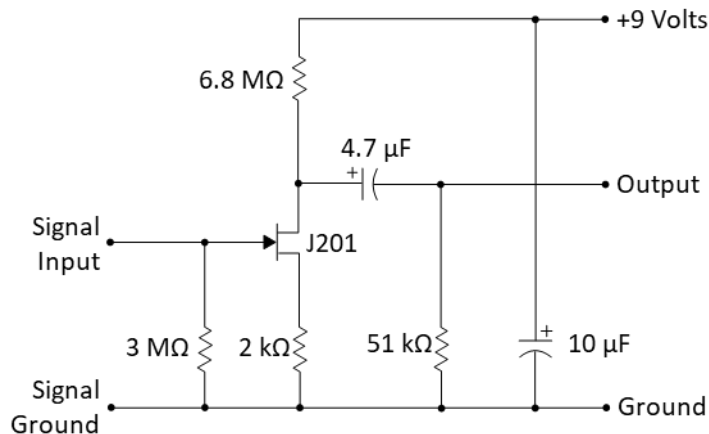
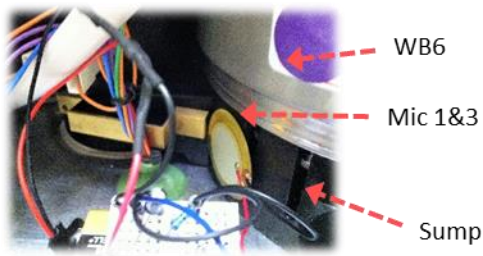


Figure 27 Picture of Microphone 3, a ceramic piezoelectric transducer, and a circuit diagram of the preamplifier used

Microphones 1 and 2 were placed in Positions 2 and 4 in accordance with the Pilot Study. Microphone 3 was placed alongside Microphone 1 in position 2 - see Figure 28 for the positions of all microphones.

### Boiler 1



### Boiler 2

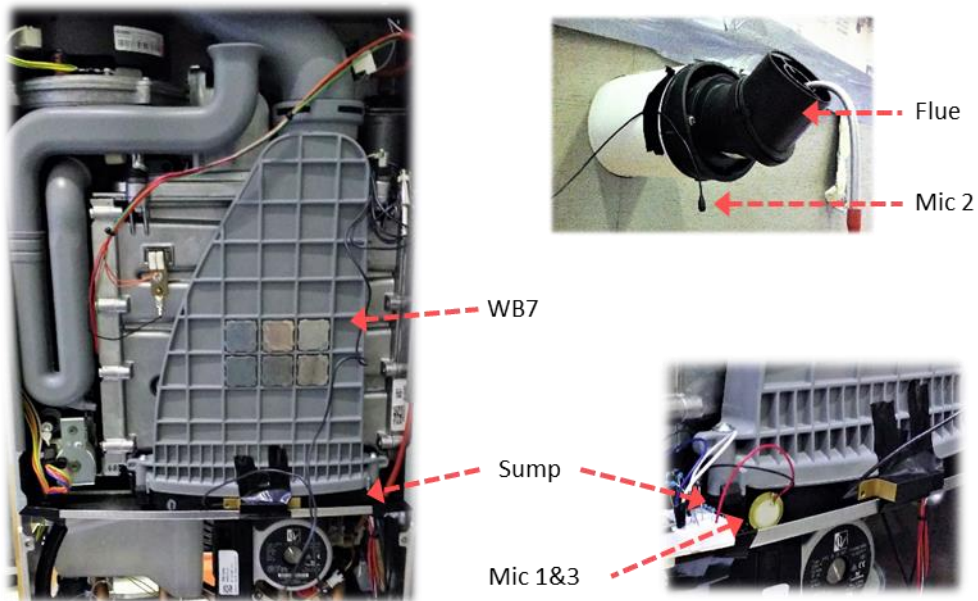


Figure 28 Pictures of the positions of all microphones for Boilers 1 and 2

Recordings from all microphones were made on separate laptops using Audacity version 2.1.2 (Audacity, 2016) at a sampling frequency of 44.1 kHz. Computer clocks on all recording equipment were synchronised and regularly checked.

## 5.1.2 Experiments

### 5.1.2.1 Cold-flow Recordings

Cold-flow recordings were required to eradicate uncertainties regarding the source of acoustic variations. These recordings were performed on Boilers 1 and 2. The aim of these experiments was to capture all noises produced during normal operation of the boiler but without a flame being present to isolate combustion noise. Non-combustion related noises included noise from the: premix fan, circulation pump, air-flow, water-flow, and electronic noises (e.g. magnetostriction of transformers).

Cold-flow recordings were performed by overriding all boiler components and forcing them to operate in normal operation regardless of flame presence. An in-house purpose-built appliance was required to override premix fan operation. The on-board boiler controller was used to activate components and operate the circulation pump. The test-rig was used to control water flow as before. For three different fan speeds, two sets of six minute recordings were made for both boilers using all microphones. During this period fan speed, pump speed etc. were noted.

Note, the differences between cold-flow recordings and normal boiler operation included:

- Flame presence.
- Water temperature within the system. This was due to lack of combustion.
- Non-combustible gas being delivered to the gas valve. Due to obvious safety concerns combustible gas was not delivered to the combustion chamber, instead only air could flow through the gas valve to the combustion chamber.

#### *5.1.2.2 Varying Burner*

For Boiler 1 three burners were tested. For each burner, the gas valve was manually adjusted in 12 steps so that the full ranges of  $\phi$  values from 0.75 to 0.88 were tested. For each step in  $\phi$  six minutes of consecutive data was recorded from all microphones. This was performed for G20 gas only. Note, special care was taken between changing burners to not disturb the positioning of the microphones.

#### *5.1.2.3 Varying Gas Type*

To test if the methods developed within the Pilot Study could be applied to other gas types, and to test if algorithms could be developed to identify  $\phi$  independent of gas type, different gases were tested for all  $\phi$  values. Gas types included G20, G23, G25, G21 and G222. The gas compositions have been summarised in Table 4. The  $\phi$  was varied by altering the partition on the gas valve. For Boiler 1 all gas types listed above were tested. For Boiler 2 only G20, G21 and G222 were available for testing.

Gas Type	% CH <sub>4</sub>	% N <sub>2</sub>	% H <sub>2</sub>	% C <sub>3</sub> H <sub>8</sub>
G20	100	-	-	-
G23	92.6	7.4	-	-
G25	86	14	-	-
G21	87	-	-	13
G222	77	-	23	-

Table 4 Table summarising compositions of all gas types tested

#### 5.1.2.4 Varying Air Intake

To thoroughly test the impact of varying  $\varphi$  values, without the impact of varying gas volumes,  $\varphi$  was varied by changing the flow of air rather than the flow of gas. Thus, for these recordings the gas valve partition was held constant while the speed of the premix fan was altered (to vary air flow).

To do this the following method was implemented:

1. The boiler was operated as normal at maximum power output i.e. the premix fan set to maximum (108 Hz for Boiler 1 and 91 Hz for Boiler 2). The  $\varphi$  value was set to 0.75 by varying the gas valve partition and observing CO<sub>2</sub> concentrations. The flow of gas going into the combustion chamber ( $G_{\text{Rate}}$ ) was noted.
2. Recordings were made from all microphones simultaneously for a six-minute duration.
3. The gas partition was opened until the next  $\varphi$  value was attained. The speed of the fan was then reduced until the gas meter reading matched the previous value of  $G_{\text{Rate}}$ .
4. Recordings were again made from all microphones.
5. Steps 3 and 4 were repeated until all recordings were made.

By following the above method  $\varphi$  was varied without varying the volume of gas entering the combustion chamber. The above was performed for Boiler 2 and G20 gas only.

#### 5.1.3 Data Analysis

For the data collected, the primary aim of this investigation was to develop algorithms approximating  $\varphi$  from combustion acoustics i.e.

$$\text{Alg}(\mathbf{A}) \cong \varphi : (\mathbf{A}^{(1)}, \varphi^{(1)}), \dots, (\mathbf{A}^{(n)}, \varphi^{(n)}).$$

Where  $\mathbf{A}^{(i)}$  contains the values of  $d$  acoustic features for the  $i^{\text{th}}$  instance from a total of  $n$  instances.

As concluded in Section 2.4, the relationship between combustion acoustics and  $\varphi$  is extremely complex. To help with this problem Machine Learning (ML) techniques were thus utilised, as they are well suited to creating approximate relations for ill-posed and complex problems. Critical in application of ML techniques is the selection of the features representing the system in question, it "...is probably the most important issue facing the designer." (Liu and Motoda, 2012, p.2).

Regarding selection of acoustic features, characteristics that encompass the variability of sound include: loudness, pitch and timbre (aka quality). Timbre is loosely defined and includes a range of characteristics which together explain why a listener can distinguish between two sounds of the same pitch and loudness; such characteristics include harmonic content, attack and decay, and vibrato/tremolo (Agostini et al., 2003). Within a fixed environment, such as a combustion chamber, timbre would not be expected to vary significantly and thus was not selected as an acoustic feature of interest. Loudness can be defined as the acoustic power of a signal for a fixed setup. It was not selected as a feature of interest due to it being a relative quantity and thus potentially unreliable in a practical scenario. Accordingly, this study focused on exploring pitch related acoustic features with normalised amplitudes. This aligned with the Pilot Study, which concluded that variations in pitch could be used to accurately determine  $\varphi$ .

For the data gathered in Sections 1.1.2.1 and 1.1.2.3, the analysis procedure has been described in Sections 4.1.1.1 to 4.1.1.7. The following is a summary of the procedure:

- Isolate combustion noise from other boiler noises
- Estimate the normalised frequency components of the resultant signals
- Determine the relative predictive power (for predicting  $\varphi$ ) of each frequency component
- Select specific frequency combinations of interest for application using ML algorithms
- Determine the Mel-Frequency-Cepstral-Coefficients (MFCCs) of the signals for application using ML algorithms
- Analyse the predictive ability of various ML algorithms on different acoustic features
- Determine the ideal combination of features to minimise dimensions while maintaining ML accuracies
- Compare the predictive performance of ML algorithms based on acoustic data, with algorithms based on ionisation current and CO concentration data

### 5.1.3.1 Isolating Combustion Noise

Cold-flow recordings can be used to isolate combustion noise from other boiler noises such as the fan, pump etc. This can be done by performing spectral subtraction on the noisy signal; where the noisy signal contains both cold-flow and combustion noise. Note that combustion noise in this context is combustion noise within a confined chamber that has been modified by the surrounding environment.

If  $\hat{X}(f)$ ,  $Y(f)$  and  $N(f)$  are the Fourier transforms of the estimated combustion noise, the noisy signal and the cold-flow noise respectively, one can estimate combustion noise via the following relation (Boll, 1979):

$$\hat{X}(f) = [|\overline{Y(f)}| - \overline{N(f)}]e^{i\theta_y(f)}$$

Where  $\theta_y(f)$  is the phase of  $Y(f)$  and  $\overline{N(f)}$  is the time-averaged Fourier transform of the cold-flow signal. For this study, because the background noise was constant for a fixed premix fan speed,  $\overline{N(f)}$  was time-averaged for the duration of a cold-flow recording. The time averaging applied to  $Y(f)$  is referred to as ‘magnitude averaging’ by Boll (1979) and implemented in order to reduce the error in estimating  $X(f)$ . For nonstationary signals the window width must be limited and its value dependent on experimentation, for speech this is in the range of 38ms. For this investigation, the signal was stationary for extended durations, thus a value of two seconds was selected as based on experimentation. For frequency bins where  $|\overline{Y(f)}|$  was less than  $\overline{N(f)}$  the output was set to zero, this modification is referred to as half-wave-rectification by Boll. The input signal in this investigation was not a mix of noisy and noise-only periods, thus many of Boll’s proposed modifications, including ‘residual noise reduction’, were not required. Once calculated  $\hat{X}(f)$  was plotted for all recordings and analysed visually.

### 5.1.3.2 Frequency Components

The frequency components of the signal were estimated using Welch’s method (Welch, 1967). Welch’s method is a modification of the basic periodogram of a signal - said modification reduces both the variance and bias of the periodogram. Welch’s method splits a sampled signal into overlapping segments, applies a window function to these segments, calculates the periodogram (by calculating the discrete Fourier transform (DFT)) of the windowed functions and averages out the resultant periodograms over a fixed interval.

The window selected for this analysis was a Hamming window of length of 4ms; the overlap was 60%; the number of DFTs applied depended on the granularity required and the frequency range being investigated; and the interval length was one second. Note, to save on processing requirements the acoustic data was down-sampled depending on the maximum frequency under investigation (without breaching sampling theorem). Once the average periodogram for the one second interval was calculated, it was normalised by dividing it by the mean energy per frequency bin; accordingly, a value of one represented the mean. Therefore, if one interval was on average louder than the next, this would not be discernible from the feature vector; hence loudness was not used as a feature.

In preparation of frequency bin data for use in ML algorithms and for general analysis purposes, the relative predictive potential of frequency bins was analysed. Removal of unnecessary features was essential to the performance of ML algorithms as noisy data “distracts a learning algorithm” (Liu and Motoda, 2012) and often leads to over-fitting. “Feature selection is a process that chooses an optimal subset of features according to a certain criterion.” (Liu and Motoda, 2012, p.10). According to Guyon and Elisseeff (2003) Wrapper methods (see Section 4.1.1.5) may be most suited in determining the optimal subset of features for ML application. However, due to the high number of dimensions, this method was computationally intractable, even with the use of non-exhaustive search methods a maximum of 50 dimensions could be analysed for these datasets. Consequently, variable ranking methods were selected; such methods included single-attribute evaluators such as information-gain, gain-ratio and one-rule. Single-attribute evaluators quantify the predictive potential of each attribute independently- refer to Witten et al. (2016) for a description. The output of the algorithms informed the selection of frequency bins for analysis using ML algorithms. In addition, it informed the discussion of frequency ranges of interest. Note dimensionality reduction methods, such as principal component analysis, were not considered suitable as these algorithms would not reduce the frequency space under consideration and not provide considerable insight.

### *5.1.3.3 MFCCs*

The MFCCs were calculated for all datasets using a range of coefficients. Mel-Frequency-Cepstral-Coefficients (MFCCs) are a popular technique for summarizing the overall ‘shape’ of a frequency distribution in a small number of features. The ‘shape’ of a distribution is known as the spectral-envelope and represents the slowly varying parts of the spectrum without the spectral-details. Typically, in speech and musical analysis this spectral-envelope carries the information required to distinguish the class of interest (see Section 3.3.3).

The spectral-details are separated from the spectral-envelope by taking the squared magnitude of inverse-Fourier transform of the log of the original spectrum (called the power Cepstrum), and filtering out high-frequency components. The remaining low-frequency components of the power Cepstrum represent the spectral-envelope of the original spectrum. The MFCC are a non-uniform discretised representation of the spectral-envelope. This is performed by applying triangular band-pass filters across the frequency axis. The positioning and width of the band-pass filters are determined from the Mel-scale. The Mel-scale discretisation is designed to replicate the human auditory response. As there was no theoretical reason why the Mel-scale would be useful in this context, a linear scale was also tested; this is also known as the linear-frequency cepstral coefficients (LFCCs). Calculating the MFCCs results in there being more filters (and thus coefficients) in the low frequency regions relative to the high frequency regions as compared to the LFCCs. The total number of coefficients, and the frequency range of interest, can be varied for the specific application. The MFCC/LFCC implementation applied in this investigation was that reported by Young et al. (2002). The Matlab code used was made available by Wojcicki (2011).

#### *5.1.3.4 Machine Learning Algorithms*

A range of algorithms representing the main techniques applied in ML were applied to all datasets. These included: Linear Regression (LR); Support Vector Machines (SVMs); k-Nearest-Neighbour (kNN); M5Base (M5P); and Artificial Neural Networks (ANNs). Beside for M5P, descriptions of these algorithms have been provided in Section 3.2.2. M5P is a decision-tree based learning algorithm but with multivariate linear models as leaves. Thus, it is analogous to piecewise linear functions. The tree is created via the divide-and-conquer method. The linear models are constructed via standard regression techniques. The original algorithm was invented by Quinlan (1992), the version used in this analysis contains modifications proposed by Wang and Witten (1996).

The ML algorithms selected represent some of the fundamental methods of supervised ML, namely linear models (LR), tree algorithms (M5P), instance-based learners (kNN) and artificial neural networks (ANNs). The tools used to implement the algorithms mentioned included a mix of the Python module scikit-learn (Pedregosa et al., 2011) and WEKA (Hall et al., 2009). WEKA is licensed under the GNU General Public license and scikit-learn under the BSD License i.e. both tools are free and open-source.

By splitting the dataset  $(\mathbf{A}^{(1)}, \varphi^{(1)}), \dots, (\mathbf{A}^{(n)}, \varphi^{(n)})$  into training  $(\mathbf{A}^{(T)}, \varphi^{(T)})$  and testing data  $(\mathbf{A}^{(t)}, \varphi^{(t)})$ , ML algorithms can be developed and tested for their ability to predict  $\varphi$  for an unknown acoustic signal. A thorough method for testing the predictive accuracy of a ML algorithm on a given dataset is to apply 'stratified  $k$ -fold cross-validation (CV)'.  $k$ -fold CV randomly partitions the data into  $k$  equal groups; trains the algorithm on  $k-1$  of the groups; tests the algorithm on the remaining group; and repeats this  $k$  times so that every group has been used once for testing and  $k-1$  times for training. Stratified  $k$ -fold CV ensures that when the data is divided into  $k$  segments, each segment has the same proportion of each class value. The output of  $k$ -fold CV is the average result of the  $k$  tests. In this way training and testing data are segregated, so that testing is never performed on training data, thus avoiding a false analysis of the algorithm's performance. Additionally, the performance estimate is less sensitive to the partitioning of the training/testing data and less data is wasted compared to other testing methods. For completeness 10-fold CV was repeated ten times using a different random number seed to split the data on each iteration. The output of multiple  $k$ -fold CV is the average of each of the  $k$ -fold CV tests and the variance of said average. Due to the computational time required to run ANNs, only one instance of stratified  $k$ -fold CV was performed. The error metric selected to compare ML algorithms was that of the root-relative-squared-error (RRSE), this was selected because it returns an absolute value and considers what the error would have been if a 'simple predictor' had been applied – refer to Equation 3.5 for more information.

For classification data, the average Kappa statistic was selected as an error metric. The calculation takes the difference between the observed and expected accuracy and divides it by one minus the expected accuracy. According to (Fleiss et al., 2013) Kappas  $> 0.75$  are considered 'excellent',  $0.40-0.75$  are 'fair to good', and  $< 0.40$  'poor'. Importantly the Kappa statistic takes into account the expected accuracy i.e. the accuracy a classifier would achieve by random chance.

Features consisting of various dimensions for both the normalised frequency bin data, and MFCCs, were applied using all ML algorithms. The results of which were used to assess the most suitable algorithm and feature combinations. Aiming to minimise the number of dimensions required while maintaining accuracies. From this, the feature space was small enough to consider the application of wrapper methods for a final phase of feature selection. Thus, optimising the dimensions required for specific ML algorithms. Note, due to the run times of MLP algorithms, fewer combinations of dimensions were tested relative to all other algorithms.

#### *5.1.3.5 Wrapper Methods*

Wrapper methods are a subset of the feature reduction schemes discussed in Section 3.2.3. For a given ML algorithm, wrapper methods evaluate all feature combinations and select that which maximises the testing accuracy of the ML algorithm when built on that feature combination. For each combination of features  $k$ -fold CV is applied and the set of features returning the highest  $k$ -fold CV score are returned. The wrapper method applied was developed by Kohavi and John (1997). Wrapper methods are particularly costly as they require an ML algorithm to be trained and tested on every feature combination. However, the feature space can be reduced significantly by employing a search strategy; for this study a best-first method was used. Best-first “Searches the space of attribute subsets by greedy hill climbing augmented with a backtracking facility. Setting the number of consecutive non-improving nodes allowed controls the level of backtracking done (this was set to five). Best first may start with the empty set of attributes and search forward, or start with the full set of attributes and search backward, or start at any point and search in both directions (by considering all possible single attribute additions and deletions at a given point).” (WEKA, 2017)

#### *5.1.3.6 Ionisation Current and CO concentration Data*

During all recordings for Boiler 2, both ionisation current and CO concentration data streams were logged. This data was thus used to test the performance of other combustion sensor schemes as summarised in Section 6.2. All efforts were made from these datasets to develop algorithms to determine  $\varphi$ . As each dataset only consists of one feature, feature selection or analysis schemes were not required. If required however ML algorithms were applied to these datasets. In addition, differing time-smoothing functions were considered.

## 6. Results of Primary Study

The following sections summarize the primary results of the investigation. Results for predicting both  $\varphi$  and gas type using combustion acoustics as a combustion sensor will first be given, this will then be compared with predictions using ionisation probe and CO concentration data. A discussion will then commence regarding the significance of the results and relevant uncertainties.

### 6.1 Acoustic Combustion Sensor

#### 6.1.1 Predicting $\varphi$

The aim of this part of the investigation was to develop algorithms to approximate  $\varphi$  from combustion acoustics for the data collected. The idea was to apply Machine Learning (ML) techniques to a summarised set of acoustic features. To determine acoustic features, exploratory work was performed from data visualisation to feature selection schemes. As mentioned in Section 5.1.3, the study focussed on exploring pitch related acoustic features. As such two types of features were considered: the first was to somewhat naively explore the full normalised frequency space from power spectral density estimates; the second was to use an acoustic feature common in audio classification research, that of the Mel-Frequency-Cepstral-Coefficients (MFCCs). ML algorithms were then tested with differing combinations of each type of feature, resulting in an optimum selection maximising predictive accuracies while minimising dimensionality. The format of the following sections is as follows:

- Overview of datasets
- Visual analysis of combustion noise in the system
- Overview of frequency feature analysis
- Overview of MFCC feature analysis
- Application of ML algorithms
- Optimisation of ML algorithms
- Analysis of when air, instead of gas, is varied
- Analysis when the burner is varied

### 6.1.1.1 Overview of Datasets

The acoustic data collected was done so from two boilers, three microphones and four gas types. For each of these combinations  $\varphi$  was varied in 12 steps from 0.75-0.88. Before analysis, data was split by boiler and microphone type, leading to six distinct datasets (refer to Table 5). Data was not split by gas type as the aim of the investigation was to develop predictive algorithms irrespective of gas type. The label NFC or MFCC after the dataset number in Table 5 refers to the two feature sets being considered i.e. the normalised frequency components (NFCs) or Mel-Frequency Cepstral Coefficients (MFCCs). The number of instances was based on splitting all data into one second intervals. A one second interval duration was selected due to its appropriateness in matching with exhaust gas emission and ionisation current data streams. Note, unfortunately gas G25 was not available at the time of testing Boiler 2.

As observed in Table 5, acoustic data was analysed separately for each boiler and microphone combination. As such the developed predictive algorithms, would only be applicable to a specific boiler and microphone combination. Boilers were considered independently as the heat exchangers used in each boiler (WB6 and WB7) were unique in geometry and size, thus combustion noise emanating from each boiler, for a particular value of  $\varphi$ , would be characteristic for the boiler in question. Microphones were considered independently as the three microphones investigated had unique frequency response profiles and unique designs of pre-amplifier. Developing microphone independent algorithms was outside the scope of this investigation but would constitute a useful modification.

Dataset	Boiler	Mic	Gas Type	$\varphi$ range	Instances
1_(NFC/MFCC)	1	1	G20, G21, G25, G222	0.75-0.88	17,280
2_(NFC/MFCC)	1	2	G20, G21, G25, G222	0.75-0.88	17,280
3_(NFC/MFCC)	1	3	G20, G21, G25, G222	0.75-0.88	17,280
4_(NFC/MFCC)	2	1	G20, G21, G222	0.75-0.88	12,960
5_(NFC/MFCC)	2	2	G20, G21, G222	0.75-0.88	12,960
6_(NFC/MFCC)	2	3	G20, G21, G222	0.75-0.88	12,960

Table 5 Summary of datasets available for analysis

### 6.1.1.2 Isolating Combustion Noise

Before extracting acoustic features, cold-flow readings were used to remove background noises from all recordings. This was done by applying spectral subtraction as proposed by Boll (1979)

(described in Section 5.1.3.1). An example of spectral subtraction has been given in Figures 29(a) and 29(b): 'Cold-Flow' shows the spectrogram of the cold-flow/background recording, 'Signal' shows the spectrogram of the original signal and 'Cleaned Signal' shows the spectrogram of the original signal after removing the 'Cold-Flow' via spectral subtraction. Theoretically the 'Cleaned Signal' represents combustion noise only, as modified by the system and the surrounding environment. Note, a smoothing filter (moving average) with a span of nine seconds was applied to the time domain in Figures 29 and 30 to increase the contrast of the spectrograms. Note, a nine second smoothing filter was later found to improve the accuracies of predictive algorithms in addition to assisting in the visualisation of spectrograms.

As observed in Figure 29, a large majority of the acoustic energy for the cleaned signal resided within the 0-600 Hz band with little to no acoustic energy above 6 kHz. In the region of 0-80 Hz a large amount of acoustic energy was removed via spectral subtraction, this was likely due to most boiler noises occupying the low frequency ranges from 30-120 Hz (Neeld et al., 2016).

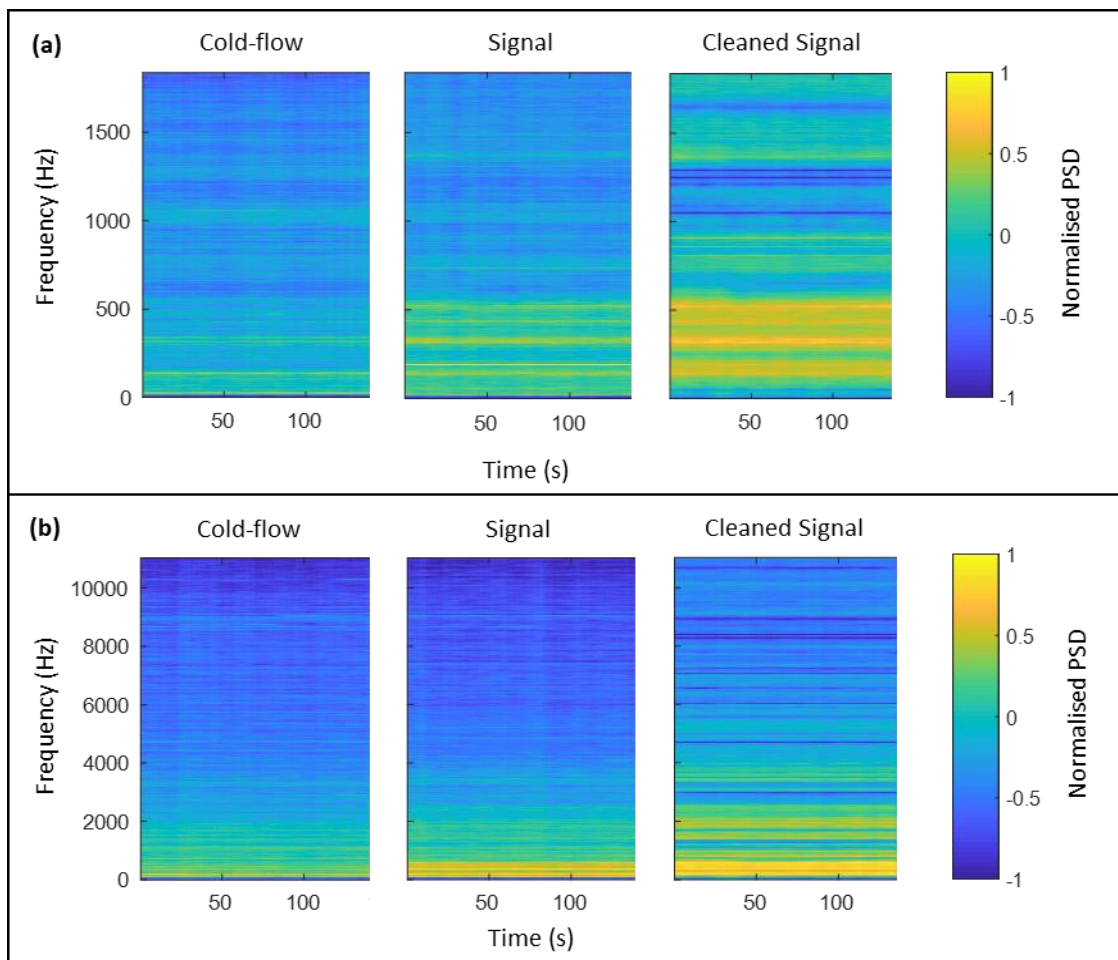


Figure 29 Spectrograms of recordings from Dataset 5 for G20 gas. The 'Cold-Flow' represents all boiler noises without the presence of combustion, the 'Signal' represents the original recording with combustion

present and the 'Cleaned Signal' is a spectral subtraction of the two previous signals. A smoothing filter of nine seconds was applied to all images. Figure (a) displays the frequency range from 0-2 kHz. Figure (b) displays the frequency range from 0-11 kHz

Once spectral subtraction had been applied to all recordings, spectrograms of differing values of  $\varphi$  could be analysed visually. This data visualisation stage was useful in cementing the analysis performed during the study. As observed in Figure 30, there were clear variations in the spectrogram for differing values of  $\varphi$ . Specifically, the frequency regions of 300, 400 and 500 Hz varied relative to one another depending on  $\varphi$ : for  $\varphi=0.83$  the 300 and 500 Hz regions were relatively strongly pronounced, for  $\varphi=0.89$  the 300 Hz region was relatively strongly pronounced, for  $\varphi=0.75$  all three regions were relatively similarly pronounced. In addition to the relative amplitudes, the shapes of these three regions also appear to vary with  $\varphi$ . It was therefore expected, that during feature analysis, some if not all these frequency ranges would be highlighted as useful features for predicting  $\varphi$  for Dataset 5 (see Section 6.1.1.5.4).

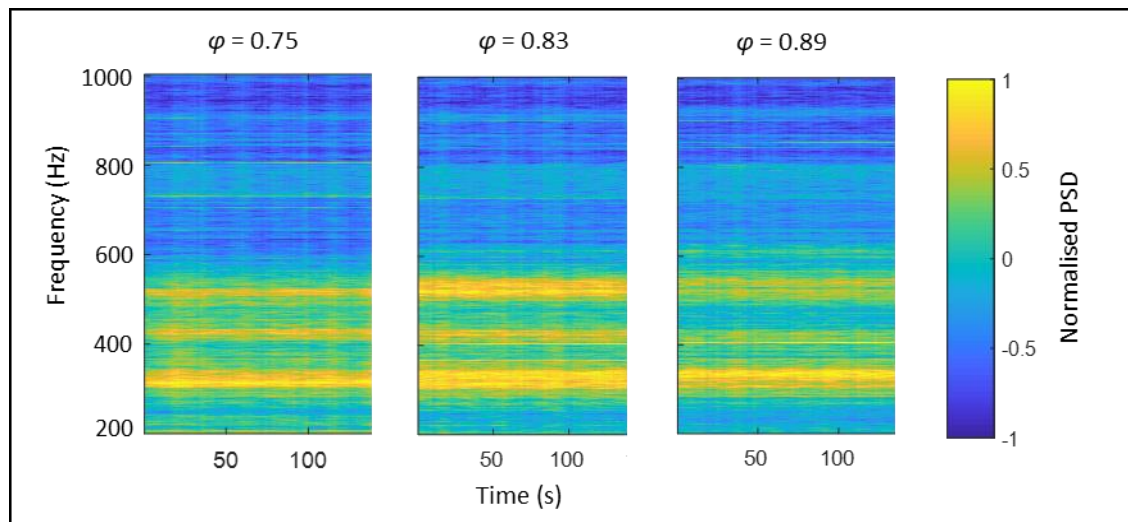


Figure 30 Spectrograms of three separate recordings for Microphone 2, Boiler 2 and G20 gas. The value of  $\varphi$  was varied between each recording as indicated at the top of each image. The PSD has been normalised to a range of -1 to 1. The frequency range is limited to 200-1000 Hz to highlight changes occurring in the spectrogram. A smoothing filter of nine seconds was applied to all images

### 6.1.1.3 Frequency Features

The following provides an overview of frequency feature extraction, analysis and feature reduction.

Acoustic data was converted into normalized-frequency-components (NFCs) for each second of each recording. This was performed by calculating the power spectral density using Welch's method for the range of 0-10 kHz. A granularity of 2.2 Hz was achieved by applying 10,000 DFTs to the down-sampled recordings. For a unique combination of boiler, microphone and gas type,

4320 seconds of acoustic data, each with 4353 frequency bins, was thus available for analysis. The amplitude of each frequency bin was normalised by dividing it by the mean energy of the signal for that one second interval. Each frequency bin was smoothed in time using a moving average with window spans of: one second (no smoothing), five seconds, nine seconds and 19 seconds. All time smoothing span durations could thus be tested. Note, in accordance with Table 5 the nomenclature 'Datasets 1\_NFC' refers to the use of NFC features for Boiler 1, Microphone 1 and gas types G20, G21, G25 and G222.

The frequency range of 0-10 kHz with a granularity of 2.2 Hz likely contains more information than necessary for predicting  $\varphi$ . Invoking learning algorithms on datasets containing large proportions of unnecessary information may result in models which over-fit, may be unstable ('curse of dimensionality') and be computationally costly. Consequently, feature reduction schemes were applied (refer to Section 3.2.3 for an overview of feature reduction methods). Due to the large data volumes and consequently the large computational costs associated with wrapper methods, univariate filters were applied at this stage with a plan to apply wrapper methods once the feature space was reduced - this approach was equivalent to that proposed by Saeys et al (2007). The univariate filters tested on all NFC datasets included information-gain (IG), gain-ratio and one-rule. It was noted all algorithms gave similar results, and thus IG was arbitrarily selected as the evaluation metric of choice. Note, IG evaluates the worth of an attribute by measuring the information gain with respect to the class, if the only information available is the feature values and the corresponding class distribution.

The IG evaluator was applied to all datasets using 10-fold CV. The output was the average merit and associated variance given to a frequency bin. The higher the average merit score, the more information that bin provided with respect to the class ( $\varphi$ ). It was necessary at this point to convert the continuous variable,  $\varphi$ , into a class label. As  $\varphi$  was varied in 12 distinct steps during experiments, a class label was given for each step. This was feasible since the variance within each step was very small: for three standard deviations, a maximum variance of 1% was observed throughout all datasets.

Figure 31 shows a typical result of applying the IG evaluator. As observed in the figure, and across all datasets analysed, there were several clear peaks where the evaluators returned high scores; in Figure 31 examples of these peaks were 3100 Hz, 4700 Hz and 7300 Hz. The width of slopes leading to these peaks spanned regions of 100-300 Hz. Although each frequency bin was taken independently, the merit score across neighbouring bins were similar in value. This observation, and the overall shape of the single-attribute evaluation plots highlighted that tonal

shifts were occurring in frequency bands in response to changes in  $\varphi$ . The bands had a minimum width of 20 Hz and in general occurred at different points for each dataset. Note, when applying the IG evaluator to the 10-20 kHz bands, the evaluated merit scores were very low compared to the 0-10 kHz region, thus the 10-20 kHz bands of the NFCs were not considered.

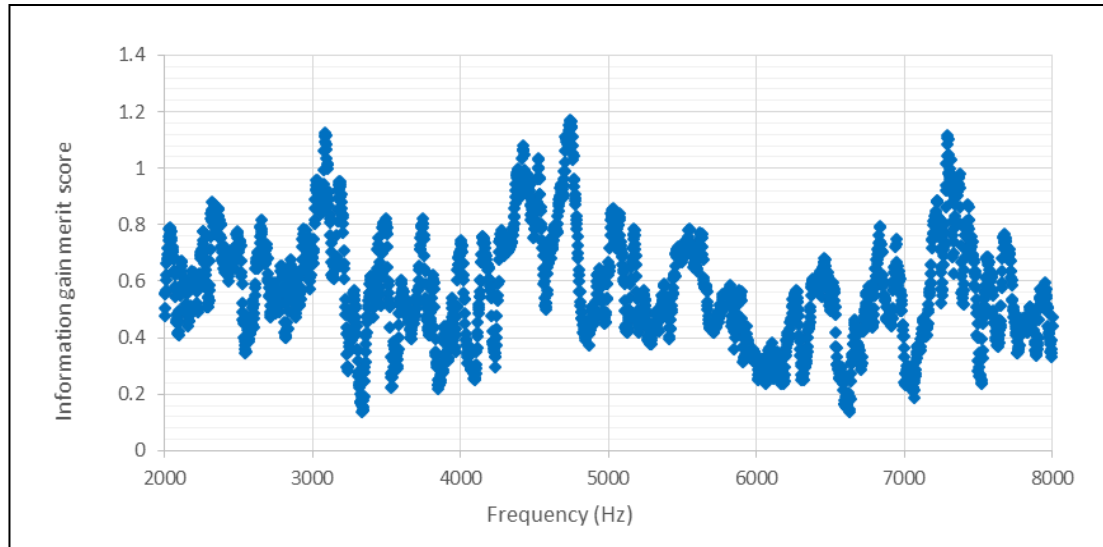


*Figure 31 Information-gain merit score for each frequency bin of Dataset 1\_NFC. The frequency range is limited from 2-8 kHz for illustration purposes only*

For analysis purposes Dataset 1\_NFC was split by gas type and the information-gain evaluator applied. The result of which was reported in Figure 32 for the 2-4 kHz range. As observed different gas types returned normalised merit scores that peaked at distinctly different frequencies. The observation highlights an important point: that for a  $\varphi$  and gas type combination, there may be a unique acoustic signature for a gas type, thus it may be possible to determine gas type from acoustics; this idea has been further investigated in Section 6.1.2.

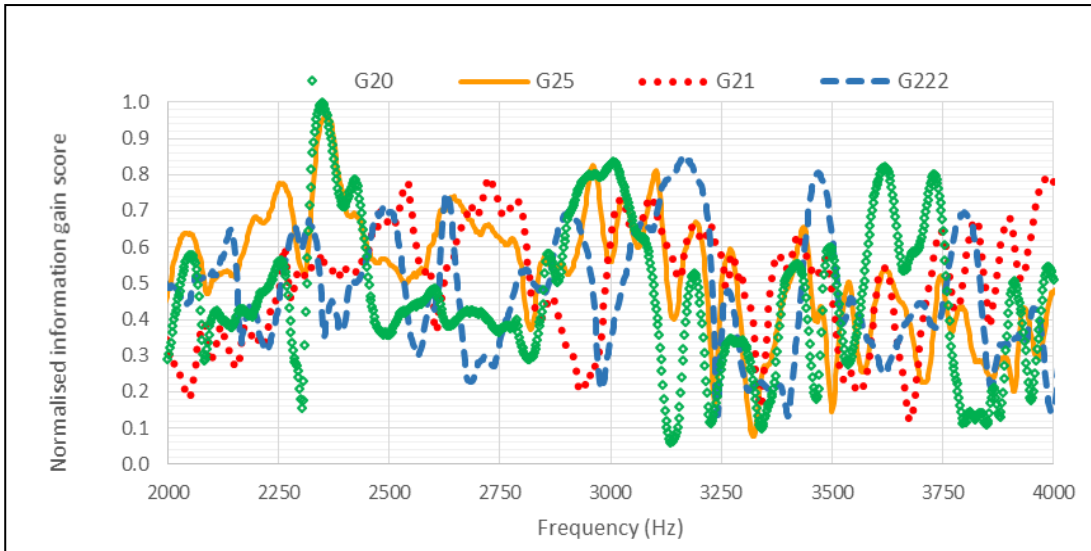


Figure 32 Information-gain merit score for each frequency bin of Dataset 1\_NFC as split by gas type for the frequency range of 2-4 kHz

From the results of the information-gain evaluator, a subset of NFCs was selected. For each dataset, the selection criteria were: the top seven peak frequency regions with a width of 300 Hz. This criterion was selected as the IG evaluator showed about 4-7 clear peak regions for each dataset and the peak regions had widths from 100-300 Hz. Additionally, it made intuitive sense to select frequency regions, instead of individual frequency bins, because tonal variations are expected to be expressed over a frequency range such as the ranges observed. Figure 33 illustrates the selection of the top seven peaks for Dataset 1\_NFC. Table 6 lists the top seven peak frequency regions for each dataset as determined from the information-gain evaluator. Datasets 1-6\_NFC were restricted to the seven frequency regions listed in Table 4, resulting in datasets with a maximum of 950 dimensions. Note, as most non-combustion related noises from domestic boilers were contained in a 5-120 Hz frequency range (Neeld et al., 2016), frequencies below 150 Hz, unless necessary, were not considered further.

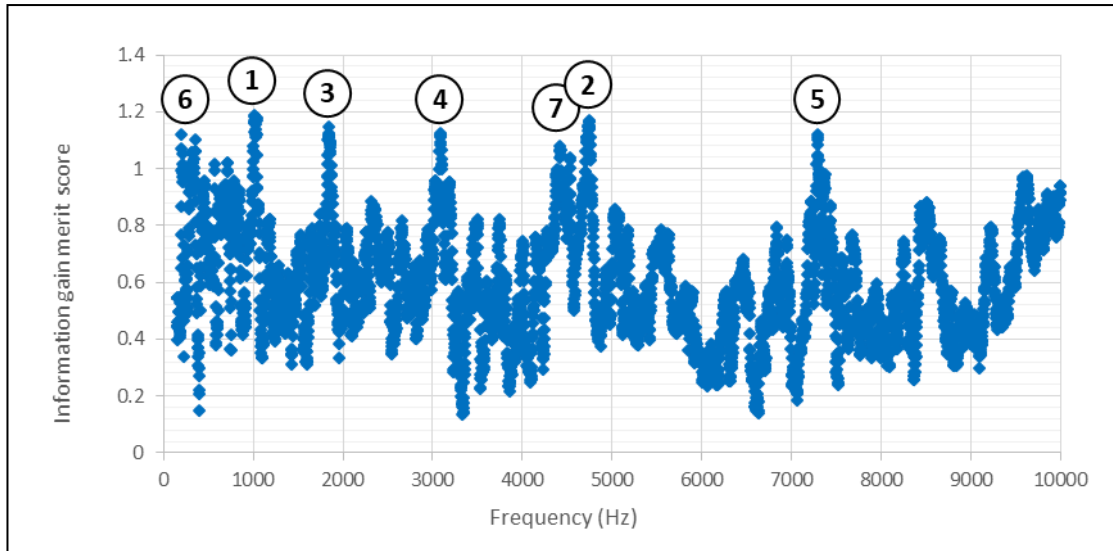


Figure 33 Information-gain merit score for each frequency bin of Dataset 1\_NFC. Labelled are the top seven peak frequency regions from 150-10000 Hz

Dataset	Frequency region of interest ordered by ranking						
	1	2	3	4	5	6	7
1_NFC	1010 ±150	4739 ±150	1837 ±150	3083 ±150	7292 ±150	351 ±150	4421 ±150
2_NFC	2476 ±150	1905 ±150	529 ±150	1266 ±150	908 ±150	5614 ±150	3996 ±150
3_NFC	2556 ±150	4717 ±150	4432 ±150	333 ±150	5685 ±150	3546 ±150	9122 ±150
4_NFC	551 ±150	1396 ±150	1607 ±150	2236 ±150	7791 ±150	4029 ±150	4972 ±150
5_NFC	549 ±150	227 ±150	796 ±150	1356 ±150	1601 ±150	2419 ±150	3277 ±150
6_NFC	7795 ±150	2448 ±150	803 ±150	1162 ±150	4862 ±150	1636 ±150	5795 ±150

Table 6 Frequency region ranking for each dataset as based on the information-gain evaluator

#### 6.1.1.4 MFCCs

The second acoustic feature under consideration was that of the MFCCs. As discussed in Section 5.1.3.3, the implementation applied in this investigation was that reported by Young et al. (2002). For the power spectrums, a Hamming window was applied with a frame duration of 500ms and an analysis frame shift of 50ms. A lifter parameter was used to re-scale the cepstrum coefficients to similar values, this was set to 22 – refer to p.75 of Young et al. (2002). MFCCs were calculated for a frequency range of 150-8000 Hz and the number of coefficients was varied from 10-70 in steps of 10. The frequency range was selected as based on the analysis of

frequency features summarized in Table 6. Over each one second interval the MFCCs were averaged to give 4320 instances per gas type. MFCCs were smoothed in time using a moving average with window spans of: one second (no smoothing), five seconds, nine seconds and 19 seconds. For all instances of each feature a normalizing function was applied to scale MFCC values between -1 and 1. Within the contexts of the datasets, the MFCC features were contained in Datasets 1-6\_MFCC in accordance with Table 5.

Figure 34 shows the normalized average values of 20 MFCCs for (the average of) the twelve distinct steps in  $\varphi$  investigated. As observed in the figure, each set of MFCC values appear to vary depending on the value of  $\varphi$ , indicating potential correlation. Regarding feature reduction, the range of 10-70 MFCCs were found to be sufficiently large as to show limiting behaviour under application of ML algorithms (see Section 6.1.1.5.3), but sufficiently small to run wrapper methods for feature selection (see Section 6.1.1.5.4). Consequently, no additional feature reduction steps were necessary before testing Datasets 1-6\_MFCC using ML algorithms.

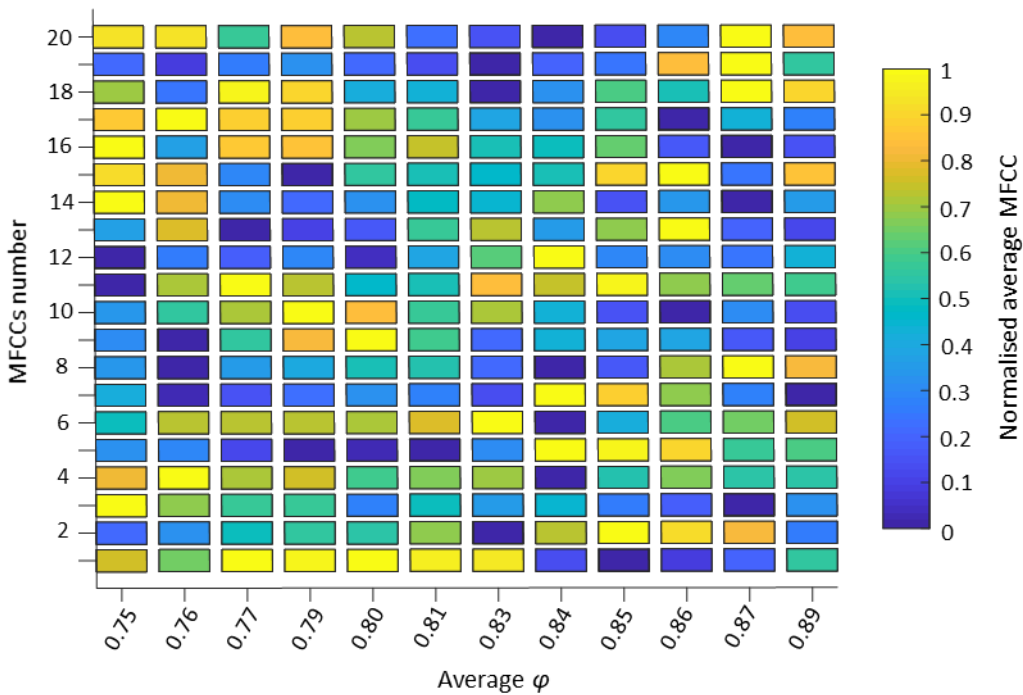


Figure 34 Normalized average values of 20 MFCCs for Dataset 3\_MFCC

### 6.1.1.5 Application of Machine Learning

The overall aim of this section was to develop and test ML algorithms on all datasets in Table 5 and track how additional dimension reduction impacted the predictive accuracies attained. At the point where predictive accuracies start to get significantly worse was the point at which the

selection of dimensions was approaching an optimum. Wrapper methods were then applied for additional feature reduction.

The ML algorithms selected for testing included k-Nearest-Neighbour (kNN), Linear Regression (LR), M5Base (M5P), Artificial Neural Networks (ANNs) and Support Vector Machines (SVMs) - refer to Kantardzic (2011) and Witten et al. (2016). Note, a modified kNN algorithm was employed which searches through a specified range of k values and selects the value with the best result. The method selected for training and testing was ten iterations of stratified 10-fold CV (see Section 3.2.4). The output of said test was the average root-relative-squared-error (RRSE) (see Equation 3.5) and variance of the RRSE. Due to the computational time required to run ANNs and SVMs, only one instance of stratified  $k$ -fold CV was performed once a subset of features had been selected - the results from ANNs and SVMs were reported separately in Section 6.1.1.5.6.

#### *6.1.1.5.1 Time smoothing*

Before testing ML algorithms, a preliminary analysis was made to decide what span should be applied to the moving average time filter. From a practical standpoint, the width of the moving average should be as small as possible so long as predictive accuracies are not impacted. This is so estimates, and consequently adjustments of  $\varphi$  can be made quickly within the control system of a domestic appliance. By applying a smoothing function the assumption is being made that the value of  $\varphi$  is stationary during the smoothing period.

The smoothing filter widths tested were: one second (no smoothing), five seconds, nine seconds and 19 seconds. These were arbitrarily selected but required to be odd in number to operate as a moving filter. For a select set of features for Datasets 1-6\_NFC and 1-6\_MFCC, ML algorithms were tested to determine a suitable selection for the filter width. For this analysis, LR and kNN algorithms were applied. For Datasets 1-6\_NFC the top six frequency regions (per Table 5) were used with a granularity of 15 Hz leading to 76 dimensions in total. For the Datasets 1-6\_MFCC, 70 MFCCs were used.

It was found that applying a time smoothing filter improved the performance of both algorithms substantially across all datasets. For LR, on average applying a five second filter improved RRSE scores by about 6.0%, increasing to nine seconds gained an extra 2.2% and to 19 seconds an extra 1.8%. For kNN, an initial improvement of 6.1% was observed moving to five seconds, with an extra 0.1% and 0.0% moving to nine and 19 seconds respectively. Thus, a nine second span

was deemed suitable and from this section onwards all acoustic feature vectors have had a nine second moving average filter applied.

### 6.1.1.5.2 Normalised Frequency Components

The following presents the results of ML algorithms as applied to Datasets 1-6\_NFC with a nine second moving average filter applied. For these datasets, features were first limited to the seven frequency regions summarised in Table 6. NFC dimensions were then further reduced in two ways: by reducing the granularity of the frequency bins; and by reducing the number of frequency regions considered. Note, a label of '7' indicated that all seven frequency regions were being included, a label of '6' indicated that the top six frequency regions were being included (according to Table 6), a label of '5' the top five etc.

Table 7 shows the lowest RRSE scores achieved for each dataset and ML algorithm combination for dimensions less than 100. The predictive accuracies of all ML algorithms, except LR, were found to asymptote in the range of 50-70 - for LR, large increases in dimensions resulted in very minor improvements in accuracy; for example, for Dataset 1\_NFC, increasing dimensions from 90 to 960 lowered the RRSE of LR from 10.5% to 8.8%.

Initial observations reveal the following:

- kNN significantly outperformed all other algorithms tested and LR performed poorest.
- The ML algorithms based on data from Boiler 1 returned significantly higher predictive accuracies than those based on data from Boiler 2 (refer to Section 7.4.2 for a discussion).
- The contact microphones outperformed the contactless microphone.

Dataset	LR		M5P		kNN (k=1)		kNN (k=2)	
	Ave. RRSE(%)	Std. dev						
1_NFC	10.48	0.242	4.68	0.429	0.53	0.028	0.43	0.043
2_NFC	16.42	0.363	8.41	0.69	0.65	0.388	0.93	0.469
3_NFC	9.38	0.203	4.68	0.523	0.56	0.062	0.48	0.093
4_NFC	18.44	0.41	6.46	1.747	3.26	0.118	2.67	0.103
5_NFC	23.96	0.61	7.58	0.874	3.37	0.165	2.9	0.145
6_NFC	47.92	0.861	15.78	2.664	3.23	0.114	2.67	0.105

Table 7 The lowest RRSE values achieved for each of the machine learning algorithms tested for each dataset. Also included is the standard deviation of the average RRSE

Figure 35 shows the RRSE of kNN algorithms on all datasets for a wide range of dimensions. Dimensions were adjusted by increasing the granularity of power spectral density estimates and

reducing the number of frequency regions considered from '7' to '1'. Included in the plots, displayed as error bars, are the standard deviations of the ten iterations of 10-fold CV. As observed for all datasets the error rates asymptote in the range of 20-50 dimensions. An optimum combination of dimensions for kNN was selected from these plots. This optimum selection was made by selecting the data point containing the fewest dimensions at the point at which error rates asymptote. For example, in Dataset 1\_NFC this occurred for the data point with 47 dimensions and an RRSE value of 0.43% containing frequency data in the top six frequency regions. The optimum selection of NFCs for all datasets, for kNN, was summarised in Table 8.

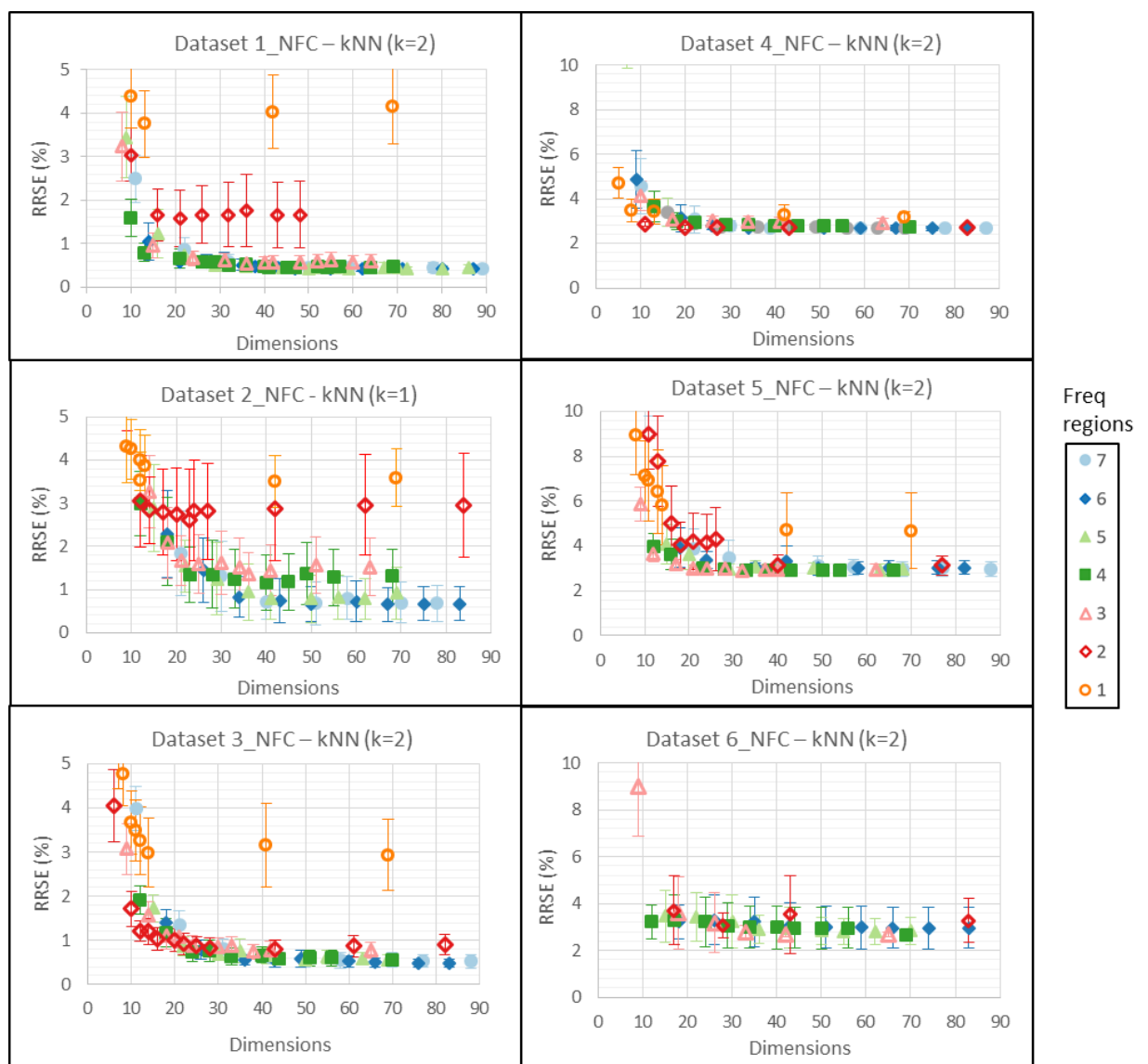


Figure 35 Plots of the resultant average RRSE after running ten iterations of 10-fold CV using kNN algorithms split by dataset, plotted against the number of dimensions in the data. The data used in the algorithms was varied by changing the granularity of frequency bins and by removing the number of frequency regions from '7' to '1'

Dataset	Algorithm	Frequency ranges inc.	No. of dimensions	Frequency granularity(Hz)	Ave. RRSE(%)	std.dev
1_NFC	kNN (k=2)	6	47	38.2	0.43	0.043
2_NFC	kNN (k=1)	6	50	36.3	0.65	0.401
3_NFC	kNN (k=2)	6	36	50	0.55	0.106
4_NFC	kNN (k=2)	2	20	30	2.69	0.105
5_NFC	kNN (k=2)	3	21	40.5	2.99	0.151
6_NFC	kNN (k=2)	3	42	21.4	2.7	0.109

*Table 8 The average RRSE after running ten iterations of 10-fold CV using kNN algorithms split by dataset. The selection of dimensions is based on selecting data-point with the lowest dimensions at the point that algorithms asymptote. Included in the table are the frequency regions, the number of dimensions and the frequency granularity*

As observed in Table 8, for Datasets 1-3\_NFC (Boiler 1) the top six frequency ranges were required to achieve optimum selection, however for Datasets 4\_NFC-6\_NFC (Boiler 2) only the top three were required. Across all datasets, a frequency bin granularity of 21-50 Hz was sufficient with dimensions ranging from 20-50. RRSE values ranged from 0.43-0.65% for Boiler 1 and 2.69-2.99% for Boiler 2. As the number of dimensions was low enough, and the kNN algorithm fast enough, wrapper methods could be applied using kNN to remove additional dimensions – see Section 6.1.1.4.4.

### 6.1.1.5.3 MFCCs

The following presents the results of ML algorithms as applied to Datasets 1-6\_MFCC with a nine second moving average filter. In general, the predictive accuracies achieved applying the kNN, LR and M5P ML algorithms to Datasets 1-6\_MFCC were comparable to that of Datasets 1-6\_NFC: kNN returned the lowest RRSE scores across all MFCC datasets and LR performed worst; additionally, algorithms were found to asymptote for dimensions less than 80.

The result of applying kNN across all Datasets 1-6\_MFCC, for the range of dimensions tested, have been summarised in Figure 36. Similarly, to the results from NFC data, algorithms on MFCC features perform best for Boiler 1, achieving RRSE in the range of 0.42-0.76%, this is compared to 2.71-2.82% for Boiler 2. The accuracies between contact microphones (Microphones 1 and 3) did not vary considerably. The accuracies achieved from the contactless microphone (Microphone 2), were slightly worse than the contact microphones, and in general showed a larger variance. As observed in Figure 36, the optimum selection (minimise dimensions while maintaining accuracies) for the number of MFCC dimensions was in the range of 40-60.

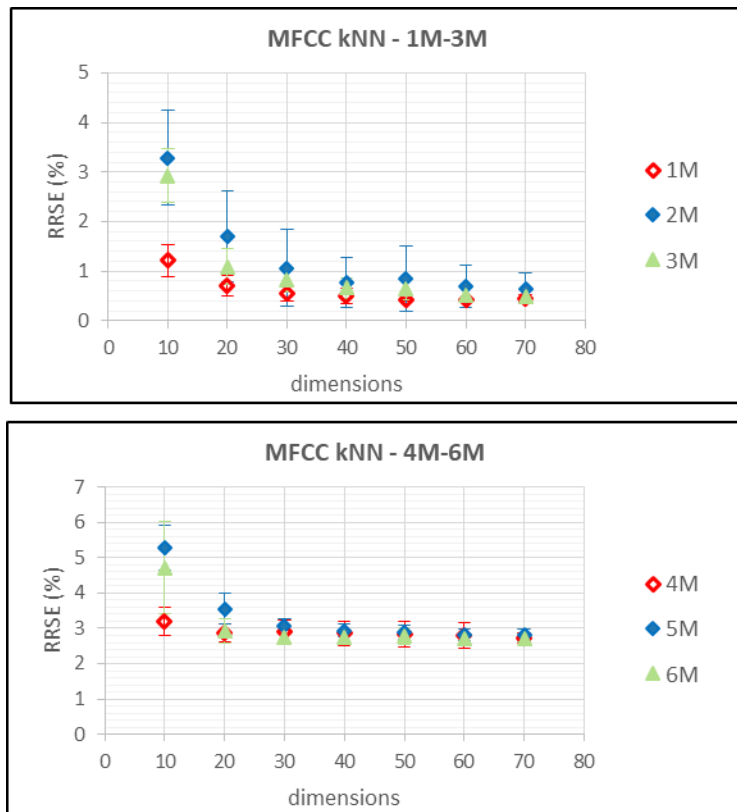


Figure 36 Plots of the resultant average RRSE after running ten iterations of 10-fold CV using kNN algorithms split by dataset, plotted against the number of dimensions in the data. The data used in the algorithms varied by the number of MFCCs calculated over the same range of frequencies

As explained in Section 5.1.3.3, MFCCs are mapped from a frequency scale to a Mel-scale for the purposes of replicating the human auditory response. However, when removing this mapping, the results of ML algorithms appear to not be impacted. Thus, MFCCs can be replaced by a linear-frequency cepstral coefficients (LFCCs) without any notable loss in accuracies. This should not be surprising as there is no logical reason for a Mel-scale in the instance of non-human related audio.

#### 6.1.1.5.4 Wrapper Methods

Wrapper methods evaluate attribute sets by using a learning scheme, the method used was developed by Kohavi and John (1997). The search method for determining the subset of attributes to test was best-first. The learning scheme tested was kNN with  $k=1$  or  $k=2$  depending on the dataset being analysed.

Table 9 and 10 show the results of running wrapper methods with kNN algorithms, across all datasets. In the tables, the 'original' selection refers to the reduced feature selection as determined in Sections 6.1.1.5.2 and 6.1.1.5.3. The results 'Wrapper' refer to the results gained

after reducing the feature space by applying wrapper methods. The results after applying wrapper methods show no significant loss in accuracies while reducing dimensions from ranges of 21-50 to 12-27. For completeness, in addition to running multiple iterations of 10-fold CV, bootstrap aggregation (bagging) (Breiman, 1996) was also tested for all datasets after the wrapper method had been applied. Bagging in this case was performed using 50 bags, each containing the same number of samples (randomly sampled with replacement) as the number of instances. RRSEs achieved applying 'bagging' align closely with 10-fold CV, cultivating confidence in the observed predictive accuracies.

Dataset	Original – kNN 10-fold CV		Wrapper – kNN 10-fold CV		Wrapper – kNN Bagging	
	RRSE ± std.dev	dimensions	RRSE ± std.dev	dimensions	RRSE ± std.dev	dimensions
1_NFC	0.43 ± 0.043	47	0.47 ± 0.061	26	0.49 ± 0.065	26
2_NFC	0.65 ± 0.401	50	0.74 ± 0.403	24	0.83 ± 0.367	24
3_NFC	0.55 ± 0.106	36	0.55 ± 0.109	27	0.56 ± 0.117	27
4_NFC	2.69 ± 0.105	20	2.73 ± 0.097	12	2.83 ± 0.086	12
5_NFC	2.99 ± 0.151	21	3.02 ± 0.192	14	3.06 ± 0.129	14
6_NFC	2.70 ± 0.109	40	2.82 ± 0.330	16	2.91 ± 0.161	16

*Table 9 Resultant average RRSE before and after running wrapper methods for Datasets 1-6\_NFC. Also listed are the changes in dimensions*

Dataset	Wrapper – kNN 10-fold CV		Wrapper – kNN 10-fold CV		Wrapper – kNN Bagging	
	RRSE $\pm$ std.dev	dimensions	RRSE $\pm$ std.dev	dimensions	RRSE $\pm$ std.dev	dimensions
1_MFCC	0.50 $\pm$ 0.150	40	0.57 $\pm$ 0.143	22	0.60 $\pm$ 0.101	22
2_MFCC	0.77 $\pm$ 0.499	40	0.99 $\pm$ 0.664	23	1.03 $\pm$ 0.566	23
3_MFCC	0.66 $\pm$ 0.206	40	0.66 $\pm$ 0.164	25	0.67 $\pm$ 0.114	25
4_MFCC	2.86 $\pm$ 0.352	40	2.78 $\pm$ 0.132	16	2.88 $\pm$ 0.110	16
5_MFCC	2.94 $\pm$ 0.171	40	3.04 $\pm$ 0.175	26	3.12 $\pm$ 0.194	26
6_MFCC	2.73 $\pm$ 0.121	40	2.81 $\pm$ 0.165	22	2.87 $\pm$ 0.135	22

*Table 10 Resultant average RRSE before and after running wrapper methods for Datasets 1-6\_MFCC. Also listed are the changes in dimensions*

Of note, after application of wrapper methods for Dataset 5\_MFCC, 14 frequency components in the 200-1000 Hz region were left, each with a range of approximately 40 Hz. This selection reconciles well with the conclusions made during data visualisation in Figure 29; namely that the 300, 400 and 500 Hz regions of the acoustic spectra should be important in distinguishing values of  $\varphi$ .

#### 6.1.1.5.5 Analysis of kNN

The ‘curse of dimensionality’ is a potential issue when applying kNN: As the feature space becomes large, distances to nearest neighbours approach the distances to farthest neighbours, making nearest neighbour matching meaningless – refer to Beyer et al. (1999). To test this phenomenon, one can: (a) Analyse the ratio between farthest neighbours and nearest neighbours (when this ratio approaches unity the application of kNN is meaningless); and (b) Analyse how many nearest neighbours exist in incrementally increasing radiuses.

Performing said analysis highlighted several ‘worst performing’ data points. A large majority of which (over 86%) corresponded to the first five or last five seconds of recordings i.e. data points where full time-smoothing, spanning nine seconds, had not been applied. Such points were not as well clustered as the rest of the dataset, highlighting the potential instability of acoustic data with no time smoothing applied. By removing the points at the start and end of recordings, reducing instances by 2.5% and 3.8% for Datasets 1-3 and 4-6 respectively, small improvements

can be observed in kNN performance; this has been summarised in Figure 37. Note, in Figure 37 the 'Reduced' label refers to datasets where data points have been removed.

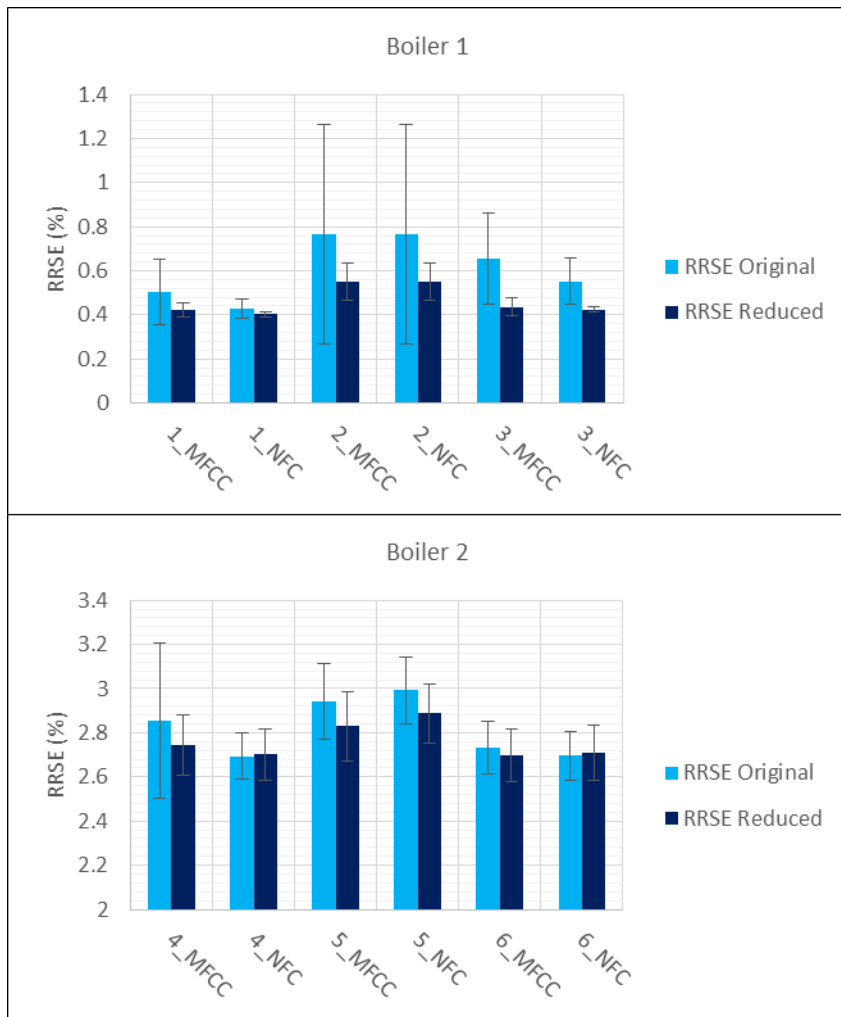


Figure 37 RRSE results of kNN using 10-fold CV to all datasets (before application of wrapper methods). 'Original' refers to the original datasets (Datasets 1-6) without the removal of any instances. 'Reduced' refers to datasets with non-fully time-smoothed data points removed (2-4% fewer instances)

By analysing the 'worst' performing data point for each dataset after removing non-fully time-smoothed data points via method (b) above, the data, in a feature space of up to 40 dimensions, was shown to be well clustered: Via method (b) a variable  $\epsilon$  was used to indicate how many multiples of the nearest neighbours is required to enclose all points, after removing non-fully time-smoothed data the value of  $\epsilon$  required to enclose all points was greater than 40 for the worst performing data point and dataset combination; all other data had an  $\epsilon$  value greater than 100. This can be compared to a  $\epsilon$  value of 10 presented by Beyer et al. (1999) for a 10 dimensional dataset. Thus, the data presented in this analysis is well clustered in comparison and should not be susceptible to the 'curse of dimensionality' i.e. application of kNN appears robust.

### 6.1.1.5.6 Artificial Neural Networks and Support Vector Machines

At this point ANNs and SVMs were tested on a broad range of dimensions for both sets of acoustic features (MFCCs and NFCs). Feature selection was influenced by the results kNN analysis (Figures 35 and 36). Figure 38 shows the most relevant results of applying ANNs and SVMs as compared to kNN for all datasets - the size of the bubbles in the chart represents the number of dimensions in the feature space. As observed SVMs performed significantly better than ANNs, particularly for the case of MFCC features. Both ANNs and SVMs performed worse than kNN but better than M5P. Details of the ANN and SVM algorithms applied have been provided below. Wrapper methods have not been applied to ANN and SVM algorithms, however if done so additional dimension reduction may be feasible.

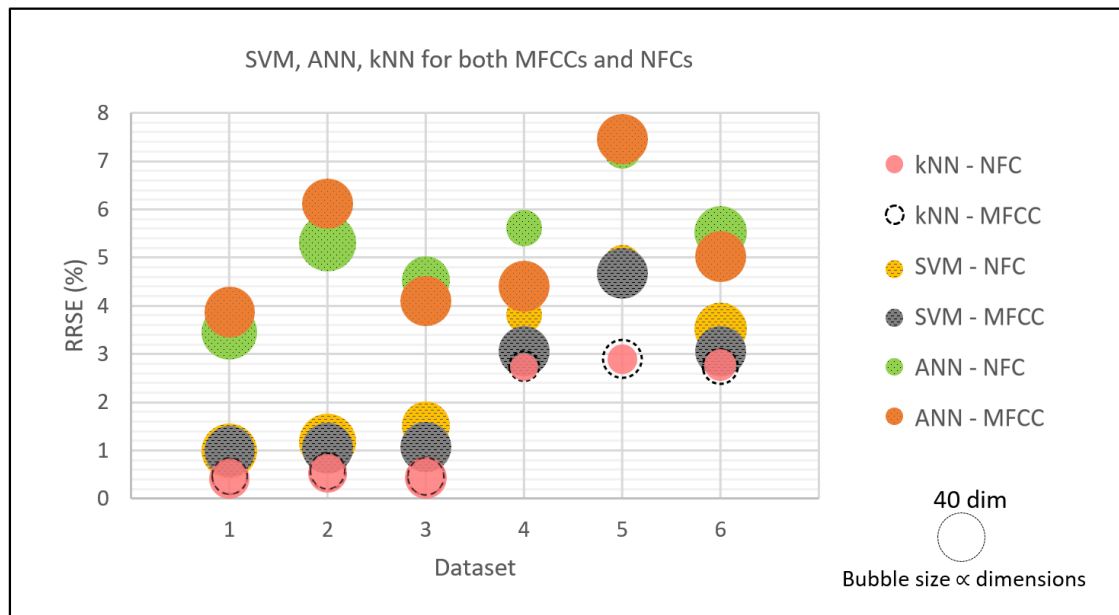


Figure 38 A bubble chart of the resultant average RRSE after running 10-fold CV using kNN, SVM and ANN algorithms on both NFC and MFCC features for all datasets. The size of bubbles represents the number of dimensions

The ANNs tested contained two fully connected layers of hidden neurons, the number of which was based on the number of input features: The first layer was equal to the number of features plus one neuron, the second layer contained half the number of neurons in the first. Sigmoid functions were used as activation functions for all neurons except the output neuron which was an unthresholded linear unit. The learning rate was set to a constant value of 0.3 and momentum term to 0.2. The number of epochs for training was limited to 1000.

The SVMs tested used a Pearson VII universal kernel (PUK) with a stopping criteria formulated by Shevade et al. (2000). The application of the PUK kernel avoided the requirement of testing

multiple ‘standard’ kernels (Üstün et al., 2006). The complexity parameter of the SVM model was set at 1.0 and the tolerance set at 0.001. The Omega and Sigma values of the PUK kernel were both set to 1.0.

It is likely that the performance of both SVMs and ANNs could be improved by tweaking the architecture and parameters of the algorithms. To do so the use of a grid search or genetic algorithm (Wu et al., 2007, Leung et al., 2003) would be appropriate. Additionally, as SVMs appear to provide a good framework to tackling this problem, a genetic SVM algorithm could be useful for initial feature selection (Frohlich et al., 2003).

#### 6.1.1.6 Varying Air Intake

All results reported thus far are applicable for cases where variations in  $\varphi$  have been due to varying gas rate. If combustion acoustics are indeed related to  $\varphi$  values, then it should also be possible to develop accurate learning algorithms for predicting  $\varphi$  for cases when incoming air is adjusted and gas rates held constant. Data was thus collected from all microphones over the same range of  $\varphi$  values while adjusting air rates. The method of this data collection has been summarised in Section 5.1.2.4.

As before NFC features MFCCs were calculated for each boiler and microphone combination. This resulted in the datasets summarised in Table 9; unfortunately, due to a technical failure recordings from Microphone 2 were not available.

Dataset	Boiler	Microphone	Gas Type	$\varphi$	Instances
7_(NFC/MFCC)	1	1	G20	0.75-0.88	4536
8_(NFC/MFCC)	1	3	G20	0.75-0.88	4536

Table 11 Summary of datasets available for analysis for Section 6.1.2

The same method of data analysis was applied to Datasets 7 and 8 as done so in Sections 6.1.1.3, 6.1.1.5.2 and 6.1.1.5.3. For NFCs, feature selection via information-gain evaluation metric resulted in a subset of seven frequency regions. As before, from the range of ML algorithms tested, the kNN algorithm was the most successful for both the NFC and MFCC datasets. The average RRSE value of ten iterations of 10-fold CV for kNN has been summarised in Figures 39 and 40 during variations in the number of dimensions.

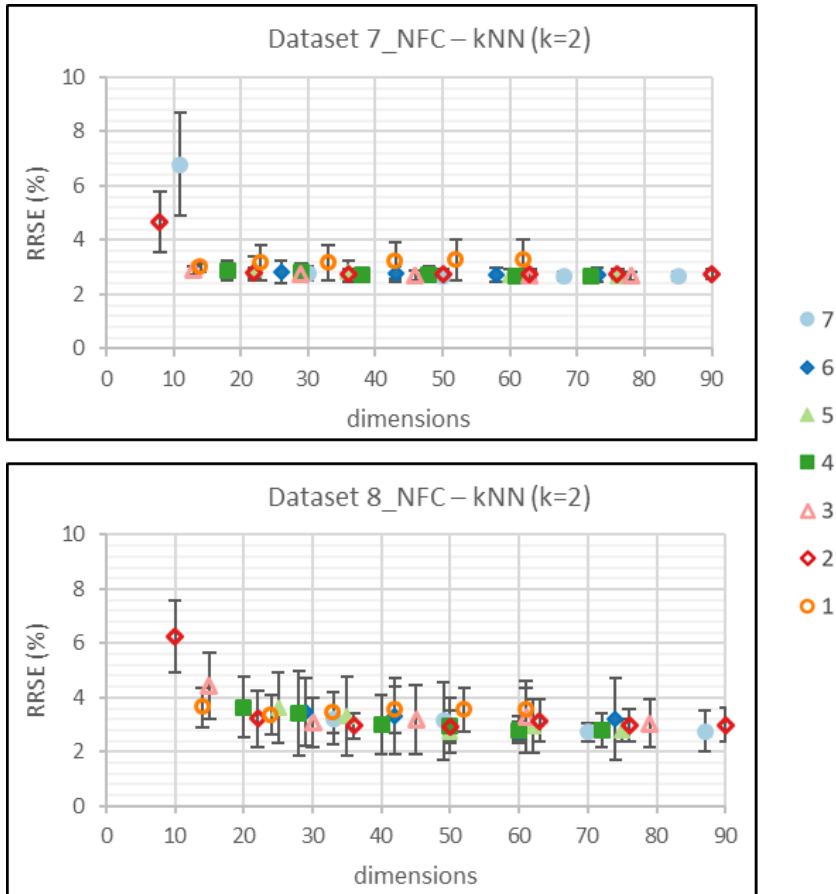


Figure 39 Plots of the resultant average RRSE after running ten iterations of 10-fold CV using kNN algorithms split by dataset, plotted against the number of dimensions in the data. The data used in the algorithms was varied by changing the granularity of frequency bins and by removing the number of frequency regions included from 7 to 1

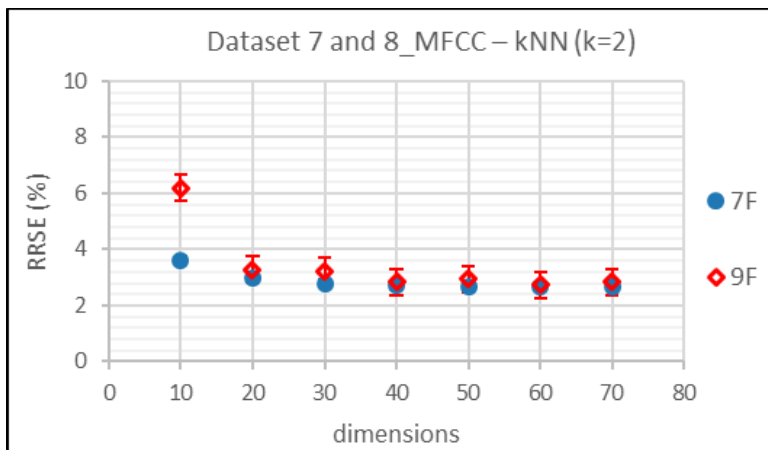


Figure 40 Plots of the resultant average RRSE after running ten iterations of 10-fold CV using kNN algorithms split by dataset, plotted against the number of dimensions in the data. The data used in the algorithms was varied by changing the number of MFCCs included from 70 to 10

As observed, for Datasets 7\_NFC and 8\_NFC RRSE results of  $2.70 \pm 0.177\%$  and  $2.77 \pm 0.341\%$  were achieved for 46 and 50 dimensions respectively. For Datasets 7\_MFCC and 8\_MFCC RRSE

results of  $2.71 \pm 0.171\%$  and  $2.84 \pm 0.341\%$  were achieved for 40 dimensions. These results are comparable to the results of Datasets 4-6\_NFC and 4-6\_MFCC. Thus, it appears combustion acoustics can be used to accurately predict  $\varphi$  irrespective of adjusting air or gas rates.

#### *6.1.1.7 Varying Burner*

For Boiler 1 three different burners were tested. Images of the burners and descriptions of the differences between them have been given in Section 5.1.1. For each burner, recordings were made for the full range of  $\varphi$  (0.75-0.88) for G20 gas only. From the recordings, it was possible to develop logistic regression or kNN algorithms to predict which burner was in the system to 100% accuracy (kappa statistic of 1) using 28 NFCs. Thus, combustion noise from each burner was unique in a way which was independent of  $\varphi$ . Consequently, it would be expected that a different algorithm would need to be trained for each burner type, or that training datasets contain examples for all burner types. For a dataset containing examples for all three burners, it was possible to use kNN algorithms to accurately determine  $\varphi$ , independent of burner type, with an RRSE of  $2.66 \pm 0.113\%$  using 44 NFCs, or an RRSE of  $2.69 \pm 0.097\%$  using 40 MFCCs. Thus, similarly to gas type, burner type impacts combustion acoustics and the training data should contain the full range of burners expected, or separate algorithms should be used for each burner.

#### *6.1.2 Predicting Gas Type*

For datasets listed in Table 5, the class values were changed from  $\varphi$  to a label indicating the gas type (G20, G21, G25 or G222). The same procedure as explained in Sections 6.1.1.2 to 6.1.1.5 was then applied. This resulted in algorithms for estimating the gas type based on combustion acoustics for the complete range of  $\varphi$  investigated. As this was a classification problem, the measure of the predictive accuracy of the algorithms was given in terms of the kappa statistic. It was found that gas types could be predicted to 100% accuracy, returning a kappa statistic of 1 for all datasets using either kNN ( $k=1$ ) or logistic regression. For Datasets 1-6\_NFC, the number of required dimensions was between 8 and 21, and for Datasets 1-6\_MFCC between 20 and 30. Thus, acoustics was a very good indicator of gas type for the range investigated irrespective of varying  $\varphi$  values. Table 12 shows the confusion matrix for predicating gas type from acoustics.

Predicted Gas Type - Acoustic data		kNN	G20	G21	G25	G222
Actual	G20	4,325	0	0	0	0
	G21	0	4,320	0	0	0
	G25	0	0	4,320	0	0
	G222	0	0	0	0	4,315

Table 12 Confusion matrix showing the predicted gas type as based on acoustic data.

## 6.2 Ionisation and CO Combustion Sensor

In order to compare the predictive ability of ionisation probes and CO gas sensors (the most common CCS sensing technologies) to the proposed acoustic methods described above, a range of similar ML approaches are applied to data from these devices for comparative purposes.

### 6.2.1 Predicting the Equivalence Ratio

CO concentrations were recorded using a Siemens Ultramat 23 gas analyser. Ionisation current was measured using the built-in ionisation probe situated in the WB7 heat exchanger and collected from the on-board energy management system for Boiler 2. Both streams were logged every second and aligned with the time frames of Datasets 3-6 and thus comparable with results from Section 6.1. The ionisation current and CO concentration data was cleaned to remove anomalous data points which occurred due to resetting systems or erroneous recordings. As before time smoothing of varying widths was applied to both data streams. Once cleaned the ionisation current and CO concentration datasets contained 12,960 instances across three gas types (G20, G21 and G222); for each instance  $\varphi$  was calculated as before from CO<sub>2</sub> concentrations via Equation 5.1.

To determine the predictive power of the CO concentration and ionisation current data streams, a range of ML algorithms were tested using 10-fold CV. ML algorithms tested included kNN, LR, polynomial regression, MSP and ANNs. Table 13 shows the result of the algorithm which resulted in the lowest average RRSE for a data stream (CO concentration or ionisation current)

as split by gas type and for all gases combined. Note, a time smoothing width of nine seconds was found to maximise accuracies and so was applied to all datasets.

		G20	G21	G222	All gas types
CO concentration	ML algorithm	kNN (k=19)	kNN (k=19)	kNN (k=19)	kNN (k=19)
	Ave. RRSE (%)	4.12	3.90	4.06	10.83
	Std.dev	0.211	0.184	0.275	0.383
Ionisation current	ML algorithm	kNN (k=1)	kNN (k=1)	kNN (k=1)	M5P
	Ave. RRSE (%)	15.27	24.44	45.95	46.48
	Std.dev	3.306	2.973	2.967	1.551

*Table 13 Summary of the average RRSE results of the best performing ML algorithms for Ionisation current and CO concentration data as split by gas type and for all gas types combined*

In general ML algorithms based on CO data resulted in higher accuracies compared with ionisation current data. For both data streams accuracies significantly decreased when all gas types were included together. As shown in Figures 41 and 42, for the ionisation current this was likely due to the impact of G222 i.e. hydrogen containing gases; for CO concentration data, this was likely due to varying carbon contents of the gases ‘blurring’ the relationship between CO concentrations and  $\varphi$ .

As observed in Figure 41 the ionisation current for all gases seemingly increased with  $\varphi$ , however for G222 the relationship was less pronounced with single values of ionisation current representing a substantial range of  $\varphi$  values. For example, for G222, an ionisation current of 3800  $\mu\text{A}$  was observed for  $\varphi$  values of 0.80 and 0.89, a range covering over half  $\varphi$  values investigated. Hence ionisation current as a predictor of  $\varphi$  could be considered to fail for  $\text{H}_2$  containing gases.

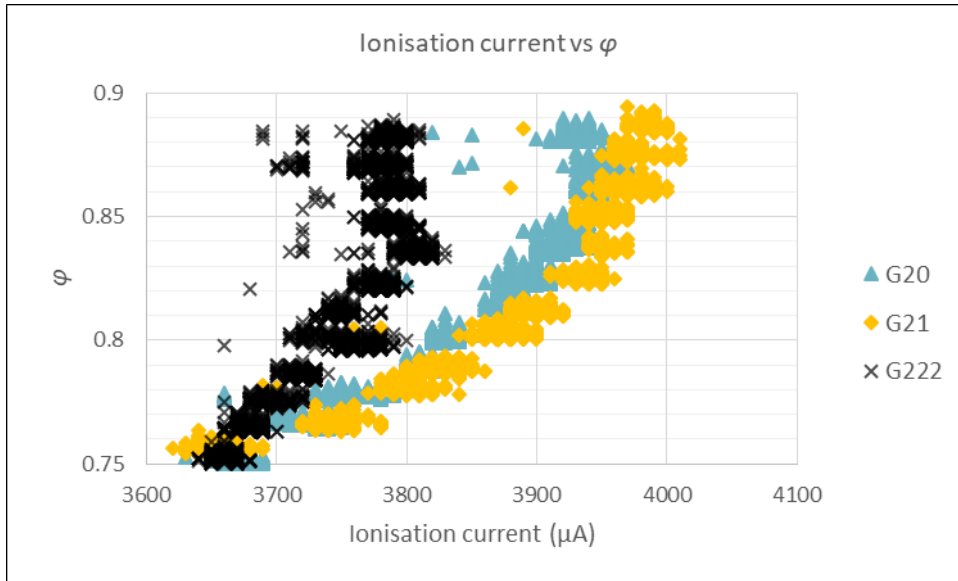


Figure 41 Plot of ionisation current against  $\phi$  as split by gas type for data collected from Boiler 2

As observed in Figure 42 the CO concentration data varied in its relationship with phi for each gas type. In the figure, for single gas types the CO vs.  $\phi$  curve was quite clearly defined, however each curve was positioned slightly differently - with G21 as the 'lower' curve and G222 as the 'higher' curve. For G222 the amount of carbon present per unit volume in the combustible mixture is less than G20, which is less than G21 and would thus produce less CO if everything else was equal. Consequently, for  $\phi=0.8$ , CO concentrations of 48-52ppm were observed for G222, 57-59ppm for G20 and 61-64ppm for G21. Note, the shape of the curves in Figure 42 indicated that polynomial regression may suited in predicting  $\phi$ , doing so leads to predictive algorithms with an RRSE 18.3%, this is compared to a RRSE of 33.3% for LR and 10.8% using kNN.

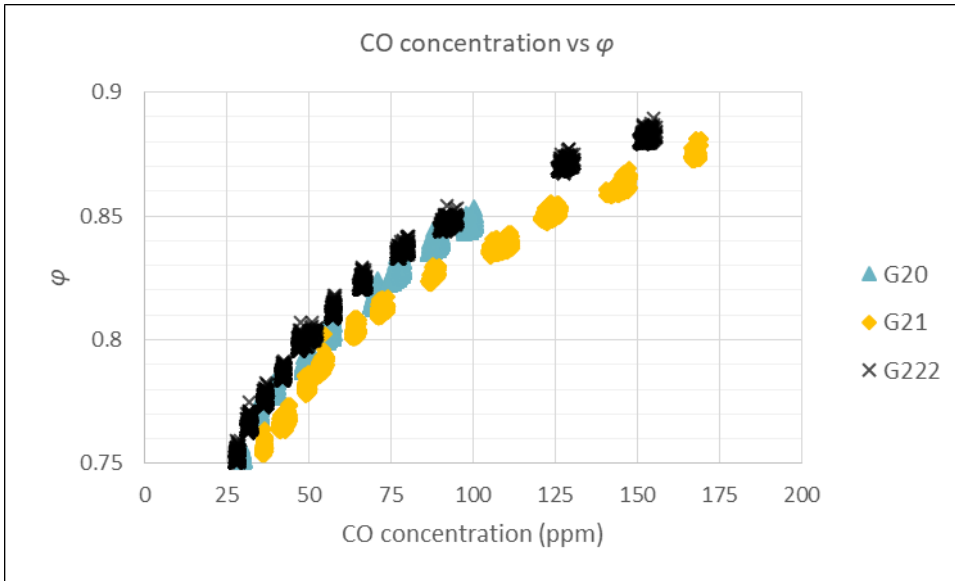


Figure 42 Plot of CO concentration against  $\phi$  as split by gas type for data collected from Boiler 2

For detection of CO concentration, the gas analyser used in this study was very accurate with an error in the range of 0.07 % (Siemens, 2017). CO gas sensors integrated within domestic appliances are likely to be much less accurate and reliable, thus would result in lower predictive accuracies than those reported. Additionally, the ionisation probe used to collect ionisation current data was a so-called ‘standard’ ionisation sensor used for flame detection. Combustion sensor specific ionisation sensors are located further into the flame to provide a stronger signal, such a sensor was not available during these tests. However one would expect the granularity of the signal from a combustion sensor specific ionisation sensor to be more granular but still suffer from the issues with regard to hydrogen containing gases as reported by E.ON Ruhrgas (Nitschke-Kowsky and Wessing, 2012) using the ‘SCOT’ ionisation sensor.

### 6.2.2 Predicting Gas Type

As summarised in Section 6.1.2, combustion acoustics can be used to predict gas type very accurately for the gas types investigated. In this section, data from the ionisation probe and CO gas sensor was tested for a range of ML algorithms to assess gas type predictive potential. As this is a classification problem the results were expressed as a confusion matrix and summarised as a Kappa statistic.

As observed in Tables 14 and 15 for Boiler 2 the ionisation sensor returned a Kappa statistic of 0.67 and CO gas sensor 0.78 for the best performing ML algorithm. The best performing ML algorithm in this instance was J48. J48 is a pruned decision tree algorithm using an information-gain metric to dictate how the tree is constructed –refer to Witten et al. (2016, pp. 189-199).

Predicted Gas Type - Ion current				
Actual	J48	G20	G21	G222
	G20	2211	410	508
	G21	708	2567	480
	G222	196	69	3590
	%correct	71%	84%	78%
Kappa: 0.67				

Table 14 Confusion matrix for predicting gas type using J48 ML algorithm for ionisation current data. Also included are the Kappa statistic and the percentage correct

Predicted Gas Type - CO concentrations				
Actual	J48	G20	G21	G222
	G20	3582	558	180
	G21	628	3441	251
	G222	162	158	3970
	%correct	82%	83%	90%
Kappa: 0.78				

Table 15 Confusion matrix for predicting gas type using J48 ML algorithm for CO concentration data. Also included are the Kappa statistic and the percentage correct

### 6.3 Summary

As summarised in Table 16, algorithms developed for predicting  $\varphi$  and gas type from acoustic data were much more accurate compared to traditional data streams (CO gas data and ionisation current data). This indicates that combustion acoustics contains much more information relative to CO concentrations and ionisation current – the extra information is being utilised by machine learning algorithms to predict  $\varphi$  and gas type to a higher accuracy. Such information is released by any flame and can be gathered without the need for invasive sensors.

The challenge in using such an approach in an operational scenario comes down to robustness over time and in the presence of background noise sources. The following discussion gives a detailed overview of the main findings of the study and their significance with respect to the wider literature. Following this limitations, assumptions and next steps are discussed

	Predicting $\varphi$ (RRSE %)	Predicting Gas Type (% correct)
Acoustic sensor	≈3.0	100
Ionisation sensor	46.5	78
CO gas sensor	10.8	85

*Table 16 Summary table of prediction results for data gathered from the acoustic sensor, ionisation sensor and CO gas sensor for all gas types (G20, G21 and G222). Boiler 2 only.*

## 7. Discussion

### 7.1 Significance of the results

#### 7.1.1 Summary

The aim of this study was to determine if combustion acoustics can be used as an indirect measure of the operational  $\varphi$  of combustion for domestic gas-fired boilers. For the two boilers investigated, this study has shown that pitch related acoustic features can be used to predict  $\varphi$  with RRSEs less than 3% by application of ML algorithms. This was achieved for an  $\varphi$  range of 0.75-0.88, independent of the gas types investigated and for the full range of microphones tested.

Microphones tested included a contact piezoelectric microphone costing 1-2 USD, in addition to two professional standard microphones, one contact, and one contactless. Gas types used in the analysis were G20, G21, G25 and G222. Acoustic features tested included NFCs and MFCCs/LFCCs. kNN algorithms were found to be the most accurate ML algorithm tested for all features, although SVMs also performed well (less than 3.6% RRSE for all contact microphones). Depending on the microphone and boiler under consideration the minimum number of dimensions required to predict  $\varphi$ , to less than 3% RRSE, varied from 12 to 26. The number of instances in these training/testing sets varied from 12,960 to 17,280. Testing/training was performed via multiple iterations of stratified 10-fold CV and, for the case of kNN, bootstrap aggregation (bagging). Time smoothing (spanning nine seconds) across acoustic features improved accuracies significantly in comparison with no time smoothing on one second windows.

ML algorithms based on pitch related acoustic features performed much better than those based on ionisation current data and CO concentration data. This has been summarized in Figure 43. The figure displays the predicted vs actual values of  $\varphi$  for all features tested using SVMs. Also plotted is the correct prediction, aka the actual. One should note that  $\varphi$  used in this figure and throughout the study is an estimate of  $\varphi$  as calculated from exhaust gases using Equation 5.1 and Table 3.

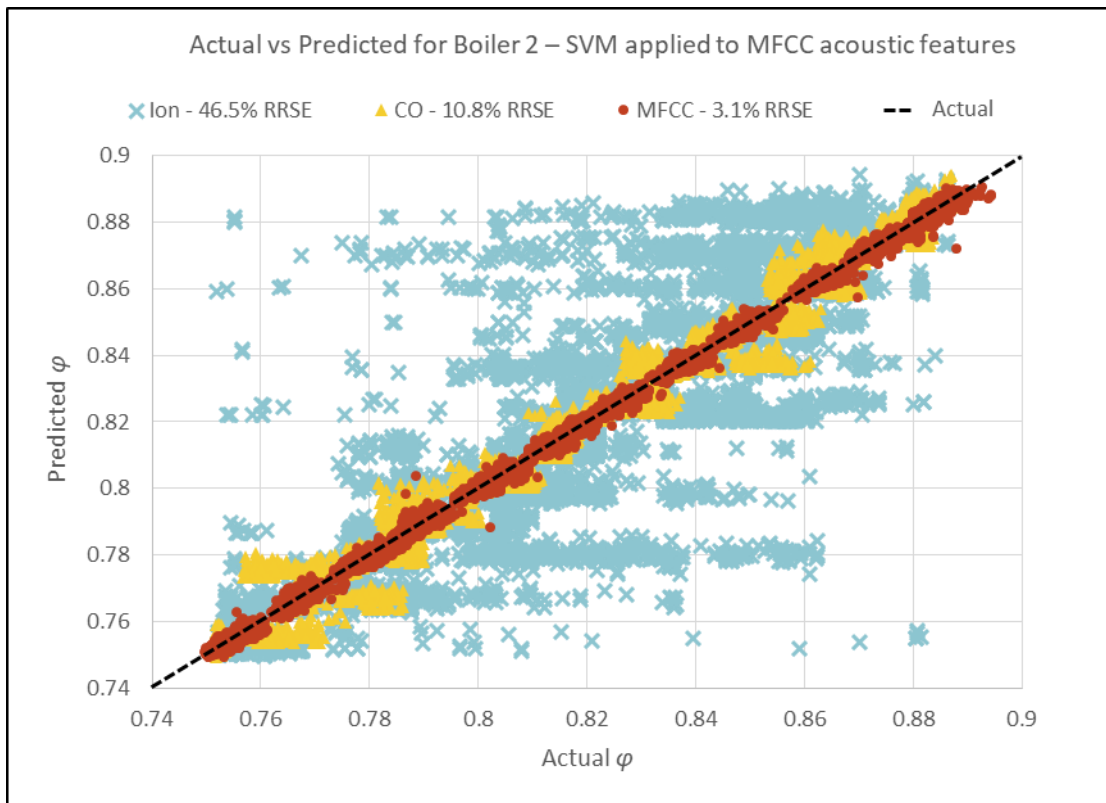


Figure 43 Actual vs predicted per estimates from SVM algorithms based on MFCC (Dataset 6\_MFCC), ionisation current (Ion) and CO concentration (CO) feature data for Boiler 2. The black dotted line represents the correct prediction

An additional aim of this study was the use of combustion acoustics as an indirect measure of gas type. For the range of gas types investigated, it was possible to predict gas type to 100% accuracy using ML algorithms based on pitch related acoustic features. This could be achieved using 8-21 dimensions depending on the boiler and microphone combination. In comparison, ionisation current and CO concentration features returned kappa values of 0.67 and 0.78 respectively (70-90% correct).

### 7.1.2 Significance

For a combination of gas composition and gas combustion system, a 'preferred' equivalence ratio exists. This preferred equivalence ratio maximizes the efficiency of the burn while remaining within the emission constraints defined by regulation (emissions include  $\text{NO}_x$  and CO). Figure 44 below shows the change in  $\text{NO}_x$  and CO concentration with equivalence ratio for a boiler and gas type combination. As one can see, a value of equivalence ratio in the range of 0.72 may be optimum for this combination of gas composition and boiler (this depends on emission constraints). However, a different gas composition would shift the equivalence ratio value (due to different calorific content) and show a different  $\text{NO}_x$  and CO curve and therefore

have a different preferred equivalence ratio value associated. In addition, a different boiler will likely produce a different emission curve and therefore a different preferred equivalence ratio. Thus, there exists a 'preferred' equivalence ratio for a combination of gas composition and gas combustion system. This preferred value should be attained operationally to maximise efficiencies in any gas combustion system.

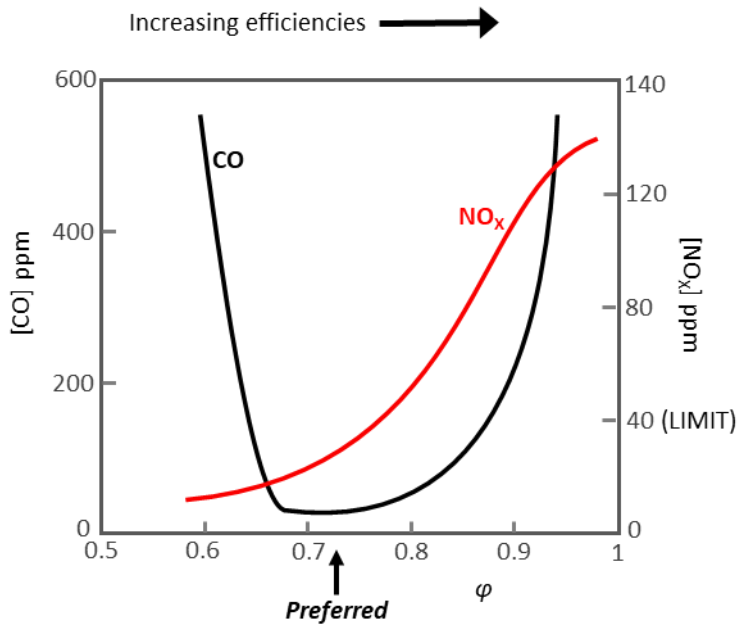


Figure 44 CO and NO<sub>x</sub> emissions for methane-air reaction at atmospheric conditions in a domestic gas-fired boiler. The boiler was a Worcester Bosch Greenstar 28i Junior. The CO and NO<sub>x</sub> trace has been averaged significantly for illustration purposes

Gas compositions in the gas network can vary within the bounds specified by the legislation of a country. For countries, such as Poland, France and Germany gas compositions vary from region to region by a significant amount. To manage the impact of varying gas compositions in these countries, many boiler manufactures have developed so-called combustion control systems to control the value of the equivalence ratio during changes in gas composition. These combustion control systems aim to maintain a set value of equivalence ratio regardless of the gas composition. This type of system may be referred to as attaining a naïve-preferred equivalence ratio. In most cases the naïve-preferred equivalence ratio value is equal to the preferred equivalence ratio for methane gas (aka G20).

Integral to a combustion control system is the method by which the current value of φ is determined. Once this value is known the system can make any necessary adjustments to φ by altering either the air or gas inlet rates. Typically, an electronic gas valve partition is adjusted to alter the gas inlet rate. Determining the operational value of the equivalence ratio is performed

by a component called a combustion sensor. The current stock of available combustion sensors aim to attain the naïve-preferred  $\varphi$  regardless of the gas being burnt. In addition to this, the current stock of available combustion sensors have many disadvantages. The primary disadvantage of which has been highlighted in this study, namely the inability to determine  $\varphi$  when significant proportions of  $H_2$  are present in the gas being burnt. For ionisation probes this is due to the unique nature of ion production and flame height variation in hydrogen-hydrocarbon gases (Näslund, 2014, p.15); for CO gas sensors this is due to the lack of carbon in the gas emissions. Considering  $H_2$  is being strongly considered in the UK (Ambrose, 2017) and elsewhere as a means to strip harmful carbon emissions from the energy system, a solution to the controlling  $\varphi$  for such gas compositions is more pertinent now than ever.

The problem being addressed in this study was thus twofold. To investigate a combustion sensor that could potentially:

- Deal with the failure of the current stock of combustion sensors to detect  $\varphi$  of high proportion  $H_2$  gas compositions
- Deal with the failure of the current stock of combustion sensors to detect the current composition of the gas type being burnt and thus develop a sensor which can attain the preferred  $\varphi$

From the literature review (Section 3.1), it was found that combustion noise was strongly related with the very nature of the flame. In addition, combustion noise of varying types (direct and indirect) is inevitable in any practical flame. Consequently, it was hypothesised that *combustion acoustics could be used to predict properties of the flame such as operational  $\varphi$* . Although no previous studies had shown, or attempted to show empirically that combustion noise could be used as an indicator of  $\varphi$ , the idea of the new solution was investigated. Such a sensor could sit external to the flame, be made cheaply and potentially provide more information that was available using other combustion sensing means.

From a pilot study (Section 4) and the primary results presented in Section 6, it appears that by applying machine learning an acoustic combustion sensor is a legitimate solution to the challenges outlined. The results of this study indicate that by interpreting combustion noise from a gas combustion system, properties of the flame such as gas composition and operational  $\varphi$  can be determined accurately. Such an acoustic combustion sensor system could be incorporated into a control loop to achieve a 'preferred'  $\varphi$ . To note, although the results of this study indicate gas composition can be accurately determined, only four gas types were

investigated. Regardless, considering the algorithms could easily categorise based on four gas types, algorithms should also be able to do a good job of categorising many more gas compositions.

The idea of acoustics as a method of flame diagnostics for determining  $\varphi$  was first proposed in the open literature by Petela and Petela (1983) and Ramachandra and Strahle (1983). However, in a relatively recent review by Ballester and García-Armingol (2010, p. 397) it was stated that “Although no subsequent application of this technique has been found in the open literature (...), these studies clearly demonstrate that the information contained in acoustic flame signals is intimately related with the very nature of the combustion process and, therefore, may offer interesting possibilities for flame monitoring.” During the literature review of this study, Sanz et al. (2008) were the only authors found to use combustion acoustics as a diagnostic tool in a practical system, however this was for a fixed gas type and a fixed  $\varphi$ . The work presented here has indicated that not only is  $\varphi$ ,  $\text{NO}_x$ ,  $\text{CO}_2$  and  $\text{CO}$  correlated to combustion acoustics, but they can be accurately predicted independent of a range of differing gas types. In addition, the exact gas type can also be predicted to a high degree of accuracy, all of which outperforms data from an ionisation and  $\text{CO}$  gas sensors.

Previous studies (Rajaram and Lieuwen, 2003, Hirsch et al., 2007) have indicated that the spectral shape observed from direct combustion noise remains constant during variations in  $\varphi$ . In the present study, it has been shown that variations in  $\varphi$  do impact the spectral shape of combustion noise from an unknown combination of direct and indirect noise sources; indeed changes in the spectral shape of combustion acoustics were significant enough to allow accurate prediction of  $\varphi$ . Understanding why this is the case is not within the scope of the study and due to the complexity of combustion acoustics, discussions on the matter are largely speculative. For example, spectral shape variations could be due to variations in indirect combustion noise phenomena; and/or the modifying effect of the combustion chamber (such as system resonances); and/or changes in turbulence in the flame etc. Although the literature on combustion noise phenomena is extensive (Dowling and Mahmoudi, 2015), specific contributions of various combustion parameters to different sources of combustion noise within a confined environment are not well understood. However, considering the results presented by authors investigating direct combustion noise, one would speculate that the origin of acoustic variability in the current study, due to variations in  $\varphi$ , is due to variations in indirect noise sources, namely variations in entropy and vorticity waves.

From a commercial context, combustion diagnostic options include ionisation sensors, flue gas sensors, emission/absorption spectroscopy and flame imaging. Both ionisation sensors and flue gas sensors have been installed in domestic appliances. Currently it appears line-of-sight techniques such as flame imaging and spectroscopy have not been considered for integration into domestic appliances; this is likely due to integration costs and robustness (spoiling of apertures etc.). The results of this study have shown that the array of practical combustion sensors should include combustion acoustics. Combustion acoustics should be considered over other options for the following reasons:

1. More accurate in determining  $\varphi$  relative to an ionisation probes or CO gas sensors
2. Potentially much cheaper than current CO gas sensors
3. Could be retrofitted to appliances, and unlike other techniques, does not require access to either the flame or exhaust gases
4. May be the only suitable combustion sensing option for high proportion hydrogen-hydrocarbon boilers

The final point is of significant importance in the UK at this time due to the push by policy to move to hydrogen for heating: £25 million is being invested via the Hydrogen for Heat Programme (Energy Live News, 2017) to investigate the potential of converting heating and cooking systems to hydrogen. Not shown in these results, but obviously apparent, is that for very large proportion hydrogen gas compositions, both ionisation and CO gas sensing approaches would fail. For CO gas sensors, this is simply because high proportion hydrogen gases contain little carbon for detection. There may therefore be a very specific application domain for an acoustic combustion sensor, that of a hydrogen or high proportion hydrogen-hydrocarbon boilers.

Outside of the scope of this study which requires further investigation for such a technique include the impacts of boiler failure modes, potential impact of environmental noise, and robustness of techniques over time. In addition, a large variety of potential gas specifications have not been tested. These aspects are discussed in the following sections.

## *7.2 Assumptions and Limitations*

### *7.2.1 Repeatability and Scalability*

Of importance for the practical application a combustion sensor is (1) repeatability and (2) scalability. Repeatability refers to the performance of an acoustic combustion sensor system (combination of algorithm and hardware) over significant periods of time. This includes impacts of combustion system wear and tear, transducer degradation/replacement and noise. Scalability refers to the applicability of the current methods to all, or a significant range, of domestic gas boiler combustion systems.

Regarding scalability, the physical phenomena underlying the observed variations in combustion acoustics are not well understood. Thus, one cannot determine if every confined gas combustion system will be suitable for the application of an acoustic combustion sensor. It may be the case that some unknown system may display combustion acoustic stability in response to variations in  $\varphi$  and gas specifications, however this is very unlikely. It is likely from theory of combustion noise (that direct noise is inevitable) and results from this study that all gas combustion systems would be suitable for application of an acoustic combustion sensor system, however each system must be tested and no presumptions can be made.

Regarding repeatability, it is imperative for any practical application of a combustion sensor that the chance of failure is very small. For a sensor based on combustion noise, background noise may be a concern. During experiments in this investigation it was not possible to completely limit background noises due to experiments being performed within an operational facility. However, only once tests have been performed will it be clear if noise is a concern for an acoustic combustion sensor. If the microphone can be installed in contact with the surface of the heat exchanger, it is likely that vibrations transmitted onto the surface of the heat exchanger would cause issues. If, however the microphone was embedded into the heat exchanger then most surface vibrations may not penetrate and noise may not be a concern. If required there are potentially both hardware and software options to explore to manage noise. One hardware solution may be to install a secondary microphone further from the source of combustion noise and use techniques of blind source separation (Vincent et al., 2006) to remove other background noise sources. Software approaches could be borrowed from areas of speech recognition, whereby robustness is tackled with the use of sophisticated feature selection, for example Kim and Stern (2012) have shown that power-normalized cepstral coefficients (PNCCs) perform better than MFCCs and perceptual linear prediction for signals with high reverberation or low

signal to noise ratios. Algorithms based on combustion noise could potentially be stabilised by the application of Bayes' inference. Bayes' inference would only work if the predictions of ML algorithms were well behaved over time i.e. if predictions produced a normal distribution around the correct value. If predictions were consistently incorrect for said period, Bayes' inference would indicate false levels of certainty.

### 7.2.2 Intermediate Gas Specifications

In a practical scenario, within certain constraints, gas qualities are varying to an unknown degree, impacting the quality of the burn. A combustion sensor is designed to detect changes in burn quality so that adjustments can be made to re-optimize  $\phi$ . Gas composition changes may occur in several forms, most common of which would be variations in the ratio of  $\text{CH}_4$  to  $\text{N}_2$ . Less common would be inclusion or removal of higher alkanes, namely  $\text{C}_3\text{H}_8$  i.e. small step shifts between G20 and G21. Not permissible in UK networks, and uncommon in EU countries, are shifts in percentages of  $\text{H}_2$  from G20 to G222. All potential shifts have been illustrated in Figure 45.

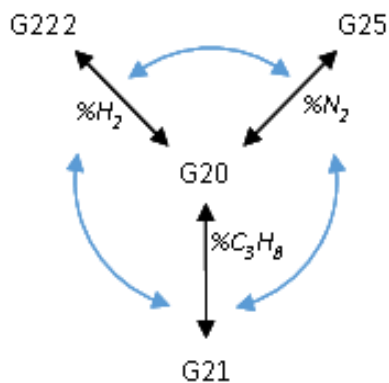


Figure 45 Illustration of the potential variations in gas type

The experiments performed in this investigation do not replicate Figure 45. However, for the case of G20,  $\phi$  was controlled by adjusting gas rates, and thus the ratio of methane to air in the combustion chamber. Since air is 78%  $\text{N}_2$ , this is roughly equivalent to the practical scenario whereby proportions of  $\text{N}_2$  are varying from higher quality methane gas to lower quality (G20 to G23 to G25). Other adjustments in the experiments were not equivalent to Figure 45: For G21 and G222, adjustments to the ratio of gas to air were not equivalent. Regardless, Sections 6.1.1.5 in conjunction with 6.1.1.6, have shown that irrespective of air or gas rate adjustments, and irrespective of gas type, it was possible to accurately determine  $\phi$  of the combustion system from acoustics. Thus, by extension, for the practical scenarios illustrated in Figure 45, it should

also be possible to infer  $\varphi$  by similar means. Despite the above, experiments should be performed whereby the proportions of CH<sub>4</sub>, N<sub>2</sub>, C<sub>3</sub>H<sub>8</sub> and H<sub>2</sub> are under complete control to simulate any potential combination of gas composition. As a quick calculation, if gases in Figure 45 were varied in 2% increments, then there would be 386 unique combinations of gas composition; if this was adjusted to 4% increments, then there would be 65 unique combinations. Consequently, a significant amount of data would be required to cover all the potential ranges in gas specification possible in a practical scenario.

To tackle this problem, it may also be advantageous to develop a two-step algorithmic approach. The first step may be to classify the gas type into a unique range, this may be achieved using some clustering model such as a density based model (DBSCAN). The next layer of the algorithm would then use an appropriate SVM or ANN for that unique gas composition and boiler combination to determine  $\varphi$ . This way results may be more reliable and accurate.

## ***7.3 Analysis of the Results***

### *7.3.1 Algorithms*

For all datasets, the most accurate predictive algorithms developed were done so using kNN. However, SVMs showed comparable predictive accuracies for most datasets and likely have additional potential for improvement. Likewise, although the ANNs tested were not as accurate as kNN or SVMs, the scope for improvement is significant. With modifications ANNs have produced the best results in many applications of machine learning including automatic speech recognition (Yu and Deng, 2014, Li et al., 2015). In such applications, performance improving modifications were mainly due to increasing network depth, including regularization techniques (such as dropout) and increasing data volumes. Increasing the depth of ANNs is referred to as deep learning (typically ANNs with eight or more layers of neurons). It is expected that if such a deep learning approach is applied to this study, that the performance of ANNs would significantly improve.

From a practical standpoint, SVMs and ANNs may be preferable option compared to kNN due to memory constraints. This is because kNN algorithms vary significantly in the way in which they learn and function. kNN is an instance based learner whereas SVMs and ANNs are eager-learners. An eager-learner commits to a single hypothesis and generalises that hypothesis to all unknown data points. Instance based learners compare an unknown data point to the full dataset of known instances upon testing and thus can effectively use a richer hypothesis space

to form an implicit global approximation to the target function. Consequently, instance based learners require a database of known instances to be kept in memory. For the case of domestic gas boilers, the on-board CPU would be used as a storage mechanism for any algorithm used. Such space is limited and thus of concern when pursuing a kNN approach. The datasets used in this investigation are 10-20 dimensions wide and about 17,000 deep, taking up approximately three megabytes of memory. If, however a database was developed to deal with a larger array of gas types and equivalence ratios, then storage may become a problem. Thus, considering that SVMs performed similarly to kNN algorithms, SVMs or other eager learners may be preferable practical option.

### 7.3.2 Boilers

The accuracy achieved by learning algorithms for Boiler 1 (Datasets 1-3) was significantly better than Boiler 2 (Datasets 4-6) across all microphones and feature sets. For Microphones 1 and 3, one explanation could be the variation in the contact point of the microphone from one boiler to the next. However, this explanation does not account for the variation in the predictive accuracy when comparing boilers for Microphone 2 - the position of Microphone 2 was identical for both boilers. Thus, the difference in observed accuracy when moving from one boiler to the other was likely due to one, or a combination of the following:

- a) Combustion noise created from Boiler 2 is less correlated with  $\varphi$  and is thus harder for learning algorithms to track.
- b) Combustion noise created within Boiler 2 is much quieter than produced in Boiler 1 and thus the signal to noise ratio is too low for such accurate tracking.
- c) The datasets used in the analysis between boilers were not comparable and therefore the results not comparable.

From the potential explanations above, c) can be easily investigated. As explained in Section 5.1,  $\varphi$  was set during experiments by adjusting the gas valve until a certain CO<sub>2</sub> concentration was achieved, once set, recordings commenced over a period of six minutes. There were 12 steps made in  $\varphi$  between recordings for both Boiler 1 and Boiler 2. These steps were identical, however upon analysis, the CO<sub>2</sub> readings from Boiler 2 showed more variation during recordings than that observed during recordings for Boiler 1. This variation was significant: For all gas types, at each of the 12 steps investigated, the average standard deviation for Boiler 2 was 47% larger than that of Boiler 1, with over 90% of all recordings for Boiler 2 having a larger variation than that of Boiler 1. This can be observed in Figure 46 below for G20 gas only. The same was

observed for recordings when air, instead of gas rates, was adjusted (Section 6.1.1.6) – in this instance the average standard deviation was 30% larger.

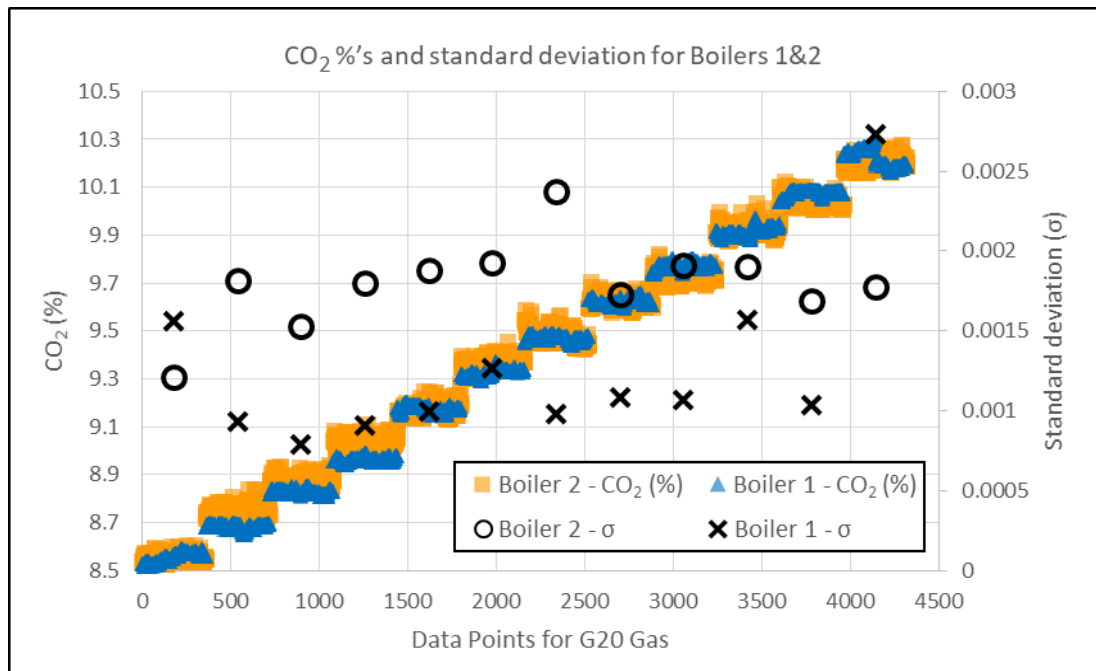


Figure 46 Plot of CO<sub>2</sub> percentages and associated standard deviations for each recording block for Boilers 1 and 2 G20 data points

For the datasets of Boiler 1, the class values are easier to predict relative to Boiler 2 therefore there is a higher chance of attaining the correct value regardless of the learned algorithm. This can be checked by running a range of algorithms using datasets without any acoustic data and only containing labels of the 12  $\varphi$  groupings i.e. a list from 1 to 12. Doing so, it was possible to predict  $\varphi$  with an RRSE of 3.2% for Boiler 1 and 4.5% for Boiler 2, thus in general it is harder to predict  $\varphi$  for Boiler 2 due to the spread of the class value ( $\varphi$ ) during recordings. In addition, compared to datasets for Boiler 2, Boiler 1 datasets contain more examples of what the acoustics 'look like' for a  $\varphi$  value (or a small range of  $\varphi$  values) and therefore the algorithms are more capable of learning. The hypothesis would therefore be: If the dataset for Boiler 2 were increased with more examples of acoustics at varying  $\varphi$  values, then it will perform better to the point of getting close to the performance of the datasets for Boiler 1. The same would be proposed to be true of the datasets analysed for varying air rates.

### 7.3.3 Microphones

For Microphones 1 and 3, once an optimum selection of features was made, the accuracy of the algorithms developed was very similar, particularly when applying kNN. The position of the

microphones were almost identical however the qualities were very different: As described in section 5.1, Microphone 1 was a professional quality microphone and was worth approximately 450 USD; Microphone 3 was custom made using a piezo disk transducer, costing 0.5 USD, with the addition of an epoxy resin for stability, and a simple preamplifier costing about 1 USD. Effectively Microphone 3 was made as cheap as possible and still resulted in predictive accuracies comparable to a professional standard microphone. Such a result suggests that the frequency response and signal-to-noise ratio of the microphone used is not crucial to the performance of learning algorithms. Significantly the result indicates that the cost of such an acoustic combustion sensor could be made very low and thus practical in a domestic appliance. In addition, it appears retrofitting a boiler with said device may be possible.

Comparing the best performing algorithms across all algorithms, the 10-fold CV accuracy achieved by Microphones 1 and 3 performed better than those developed for Microphone 2. For Boiler 1 Microphone 2 achieved  $0.65 \pm 0.388\%$  RRSE, Microphone 1  $0.43 \pm 0.043\%$  RRSE and Microphone 3  $0.48 \pm 0.093\%$ . For Boiler 2 Microphone 2 achieved  $2.90 \pm 0.145\%$  RRSE, Microphone 1  $2.67 \pm 0.103\%$  RRSE and Microphone 3  $2.67 \pm 0.105\%$ . In general, the performance of Microphone 2 could be explained in terms of distance from the source of acoustic variations. As Microphone 2 was placed external of the exhaust pipe, the level of combustion acoustics would have been significantly lower than those placed much closer; thus, the signal-to-noise was likely worse.

#### *7.4 Directions for Commercial Development*

This investigation has shown the potential of a new technique for diagnosing the properties of a flame in a practical system. The new technique relates combustion acoustics to the properties of the flame by using machine learning algorithms. Such a method is completely new to the field and as such requires investment to be developed commercially. The following will discuss some of the required investment and why from a commercial perspective such an investment may be worthwhile.

The following is required to develop an acoustic combustion sensor for integration into a combustion control system for application in domestic gas boilers:

1. Additional research:
  - a. Variable gas compositions – as a first step, similarly to this investigation, acoustic data should be collected for instances where the gas composition changes

incrementally across the range of potential variation. This has been discussed in Section 7.3.2. While acoustic data is recorded the exact composition of the gas, in addition to the concentration of CO<sub>2</sub> species in the exhaust gases, should be collected. Using this data, machine learning algorithms again can be developed for all scenarios expected in a practical situation.

- b. Noise – Not considered during this investigation was the impact of noise. By using a contact microphone, the approach is susceptible to any external vibrations on the surface of the boiler in within the direct vicinity. To manage external noises a combination of hardware and software solutions may be required. As seen in the field of automatic voice recognition, many techniques are available to guard against background noises, these include using more advanced features such as power-normalized cepstral coefficients (PNCCs) and advanced filtering techniques. Hardware solutions include embedding the microphone into the boiler, by doing so one may find background noises do not penetrate. If background noises do penetrate then more than one transducer could be used and blind source separation applied – refer to Belouchrani et al. (1997) for more information.
  - c. Failure Modes – Not considered in this investigation is how an acoustic combustion sensor would manage failure modes of the boiler. In the event of a boiler failure mode the acoustic combustion sensor must be stopped from compromising the safety of the boiler.
2. Field trials – Once suitably researched and a prototype combustion sensor developed, field trials would commence.
  3. Development of Standards – A device which controls the air-to-gas ratio of the combustion system would be required to meet certain health and safety standards. As such a combustion sensing approach is new to the field then the standards would need to be developed and agreed.

Regardless of the above, such investment may be worthwhile as the technique has been shown to be more accurate and provide more information than other combustion sensing options. Of note, an acoustic combustion sensing appears to give accurate estimates of the operational equivalence ratio even when hydrogen is introduced into the gas mix. This is compared with an ionisation sensing and flue gas sensing approach, both of which are much less accurate when hydrogen mixes are considered. In addition to this, an acoustic combustion sensing approach may prove to be more resilient and cost effective. This is because the approach does not require

access to the flame, the sensor does not sit within the flame and the sensor can be retrofitted to an existing design.

## 8. Conclusions

This investigation has shown that pitch related features from combustion acoustics can be used to accurately determine certain characteristics of the flame, including the  $\varphi$  and the gas type. To extract useful information from combustion acoustics, data processing techniques in addition to machine learning (ML) algorithms were required.

For both boilers and all microphones tested, ML algorithms were developed to determine  $\varphi$  with a RRSE of less than 3% for every second of the data independent of gas type. This was achieved using kNN algorithms with 12 to 26 NFC or MFCC/LFCC features, although SVM algorithms (with a PUK kernel) also resulted in RRSEs of less than 3%. The results were obtained for contactless and contact microphones ranging in cost from 1-2 USD to 300 USD.

The acoustic approach investigated in this study was shown to be significantly more accurate in determining  $\varphi$  relative to data based on ionisation currents or CO gas concentrations sensors (the most common CCS sensing technologies). Data from a CO gas sensor was shown to predict  $\varphi$  with (at best) a RRSE of 10.8%, data from an ionisation sensor with a RRSE of 46.5%. This indicated that combustion acoustics contains much more information regarding the state of the flame relative to CO concentrations and ionisation currents. In addition, an acoustic approach could be retrofitted to appliances and unlike other techniques, does not require access to either the flame, exhaust gases or a line-of-sight sensor.

Furthermore, it has been shown that the information contained within combustion acoustics can be used to determine the gas type to 100% accuracy, which may be of use for boiler designers looking to optimise burn conditions for various fuel compositions. For example, hydrogen-hydrocarbon gases have a much faster flame laminar flame speeds than hydrocarbon gases, as such, if hydrogen-hydrocarbon gases were detected, fan speeds could be adjusted to reduce the risk of flashback and deal with the higher flame speed.

Due to flame height variations and lack of carbon concentrations, an acoustic combustion sensing technique may be the only method which is flexible enough to accurately predict  $\varphi$  for high proportion hydrogen-hydrocarbon flames. This is particularly relevant as there is a currently a push for the development of hydrogen specific heating systems.

Next steps include: (1) to adjust  $\varphi$  by incrementally changing proportions of CH<sub>4</sub>, N<sub>2</sub>, C<sub>3</sub>H<sub>8</sub> and H<sub>2</sub> across the acceptable range in the second grouping of gas families; (2) test an embedded

contact microphone technique with increased levels of noise and adjust algorithms accordingly to deal with any impacts (potential use of PNCC, Gaussian mixture models etc.); (3) test variations in hardware to minimise impacts of noise and costs; (4) develop procedures for appliance testing so that regulation requirements can be met and such a sensor can be commercialised.

If an acoustic combustion sensor was commercialised, the combustion of gases of varying quality and composition could tightly controlled in domestic appliances. This would result in a more flexible gas network while controlling emissions, efficiencies and maintaining safety standards.

## References

- Agostini, G., Longari, M. and Pollastri, E. (2003) 'Musical instrument timbres classification with spectral features', *EURASIP Journal on Advances in Signal Processing*, 2003(1), pp. 943279.
- Allen, M. G., Butler, C. T., Johnson, S. A., Lo, E. Y. and Russo, F. (1993) 'An imaging neural network combustion control system for utility boiler applications', *Combustion and Flame*, 94(1), pp. 205-214.
- Ambrose, J. (2017) '£50bn plan for hydrogen gas sparks back to life', *The Telegraph*. Available at: <http://www.telegraph.co.uk/business/2017/09/02/50bn-plan-hydrogen-gas-sparks-back-life/>.
- Audacity (2016) *Audacity 2.1.2* Free, open source, cross-platform audio software. Available at: <http://www.audacityteam.org/>.
- Ayoola, B. O., Balachandran, R., Frank, J. H., Mastorakos, E. and Kaminski, C. F. (2006) 'Spatially resolved heat release rate measurements in turbulent premixed flames', *Combustion and flame*, 144(1), pp. 1-16.
- Bahri, B., Shahbakhti, M., Kannan, K. and Aziz, A. A. (2016) 'Identification of ringing operation for low temperature combustion engines', *Applied Energy*, 171, pp. 142-152.
- Bake, F., Michel, U. and Roehle, I. (2007) 'Investigation of entropy noise in aero-engine combustors', *Journal of Engineering for Gas Turbines and Power*, 129(2), pp. 370-376.
- Balachandran, R., Ayoola, B. O., Kaminski, C. F., Dowling, A. P. and Mastorakos, E. (2005) 'Experimental investigation of the nonlinear response of turbulent premixed flames to imposed inlet velocity oscillations', *Combustion and Flame*, 143(1), pp. 37-55.
- Ballester, J. and García-Armingol, T. (2010) 'Diagnostic techniques for the monitoring and control of practical flames', *Progress in Energy and Combustion Science*, 36(4), pp. 375-411.
- Ballester, J., Hernández, R., Sanz, A., Smolarz, A., Barroso, J. and Pina, A. (2009) 'Chemiluminescence monitoring in premixed flames of natural gas and its blends with hydrogen', *Proceedings of the Combustion Institute*, 32(2), pp. 2983-2991.
- Bellman, R. E. (2015) *Adaptive control processes: a guided tour*. Princeton university press.
- Belouchrani, A., Abed-Meraim, K., Cardoso, J. F. and Moulines, E. (1997) 'A blind source separation technique using second-order statistics', *IEEE Transactions on signal processing*, 45(2), pp. 434-444.
- Ben-Bassat, M. (1982) 'Pattern recognition and reduction of dimensionality', *Handbook of Statistics*, 2(1982), pp. 773-910.
- Benzeghiba, M., De Mori, R., Deroo, O., Dupont, S., Erbes, T., Jouvét, D., Fissore, L., Laface, P., Mertins, A. and Ris, C. (2007) 'Automatic speech recognition and speech variability: A review', *Speech communication*, 49(10), pp. 763-786.
- Beyer, K., Goldstein, J., Ramakrishnan, R. and Shaft, U. 'When is "nearest neighbor" meaningful?'. 1999: Springer, 217-235.
- Birbaud, A.-L., Durox, D., Ducruix, S. and Candel, S. (2007) 'Dynamics of confined premixed flames submitted to upstream acoustic modulations', *Proceedings of the Combustion Institute*, 31(1), pp. 1257-1265.
- Blonbou, R., Laverdant, A., Zaleski, S. and Kuentzmann, P. (2000) 'Active adaptive combustion control using neural networks', *Combustion Science and Technology*, 156(1), pp. 25-47.
- Boll, S. (1979) 'Suppression of acoustic noise in speech using spectral subtraction', *IEEE Transactions on acoustics, speech, and signal processing*, 27(2), pp. 113-120.
- Bowman, C. T. (1975) 'Kinetics of pollutant formation and destruction in combustion', *Progress in energy and combustion science*, 1(1), pp. 33-45.
- Bragg, S. L. (1963) 'Combustion noise', *J. Inst. Fuel*, 36(1), pp. 12-16.
- Breiman, L. (1996) 'Bagging predictors', *Machine learning*, 24(2), pp. 123-140.

- Breiman, L., Friedman, J., Stone, C. J. and Olshen, R. A. (1984) *Classification and regression trees*. CRC press.
- Brenez, L., Martin, J. P., Soufiani, A. and Rolon, J. C. 'Optical and spectroscopic diagnostics for the study of laminar partially premixed injectors and natural gas boilers'. 2000, 381-390.
- Briggs, F., Lakshminarayanan, B., Neal, L., Fern, X. Z., Raich, R., Hadley, S. J. K., Hadley, A. S. and Betts, M. G. (2012) 'Acoustic classification of multiple simultaneous bird species: A multi-instance multi-label approach', *The Journal of the Acoustical Society of America*, 131(6), pp. 4640-4650.
- Broenink, A. (2015) *From L-gas to H-gas*. <http://www.gasterra.nl/>. Available at: <http://www.gasterra.nl/en/news/from-l-gas-to-h-gas> (Accessed: July 2017).
- BSRIA 2015. Latest trends in the World Traditional & Renewable Heating Markets. In: Dawson, K. (ed.). BSRIA Worldwide Market Intelligence.
- Calcote, H. F. (1962) 'Eighth Symposium (International) on Combustion', *Williams and Wilkins, Baltimore*, pp. 184.
- Calcote, H. F. and King, I. R. 'Studies of ionization in flames by means of Langmuir probes'. 1955: Elsevier, 423-434.
- Candel, S. (2016) *Combustion Dynamics Lectures*. Princeton- CEFRC-CI Combustion Summer School. Youtube: Princeton. Available at: <http://youtu.be/DU8NH3WscAc> (Accessed: November 2016 2016).
- Candel, S., Durox, D., Ducruix, S., Birbaud, A. L., Noiray, N. and Schuller, T. (2009) 'Flame dynamics and combustion noise: progress and challenges', *International Journal of Aeroacoustics*, 8(1), pp. 1-56.
- CEN (2009): *BS EN 437:2003+A1:2009 - Test gases, test pressures, appliance categories and gas appliance types*: European Committee for Standardization. Available at: [http://standards.cen.eu/dyn/www/f?p=204:110:0:::FSP\\_PROJECT,FSP\\_ORG\\_ID:32589\\_6219&cs=172B4D589A066067FB3DA51F04A9AAAD2](http://standards.cen.eu/dyn/www/f?p=204:110:0:::FSP_PROJECT,FSP_ORG_ID:32589_6219&cs=172B4D589A066067FB3DA51F04A9AAAD2).
- Chan, S. H. (1996) 'An Exhaust Emissions Based Air-Fuel Ratio Calculation for Internal Combustion Engines', *Proceedings of the Institution of Mechanical Engineers, Part D: Journal of Automobile Engineering*, 210(3), pp. 273-280.
- Cheng, T.-S., Wu, C. Y., Li, Y. H. and Chao, Y. C. (2006) 'Chemiluminescence measurements of local equivalence ratio in a partially premixed flame', *Combustion science and technology*, 178(10-11), pp. 1821-1841.
- Choi, M. Y., Hamins, A., Mulholland, G. W. and Kashiwagi, T. (1994) 'Simultaneous optical measurement of soot volume fraction and temperature in premixed flames', *Combustion and flame*, 99(1), pp. 174-186.
- Chu, B.-T. and Kovásznyai, L. S. G. (1958) 'Non-linear interactions in a viscous heat-conducting compressible gas', *Journal of Fluid Mechanics*, 3(5), pp. 494-514.
- Chu, J.-Z., Shieh, S.-S., Jang, S.-S., Chien, C.-I., Wan, H.-P. and Ko, H.-H. (2003) 'Constrained optimization of combustion in a simulated coal-fired boiler using artificial neural network model and information analysis☆', *Fuel*, 82(6), pp. 693-703.
- Clements, R. M. and Smy, P. R. (1976) 'The variation of ionization with air/fuel ratio for a spark-ignition engine', *Journal of Applied Physics*, 47(2), pp. 505-509.
- Correia, D. P., Ferrao, P. and Caldeira-Pires, A. (2000) 'Flame three-dimensional tomography sensor for in-furnace diagnostics', *Proceedings of the Combustion Institute*, 28(1), pp. 431-438.
- Cover, T. and Hart, P. (1967) 'Nearest neighbor pattern classification', *IEEE transactions on information theory*, 13(1), pp. 21-27.
- Crighton, D. G., Dowling, A. P., Ffowcs-Williams, J. E., Heckl, M., Leppington, F. G. and Bartram, J. F. (1992) 'Modern methods in analytical acoustics lecture notes', *The Journal of the Acoustical Society of America*, 92(5), pp. 3023-3023.

- Davis, K. H., Biddulph, R. and Balashek, S. (1952) 'Automatic recognition of spoken digits', *The Journal of the Acoustical Society of America*, 24(6), pp. 637-642.
- Davis, S. and Mermelstein, P. (1980) 'Comparison of parametric representations for monosyllabic word recognition in continuously spoken sentences', *IEEE transactions on acoustics, speech, and signal processing*, 28(4), pp. 357-366.
- DECC, DECC (2014) *United Kingdom housing energy fact file: 2013*.
- DECC (2015) *Natural gas: Chapter 4, Digest of United Kingdom Energy Statistics (DUKES)*.
- Dehariya, V. K., Shrivastava, S. K. and Jain, R. C. 'Clustering of image data set using k-means and fuzzy k-means algorithms'. 2010: IEEE, 386-391.
- DeWitt, D. P. and Nutter, G. D. (1988) *Theory and practice of radiation thermometry*. Wiley Online Library.
- Dibike, Y. B., Velickov, S., Solomatine, D. and Abbott, M. B. (2001) 'Model induction with support vector machines: introduction and applications', *Journal of Computing in Civil Engineering*, 15(3), pp. 208-216.
- Doak, P. E. (1973) 'Fundamentals of aerodynamic sound theory and flow duct acoustics', *Journal of Sound and Vibration*, 28(3), pp. 527-561.
- Docquier, N., Belhafaoui, S., Lacas, F., Darabiha, N. and Rolon, C. (2000) 'Experimental and numerical study of chemiluminescence in methane/air high-pressure flames for active control applications', *Proceedings of the Combustion Institute*, 28(2), pp. 1765-1774.
- Docquier, N. and Candel, S. (2002) 'Combustion control and sensors: a review', *Progress in energy and combustion science*, 28(2), pp. 107-150.
- Docquier, N., Lacas, F. and Candel, S. (2002) 'Closed-loop equivalence ratio control of premixed combustors using spectrally resolved chemiluminescence measurements', *Proceedings of the Combustion Institute*, 29(1), pp. 139-145.
- Dodds, P. E. and McDowall, W. (2013) 'The future of the UK gas network', *Energy Policy*, 60, pp. 305-316.
- Domingos, P. (2012) 'A few useful things to know about machine learning', *Communications of the ACM*, 55(10), pp. 78-87.
- Dowling, A. P. and Mahmoudi, Y. (2015) 'Combustion noise', *Proceedings of the Combustion Institute*, 35(1), pp. 65-100.
- Ducruix, S., Schuller, T., Durox, D. and Candel, S. (2003) 'Combustion dynamics and instabilities: Elementary coupling and driving mechanisms', *Journal of propulsion and power*, 19(5), pp. 722-734.
- Duda, R. O., Hart, P. E. and Stork, D. G. (2012) *Pattern classification*. John Wiley & Sons.
- EASEE-gas (2008) *Common Business Practice - Harmonisation of Natural Gas Quality - Number 2005-001/02*: EASEE-gas. Available at: [https://easee-gas.eu/download\\_file/DownloadFile/4/cbp-2005-001-02-gas-quality-harmonisation](https://easee-gas.eu/download_file/DownloadFile/4/cbp-2005-001-02-gas-quality-harmonisation).
- EASEE-gas (2016) *From Producers to End Users*. Available at: <https://easee-gas.eu/> (Accessed: 02/01/2016 2016).
- Ebert, V., Fitzer, J., Gerstenberg, I., Pleban, K. U., Pitz, H., Wolfrum, J., Jochem, M. and Martin, J. 'Simultaneous laser-based in situ detection of oxygen and water in a waste incinerator for active combustion control purposes'. 1998: Elsevier, 1301-1308.
- Ebert, V., Teichert, H., Strauch, P., Kolb, T., Seifert, H. and Wolfrum, J. (2005) 'Sensitive in situ detection of CO and O<sub>2</sub> in a rotary kiln-based hazardous waste incinerator using 760nm and new 2.3 μm diode lasers', *Proceedings of the Combustion Institute*, 30(1), pp. 1611-1618.
- Edwards, J. B. (1974) *Combustion - the formation and emission of trace species*. [S.l.]: Ann Arbor Pubs.
- Energy Live News (2017) *UK project to explore hydrogen potential for heating*. [energylivenews.com](http://energylivenews.com): Energy Live News. Available at:

- <http://www.energylivenews.com/2017/11/09/uk-project-to-explore-hydrogen-potential-for-heating/> (Accessed: November 2017).
- Ersatzteilmann (2017) *Vaillant 0020026816 Sensor (CO,Keramik) VC... /2-E (CO, Keramik)*. [www.ersatzteilmann.de](http://www.ersatzteilmann.de). Available at: <https://www.ersatzteilmann.de/Vaillant/Vaillant-Ersatzteile/Vaillant-0020026816-Sensor-CO-Keramik-VC-/2-E-CO-Keramik--40186.html> (Accessed: July 2017).
- Farina, A. 'Simultaneous measurement of impulse response and distortion with a swept-sine technique'. 2000: Audio Engineering Society.
- Farina, A. 'Advancements in impulse response measurements by sine sweeps'. 2007: Audio Engineering Society.
- Fay, J. A. (1994) *Introduction to fluid mechanics*. MIT press.
- Fialkov, A. B. (1997) 'Investigations on ions in flames', *Progress in Energy and Combustion Science*, 23(5), pp. 399-528.
- Flagan, R. C. and Seinfeld, J. H. (2013) *Fundamentals of Air Pollution Engineering*. Englewood Cliffs, New Jersey.
- Fleiss, J. L., Levin, B. and Paik, M. C. (2013) *Statistical methods for rates and proportions*. John Wiley & Sons.
- Frahm, T. (2015) *Conversion from L-gas to H-gas started*. <http://www.energie-experten.org>. Available at: <http://www.energie-experten.org/experte/meldung-anzeigen/news/umstellung-von-l-gas-auf-h-gas-gestartet-4544.html> (Accessed: August 2017).
- Fridman, L. (2017) *MIT 6.S094: Introduction to Deep Learning and Self-Driving Cars*. MIT 6.S094. Youtube: MIT. Available at: <https://www.youtube.com/playlist?list=PLrAXtmErZgOeiKm4sgNOknGvNjby9efdf> (Accessed: July 2017).
- Frohlich, H., Chapelle, O. and Scholkopf, B. 'Feature selection for support vector machines by means of genetic algorithm'. 2003: IEEE, 142-148.
- Fung, G. (2001) 'A comprehensive overview of basic clustering algorithms'.
- Furlong, E. R., Baer, D. S. and Hanson, R. K. 'Real-time adaptive combustion control using diode-laser absorption sensors'. 1998: Elsevier, 103-111.
- Gasch, A. P. and Eisen, M. B. (2002) 'Exploring the conditional coregulation of yeast gene expression through fuzzy k-means clustering', *Genome biology*, 3(11), pp. research0059-1.
- Gazprom (2016) *Marketing - Europe*. Available at: <http://www.gazprom.com/about/marketing/europe/> (Accessed: January 2016).
- Gazprom Export (2016) *Foreign Partners - Bulgaria*. Available at: <http://www.gazpromexport.ru/en/partners/bulgaria/> (Accessed: January 2016).
- Glassman, I. and Yetter, R. A. (2014) *Combustion*. Academic press.
- Gorunescu, F. (2011) *Data Mining: Concepts, models and techniques*. Springer Science & Business Media.
- Griffiths, J. F. and Barnard, J. A. (1995) *Flame and combustion*. CRC Press.
- Gu, Y., Zhao, W. and Wu, Z. (2011) 'Online adaptive least squares support vector machine and its application in utility boiler combustion optimization systems', *Journal of Process Control*, 21(7), pp. 1040-1048.
- Guyon, I. and Elisseeff, A. (2003) 'An introduction to variable and feature selection', *Journal of machine learning research*, 3(Mar), pp. 1157-1182.
- Guyon, I., Weston, J., Barnhill, S. and Vapnik, V. (2002) 'Gene selection for cancer classification using support vector machines', *Machine learning*, 46(1), pp. 389-422.
- Hall, M., Frank, E., Holmes, G., Pfahringer, B., Reutemann, P. and Witten, I. H. (2009) 'The WEKA data mining software: an update', *ACM SIGKDD explorations newsletter*, 11(1), pp. 10-18.

- Hall, M. A. (1999) 'Correlation-based feature selection for machine learning'.
- Hanson, R. K., Jeffries, J. B., Xin, Z., Xiang, L., Hejie, L., Mattison, D. and Klingbeil, A. (2005) *Smart Sensors for Advanced Combustion Systems*: GCEP Technical Report, 2005.[Online]. Available: [http://gcep.stanford.edu/pdfs/QeJ5maLQQRugiSYMF3ATDA/2.6.3.hanson\\_06.pdf](http://gcep.stanford.edu/pdfs/QeJ5maLQQRugiSYMF3ATDA/2.6.3.hanson_06.pdf).
- Hao, Z., Kefa, C. and Jianbo, M. (2001) 'Combining neural network and genetic algorithms to optimize low NO<sub>x</sub> pulverized coal combustion', *Fuel*, 80(15), pp. 2163-2169.
- Hardalupas, Y., Orain, M., Panoutsos, C. S., Taylor, A., Olofsson, J., Seyfried, H., Richter, M., Hult, J., Aldén, M. and Hermann, F. (2004) 'Chemiluminescence sensor for local equivalence ratio of reacting mixtures of fuel and air (FLAMESEEK)', *Applied thermal engineering*, 24(11), pp. 1619-1632.
- Hassan, H. A. (1974) 'Scaling of combustion-generated noise', *Journal of Fluid Mechanics*, 66(3), pp. 445-453.
- Hermann, J. and Hoffmann, S. (2004) 'Implementation of Active Control in a Full-Scale Gas-Turbine Combustor', *Combustion Instabilities in Gas Turbine Engines: Operational Experience, Fundamental Mechanisms, and Modeling*.
- Hermansky, H. (1990) 'Perceptual linear predictive (PLP) analysis of speech', *the Journal of the Acoustical Society of America*, 87(4), pp. 1738-1752.
- Hernandez, R. and Ballester, J. (2008) 'Flame imaging as a diagnostic tool for industrial combustion', *Combustion and flame*, 155(3), pp. 509-528.
- Higgins, B., McQuay, M. Q., Lacas, F. and Candel, S. (2001a) 'An experimental study on the effect of pressure and strain rate on CH chemiluminescence of premixed fuel-lean methane/air flames', *Fuel*, 80(11), pp. 1583-1591.
- Higgins, B., McQuay, M. Q., Lacas, F., Rolon, J.-C., Darabiha, N. and Candel, S. (2001b) 'Systematic measurements of OH chemiluminescence for fuel-lean, high-pressure, premixed, laminar flames', *Fuel*, 80(1), pp. 67-74.
- Hirsch, C., Wäsle, J., Winkler, A. and Sattelmayer, T. (2007) 'A spectral model for the sound pressure from turbulent premixed combustion', *Proceedings of the Combustion Institute*, 31(1), pp. 1435-1441.
- HM Government (1996) *Gas Safety (Management) Regulations 1996*. The Stationery Office Limited, Norwich: Her Majesty's Stationery Office.
- Hoshen, Y., Weiss, R. J. and Wilson, K. W. 'Speech acoustic modeling from raw multichannel waveforms'. 2015: IEEE, 4624-4628.
- Howe, M. S. (1998) *Acoustics of fluid-structure interactions*. Cambridge university press.
- HRB 2017. Sensor Vaillant, 0020209505, ersetzt 0020026816. [www.hrb24.de](http://www.hrb24.de).
- Huang, Y., Yan, Y. and Riley, G. (2000) 'Vision-based measurement of temperature distribution in a 500-kW model furnace using the two-colour method', *Measurement*, 28(3), pp. 175-183.
- Huppelshausen, H., Berg, H. and Hoppe, M. 'Applications aspects of combustion control using ionization signal', *Proceedings of the International Gas Research Conference*, Amsterdam.
- Hurle, I. R., Price, R. B., Sugden, T. M. and Thomas, A. 'Sound emission from open turbulent premixed flames'. 1968: The Royal Society, 409-427.
- IBHS Ltd. (2017) *Weishaupt ignition electrodes*. [www.ibhs.co.uk](http://www.ibhs.co.uk). Available at: <https://www.ibhs.co.uk/burner-controls/ignition-electrodes/weishaupt-ignition-electrodes.html> (Accessed: June 2017).
- Ilamathi, P., Selladurai, V. and Balamurugan, K. (2013) 'Modeling and optimization of unburned carbon in coal-fired boiler using artificial neural network and genetic algorithm', *Journal of Energy Resources Technology*, 135(3), pp. 032201.

- Iliyas, S. A., Elshafei, M., Habib, M. A. and Adeniran, A. A. (2013) 'RBF neural network inferential sensor for process emission monitoring', *Control Engineering Practice*, 21(7), pp. 962-970.
- Ismail, H. M., Ng, H. K., Queck, C. W. and Gan, S. (2012) 'Artificial neural networks modelling of engine-out responses for a light-duty diesel engine fuelled with biodiesel blends', *Applied Energy*, 92, pp. 769-777.
- ITM-Power (2015) *Thuga Power-to-Gas Plant*. <http://www.itm-power.com>. Available at: <http://www.itm-power.com/project/thuga-power-to-gas> 2018).
- Jones, H. R. N. (1989) *The application of combustion principles to domestic gas burner design*. Taylor & Francis.
- Kantardzic, M. (2011) *Data mining: concepts, models, methods, and algorithms*. John Wiley & Sons.
- Karki, J. (2000) 'Signal conditioning piezoelectric sensors', *App. rept. on mixed signal products (sloa033a)*, Texas Instruments Incorporated.
- Kathrotia, T. (2011) 'Reaction kinetics modeling of OH\*, CH\*, and C2\* chemiluminescence'.
- Kiefer, M., Maas, U., Park, S., Pian, X., Kollmann, G., Loohuis, G. O., Leerkes, D., Kalk, H., Markus, D. and Langer, T. 'Combustion Control Based on Flame Ionization', *25th World Gas Conference*, Kuala Lumpur.
- Kilham, J. K. and Kirmani, N. 'The effect of turbulence on premixed flame noise'. 1979: Elsevier, 327-336.
- Kim, B., Kaneko, M., Ikeda, Y. and Nakajima, T. (2002) 'Detailed spectral analysis of the process of HCCI combustion', *Proceedings of the Combustion Institute*, 29(1), pp. 671-677.
- Kim, C. and Stern, R. M. 'Power-normalized cepstral coefficients (PNCC) for robust speech recognition'. 2012: IEEE, 4101-4104.
- Kim, Y. E., Schmidt, E. M., Migneco, R., Morton, B. G., Richardson, P., Scott, J., Speck, J. A. and Turnbull, D. 'Music emotion recognition: A state of the art review'. 2010, 255-266.
- Kimpton, S. K. and Brown, M. J. 2010. Gasqual: Future Gas Profiles *In: CEN (ed.)*. Gasqual.
- Kittler, J. (1978) 'Feature set search algorithms', *Pattern recognition and signal processing*.
- Klein, S. A. (2000) *On the acoustics of turbulent non-premixed flames*. Universiteit Twente.
- Kleppe, J. A., Norris, W. J., McPherson, D. R. and Fralik, G. C. 'The measurement of performance of combustors using passive acoustic methods'. 2004.
- Kohavi, R. 'Feature subset selection as search with probabilistic estimates'. 1994.
- Kohavi, R. and John, G. H. (1997) 'Wrappers for feature subset selection', *Artificial intelligence*, 97(1-2), pp. 273-324.
- Kohse-Höinghaus, K., Barlow, R. S., Aldén, M. and Wolfrum, J. (2005) 'Combustion at the focus: laser diagnostics and control', *Proceedings of the Combustion Institute*, 30(1), pp. 89-123.
- Kohse-Höinghaus, K. and Jeffries, J. B. (2002) 'Applied combustion diagnostics'.
- Kokanovic, S., Guidati, G., Torchalla, S. and Schuermans, B. 'Active combustion control system for reduction of NOx and pulsation levels in gas turbines'. 2006: American Society of Mechanical Engineers, 673-682.
- Koller, D. and Sahami, M. (1996) *Toward optimal feature selection*: Stanford InfoLab.
- Kopp, S.-D. (2015) *Politics, Markets and EU Gas Supply Security: Case Studies of the UK and Germany*. Springer.
- Korotcenkov, G. (2007) 'Metal oxides for solid-state gas sensors: What determines our choice?', *Materials Science and Engineering: B*, 139(1), pp. 1-23.
- Köylü, U. O. and Faeth, G. M. (1996) 'Spectral extinction coefficients of soot aggregates from turbulent diffusion flames', *Journal of Heat Transfer*, 118(2), pp. 415-421.
- Krzywanski, J., Czakiert, T., Blaszcuk, A., Rajczyk, R., Muskala, W. and Nowak, W. (2015) 'A generalized model of SO<sub>2</sub> emissions from large-and small-scale CFB boilers by artificial neural network approach: Part 1. The mathematical model of SO<sub>2</sub> emissions in air-firing,

- oxygen-enriched and oxycombustion CFB conditions', *Fuel Processing Technology*, 137, pp. 66-74.
- Lamel, L. F. (1988) 'Formalizing Knowledge used in Spectrogram Reading: Acoustic and perceptual evidence from stops'.
- Larranaga, P., Calvo, B., Santana, R., Bielza, C., Galdiano, J., Inza, I., Lozano, J. A., Armañanzas, R., Santafé, G. and Pérez, A. (2006) 'Machine learning in bioinformatics', *Briefings in bioinformatics*, pp. 86-112.
- LeCun, Y., Jackel, L. D., Bottou, L., Cortes, C., Denker, J. S., Drucker, H., Guyon, I., Muller, U. A., Sackinger, E. and Simard, P. (1995) 'Learning algorithms for classification: A comparison on handwritten digit recognition', *Neural networks: the statistical mechanics perspective*, 261, pp. 276.
- Leipertz, A., Obertacke, R. and Wintrich, F. 'Industrial combustion control using UV emission tomography'. 1996: Elsevier, 2869-2875.
- Leung, F. H.-F., Lam, H.-K., Ling, S.-H. and Tam, P. K.-S. (2003) 'Tuning of the structure and parameters of a neural network using an improved genetic algorithm', *IEEE Transactions on Neural networks*, 14(1), pp. 79-88.
- Li, J., Deng, L., Haeb-Umbach, R. and Gong, Y. (2015) *Robust Automatic Speech Recognition: A Bridge to Practical Applications*. Academic Press.
- Libbrecht, M. W. and Noble, W. S. (2015) 'Machine learning applications in genetics and genomics', *Nature Reviews Genetics*, 16(6), pp. 321.
- Liu, B., Hu, J., Yan, F., Turkson, R. F. and Lin, F. (2016) 'A novel optimal support vector machine ensemble model for NO<sub>x</sub> emissions prediction of a diesel engine', *Measurement*, 92, pp. 183-192.
- Liu, G. P. and Daley, S. (1999) 'Output-model-based predictive control of unstable combustion systems using neural networks', *Control Engineering Practice*, 7(5), pp. 591-600.
- Liu, H. and Motoda, H. (2012) *Feature selection for knowledge discovery and data mining*. Springer Science & Business Media.
- Lu, G., Yan, Y., Huang, Y. and Reed, A. (1999) 'An intelligent vision system for monitoring and control of combustion flames', *Measurement and control*, 32(6), pp. 164-168.
- MacKay, D. J. C. and Stone, T. J. (2013) 'Potential greenhouse gas emissions associated with shale gas extraction and use', *London, UK: Department of Energy and Climate Change*.
- Mahan, J. R. (1984) 'A critical review of noise production models for turbulent, gas-fueled burners'.
- Mahmoudi, Y., Dowling, A. P. and Stow, S. R. (2017) 'Acoustic and entropy waves in nozzles in combustion noise framework', *AIAA Journal*.
- Marble, F. E. and Candel, S. M. (1977) 'Acoustic disturbance from gas non-uniformities convected through a nozzle', *Journal of Sound and Vibration*, 55(2), pp. 225-243.
- Markillie, R. (2016) *National Grid HyDeploy consortium wins £7m OfGem funding for UK power-to-gas*: <http://www.itm-power.com>. Available at: <http://www.itm-power.com/news-item/national-grid-hydeploy-consortium-wins-7m-ofgem-funding-for-uk-power-to-gas> (Accessed: June 2017).
- Mayes, I. W. 'Generic NO<sub>x</sub> control intelligent system (GNOCIS)'. 1999: IET, 9-1.
- McCulloch, W. S. and Pitts, W. (1943) 'A logical calculus of the ideas immanent in nervous activity', *The bulletin of mathematical biophysics*, 5(4), pp. 115-133.
- Mercer, J. (1909) 'Functions of positive and negative type, and their connection with the theory of integral equations', *Philosophical transactions of the royal society of London. Series A, containing papers of a mathematical or physical character*, 209, pp. 415-446.
- MHS (2017) *Vaillant sensor CO 0020209505*: [www.meinhausshop.de/](http://www.meinhausshop.de/). Available at: [https://www.meinhausshop.de/Vaillant-Sensor-CO-0020209505?campaign=profitmax\\_de&spartner=profitmax\\_de&utm\\_source=profitmax\\_de&utm\\_medium=cpc](https://www.meinhausshop.de/Vaillant-Sensor-CO-0020209505?campaign=profitmax_de&spartner=profitmax_de&utm_source=profitmax_de&utm_medium=cpc) (Accessed: June 2017).

- Mitchell, T. (1997) *Machine Learning*. McGraw Hill.
- Montavon, G., Samek, W. and Müller, K.-R. (2017) 'Methods for interpreting and understanding deep neural networks', *arXiv preprint arXiv:1706.07979*.
- Moreno, P. J. (1996) 'Speech recognition in noisy environments'.
- Morfeý, C. L. (1973) 'Amplification of aerodynamic noise by convected flow inhomogeneities', *Journal of Sound and Vibration*, 31(4), pp. 391-397.
- Morgans, A. S. and Duran, I. (2016) 'Entropy noise: A review of theory, progress and challenges', *International Journal of Spray and Combustion Dynamics*, 8(4), pp. 285-298.
- Morris, C. (2017) *Germany runs out of Dutch gas*. <https://energytransition.org>: Energy Transition. Available at: <https://energytransition.org/2017/03/germany-runs-out-of-dutch-gas/> (Accessed: June 2017).
- Moseley, P. T. (1997) 'Solid state gas sensors', *Measurement Science and technology*, 8(3), pp. 223.
- Mountrakis, G., Im, J. and Ogole, C. (2011) 'Support vector machines in remote sensing: A review', *ISPRS Journal of Photogrammetry and Remote Sensing*, 66(3), pp. 247-259.
- Muruganandam, T. M., Kim, B. H., Morrell, M. R., Nori, V., Patel, M., Romig, B. W. and Seitzman, J. M. (2005) 'Optical equivalence ratio sensors for gas turbine combustors', *Proceedings of the Combustion Institute*, 30(1), pp. 1601-1609.
- Najm, H. N., Paul, P. H., Mueller, C. J. and Wyckoff, P. S. (1998) 'On the adequacy of certain experimental observables as measurements of flame burning rate', *Combustion and flame*, 113(3), pp. 312-332.
- National Grid plc (2013) *2013 Gas Ten Year Statement*, Warwick, United Kingdom: National Grid.
- National Grid plc 2016a. Future Energy Scenarios.
- National Grid plc (2016b) *Gas Ten Year Statement*, Warwick, United Kingdom. Available at: <http://www2.nationalgrid.com/uk/Industry-information/Future-of-Energy/GTYS/>.
- NBS (2012): *BS EN 15502-1:2012+A1:2015 - Gas-fired heating boilers. General requirements and tests*.
- Neeld, T., Eaton, J., Naylor, P. A. and Shipworth, D. (2016) 'A novel method of determining events in combination gas boilers: Assessing the feasibility of a passive acoustic sensor', *Building and Environment*, 100, pp. 1-9.
- Nielsen, M. A. 2015. *Neural networks and deep learning*. Determination Press USA.
- Nilsson, N. J. (1996) 'Introduction to machine learning. An early draft of a proposed textbook'.
- Nitschke-Kowsky, P. and Radtke, H. (2011) 'Testing commercially available gas-fired condensing appliances equipped with a combustion control system', *GWF International: European Journal of Gas Technologies, Distribution and Applications*, (1), pp. 3-11.
- Nitschke-Kowsky, P. and Wessing, W. 'Impact of hydrogen admixture on installed gas appliances', *World Gas Conference*, Kuala Lumpur, Malaysia: International Gas Union.
- Nori, V. N. and Seitzman, J. M. (2009) 'CH\* chemiluminescence modeling for combustion diagnostics', *Proceedings of the Combustion Institute*, 32(1), pp. 895-903.
- Norris, W. J., Kleppe, J. A., McPherson, D. R. and Fralick, G. C. 'The measurement of performance of combustors using passive acoustic methods: Additional results'. 2005.
- Näslund, M. (2014) *Combustion control in domestic gas appliances: Fuel gases containing hydrogen*, [www.sgc.se](http://www.sgc.se): Danish Gas Technology Centre.
- Obertacke, R., Wintrich, H., Wintrich, F. and Leipertz, A. (1996) 'A new sensor system for industrial combustion monitoring and control using UV emission spectroscopy and tomography', *Combustion science and technology*, 121(1-6), pp. 133-151.
- Ocak, H. and Loparo, K. A. 'A new bearing fault detection and diagnosis scheme based on hidden Markov modeling of vibration signals'. 2001: IEEE, 3141-3144.
- Ofgem (2016) *Gas Quality*. Available at: <https://www.ofgem.gov.uk/gas/wholesale-market/gas-quality> (Accessed: January 2016).

- Ortmann, S. and Glesner, M. (1998) 'Development and implementation of a neural knock detector using constructive learning methods', *International Journal of Uncertainty, Fuzziness and Knowledge-Based Systems*, 6(02), pp. 127-137.
- Ortmann, S., Rychetsky, M., Glesner, M., Groppo, R., Tubetti, P. and Morra, G. (1998) *Engine knock estimation using neural networks based on a real-world database*: SAE Technical Paper (0148-7191).
- Parliament, U. K. (2008) 'Climate change act 2008', London, UK.
- Pedregosa, F., Varoquaux, G., Gramfort, A., Michel, V., Thirion, B., Grisel, O., Blondel, M., Prettenhofer, P., Weiss, R. and Dubourg, V. (2011) 'Scikit-learn: Machine learning in Python', *Journal of machine learning research*, 12(Oct), pp. 2825-2830.
- Petela, G. and Petela, R. (1983) 'Diagnostic possibilities on the basis of premixed flame noise levels', *Combustion and flame*, 52, pp. 137-147.
- Peters, N. (2000) *Turbulent combustion*. Cambridge: Cambridge University Press.
- Polifke, W., Paschereit, C. O. and Döbbeling, K. (2001) 'Constructive and destructive interference of acoustic and entropy waves in a premixed combustor with a choked exit', *Int. J. Acoust. Vib*, 6(3), pp. 135-146.
- Price, R. B., Hurlle, I. R. and Sugden, T. M. 'Optical studies of the generation of noise in turbulent flames'. 1969: Elsevier, 1093-1102.
- Quinlan, J. R. 'Learning with continuous classes'. 1992: Singapore, 343-348.
- Quinlan, J. R. (1993) *C4.5 : programs for machine learning*. San Mateo, Calif.: Morgan Kaufmann.
- Rajaram, R. (2007) 'Characteristics of sound radiation from turbulent premixed flames'.
- Rajaram, R. and Lieuwen, T. (2003) 'Parametric studies of acoustic radiation from premixed flames', *Combustion Science and Technology*, 175(12), pp. 2269-2298.
- Rajaram, R. and Lieuwen, T. (2009) 'Acoustic radiation from turbulent premixed flames', *Journal of Fluid Mechanics*, 637, pp. 357-385.
- Ramachandra, M. K. and Strahle, W. C. (1983) 'Acoustic signature from flames as a combustion diagnostic tool', *AIAA Journal*, 21(8), pp. 1107-1114.
- Ramaswamy, S., Tamayo, P., Rifkin, R., Mukherjee, S., Yeang, C.-H., Angelo, M., Ladd, C., Reich, M., Latulippe, E. and Mesirov, J. P. (2001) 'Multiclass cancer diagnosis using tumor gene expression signatures', *Proceedings of the National Academy of Sciences*, 98(26), pp. 15149-15154.
- Reuters Staff (2016) 'UPDATE 1-Dutch government confirms cut in Groningen gas output', *Reuters*. Available at: <https://www.reuters.com/article/netherlands-gas-groningen-idUSL8N1BZ3LT>.
- Reynolds, D. A., Quatieri, T. F. and Dunn, R. B. (2000) 'Speaker verification using adapted Gaussian mixture models', *Digital signal processing*, 10(1-3), pp. 19-41.
- Roberts, J. P. and Leventhall, H. G. (1973) 'Noise sources in turbulent gaseous premixed flames', *Applied Acoustics*, 6(4), pp. 301-308.
- Rogers, H. 2011. *The impact of import dependency and wind generation on UK gas demand and security of supply to 2025*. Oxford Institute for Energy Studies.
- Rychetsky, M., Ortmann, S. and Glesner, M. 'Support vector approaches for engine knock detection'. 1999: IEEE, 969-974.
- Saews, Y., Inza, I. and Larrañaga, P. (2007) 'A review of feature selection techniques in bioinformatics', *bioinformatics*, 23(19), pp. 2507-2517.
- Sanders, S. T., Mattison, D. W., Jeffries, J. B. and Hanson, R. K. (2002) 'Sensors for high-pressure, harsh combustion environments using wavelength-agile diode lasers', *Proceedings of the Combustion Institute*, 29(2), pp. 2661-2667.
- Santosh, D. H. H., Venkatesh, P., Poornesh, P., Rao, L. N. and Kumar, N. A. (2013) 'Tracking multiple moving objects using gaussian mixture model', *International Journal of Soft Computing and Engineering (IJSCE)*, 3(2), pp. 114-9.

- Sanz, A., Ballester, J., Hernandez, R. and Cerecedo, L. M. (2008) 'Advanced monitoring of industrial burners based on fluctuating flame signals', *Fuel*, 87(7), pp. 1063-1075.
- Schölkopf, B. and Smola, A. J. (2002) *Learning with kernels: support vector machines, regularization, optimization, and beyond*. MIT press.
- Scott, D. A., King, G. B. and Laurendeau, N. M. (2002) 'Chemiluminescence-based feedback control of equivalence ratio for a continuous combustor', *Journal of propulsion and power*, 18(2), pp. 376-382.
- Senior, A. (2017) *Lecture 9 - Speech Recognition (ASR) [Andrew Senior]*. Youtube. Available at: [https://www.youtube.com/watch?v=HyUtT\\_z-cms](https://www.youtube.com/watch?v=HyUtT_z-cms) (Accessed: August 2017).
- SGN 2015. Oban Project: Opening Up the Gas Market Progress Report 3. [www.sgn.co.uk](http://www.sgn.co.uk): SGN.
- SGN 2016. Opening up the gas market - Full Report. [www.sgn.co.uk](http://www.sgn.co.uk): SGN.
- Sharkey, A. J. C., Chandroth, G. O. and Sharkey, N. E. (2000) 'A multi-net system for the fault diagnosis of a diesel engine', *Neural Computing & Applications*, 9(2), pp. 152-160.
- Shevade, S. K., Keerthi, S. S., Bhattacharyya, C. and Murthy, K. R. K. (2000) 'Improvements to the SMO algorithm for SVM regression', *IEEE transactions on neural networks*, 11(5), pp. 1188-1193.
- Shivashankara, B. N., Strahle, W. C. and Handley, J. C. (1975) 'Combustion noise radiation by open turbulent flames', *Progress in Astronautics and Aeronautics*, 37, pp. 277-296.
- Siddall, R. G. and McGrath, I. A. 'The emissivity of luminous flames'. 1963: Elsevier, 102-110.
- Siemens (2017) *Ultramat 23*. [w3.siemens.com](http://w3.siemens.com): Siemens. Available at: <http://w3.siemens.com/mcms/sensor-systems/en/process-analytics/extractive-continuous-process-gas-analytics/pages/ultramat-23.aspx> (Accessed: August 2017).
- Silver, D., Huang, A., Maddison, C. J., Guez, A., Sifre, L., Van Den Driessche, G., Schrittwieser, J., Antonoglou, I., Panneershelvam, V. and Lanctot, M. (2016) 'Mastering the game of Go with deep neural networks and tree search', *Nature*, 529(7587), pp. 484-489.
- Silver, D., Hubert, T., Schrittwieser, J., Antonoglou, I., Lai, M., Guez, A., Lanctot, M., Sifre, L., Kumaran, D. and Graepel, T. (2017a) 'Mastering Chess and Shogi by Self-Play with a General Reinforcement Learning Algorithm', *arXiv preprint arXiv:1712.01815*.
- Silver, D., Schrittwieser, J., Simonyan, K., Antonoglou, I., Huang, A., Guez, A., Hubert, T., Baker, L., Lai, M. and Bolton, A. (2017b) 'Mastering the game of go without human knowledge', *Nature*, 550(7676), pp. 354.
- Sinai, Y. L. (1980) 'The generation of combustion noise by chemical inhomogeneities in steady, low-Mach-number duct flows', *Journal of Fluid Mechanics*, 99(02), pp. 383-397.
- SITGroup (2017) *VestaSIT*. Available at: <http://www.sitgroup.it/en/product/vestasit-2/> (Accessed: July 2017).
- Skalak, D. B. 'Prototype and feature selection by sampling and random mutation hill climbing algorithms'. 1994, 293-301.
- Smith, S. W. (1997) 'The scientist and engineer's guide to digital signal processing'.
- Smith, T. J. B. and Kilham, J. K. (1963) 'Noise generation by open turbulent flames', *The Journal of the Acoustical Society of America*, 35(5), pp. 715-724.
- Smola, A. J. and Schölkopf, B. (2004) 'A tutorial on support vector regression', *Statistics and computing*, 14(3), pp. 199-222.
- Solomon, P. R., Best, P. E., Carangelo, R. M., Markham, J. R., Chien, P.-L., Santoro, R. J. and Semerjian, H. G. 'FT-IR emission/transmission spectroscopy for in situ combustion diagnostics'. 1988: Elsevier, 1763-1771.
- Song, J., Romero, C. E., Yao, Z. and He, B. (2017) 'A globally enhanced general regression neural network for on-line multiple emissions prediction of utility boiler', *Knowledge-Based Systems*, 118, pp. 4-14.
- Spindt, R. (1965) 'Air-Fuel Ratios from Exhaust Gas Analysis', *SAE Technical Paper 650507*.

- Stanimirova, I., Üstün, B., Cajka, T., Riddelova, K., Hajslova, J., Buydens, L. M. C. and Walczak, B. (2010) 'Tracing the geographical origin of honeys based on volatile compounds profiles assessment using pattern recognition techniques', *Food Chemistry*, 118(1), pp. 171-176.
- Stern, R. M. and Morgan, N. (2012) 'Features based on auditory physiology and perception', *Techniques for Noise Robustness in Automatic Speech Recognition*, pp. 193227.
- Stevens, K. N. (2000) *Acoustic phonetics*. MIT press.
- Strahle, W. C. (1971) 'On combustion generated noise', *Journal of Fluid Mechanics*, 49(02), pp. 399-414.
- Strahle, W. C. and Shivashankara, B. N. 'A rational correlation of combustion noise results from open turbulent premixed flames'. 1975: Elsevier, 1379-1385.
- Syred, N. (2006) 'A review of oscillation mechanisms and the role of the precessing vortex core (PVC) in swirl combustion systems', *Progress in Energy and Combustion Science*, 32(2), pp. 93-161.
- Taghavifar, H., Taghavifar, H., Mardani, A., Mohebbi, A., Khalilarya, S. and Jafarmadar, S. (2016) 'Appraisal of artificial neural networks to the emission analysis and prediction of CO<sub>2</sub>, soot, and NO<sub>x</sub> of n-heptane fueled engine', *Journal of Cleaner Production*, 112, pp. 1729-1739.
- Tam, C. K. W., Parrish, S. A., Xu, J. and Schuster, B. (2013) 'Indirect combustion noise of auxiliary power units', *Journal of Sound and Vibration*, 332(17), pp. 4004-4020.
- Tan, C. K., Wilcox, S. J. and Ward, J. (2006) 'Use of artificial intelligence techniques for optimisation of co-combustion of coal with biomass', *Journal of the Energy Institute*, 79(1), pp. 19-25.
- Tan, C. K., Wilcox, S. J., Ward, J. and Lewitt, M. (2003) 'Monitoring near burner slag deposition with a hybrid neural network system', *Measurement Science and Technology*, 14(7), pp. 1137.
- Tandon, N. and Choudhury, A. (1999) 'A review of vibration and acoustic measurement methods for the detection of defects in rolling element bearings', *Tribology international*, 32(8), pp. 469-480.
- Tao, W. and Burkhardt, H. (1995) 'Vision-Guided Flame Control Using Fuzzy Logic and Neural Networks', *Particle & particle systems characterization*, 12(2), pp. 87-94.
- Tao, W., Mazur, M., Huet, M. and Richecoeur, F. (2016) 'Indirect Combustion Noise Contributions in a Gas Turbine Model Combustor with a Choked Nozzle', *Combustion Science and Technology*, 188(4-5), pp. 793-804.
- Teichert, H., Fernholz, T. and Ebert, V. (2003) 'Simultaneous in situ measurement of CO, H<sub>2</sub>O, and gas temperatures in a full-sized coal-fired power plant by near-infrared diode lasers', *Applied Optics*, 42(12), pp. 2043-2051.
- Tenenbaum, J. B., De Silva, V. and Langford, J. C. (2000) 'A global geometric framework for nonlinear dimensionality reduction', *science*, 290(5500), pp. 2319-2323.
- Thissen, U., Pepers, M., Üstün, B., Melssen, W. J. and Buydens, L. M. C. (2004) 'Comparing support vector machines to PLS for spectral regression applications', *Chemometrics and Intelligent Laboratory Systems*, 73(2), pp. 169-179.
- Thomas, A. and Williams, G. T. 'Flame noise: sound emission from spark-ignited bubbles of combustible gas'. 1966: The Royal Society, 449-466.
- Tillman, D. J. (2005) *A Discrete FET Guitar Preamp*. <http://www.till.com>. Available at: <http://www.till.com/articles/GuitarPreamp/index.html> (Accessed: 02-Aug 2017).
- Toivonen, H., Onkamo, P., Hintsanen, P., Terzi, E., Sevón, P., Zurada, J. and Kantardzic, M. 'Data mining for gene mapping'. 2005: Citeseer.
- Tsai, J.-T., Chou, J.-H. and Liu, T.-K. (2006) 'Tuning the structure and parameters of a neural network by using hybrid Taguchi-genetic algorithm', *IEEE Transactions on Neural Networks*, 17(1), pp. 69-80.

- Tsanas, A., Little, M. A., McSharry, P. E. and Ramig, L. O. (2010) 'Accurate telemonitoring of Parkinson's disease progression by noninvasive speech tests', *IEEE transactions on Biomedical Engineering*, 57(4), pp. 884-893.
- Tüske, Z., Golik, P., Schlüter, R. and Ney, H. 'Acoustic modeling with deep neural networks using raw time signal for LVCSR'. 2014.
- URSO 2014. Regulatory Office for Network Industries - Annual Report.
- Vaillant 2017. ecoTEC plus 825, 832, 838 and 938. [www.vaillant.co.uk](http://www.vaillant.co.uk).
- van der Voort, N. and Vanclay, F. (2015) 'Social impacts of earthquakes caused by gas extraction in the Province of Groningen, The Netherlands', *Environmental Impact Assessment Review*, 50, pp. 1-15.
- Vapnik, V. (1995) *The nature of statistical learning theory*. New York ; London: Springer.
- Vapnik, V. N. and Chervonenkis, A. J. (1974) 'Theory of pattern recognition'.
- Vapnik, V. N. and Kotz, S. (1982) *Estimation of dependences based on empirical data*. Springer-Verlag New York.
- Viessmann (2013) *Boiler and combustion management system for the Vitodens 200-W, B2HA and Vitodens 222-F, B2TA*. [www.viessmann-us.com](http://www.viessmann-us.com): Viessmann Manufacturing. Available at: [http://www.viessmann-us.com/content/dam/vi-brands/CA/pdfs/wall-mount/lambda\\_pro\\_b2ha\\_flyer.pdf/jcr\\_content/renditions/original.media\\_file.inline.file/file.pdf](http://www.viessmann-us.com/content/dam/vi-brands/CA/pdfs/wall-mount/lambda_pro_b2ha_flyer.pdf/jcr_content/renditions/original.media_file.inline.file/file.pdf) (Accessed: 23/06 2016).
- Viessmann (2017) *Viessmann Vitodens 200-W Wall Mounted Gas Condensing Boiler*. [www.viessmann.co.uk](http://www.viessmann.co.uk). Available at: <https://www.viessmann.co.uk/en/residential-buildings/gas-boilers/gas-condensing-boiler/vitodens-200w.html> (Accessed: July 2017).
- Vincent, E., Gribonval, R. and Févotte, C. (2006) 'Performance measurement in blind audio source separation', *IEEE transactions on audio, speech, and language processing*, 14(4), pp. 1462-1469.
- Von Drasek, W. A., Charon, O. and Marsais, O. 'Industrial combustion monitoring using optical sensors'. 1999: International Society for Optics and Photonics, 215-225.
- Wang, H. 2015. Combustion Chemistry Lecture Series. In: Princeton-CEFRC (ed.) *2015 Princeton-CEFRC Combustion Summer School*. Princeton University.
- Wang, Y. and Witten, I. H. (1996) 'Induction of model trees for predicting continuous classes'.
- Warnatz, J. (1981a) 'Flame velocity and structure of laminar hydrogen air flames', *Prog. Astronaut. Aeronaut.*, 76, pp. 501.
- Warnatz, J. 'The structure of laminar alkane-, alkene-, and acetylene flames'. 1981: Elsevier, 369-384.
- Weishaupt (2017) *SCOT system*. <http://www.weishaupt.co.uk>. Available at: <http://www.weishaupt.co.uk/service/fachwortlexikon/scot-system> (Accessed: June 2017).
- WEKA (2017) *Class BestFirst*: University of Waikato. Available at: <http://weka.sourceforge.net/doc.dev/weka/attributeSelection/BestFirst.html> (Accessed: May 2017).
- Welch, P. (1967) 'The use of fast Fourier transform for the estimation of power spectra: a method based on time averaging over short, modified periodograms', *IEEE Transactions on audio and electroacoustics*, 15(2), pp. 70-73.
- Weston, J., Elisseeff, A., Schölkopf, B. and Tipping, M. (2003) 'Use of the zero-norm with linear models and kernel methods', *Journal of machine learning research*, 3(Mar), pp. 1439-1461.
- Witten, I. H., Frank, E., Hall, M. A. and Pal, C. J. (2016) *Data Mining: Practical machine learning tools and techniques*. Morgan Kaufmann.
- Wojcicki, K. (2011) *HTK MFCC MATLAB*. Matlab File Exchange. Available at: <https://uk.mathworks.com/matlabcentral/fileexchange/32849-htk-mfcc-matlab> (Accessed: 10 September 2016).

- Worcester Bosch Group (2013) *Greenstar 24-28 i Junior Combi Installation and Servicing Instructions*. [www.worcester-bosch.co.uk](http://www.worcester-bosch.co.uk): Worcester Bosch Group. Available at: <https://www.worcester-bosch.co.uk/professional/support/literature/greenstar-i-junior-combi-installation-instructions> (Accessed: June 2017).
- Worcester Bosch Group (2015) *Greenstar 25-30 Si Compact ErP Installation and Servicing Instructions*. [www.worcester-bosch.co.uk](http://www.worcester-bosch.co.uk): Worcester Bosch Group. Available at: <https://www.worcester-bosch.co.uk/professional/support/literature/greenstar-si-compact-combi-installation-instructions> (Accessed: July 2017).
- Wu, C.-H., Tzeng, G.-H., Goo, Y.-J. and Fang, W.-C. (2007) 'A real-valued genetic algorithm to optimize the parameters of support vector machine for predicting bankruptcy', *Expert systems with applications*, 32(2), pp. 397-408.
- Xuan, Y. and Blanquart, G. (2016) 'Two-dimensional flow effects on soot formation in laminar premixed flames', *Combustion and Flame*, 166, pp. 113-124.
- Yapanel, U. H. and Hansen, J. H. L. (2008) 'A new perceptually motivated MVDR-based acoustic front-end (PMVDR) for robust automatic speech recognition', *Speech Communication*, 50(2), pp. 142-152.
- Yoon, H. J., Yang, J. H., Zhou, Z., Yang, S. S. and Cheng, M. M.-C. (2011) 'Carbon dioxide gas sensor using a graphene sheet', *Sensors and Actuators B: Chemical*, 157(1), pp. 310-313.
- Young, S., Evermann, G., Gales, M., Hain, T., Kershaw, D., Liu, X., Moore, G., Odell, J., Ollason, D. and Povey, D. (2002) 'The HTK book', *Cambridge university engineering department*, 3, pp. 175.
- Yu, D. and Deng, L. (2014) *Automatic speech recognition: A deep learning approach*. Springer.
- Zeldovich, Y. B., Sadovnikov, P. Y. and Frank-Kamenetskii, D. A. 1947. Oxidation of Nitrogen in Combustion. Academy of Sciences of USSR, Institute of Chemical Physics, Moscow-Leningrad: Shelef. Trans.
- Zhou, H., Zhao, J. P., Zheng, L. G., Wang, C. L. and Cen, K. F. (2012) 'Modeling NO<sub>x</sub> emissions from coal-fired utility boilers using support vector regression with ant colony optimization', *Engineering Applications of Artificial Intelligence*, 25(1), pp. 147-158.
- Üstün, B., Melssen, W. J. and Buydens, L. M. C. (2006) 'Facilitating the application of support vector regression by using a universal Pearson VII function based kernel', *Chemometrics and Intelligent Laboratory Systems*, 81(1), pp. 29-40.

# 9. Appendix

## 9.1 Heat Exchangers

*Figure 47 Blue prints of the WB6 Heat Exchanger*

*Figure 48 Blue prints of the WB7 Heat Exchanger*